UNIVERSITY OF NOVA GORICA
GRADUATE SCHOOL

COMBINATION OF CONSTRUCTED WETLAND AND TiO_2 PHOTOCATALYSIS FOR TEXTILE WASTEWATER TREATMENT

DISSERTATION

Dunja Mahne

Mentors: prof. dr. Polonca Trebše
prof. dr. Urška Lavrenčič Štangar

Nova Gorica, 2012

ZAHVALA

“Hear me, four quarters of the world – a relative I am!
Give me the strength to walk the soft earth, a relative to all there is!
Give me the eyes to see and the strength to understand, that I may be like you.
With your power only can I face the winds!”

Black Elk (1863-1950)
Oglala Sioux holy man

“Vizija brez naloge ni drugega kot sen, naloga brez vizije je tlaka, vizija in naloga pa sta upanje sveta.”

iz cerkve v Sussexu, Anglija, okr. 1730

Hvala vsem, ki ste mi pomagali uresničiti vizijo in jo spremeniti v nalogo!

POVZETEK

Doktorska naloga ima naslov »Kombinacija rastlinske čistilne naprave in TiO_2 fotokatalize za čiščenje tekstilne odpadne vode«.

Umetna barvila zelo različnih kemijskih struktur so široko uporabljana v tekstilni, prehranski, papirni in kozmetični industriji. Barvila predstavljajo eno največjih skupin organskih molekul. Tekstilna industrija, ki je velik porabnik umetnih barvil, ima pomembno vlogo v vsakdanjem življenju, hkrati pa je velik porabnik in onesnaževalec vode. Ocene kažejo, da se približno 15 % celotne proizvodnje barvil izgubi med barvanjem in procesiranjem tekstilnih vlaken. Če te vode niso čiščene, povzročajo estetsko onesnaženje, zmanjšujejo prodornost svetlobe v vodno telo in nastopajo kot motilci bioloških procesov v vodi. Nekatera barvila so toksična in kancerogena. Prav tako so lahko vir nastanka strupenih razgradnih produktov, ki so rezultat hidrolize, oksidacije in drugih reakcij razgradnje, ki potekajo v vodnem okolju. Ker imajo onesnažene vode iz tekstilne industrije kompleksno sestavo, so težko biološko dostopne in razgradljive, je bilo veliko naporov vloženih v njihovo čiščenje in zmanjševanje okoljskega bremena, ki ga predstavljajo. Tradicionalne fizikalno kemijske in biološke metode pri tem niso posebno uspešne, saj je zanje značilen prenos onesnaženja in visoki stroški obratovanja; nove metode so tako večkrat predlagane kot bolj učinkovite. Glavni cilji raziskave so bili: (1) sinteza dopiranih TiO_2 polprevodniških tankih plasti s povečanim izkoristkom sončne svetlobe kot vira energije za fotokatalitske reakcije; (2) postavitev in preizkus/uporaba modela rastlinske čistilne naprave; (3) eksperimenti fotokatalitske razgradnje v reaktorju laboratorijske in realne velikosti s pripravljeno tekstilno odpadno vodo; (4) primerjava dolžine obsevanja in stopnje mineralizacije med predčiščeno in surovo odpadno vodo.

TiO_2 tanke plasti z različnim številom slojev so bile sintetizirane po sol-gel metodi. Ko sem TiO_2 polprevodnik dopirala z različnimi količinami železa, se je energijska špranja polprevodniškega materiala premaknila v smer višje

absorpcije vidnega dela spektra. Za določitev fizikalno kemijskih lastnosti dopiranih tankih plasti sem uporabila različne tehnike karakterizacije materialov. Rezultati preizkusa fotokatalitskih lastnosti dopiranih tankih plasti so pokazali, da je imelo dopiranje neugoden vpliv na fotokatalitsko učinkovitost. To pripisujem dejstvu, da pomeni dodatek dopanta v kristalni strukturi prisotnost mest, na katerih poteče rekombinacija. Prav tako je z dopiranjem prišlo do nastanka skupkov na površini tankih plasti in zmanjšanja kristaliničnosti anataza. Ob preizkusu fotokatalitske učinkovitosti TiO_2 in Au/TiO_2 vzorcev sem ugotovila, da je pri TiO_2 tankih plasteh brez dodatkov število nanesenih plasti tisto, ki igra najpomembnejšo vlogo pri določanju učinkovitosti. Ne dopiranje z železom ne naparevanje zlata na površino tankih plasti v primeru večplastnega TiO_2 ni izboljšalo fotokatalitske učinkovitosti katalizatorja. Naparevanje zlata pa je izboljšalo učinkovitost v primeru, ko je bilo zlato naparjeno na enoplasten TiO_2.

Postavljen je bil model rastlinske čistilne naprave. Za pripravo treh vrst tekstilne odpadne vode, ki je bila čiščena v modelu, sem uporabila tri strukturno različna barvila. Učinkovitost modela sem spremljala preko meritev razbarvanja, spremembe absorpcije v UV in Vis delu spektra, z merjenjem biološke in kemijske potrebe po kisiku in toksičnosti (*Vibrio fischeri*) vzorcev na vtoku in iztoku iz modela. Predčiščenje v modelu je imelo enak učinek na vsa tri barvila – absorpcija v Vis delu je bila znižana in v UV delu spektra povišana. Primerjava stopnje znižanja kemijske potrebe po kisiku in stopnje razbarvanja s podobnimi sistemi je pokazala, da je imel model nižjo učinkovitost od pričakovane. To pripisujem nizkim koncentracijam na vtoku, dolžini inkubacije in rednemu prezračevanju substrata med zaporednimi poskusi. Povišane absorpcije v UV delu potrjuje nastanek toksičnih aromatskih aminov, ki nastanejo z redukcijo azo vezi.

Vzorci predčiščene in surove odpadne vode so bili obsevani v fotoreaktorju laboratorijskih dimenzij. Merjene so bile spremembe v absorpciji in kemijski

potrebi po kisiku. Narejena je bila primerjava med fotokatalitsko oksidacijo in ozonacijo vseh treh različnih barv. Nepričakovano je bilo v primeru modrega barvila ugotovljeno, da potrebna dolžina obsevanja za predčiščene vzorce ni bila krajša v primerjavi s tisto, ki je bila potrebna za razbarvanje surovih vzorcev. Pri fotokataliski ozonaciji je razbarvanje pričakovano nastopilo hitreje kot pri fotokatalitski oksidaciji. Začetna intenziteta obarvanja vzorca je vplivala na potrebno dolžino obsevanja za razbarvanje.

Rezultati iz reaktorja realne velikosti so potrdili rezultate laboratorijskega fotoreaktorja – za modro barvilo je bila ravno tako potrebna enaka dolžina obsevanja za razbarvanje predčiščenih in surovih vzorcev. Razbarvanje ostalih dveh vzorcev je bilo z uporabo predčiščenja pospešeno; mejne vrednosti, tudi za razbarvanje, so bile dosežene po 12ih urah obsevanja. Vzorci s črnim barvilom so imeli visoke vrednosti toksičnosti ves čas trajanja obsevanja. Vrednosti toksičnosti za modro in rdeče barvilo pa so se med obsevanjem znižale. Vrednosti kemijske potrebe po kisiku so se znižale, vendar je bilo znižanje v primerjavi z razbarvanjem počasnejše; kljub temu so bile dovoljene mejne vrednosti za izpust za kemijsko potrebo po kisiku dosežene hitreje kot mejne vrednosti za izpust obarvanih vzorcev.

Na podlagi rezultatov opravljenih eksperimentov in narejeni analizi stroškov, je kombinacija uporabe rastlinske čistilne naprave in fotokatalitsko obsevanje vzorcev z naravno svetlobo tista kombinacija, ki je predlagana kot najbolj ugoden pristop za čiščenje tekstilne odpadne vode.

Ključne besede: *fotokataliza, TiO_2 tanke plasti, dopiranje, rastlinska čistilna naprava, tekstilna odpadna voda*

SUMMARY

Synthetic dyes may be found in many structural varieties and are widely used as colouring agents in textile, food, paper and cosmetics production. They also represent one of the largest groups of organic molecules. Textile industry, large consumer of synthetic dyes, plays an important role in everyday life and it also consumes large quantities of water and produces large amounts of wastewater. It is estimated that approximately 15 % of the total textile colorant production is lost during dyeing and processing of textile fibres. These wastewaters, left untreated, cause aesthetical pollution, reduce light penetration into the water body and interfere with aquatic biological process like photosynthesis. Some of the dyes exhibit toxic and carcinogenic effects and can also be the origin of dangerous by-products formation through oxidation, hydrolysis and other reactions taking place in the water phase. Because of the complex, recalcitrant and bio-resistant character of textile effluents, a lot of attention has been dedicated to their remediation and pollution abatement. Since traditional physicochemical methods and biological approaches were not found to be successful in pollution abatement without phase transfer or high treatment costs, new approaches have been proposed. The goals of my Ph.D. research were to combine two promising treatment approaches for textile wastewater treatment. The major goals of my research were: (1) synthesis of doped TiO_2 semiconductor thin films with enhanced ability to use sunlight as a light source to perform photocatalytical reactions; (2) set up and operation of a constructed wetland (CW) model; (3) lab scale and pilot scale photodegradation experiments on prepared textile wastewater; (4) comparison of length of irradiation and degree of mineralization of CW pre-treated and raw samples.

TiO_2 thin films of several layers were synthesised by a sol-gel method. When TiO_2 semiconductor was doped with different amounts of iron, the band gap shift was achieved towards Vis light absorption. Different techniques were used to characterise physico-chemical properties of doped thin films. Photocatalytic

performance of doped films was tested and results showed that doping had an overall detrimental effect on films performance. This was attributed to the fact, that doping forms recombination sites which deteriorate the semiconductor performance and also to particles' agglomeration and crystallinity loss exhibited in the doped samples. When photocatalytic activity of TiO_2 and Au/TiO_2 samples was tested the number of layers was found to play the most important role in determining photocatalytic performance in the case of pure TiO_2 samples. In the case of multilayer films both types of modifications exhibit deteriorating effect on the films performance. Gold addition substantially increased photocatalytic performance only when it was sputtered onto the one layer film.

A CW model was set up and put in operation. Prepared wastewater with three structurally different textile dyes was treated in several sequential experiments. Model's performance was followed by measuring decolouration, change in UV-Vis absorbance spectra, BOD, COD and toxicity (*Vibrio fischeri*) values at the inflow and outflow from the model. Pre-treatment in the CW model proved to have a uniform effect on all the three dyes – it decreased absorbance in the Vis part of spectra and increased it in the UV part. When COD removal reduction and decolouration rate were compared to those reported for similar systems treating textile wastewater, those obtained in our system were lower. This was attributed to the inflow concentrations, length of incubation and periodic aeration in the media. Increase in the samples' UV absorbance confirmed the formation of toxic aromatic amines' through reductive azo bonds' cleavage.

Pre-treated and raw samples of textile wastewaters were irradiated in Carberry photoreactor. Absorbance changes and COD decrease were measured. Photocatalytic oxidation and ozonation of three different dyes were compared. Unexpectedly for blue dye the irradiation time needed to decolorize the sample solution was not shortened by the pre-treatment in the CW model. When photocatalytic ozonation was applied, decolouration was observed in

considerably shorter time compared to photocatalytic oxidation. Initial colouration intensity was found to influence the overall irradiation time.
The CPC reactor irradiation results confirmed the results obtained in the Carberry type photoreactor - for blue dye again the same length of irradiation was needed to decolourise raw and pre-treated samples. Decolouration of pre-treated samples was much faster for the other two tested dyes; limit values as well as decolouration were achieved after 12 h of irradiation. Black dye exhibited high toxicity values throughout the entire experiment. But toxicity of red and blue samples decreased in the course of irradiation. COD values decreased at a slower rate compared to colouration, nevertheless, for red and black dye, the legislative limit COD values were reached before colouration limits.

Based on results obtained in the experiments and cost estimation analysis, an improved biological stage CW with natural irradiation source in a post photocatalytic oxidation step is thus proposed as the best treatment approach.

Key words: *photocatalysis, TiO_2 thin films, doping, constructed wetland, textile wastewater*

LIST OF CONTENTS

LIST OF FIGURES

LIST OF TABLES

ABBREVIATIONS

AFM = atomic force microscopy

AOPs = advanced oxidation processes

BE = binding energy

BOD_5 =biological oxygen demand

CB = conduction band

COD = chemical oxygen demand

CPC = compound parabolic concentrator

CW = constructed wetland

D = diameter of the particles

DMS = dimethylsulfide

DO = dissolved oxygen (concentration)

EC = electric conductivity (measurement)

ERL = electrostatic repulsive effect

FE-SEM = field emission scanning electron microscopy

FWS = free water surface wetlands

HDPE = high density polyethylene

HLR = hydraulic loading rate

HRT = hydraulic retention time

HSSF = horizontal subsurface flow wetlands

L = length

ORP = oxidation-reduction potential

PAH = polycyclic aromatic hydrocarbons

PCOx = photocatalytic oxidation

PCOz = photocatalytic ozonation

POD = peroxidase enzymes

RBK5 = Reactive Black 5

RBL19 = Reactive Blue 19

RF = Radio frequency

ROS = reactive oxidative species

RRD22 = Reactive Red 22

SAC = Spectral Absorption Coefficient

T = temperature

TN = total nitrogen

TOC = total organic carbon

TP = total phosphorus

VB = valence band

VFW = vertical flow wetlands

W = width

WWTP = wastewater treatment plant

XPS = X-ray photoelectron spectroscopy

XRD = X-ray diffraction

1. INTRODUCTION

The main courses of surface and ground water contamination are industrial discharges, which can be harmful also in low quantities and concentrations, and insufficient domestic wastewater treatment. More than 45 % of the Slovenian terrain is on karst bedrock. A very high permeability of bedrock is characteristic for this region. As a consequence almost all water from the surface penetrates very quickly into the underground. Since the penetration process is quick, the filtration and purification processes are very low or nonexistent (sinkholes). Consequently, all pollution reaching the ground very easily reaches underground waters where remediation potential is inherently low and the possibilities of polluting water resources very high (Drew and Hötzl, 1999).

Among the twelve principles of green chemistry we can also find the following: catalysis, design for degradation, real-time analysis for pollution prevention, use of renewable feedstock and design for energy efficiency (Herrmann et al., 2007). I would like to point out the last of the named principles which, together with the other listed ones, was the leading notion when the work on a combination of two different systems was started. That is a combination of two methods based on two very different principles with the aim to treat wastewater in an efficient way. Efficient from two different points of view: pollution reduction to meet the legislative limit values and cost benefit point of view. A laboratory scale constructed wetland model was coupled with photocatalytic degradation with TiO_2 photocatalytic paper as a semiconductor photocatalyst under near UV light for textile wastewater treatment.

Photocatalytic degradation of various toxic or bio-recalcitrant or not biodegradable (due to being biologically non-accessible) substances has been proposed as a viable process to detoxify water. Through formation of highly reactive chemical species in the oxidation process, recalcitrant molecules are degraded into biodegradable ones or even completely mineralized. However,

some degradation products can be more toxic than the parent compounds. All these processes are called advanced oxidation processes or sometimes advanced oxidation technologies (Robert and Malato, 2002).

Titanium dioxide's use has long been present in applications which require high opacity and brightness as coatings, paints, plastics, ink and paper since it exhibits unique optical properties like high refractive index and whiteness. It has attracted new attention since the discovery of Fujishima-Honda effect in 1972 and up to present day it stays very attractive due to its photosensitivity, low cost, non-toxicity and chemical stability (Ko et al., 2009). Photocatalytic paper as one of the forms of supported TiO_2 catalysts was defined to be a smart composite which exhibits light activated catalytic function and is able to decompose organic pollutants and kill pathogens (Ko et al., 2009).

Another favourable approach to wastewater treatment from the energy and cost reduction point of view is treating wastewater by passing it through a constructed wetland. Constructed wetland is a setup which imitates natural ecosystem. In nature, water ecosystems are able to decompose some of the substances from wastewater by mechanical interactions with media and metabolic action of organisms in the media (Bulc and Ojstršek, 2008). Decrease in organic load occurs as aerobic decomposition takes place in the presence of oxygen and anaerobic decomposition in oxygen depleted zones (Vrhovšek and Kroflič, 2007).

With combining these two systems, biological degradation in constructed wetland model and chemical degradation with advanced oxidation methods, we aimed to attain a system which would provide a satisfactory cost-effect relationship for textile wastewater treatment for both - organic load and specific bio-recalcitrant pollutants. Synthetic dyes are used in a very wide selection of industrial processes and services such as paper production, food technology, in

construction, automobile industry and hair colourings (Forgacs et al., 2004). But in terms of quantities, textile industry precedes all the other named consumers (Hai et al., 2007).

A laboratory scale constructed wetland (CW) model had a similar design to a model used by (Zupančič, 2001) to establish relationship between media and metal ion removal. The CW model was setup to test overall performance for treatment of textile wastewater. As recalcitrant substances were not expected to be completely degraded in the wetland model, the aim was to combine it with one of the advanced oxidation methods. With the use of such a combination complete decolouration and mineralization of present pollutants was expected (Hai et al., 2007).

2. RESEARCH GOALS

The research goals are divided into two major groups.

In the first part the focus was on research of advanced oxidation methods and its application in catalysis used in wastewater treatment. In the frame of this research, synthesis of doped TiO_2 semiconductor thin films and investigation of their functional properties and photocatalytic performance was conducted. A "soft chemistry" sol-gel procedure was adopted to synthesize thin films on glass support by dip coating. The main goal to be achieved by a doping procedure was enhancement of ability of the semiconductor to use sunlight as a light source to perform photocatalytic reactions. TiO_2 catalyst thin films were doped with various amounts of iron (and also sputtered with gold) with the aim to achieve a "red shift" in absorbance onset of the films and so to obtain a better photocatalytic performance with the use of visible light.

Second part of the research was dedicated to setup and operation of a CW model. A laboratory scale model with controlled experimental conditions of the inflow water quality and hydraulic loads was set up based on a previously

constructed model by (Zupančič, 2001). Its design and operational parameters were chosen according the literature data (EPA, 2000; Bulc and Ojstršek, 2008). In the model, operating conditions for microbiologic colour reduction were established. The model was filled with prepared textile wastewater and changes in various parameters were followed: colour, total organic carbon (TOC), biological oxygen demand (BOD_5), chemical oxygen demand (COD) and toxicity removal efficiency.

At the end, two above-mentioned systems were combined. First set of photocatalytic degradation experiments was done in a small volume Carberry photocatalytic reactor where 280 mL of prepared wastewater was irradiated. Experiments were done under two different conditions; samples were purged either with oxygen or with ozone, with the aim to compare two different methods - photocatalytic oxidation and photocatalytic ozonation. Pre-treated wastewater in the CW model and raw wastewater was irradiated for the same length of time and results were compared. In the second set of experiments photocatalytic degradation was performed in a real scale compound parabolic collector reactor (CPC) where 17.5 L of prepared wastewater were photocatalytically irradiated. Irradiation results of the CW pre-treated and raw wastewater were compared. An estimate of costs of each of the treatment approaches was done.

3. THEORETICAL BACKGROUND

3.1. TEXTILE DYES

Synthetic dyes are found in the following structural varieties based on auxochrome group: acidic, reactive, disperse, direct, vat, basic, mordant, pigment, anionic dyes (dos Santos et al., 2007). They are widely used as colouring agents in textile, food, paper and cosmetics production and represent one of the largest groups of organic molecules. Textile industry plays an important role in everyday life but it also consumes large quantities of water and

produces large amounts of wastewater. The estimation is that approximately 15 % of the total colorant production is lost during dying and processing of textile fibres (Pekakis et al., 2006). High variety is characteristic for the dyes' and auxiliary chemicals' composition used in the process and found later in textile wastewater which are generally organic and have complex structure (Akpan and Hameed, 2009).

Reactive dyes are the only sort of textile dyes which are designed to covalently bond with OH-, NH- or SH- groups to prevalently cellulosic fibres (also used for silk and nylon fibres). Covalent bond with an additional electrostatic interaction, when the dye ion and fibre have opposite charges, is the strongest dye-fibre attachment. Consequently and also because a large variety of colours is available and high wet fastness and ease of application are characteristic, they are extensively used in textile industry. In general they are used for cotton fibres colouring but can also be used for wool and polyamide fibres. Reactive dyes represent about 20-30 % of the total market share. Another source cites a 60-70 % share of azo dyes in the world's dye market (Garcia et al., 2009). The next most common chromophore group is the anthraquinone one. Reactive dyes were developed with the aim to resist fading when exposed to sweat, soap, water, and light or oxidising agents (Lee and Pavlostathis, 2004). In the light of the efforts made for their degradation in wastewaters, this hints to the fact that their resistance implies also to degradation.

3.1.1. Dye structure

By chemical structure the reactive dyes are azo, anthraquinone, phthalocyanine and ortriphenilmethylene dyes. They are highly sulfonated and consequently highly water soluble, also they don't adsorb well onto the biomass (Beydilliet al., 2000).

The structure of reactive dyes is composed of solubilising components (sulphone of sulphide groups), chromophore (azo/keto-hydrazone groups) and reactive centre. The colour changes with the change of the chemical structure of the chromophore:

- monoazo dyes structures are used for yellow, orange and red casts;
- mono and diazo structures are used for violet and navy blue casts;
- anthraquinone and phthalocyanine derivatives and copper complexes are used for blue and green casts (dos Santos et al., 2007).

Reactive centres can be divided by the mechanism of bond formation between the dye molecule and the media. The reactive centre can be monofunctional, bifunctional and polyfunctional. Monofunctional centre has one, two, three or more reactive groups like 2-sulphatoethylsulphone or sulphatoethylsulphonamide, aminofluortryazine, tri- or tetrachloropyrimidine. Bifunctional and polyfunctional centres have one of the following combinations:

- one diazo chromophore and one reactive system on each side of the molecule;
- two chromophores bonded by two reactive systems;
- one chromophore and two reactive systems on one side of the molecule.

3.1.2. Dyeing process

A common textile-processing setup consists of the following processes which occur in sequential steps (dos Santos et al., 2007):

- *Sizing*: sizing agents provide strength of fibres and minimize breakage (starch, polyvinyl alcohol, carboxymethyl cellulose).
- *Desizing*: this step removes the redundant sizing material from the previous step.
- *Scouring/Washing*: fibreimpurities breakdown (natural oils, fats, waxes, surfactants); emulsification and suspension in the alkali scouring bath (NaOH).

- *Bleaching*: naturally occurring colour removal by sodium hypochlorite (NaClO) and H_2O_2.
- *Mercerising*: concentrated alkaline solution and acid solution to increase dye-ability, lustre (brightness) and fibre appearance.
- *Dyeing*: adding colours to fibres (large amount of water).
- *Rinsing*: several rinsing cycles to remove the unfixed, redundant colouration.

As a discharge of the named processes the following compounds can be found in the wastewater: size agents, enzymes, starch, waxes, ammonia, H_2O_2, sodium silicate, disinfectants, insecticide residues, NaOH, soaps, fats, pectin, waxes, oils, antistatic agents, and colour. Also surfactants, metals, salts, organic stabilizers (sulphide, formaldehyde) are found in the discharge.

Textile auxiliaries which are added to the dyebath in colouration procedure are generally divided into wetting agents and sequestering agents. They can be irritating at direct contact to human skin, exhibit low degradability and significantly increase degree of pollution of the technological water (Ojstršek, 2007). For the most part, organic pollution arises from the desizing/scouring step and colour pollution of the wastewaters from the dyeing/rinsing step. Different wastewaters from the single process steps exhibit extreme fluctuations in pollution parameters - pH, COD and BOD values fluctuations (dos Santos et al., 2007).

High losses are especially characteristic for reactive dyes and are a consequence of low levels of dye-fibre fixation when hydrolysed dye molecules are in the dyebath. Hydrolysis arises from the fact that the dye molecules are highly soluble in water and have a characteristic brightness (Pearce et al., 2003). When applying typical reactive dye dyeing conditions (pH ≥ 10, T ≥ 60 °C, salts 60-100 g/L), 20-50 % of all the applied dyes remain unfixed in their hydrolyzed form in which they exhibit no affinity towards fabric (Lee and

Pavlostathis, 2004). This is the amount ending in textile wastewaters. To dye 1 kg of cotton fibres, about 150 L of water is needed and large amounts of wastewater are generated (Jadhav et al., 2010).

Presence of unnatural colours in watercourses is associated with contamination and creates an aesthetic problem. Very low dye concentrations are visible in clear river water, as low as 0,005 mg/L (Nigam et al., 1996). When colour standards were set by the UK Environmental Agency for several different wavelengths, the limit taken into account was capacity of the human eye to detect colour in 1 ppm concentration (Pearce et al., 2003).

3.1.3. Removal methods

Textile wastewater effluent discharged into a natural environment represents an aesthetic and environmental problem. Colouration is correlated with pollution and light absorbance by dye molecules in the body of water; it interferes with aquatic biological process like photosynthesis due to reduced light penetration (Alinsafi et al., 2006).

In many cases and also Tekstina, a textile company in Ajdovščina, Slovenija, discharges its effluents to the sewage system leading to local wastewater treatment plant. At higher load events, after days when colouring processes are more frequent, the treatment plant has operation problems due to Tekstina discharges since the pollution (colouration) abatement is not sufficient (Krečič, 2009).

Also elsewhere the practice of treating textile effluents in common wastewater treatment plants has shown that an industrial scale decolouration system is needed prior to discharge to sewage works. Regarding the location there are two possibilities, where the textile industry effluent should be treated in terms of colour removal. The first one foresees treatment within the industrial grounds,

where wastewater is either first decoloured and then discharged to the sewage or it is treated to the point, which allows partial or full reuse of the water in the technological process. The second one places the decolouration step before or after the treatment process applied at the location of the sewage treatment plant (Pearce et al., 2003).

Due to a large number of different dye molecules which can react differently during the treatment procedure, seasonal variations due to fashion cycles and production routines, and also high investment and operational costs of treatment plants and low efficiency, a uniform end-of-pipe solution which would be universally applicable to all kinds of textile effluents is not to be expected; and is not even being looked after.

Currently there are several different treatment methods, summarised in Fig. 1, applied to abate the textile wastewater pollution and can be divided into the following classes:

- chemical methods;
- physical and physico-chemical methods;
- biological approaches.

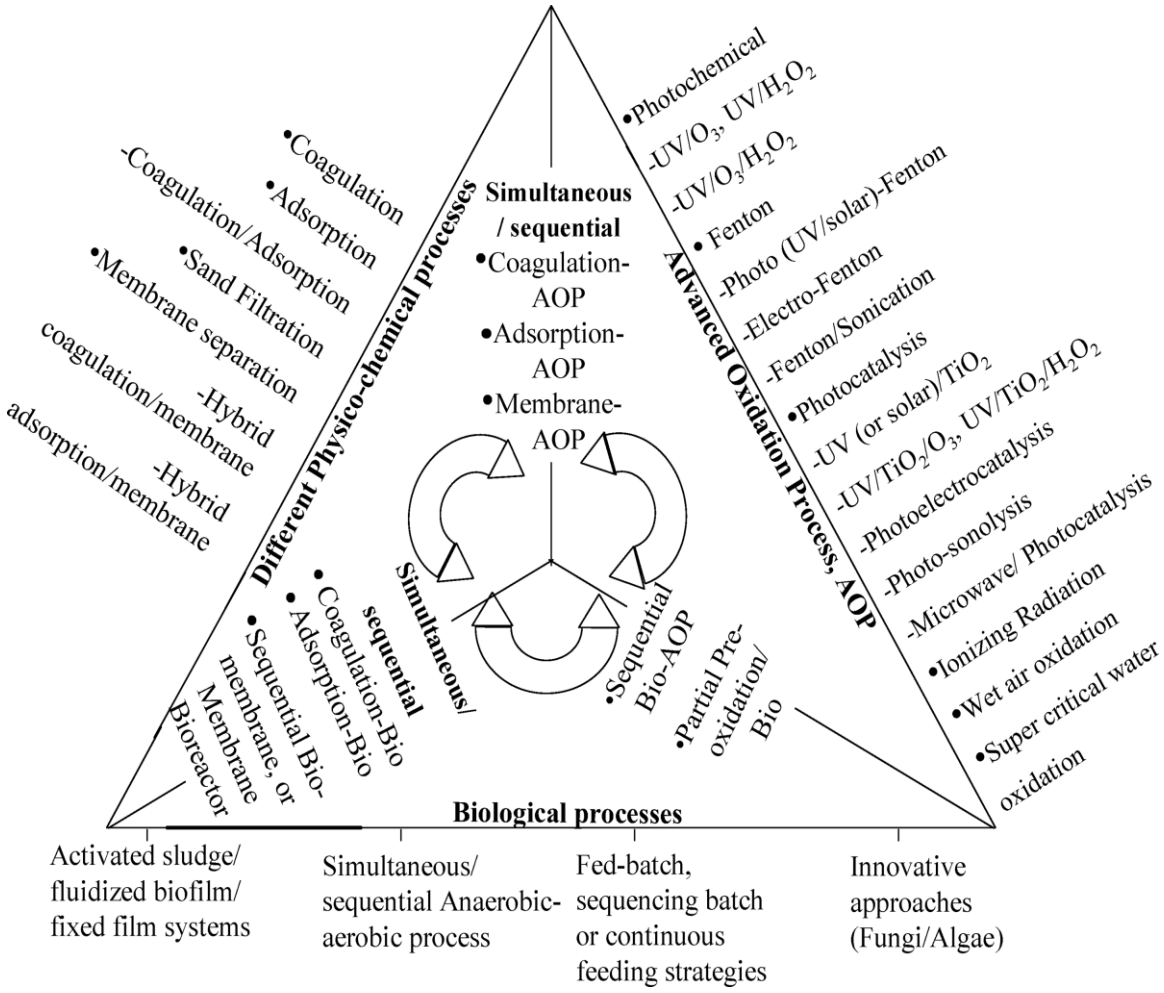

Figure 1: Simplified representation of broad spectrum of combinations proposed in the literature for textile wastewater treatment (after Hai et al., 2007).

The most prominent drawback of most of the physico-chemical methods is in secondary waste production (sludge), membrane fouling and costly adsorbent regeneration. IPPC (Integrated pollution prevention and control) regulations suggest that the mass transfer methods should be abandoned in favour of destruction technologies, as the transfer of pollution should be, if possible, avoided.

Biological treatment methods on the other hand are considered to be inherently environmentally friendly and cheaper compared to chemical ones (Harrelkas et al., 2008). In biological treatment, the anaerobic phase is important for the

decolouration since reductive cleavage of azo bonds takes place in anaerobic environment. In the aerobic phase biomineralization of the cleaved aromatic amines is predicted to take place, but there are some limitations, since it is not certain whether all aromatic amines can be degraded and the complete removal of other components is also questionable (van der Zee and Villaverde, 2005). Anaerobic and aerobic degradation are described in detail in 3.2.6.

Due to environmental implications and limitations of each of the above named treatment methods, more and more research and promise of successful outcome is focused on combining one of the biological treatment methods with other techniques to ensure a cost effective and pollution destruction technology as the best approach to pollution abatement (Hai et al., 2007).

3.1.4. Dye toxicity

Toxicology of the azo dyes presumably arises from reductive cleavage of azo bond and subsequent formation of aromatic amines as a key metabolic step leading to toxicity and carcinogenic activation of the dye. Mutagenic activity was confirmed in a number of studies on effluents from textile and other dye industries. Compared to an array of different effluents, the dye industry generated wastes rank as moderately mutagenic (Mathur et al., 2005).

When toxicity of different colours and their metabolites after azo bond reduction has been compared before and after reductive cleavage, different toxicity levels were exhibited. Toxicity of C.I. Acid Orange 7 and C.I. Food Yellow dyes was similar before reduction; after reduction the toxicity of Food Yellow slightly decreased, but it increased a 100-fold for Acid Orange (Gottlieb et al., 2003).

When toxicity test was done directly on aromatic amines' standards - those expected to be formed during azo cleavage, the obtained results differed substantially and were found to be dependent on the type and position of the

substitution group. Position of sulphonic group in the naphthalene ring was found to play an important role in its final toxicity. Position 1' turned out to be more toxic compared to position 2'. Toxicity of 1-amino-2-naphtol was very high compared to its sulphonated analogue. It is believed that the lack of sulphonate group increases lipid solubility and higher uptake by the test organism. This was the reason why toxicity of the two compared colours differed so much after the reduction. Toxicity increased also in the case of Reactive Black reduction by *C. butricum* (Gottlieb et al., 2003).

When different test organisms were used for the reduction step and toxicity after reduction was compared it has been shown, that toxicity for some dyes is and for some dyes is not dependent on the reduction method. This is attributed to the fact that different bacterial strains used for the reduction produce different end products which exhibit different toxicity (Gottlieb et al., 2003).

Dyes and textile effluents affect chromosomes and cell division. A decreased mitotic index of meristematic cells showed presence of cytotoxic compounds but in experiment with textile effluent increased mitotic index indicated presence of factors which increase cell division which eventually leads to uncontrolled proliferation and tumour formation. Strong genotoxic effects (mitotic cell aberrations) were detected at an effluent concentration as low as 10 %. Effluent treatment resulted in significant reduction in percentage of aberrant mitotic cells (Jadhav et al., 2010).

Bioaccumulation of dyes depends on the chemical structure, size of the molecule, number of sulphonic groups and solubility in lipids. Bioaccumulation is not characteristic for the water-soluble dyes like reactive dyes. Disperse dyes do accumulate in fish organisms up to some extent but the passage through the biological membranes is impeded by their high molecular weight (Gonçalves et al., 2000).

3.2. CONSTRUCTED WETLAND FOR (TEXTILE) WASTEWATER TREATMENT

Treatment of textile effluents containing azo dyes from textile industry represents a challenging issue due to their complex aromatic structure which is designed with the aim to be resistant to fading when exposed to sweat, light, washing liquids and oxidising agents (Davies et al., 2005).

CW's are systems which mimic the functions and processes in natural wetlands. The processes involve wetland vegetation, soil and associated microbial community for water quality improvement. The specific design of a constructed wetland elevates treatment efficiency compared to natural systems. The CW design enables them to take advantage of the processes which occur in natural wetlands by conducting them in a more controlled environment of CW setup (Vymazal, 2005). In another way CWs are made to mimic natural marshes and are a low-cost alternative to conventional secondary and tertiary wastewater treatment (Thullen et al, 2005).

In 1970s and 1980s the CWs were used only for treating domestic, municipal sewage. But since the 1990s they have been used for wider spectra of wastewaters. There are several runoffs treated by CWs: landfill leachate, urban, highway, airport runoff, etc. Also waters from food processing industry – vinery, dairy and animal operations can also be treated by CWs. They are also used for industrial wastewater treatment like that from wood handling, pulp and paper mills, oil refineries and fertilizer manufacture (Kadlec and Wallace, 2008, pp. 841).

3.2.1. Types of constructed wetlands

Varying conditions in CW beds enable development of specific ecological niches which favour development of specific microbial biofilms with functionally different respiration and in turn pollution removal processes (Wiessner et al., 2005). The

basic classification is based on the type of macrophytic growth and on the water flow regime, as presented in Fig. 2.

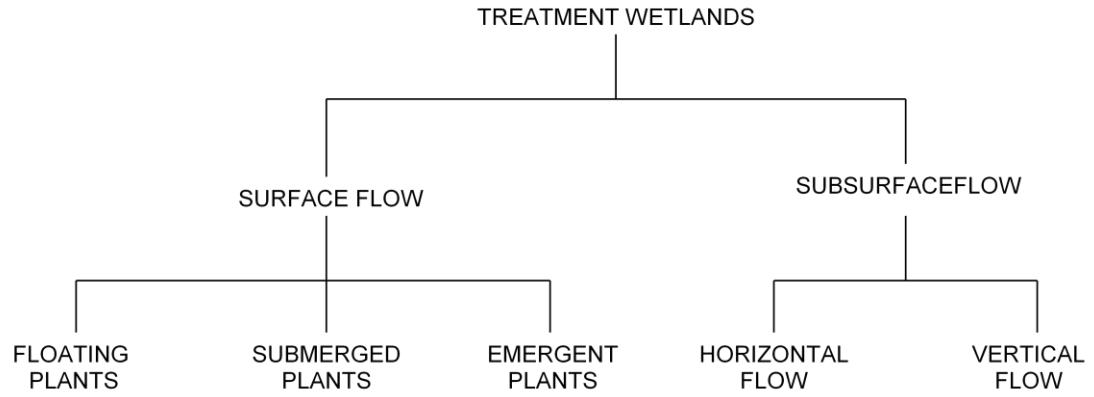

Figure 2: Constructed wetland types (after Kadlec and Wallace, 2008).

3.2.1.1. Free water surface wetlands

Free water surface wetlands (FWS) are characteristic for their areas of open water and are the most similar to natural marshes in their appearance. Floating vegetation and emergent plants are found in FWS and also a wide variety of wildlife is attracted to them from insects, water animals to birds and mammals. The most common application of FWS is advanced (tertiary) treatment after secondary wastewater treatment and is an exclusive choice for agricultural, industrial and urban stormwater treatment since they are able to deal with pulse flows and changes in level (Kadlec and Wallace, 2008, pp. 5).

Anoxic conditions prevail in this type of CW. There is a thin aerobic layer at the surface caused by passive aeration through oxygen diffusion. Below this zone the redox potential decreases with the lowest value in the upper soil bed where sedimentation of particulate matter forms a zone with high microbial activity and very high oxygen demand. Below this depth the potential in some cases increases again due to low pollution diffusion through the matrix and plant rhizosphere oxygenation, but the conditions remain highly reduced (Faulwetter et al., 2009).

3.2.1.2. Vertical flow wetlands

Since horizontal subsurface flow wetlands (HSSF) (in 3.2.1.3.) have limited capacity to oxidise ammonia due to low oxygen transfer ability, vertical flow wetlands (VFW) were developed with the aim to treat wastewaters with high ammonia levels, higher than those in municipal wastewaters and are used to treat very concentrated wastewaters like leachates and food processing wastewaters etc. A version of VFW is flooded with water to minimise oxygen transport into the body of wetland and is used to create anaerobic, reducing conditions for sulphur management purposes and metals immobilisation. It can also be used for biosolids and sludge dewatering (Kadlec and Wallace, 2008, pp. 7).

The vertically percolating water creates unsaturated, highly oxidised conditions. Consequentially high redox conditions favour aerobic processes with high biological BOD removal and nitrification and low denitrification compared to FWS and HSSF (Li et al., 2008). High nutrient content and oxygen rate both promote microbial growth with maximum density and activity in the first 5-10 cm of the filter material (Faulwetter et al., 2009). Plant contribution to oxygenation is considered negligible since the concentration is already very high.

3.2.1.3. Horizontal subsurface flow wetlands

In horizontal subsurface flow wetlands (HSSF) water is under the surface of gravel and soil beds where it flows through the media with plants' roots and rhizomes. Most commonly they are used for one house or small community domestic wastewater treatment but also for certain industrial wastewaters. The main consideration is the media clogging possibility (Kadlec and Wallace, 2008, pp. 6).

Horizontal sub-surface flow CWs are the most commonly used type of CWs in Europe. A typical CW setup is presented on Fig. 3. Design of such a CW

consists of a rectangular bed, filled with appropriate media and planted with the common reed (*Phragmites australis*). The rectangular space is lined with an impermeable membrane.

The wastewater has to be mechanically pre-treated before it can enter the CW. Water passes slowly through the filtration medium under the surface of the bed in a more or less horizontal path until it reaches the outlet zone. As it reaches the outlet it can be collected before discharge via a level control. During the passage through the reed bed the wastewater makes contact with a network of aerobic, anoxic and anaerobic zones (Vymazal, 2005).

Suspended solids, which are not removed by pre-treatment, are removed by filtration and settlement in the first few meters on the CW. An effective pre-treatment is needed to avoid clogging events. Clogging is a consequence of accumulation of trapped solids and is highly undesirable.

Length and depth of the wetland among other factors influence redox conditions in this type of CW. Oxidised and reduced zones are present, but overall the reduced environment prevails (Headley et al., 2005). Redox potential increases with length due progressive pollution degradation and mechanical filtration. And it decreases with depth; namely higher potential close to surface zone (5-20 cm) is a result of passive oxygen diffusion and plant oxygen release (Faulwetter et al., 2009). However since there is vertical mixing of water present in the matrix, depth variation is not always present. Vertical redox profile varies with the CW length, being more pronounced at the outlet compared to the inlet. Shallower (0.27-0.5 m) CWs reportedly have higher redox potentials compared to deeper ones (0.5-1m) and so are more efficient in COD, BOD, NH_3 and P removal (Headley et al., 2005).

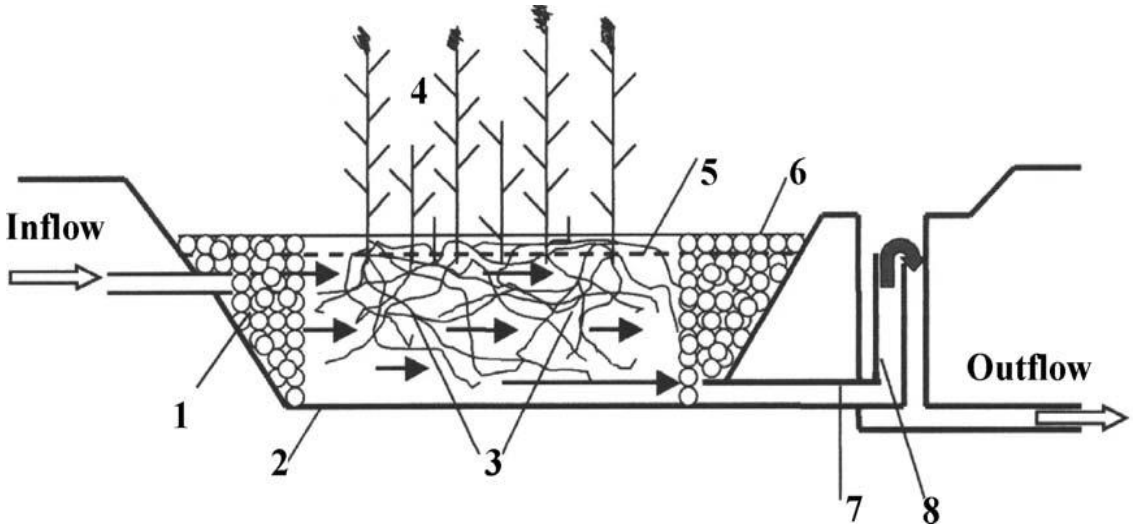

Figure 3: Schematic representation of a treatment wetland with horizontal sub-surface flow. 1 - distribution zone filled with stones, 2 - impermeable liner, 3 - filtration medium (gravel, crushed rock), 4 - vegetation, 5 - water level in the bed, 6 - collection zone filled with large stones, 7 - collection drainage pipe, 8 - outlet structure for maintaining the water level in the bed. The arrows indicate only a general flow pattern (after Vymazal, 2005).

As wastewater passes through the CW rhizosphere, it is cleaned by microbial degradation, physical and chemical processes of binding the particles and in a low amount, by plant harvesting. Also combinations of various types of CWs, the so-called hybrid systems are known, which have been used to enhance the treatment effect. The inability of HSSW or VFW to provide together nitrification and denitrification step and decrease total nitrogen load in a single HF or VF CW, lead to a combination of both systems into a hybrid one (Vymazal, 2005).

CW models are laboratory scale models used to investigate relations between different pollutants, removal pathways for different pollutants and their removal rates. Laboratory scale planted or unplanted systems allow a high level of control over experimental conditions. There is a complete control over the inflow water quality and consequently concentrations of the introduced pollutant which represent the systems' load. Also the hydraulic load conditions are varied according to the expected removal efficiency.

3.2.2. Design parameters

Design of the CW can be roughly divided into two categories. The first are sizing calculations which require characterisation of the incoming water and regional climate and goals of treatment to be achieved. Prescriptive sizing criteria, loading charts and scaling factors are design tools used in this phase. The second category is physical specifications which include number of cells, layout, liners, bed depth, media size, plants and level control (Kadlec and Wallace, 2008, pp. 715).

Area, calculated to achieve treatment goals may be arranged in a number of ways. Number of independent flow paths, number of cells in each flow path and aspect ratio of the cells or flow path are the principal decisions to be taken. Among general recommendations for an individual wetland cell is a recommendation to avoid small length-to-width ratio and maintenance of good bottom uniformity during construction and start-up (Kadlec and Wallace, 2008, pp. 659).

The aspect ratio is important in basin design since it effects the flow distribution and hydraulic short circuiting. It is presumed that long, narrow paths are closer to plug-flow compared to shorter, wide ones. Ratios between 2 : 1 <L : W < 4 : 1 are recommended by (EPA, 2000). Effective flow distribution is the goal of calculations and optimisation of other parameters such as deep zones, speed bumps and banded or clumped vegetation (Kadlec and Wallace, 2008, pp. 660-664).

Design criteria for subsurface flow CW was proposed by Kikuth in 1977 (Eq. 1) and is up to date used for sizing of systems for domestic sewage treatment and a base for calculations for other wastewaters.

$$A_h = \frac{Q_d\,(\ln C_{in} - C_{in})}{K_{BOD}} \qquad (1)$$

In Eq. 1 A_h is the surface of the flow bed (m^2), Q_d is the average flow rate (m^3/day), C_{in} is the influent BOD_5, C_{out} is the effluent BOD_5 and K_{BOD} is the rate constant.

The type of bed – its aspect ratio also influences the removal efficiency. It has been shown, that aspect ratio 2.5 : 1 is the most efficient one in removal of volatile fatty acids and alkylsulfides compared to aspect ratios of 1 : 1 (square), 1.5 : 1 and 2 : 1 (Huang et al., 2005). Depth of the filtration bed is usually 0.6 to 0.8 m so the macrophyte roots of wetland plants can penetrate the whole bed and ensure oxygen release in throughout the bulk of the media (Farooqi et al., 2008).

The design of constructed wetland can promote either a wide range of redox conditions, allowing many different biological processes to take place, aimed at removing many different pollutants in the same bed. Or it can promote a chosen, limited range of conditions, targeted to promote growth of a specific microorganisms' group with the aim to remove a specific pollutant (Faulwetter et al., 2009).

3.2.2.1. Water depth, hydraulic loading rate and hydraulic retention time

The hydraulic loading rate (HLR) is the flow rate divided by the surface area of the beds. Hydraulic retention time (HRT) is the time when a certain volume of water remains within the CW (Akratos and Tsihrintzis, 2007).

For the following compounds studied - volatile fatty acids and alkylsulfides - the results suggest that the HRT and water depth are two major factors which control the performance of CW. These hydraulic variables affect the duration of the contact between the pollutants and the microbial population within the CW matrix. In general it has been proven that longer HRT generates more aerobic

conditions and provides higher pollution removal rates. These results suggest that these two factors should be an important consideration in CW design and construction. Water depth affects the surface aeration which drives redox conditions and biochemical reactions of the beds. The water in shallow beds (depth 0.27 m) showed higher redox potentials than in deep beds (depth ranged from 0.47-0.51 m), promoting more variable and energetically favourable reactions in shallow beds (such as denitrification) (Huang et al., 2005).

Results concerning the relationship between concentrations of target analytes and water depth (or water level) also show the same relationship. A higher removal of ammonium, phosphate and nitrate was found at lower media depth when comparing 46 cm with 30 cm systems (Huang et al., 2005). A general observation when different experimental units with different media, sizes and pollutants were compared is that effluent concentrations increase as loading is increased. So the efficiency decreases when higher wastewater load is introduced to the system. This is expected, since higher loading implies smaller HRT, and thus, lower removal efficiency.

Mean removals were investigated for retention times of 6, 8, 14 and 20 days, for removal efficiencies of different pollutants and with different gravel sizes. With medium gravel (4-25 mm) media, the results exhibited a significant difference in organic matter removal between 6- and 8-day retention times (77 % and 90 % COD removal, respectively), and no significant difference between 14 and 20 days (92 % and 93 % COD removal, respectively). This leads to the conclusion that HRT longer than 8 days is adequate for relatively high removal of organic matter. The use of fine gravel (0.25-16 mm) and cobbles (30-180 mm) influenced the efficiency of removal up to some extent. At 8 days HRT, the BOD efficiency was 92 and 87 % for fine gravel and cobbles, respectively.

For total nitrogen (TN) and ammonia, HRT plays a more significant role for removal efficiency. A 6-day HRT resulted as not sufficient but there was a relatively high removal for HRT of 8 days and above. Much higher removal efficiencies were observed for a 20-day HRT compared to 14-day HRT. Removal efficiency was found to substantially depend on the type of media used (Akratos and Tsihrintzis, 2007).

3.2.3. Operation modes

- BATCH FEED OPERATION

In a sequential process the CW is filled with water for a certain HRT and afterwards completely drained before being filled again. This type of feeding creates a pronounced temporal redox variation. When water enters the bed, the potential drops, later it gradually increases as the pollution is removed. Alternating reduced and oxidised conditions fundamentally influence microbial consortia, favouring aerobic facultatives adjusted to varying nutrient and redox conditions. Compared to continuous flow feeding, the batch feed enables more oxidised conditions and so better performance of COD removal (Faulwetter et al., 2009).

- INTERMITTENT FLOW FEED

On contrary to batch, in the intermittent feed regime wastewater is fed into the system before previous load is completely drained. Vertical mixing is present along the length and depth of the bed as confirmed by tracer studies. The feeding regime creates temporal (as in batch feed) and spatial redox potential variation. Mixing of fluid between anaerobic bottom zones and aerobic and anoxic micro-sites in the rhizosphere gives an explanation of a higher redox potential compared to the one in continuously fed beds. The system shows higher ammonium and lower sulphate removal, but there was no difference in COD removal exhibited between intermittent and continuous flow fed beds (Headley et al., 2005).

- CONTINUOUS FLOW FEEDING

As water is continuously fed into the system, this represents the simplest of the named feeding techniques. It results in generally lower redox potential compared to the batch and intermittent feed and is consequently less effective for aerobic pollutant removal. Spatial gradient is formed along the length, with high nutrient loads and anoxic conditions in the first part and low nutrient loads and more aerobic conditions towards the outlet (Faulwetter et al., 2009).

3.2.4. Removal mechanisms

3.2.4.1. Physicochemical mechanisms of filtration and matrix adsorption

Filtration takes place during the water flow through media and rhizosphere. There are physical and chemical processes which take place and remove the suspended particles and dissolved substances. Filtration depends on the sort of media, media particle size, depth, the overflow and flow rate.

There are 3 main filtration ways. The first is conventional filtration, which retains particles smaller than pore size but there are no additional forces of retaining. The second is physicochemical bonding of impurities to the media due to the action of intermolecular forces of the surface active substrates. These include intermolecular forces like dipole-dipole interactions, hydrogen bonds, and induction forces (Henze et al., 1996).

The third group of chemical reactions is chemical bonding of impurities to the media. The media in question are actively involved in the process of biochemical degradation of pollutants. They chemically bond a substance or release it by ionic exchange or other chemical reaction (Henze et al., 1996). Ion exchange reactions are done by either cationic or anionic exchangers, natural or artificial ones. Organic ion exchangers are based on polymer resins, inorganic

exchangers are zeolites and bentonites. Humic acids which are often present in the CWs contain a lot of hydroxyl and carboxyl functional groups which act as cationic exchangers. Cation exchange capacity of macrophytes is attributed to humic acids present in the plant tissue. Cation exchange capacity of media is a measure of the number of binding sites per volume and mass (Vymazal et al., 1998).

Chemical reactions in the media take place between inorganic pollutants (phosphates, sulphates, nitrates, nitrites…) and corresponding inorganic substances in the media. In the case an unstable organic material (i.e. peat) is used, reactions between organic pollutants and the media (humic acids, lactic acid, tenzides…) take place.

In the case of phosphorus, inorganic P is adsorbed on hydrous oxides of Fe and Al, and can precipitate as insoluble Fe-phosphates and Al-phosphates. Insoluble Ca-P precipitation dominates at pH > 7. But it is yet unclear whether adsorption via ligand exchange or precipitation reactions is the major mechanism of removal. In the case of nitrogen, ammoniacal N is stable and is adsorbed onto active sites in the bed matrix. But ion exchange of NH_4^+-N on cation exchange sites is rapidly reversible since the equilibrium between the adsorbed NH_4^+-N and the one in solution is quickly established.

In reactions for metals removal cation exchange capacity and adsorption capacity depend on the plant's surface to volume ratio. It is obvious that plants with high surface to volume ratio act in favour of adsorption and exchange reactions. In cation exchange reactions with metals stronger positively charged metal cations displace cations from the media (Vymazal et al., 1998).

3.2.4.2. Role of media in removal efficiency

Different coarse and fine gravel beds were compared for dimethylsulfide (DMS) removal. Coarse gravel included particles with 10 mm average size and fine gravel was 3.5 mm in size. An average effluent DMS concentration in the beds containing coarse gravel was not statistically different than in those containing finer gravel. But in the case of acetic acid the beds containing coarse gravel had an average effluent concentration slightly higher than the one containing finer gravel. TN removal showed high dependence on porous media size and type. By comparing mean removal efficiencies it was shown that finer porous media are more effective than coarser.

Since the main mechanism for phosphorus removal is adsorption and precipitation, $P\text{-}PO_4^{3-}$ and total phosphorus (TP) removal efficiency is predominantly affected by the porous media size and type. Media which include minerals with reactive Fe- and Al- hydroxide on their surfaces, or calcareous materials which promote Ca-phosphate precipitation are rather efficient in phosphorus removal. It has been suggested that in an acidic pH, phosphorus precipitation as iron and sulphate precipitates becomes the most important mechanism (Akratos and Tsihrintzis, 2007).

3.2.4.3. Microbial degradation

Aerobic respiration and fermentation are the most important type of reactions by which microorganisms brake down the pollution into CO_2, N_2 and H_2O. In some cases end products of these reactions induce other reactions contributing to pollution removal, like sulphide promoting precipitation and sequestration of heavy metals (Dvorak et al., 1992). Microbial transformations are prevailing in organic carbon degradation in CWs. Also sulphate reduction may play an important role in carbon removal (Faulwetter et al., 2009). As the energy yield for the microorganisms is consistent with the type of reactions being highest in the aerobic and lowest in anaerobic conditions, the highest organic carbon

consumption and pollution removal is characteristic for the oxidised conditions and lowers towards reduced ones (Faulwetter et al., 2009).

Microbial community is attached to the underground parts of plants and to the particles' surface. As the usual depth of a CW filtration bed is 0.5-0.8 m, this depth still permits the plants' rhizomes to penetrate the whole depth and so ensure oxygenation. Oxygenation is enabled through release of oxygen from the roots. A wetland plant, through its aerenhim - a hollow, air filled channels connected to the atmosphere - serves the purpose to transport oxygen to the roots. But some of the oxygen is lost from the roots and rhizomes to the rhizosphere. Oxygen leaving to the rhizosphere is not enough to provide aerobic conditions in the whole bulk of media but there are aerobic regions present around the roots and rhizomes. Aerobic degradation is mostly done by aerobic heterotrophic bacteria. There are also ammonifying bacteria degrading compounds containing nitrogen and nitrifying bacteria living in aerobic conditions but the heterotrophic bacteria outcompete the other two in having the fastest metabolic rates (Faulwetter et al., 2009).

The amount of released oxygen is not enough to meet the needs of aerobic degradation and nitrification of ammonia substances. As a result, substances are also degraded anaerobically. Anaerobic degradation starts below Fe^{3+} reduction zone and is carried out by either facultative or obligate anaerobes in a multi-step process in which high molecular weight carbohydrates are broken down to lower weight compounds (Vymazal et al., 1998). In anaerobic degradation – fermentation processes, the end products are acetic acid, butyric and lactic acids and alcohols and in aerobic CO_2 and H_2 gasses. Fermentation reactions by fermentative bacteria take place and the end products represent substrate for the strictly anaerobic sulphate reducing and methanogenic bacteria. Both types of organisms play an important role in decomposition and consequently carbon cycling in the system.

3.2.4.4. Nitrogen removal

Removal mechanisms for nitrogen are ammonia volatilization, nitrification and denitrification reactions, ammonification, and plant uptake and matrix adsorption. Nitrifying bacteria are strict aerobes, so nitrification in the media is limited to areas adjacent to roots and rhizomes. Prevailing anaerobic and anoxic conditions are suitable for denitrification but the limiting step is the nitrate formation since the majority of nitrogen entering wastewater is in the form of ammonia (Huett et al., 2005).

Another reaction for ammonia production is mineralization of organic nitrogen – ammonification under anaerobic or aerobic conditions which adds ammonia to the system. The fine grain soil exhibits higher nitrogen removal compared to coarse grain one due to higher elimination rate caused by higher cation exchange capacity of the fine-grained soils (Huett et al., 2005).

Significant losses of ammonia occur through physicochemical process where ammonium nitrogen is in equilibrium between gaseous and hydroxyl form. Volatilization occurs at pH around 9 when ratio between ammonia and ammonium ion in the system is 1 : 1 (Vymazal et al., 1998). Ammonium and TN in the effluent have been reported to decrease exponentially with increase in the wastewater residence time (Akratos and Tsihrintzis, 2007).

3.2.4.5. Phosphorus removal

Biological oxidation of phosphate results in conversion of all phosphate forms into orthophosphate. The following pathways are used for phosphorus removal in wetland treatment: adsorption, plant absorption, complexation and precipitation and bacterial removal. Removal is mainly done by ligand exchange reactions in which phosphate exchanges water or hydroxyl groups on the surface of Fe and Al hydrous oxides. The sediment/peat accumulation is the major long term P sink (Akratos and Tsihrintzis, 2007).

Bacteria removal and plant uptake are responsible for P-PO_4^{3-} removal, while precipitation and adsorption are responsible for the removal of all phosphorus forms (Akratos and Tsihrintzis, 2007). But media usually used in horizontal flow CWs (gravel and stones) have generally low phosphorus removal rates due to low quantities of Fe, Al and Ca present. The more aerobic planted wetlands are more favourable for phosphorus removal in the sorption and co-precipitation reactions. Phosphorus removal was greater than 80 % when the residence time was 40 h. But in the case of shorter residence time, the removal was only 39 %. Phosphorus uptake by bacteria is a cyclic process. Bacteria use the phosphate as an energy reserve which can be used in nutrient uptake under anaerobic conditions. Phosphate reserve regeneration is carried out in aerobic and also anoxic conditions (Akratos and Tsihrintzis, 2007).

3.2.4.6. Pathogen removal

Pathogen inactivation is also an important issue when performance in CW beds is considered. The degree of bacterial removal depends on several environmental factors such as HRT, granular medium and type of plants used in CW (Ottova et al., 1997). So far several researchers obtained contradictory results on influence of environmental factors. For now influence of environmental factors on microbial removal is still not definitively proved.

HRT and inactivation are positively correlated. A HRT not long enough means unsatisfactory removal. But inactivation could also be dependent on the type of plant used in the CW (Ottova et al., 1997). In most of the studies, the rate of removal corresponded to the HRT length. In the case of faecal coliform bacteria the HRT affects the inactivation 3 times more compared to variation in granular medium. But in the case of somatic coliphage removal, HRT and granular media exhibit approximately the same variance in inactivation. But as the HRT reaches 3 days, the inactivation reaches saturation values. Further prolongation is not effective. At the saturation level, the inactivation ratio depends on granular

medium in the bed. Smaller sized particles proved to be more efficient for both faecal coliform and somatic coliphage inactivation (Ottova et al., 1997).

In some cases a difference between planted and unplanted beds was confirmed and in other no difference was observed at all. When difference is present, it is in favour of planted beds which exhibit higher removal efficiency. The planted bed advantage is connected to a higher number of ciliated protozoa present and in turn larger number of bacteria grazed. But the most important effect of plants being present in the bed is suggested to be the air transport through the plants, which results in media aeration (Garcia et al., 2003). To obtain the highest results for bacterial inactivation (3 log-units) the specific surface area needed is 3 m^2/person-equivalent. This is a significant number in the places where availability and in turn cost of land is an issue.

The performance of a bed with a finer medium (sand) was better compared to the one with gravel. Another study reports no significant difference in rate of removal between soil and gravel media. This suggests that the type of media doesn't play a key role in determining the rate of inactivation (Garcia et al., 2003).

3.2.5. Role of wetland vegetation

The main role of vegetation through growth of roots and rhizomes is attributed to modification of soil texture, hydraulic conductivity, soil chemistry, release of exudates like vitamins and antibiotics, release of oxygen to oxygenate the media, creating aerated microaerobic degradation zones within the bed (Davies et al., 2005). In temperate regions the plant removal rate is limited by the fact that harvesting regime prevents harvesting in the peak nutrient standing stock, which is in late summer. Even at the peak standing stock the amount of N and P that could be removed by harvesting, forms less than 10 % of the total removed nutrients in the CW (Vymazal, 2005). In the tropics on the other hand, the

nutrient translocations are minimal so the harvesting is more favourable to remove the nutrient load.

Plant removal is also suggested to be favourable in the case of wastewater tertiary treatment, when the nutrient load rates are lower so the plant uptake forms a higher portion of nutrients to be removed (Vymazal, 2005). The quantities of nutrients which can potentially be removed by harvesting plants are generally insignificant compared to nutrient loads to the treatment system. The amount of nitrogen removal by plants at optimum conditions is 10-16 % (Vymazal et al., 1998).

The results of experiments on several pollutants like polycyclic aromatic hydrocarbons (PAH), chlorinated pesticides, explosives and some surfactants have proved a more rapid degradation in rhizosphere compared to the bulk of soil (Macek et al., 2000). Studies indicate that degradation of xenobiotics is carried out through exoenzymes, excreted by plants roots into the rhizosphere, microorganisms' enzymes present in the rhizosphere and intrinsic enzymatic machinery of the plant body itself (de Araujo et al., 2002).

Active uptake of the xenobiotic molecule is followed by adsorption; it is either exported into the cell vacuole or into the extracellular space. Through covalent bonds with macromolecules like lignin, hemicellulose, cellulose and pectin it becomes integrated into the lignin or cell membrane and so becomes non extractable from the plant matrix (Davies et al., 2005). Peroxidase enzymes (POD) represent a large group of enzymes, common in many microorganism and plant cells. Elevated POD activity is an indicator of various pollution stresses plants have been exposed to since they are considered to be a non specific oxidative activity towards xenobiotic molecules. Hydrogen peroxide is used as the oxidant by the POD and the heme as the site of oxidation of the protein (Davies et al., 2005). A non specific oxidative polymerisation occurs in

the cell wall and when lignin is produced it contributes to improvement of mechanical defence in the cell wall.

Other enzymes identified as a defence at xenobiotic uptake are: cytochrome P450, peroxygenases, glutathione-S-transferase, carboxylesterases. They all take part in xenobiotic metabolism either in transformation, conjugation, transport or cellular compartmentalisation process. In the case of a VFW model azo dye removal efficiency was studied in moderate and high oxidative stress conditions. The dye, TOC and COD removal efficiencies were similar and were not dependant on the inflow concentrations (Davies et al., 2005). At increased dye concentration conditions the POD activity decreases but after two days of exposure it reaches the level which enables the plat to adjust its metabolism to the high stress conditions. *Phragmites australis* crude tissue extract proved to degrade the dye itself and also aromatic amines released during degradation (Davies et al., 2005).

3.2.6. Textile wastewater treatment in CW

3.2.6.1. Decolouration

Decolouration of textile wastewaters in CW is attributed to biological decolouration under anoxic-anaerobic conditions. Also sulphate reducing bacteria play a role in dye decolouration as they reduce sulphate to sulphide which in turn chemically decolourises dyes. Decolouration is likely to take place under highly reducing conditions (Mbuligwe, 2005).

Biodegradation process can be aerobic, anaerobic or a combination of the two: but there are significant differences in physiology of the microorganisms grown under the named conditions. Aerobic bacteria must be specifically adapted to decolouration of a certain dye which is achieved through a long term growth in continuous culture in presence of a simple azo compound. Bacteria

consequently synthesize a specific azoreductase enzyme which can reductively cleave the azo group in the presence of oxygen (Pearce et al., 2003).

Aromatic amines, formed during azo dye reduction are reportedly more easily degraded under aerobic conditions. A large number of bacterial strains have proven the ability of the degradation leading to complete mineralization. But there is a group of aromatic amines, which is difficult to degrade also under aerobic conditions (aryl sulfonates, aminobenzene and aminonaphthyl sulfonates). Also autooxidation of a few aromatic amines has been reported. Oxygen via free radical reactions reacts with aromatic amine and sometimes coloured oligomers and polymers are formed (reoccurring colouration of the sample). Products can be more recalcitrant to biological degradation compared to parent compound (Pandey et al., 2007).

On contrary, the reduction under anaerobic conditions is relatively unspecific with regard to the azo compounds to be decolourised. Colour removal under anaerobic conditions is also referred to as dye reduction. The cleavage of azo bond involves transfer of four electrons (reducing equivalents) which takes place in two stages – two electrons in each, with the dye molecule as the final acceptor. As most of the dyes have sulphonated substituent groups and high molecular weight, they are unlikely to pass the cell membranes. The current hypothesis is that the reduction mostly occurs in extracellular space by extracellular or membrane bound mediators. A co-metabolic reaction is probably the main mechanism of dye reduction with reducing equivalents or reduced cofactors such as NADH, NAD(P)H, $FMNH_2$, $FADH_2$ which act as secondary electron donors (dos Santos et al., 2007). Namely a link between intracellular electron transport system and extra-cellular environment must be established.

Presence or addition of low molecular redox mediators facilitates the reduction and may substantially increase the reaction rates (dos Santos et al., 2007).

Concentrations of electron donors in auxiliary substrate stimulate the reduction cleavage of azo bonds since this concentration controls the rate of reduced equivalents formation. Also products of cell lysis may act as electron donors (Pandey et al., 2007). Under anaerobic conditions, no further dye degradation is observed after the reduction of azo bond. Aromatic amines are degraded in the presence of oxygen via hydroxylation and ring opening (Pearce et al., 2003).

3.2.6.2. COD removal

It has been established that the wetland performance is higher at higher loads and removal rates are consequently higher when the system is exposed to higher pollution loads (Kadlec and Reddy, 2001). Moreover, a clear difference has been shown between planted and unplanted CW performance in terms of COD removal. The planted beds, containing aerobic microlocations in the roots and rhizomes of the macrophytes exhibited up to 21 % higher removal rates compared to the unplanted ones (Mbuligwe, 2005). This is attributed to the fact that in planted CW, aerobic microlocations are present in the vicinity of roots and rhizomes of the plants.

Performance of the CW treating textile wastewater was lower compared to domestic wastewater treatment. This might arise from the fact that some organics in the wastewater and products of biological reduction of textile effluents are more recalcitrant compared to components in other type of wastewaters being treated in CW (Baughman and Perkins, 2002). It has been suggested that a part of anaerobic degradation metabolites (colourless compounds) cannot enter further biological degradation and in consequence prevent the complete COD removal under a combination of aerobic and anaerobic conditions (Mbuligwe, 2005).

In a study with an anaerobic - aerobic reactor of 2.5 L in volume, HRT proved to be a determining criterion influencing COD removal efficiency. At the HRT of

100 days, the COD removal was 80 %. As the HRT was decreased to 6 h, the colour removal remained almost the same, but the COD removal dropped to 29 % (Isik and Sponza, 2008). The quoted experiment proves the presumption, that the HRT plays an important role in COD removal since the metabolites released during decolouration are recalcitrant and need adequate length in both anaerobic and aerobic conditions for an ultimate decolouration to be achieved. The same has been found out in the case of an anaerobic reactor, where textile dyes were degraded under methanogenic conditions where the removal rate doubled as the initial dye concentration increased from 50 mg/L to 100 and 200 mg/L (Lee and Pavlostathis, 2004).

In another experiment in an anaerobic upflow packed bed reactor 24 % COD removal was achieved at HRT of 5 days for a simulated wastewater (Talarposhti et al., 2001), but different efficiency is reported for the anaerobic decolouration at the HRT of 10 days. COD removal was in the range of 78-94 % which is undoubtedly higher compared to all other literature data (Manu and Chaudhari, 2002). In the same study an interesting issue was raised, namely the COD and colour removal were correlated and it has been shown that at the addition of nutrients (starch) when the reducing equivalents were produced in sufficient quantity by degradation of starch, only dye reduction took place (Manu and Chaudhari, 2002).

3.3. PHOTOCATALYSIS

TiO_2 powders were used as white pigments from ancient times. It is not clear, when exactly utilization in photochemistry started; there are reports from Japan from the 1950s when autooxidation of TiO_2 as a photocatalyst was described under UV irradiation. In the 1960s photoelectrolysis of water was investigated since TiO_2 exhibited a positive enough valence band edge to oxidise water to oxygen. In 1969 solar photoelectrolysis was demonstrated for the first time and named Honda-Fujishima effect (Fujishima and Honda, 1972). Light assisted

water splitting was popular also in the 1980s due to the second big oil crisis since it was seen as one of the promising methods for hydrogen production. First reports of decomposition in the presence of aqueous TiO_2 solutions are from 1977 when cyanide was decomposed (Hashimoto et al., 2005).

Later follow the reports on detoxification of harmful substances in water and air suggesting TiO_2 usage as a promising technology for water and air pollution reduction. The dilemma of industrial scale application of supported versus slurry TiO_2 and further problems caused by the need of water filtering after the treatment procedure remains an open issue up-to-date and both, supported and dissolved TiO_2 applications are being developed (Hashimoto et al., 2005).

Application range of TiO_2 coatings largely widened after the discovery of change in wettability of the TiO_2 surface before and after UV irradiation. Applications arising from this phenomenon are “self-cleaning materials” and “anti-fogging properties”. Stains which are adsorbed onto the TiO_2 surface are washed away by the water droplets since water soaks in-between the stain and the TiO_2 surface (Hashimoto et al., 2005). Coatings are being applied on various glass surfaces and mirrors in commercial use.

Other applications are the indoor air cleaning applications, anti-bacterial function and photocatalytic decomposition of pollutants in water, air and soil (Hashimoto et al., 2005). Current limitations to applications of TiO_2 photocatalyst are set by the less than 3 % of available sunlight. Namely its bang gap has the energy $E_{bg} \approx 3.2$ eV which corresponds to wavelength of 388 nm or lower. This means that it can only be excited by light with energies higher than 3.2 eV which corresponds to shorter wavelengths (Rampaul et al., 2003). Enhancing the visible light activity stays the most important issue to be overcome in developing large scale environmental applications.

3.3.1. Heterogenous photocatalysis

Heterogeneous photocatalysis is able at the same time to be efficient in green chemistry, in fine chemicals and in so called Advanced Oxidation Processes (AOPs) (Herrmann et al., 2007). Photocatalytic degradation of pollutants in water using TiO_2 and solar light has been proposed as an effective alternative for waste water treatment (Gelover et al., 2004).

For all AOPs a common chemical feature is characteristic - its capability to form highly reactive chemical species such as $OH^{\cdot}$ and $O_2^{-\cdot}$ radicals which drive oxidation processes. And through oxidation processes the degradation or complete abatement through mineralization of substances is achieved. The $OH^{\cdot}$ radicals are strong reactive species with oxidation potential 2.8 V. They attack most of the organic molecules and very little or no selectivity is characteristic. This is a useful attribute for an oxidant used in wastewater treatment and for solving pollution problems (Malato et al., 2002).

3.3.2. General mechanism of TiO_2 semiconductor photocatalysis

Bonding and electron distribution in a solid material is described by a band theory. Semiconductors can be characterized by two types of energy bands: a filled low energy valence band and a high (empty) energy conduction band which gives rise to an energy gap (“band gap”) between these two bands, with a low probability of thermal electron excitation from valence to conduction band, resulting in low electrical conductivity. However light excitation of a semiconductor can promote electrons from valence to conduction band if light with energy higher than the semiconductor band gap is absorbed (Carneiro et al, 2007).

Basic process of TiO_2 photocatalysis consists of the following sub-processes: electron (e^-) is ejected from the valence band (VB) of the semiconductor into the

conduction band (CB) creating a hole (h^+) in the valence band. The electron ejection takes place due to UV irradiation of the TiO_2 semiconductor with energies equal or higher than 3.2 eV (Robert and Malato, 2002). The existence of a band gap in the semiconductor prevents rapid deactivation of the excited e^-_{CB} and h^+_{VB} pairs, which can be deactivated only by recombination. This assures that an e^-_{CB} + h^+_{VB} life time is sufficiently long to participate in interfacial redox reactions (Carneiro et al., 2007). Also nanoparticulate crystalline structure prevents rapid recombination.

Nevertheless a non-feasible recombination of the electron e^-_{CB} and hole h^+_{VB} can take place and no oxidation of OH^- or pollutant species occurs (Robert and Malato, 2002). To increase visible light absorption and to improve photocatalytic activity by decreasing the band gap or preventing e^-_{CB} / h^+_{VB} pair recombination by electron / hole trapping, the addition of transitional metals or non-metal ions has been introduced (Carneiro et al., 2007).

The question whether to use dissolved TiO_2 catalyst in the bulk of the sample or to use a deposited catalyst on glass or other support remains an open question. The advantage of using a deposited, immobilized catalyst lies in the possibility of its sequential use and avoidance of separation problem at the end of the treatment. On the other hand TiO_2 slurries using Degussa P25 powder as catalyst exhibit higher photocatalytic performance, but their application in industrial scale suspensions encounters the problem of separation of the catalyst from the treated water and its recycling at the end of the treatment. Because of the small TiO_2 particles size (< 0.5 μm) a complete separation is very expensive (Robert and Malato, 2002).

3.3.3. Sol-gel thin films (deposited catalyst)

Thin films can be prepared by a variety of deposition techniques: sol-gel process, chemical vapour deposition, evaporation and various sputtering

depositions. The sol-gel process can be described as a process where materials are formed via a sol; the gelation of sol takes place and solvent is removed at the end. Due to the course of the meta-stable oxide materials synthesis procedure, the method is called “chimie douce” or a soft chemical approach (Schubert and Hüsing, 2005).

“Sol” is defined as a colloidal suspension of solid particles in a liquid. The particles can be amorphous or crystalline. “Colloid” is a suspension in which the dispersed phase is so small that gravitational forces are negligible and interactions are dominated by short range forces. If a monomer can make more than two bonds, then there is no limit on the size of the molecule that can form. “Gel” is a substance, where one molecule reaches macroscopic dimensions and so extends throughout the solution (Brinker and Scherer, 1990, pp. 2, 8, 14). Thin films are prepared by standard coating technologies which are dip coating, spin coating or spraying. The gel is formed from the sol - gelation occurs during preparation of the film, due to rapid evaporation of the solvent (Schubert and Hüsing, 2005).

Advantages of the sol-gel method are in the possibility of micro-structural control through low processing temperatures; metastable, porous structures created in the solution are preserved. Through micro structural control the pore volume, size and surface area can be controlled. Control over the rate of hydrolysis and condensation, and over colloid particle size and pore size is possible so final porosity level can be achieved through appropriate chemical modification of the precursors. Additional pore size and mechanical strength control can be achieved through control of ageing and drying conditions (Schubert and Hüsing, 2005).

Low temperature of preparation also saves energy, minimizes evaporation losses and consequently air pollution. Low temperatures result in nanocrystalline

solids outside the range of glass formation by avoiding crystallisation or phase separation (Brinker and Scherer, 1990, pp 841). The sol-gel method has many advantages over other fabrication techniques such as purity, homogeneity and flexibility in introducing dopants in large concentrations, stoichiometry control, ease of processing, control over composition and ability to coat large and complex areas (Carp et al., 2004).

3.3.4. TiO_2 Doping

Titanium dioxide, which size and shape ranges from clusters to colloids, powders and large single crystals, is close to being an ideal photocatalyst. But there is one exception - it does not absorb visible light (Carp et al., 2004). There are three principal forms of TiO_2: anatase, rutile and brookite. But only rutile and anatase are straightforwardly synthesized in the “soft chemistry” procedures like sol-gel procedure. Anatase and also rutile are semiconductors, with a band gap around 3.2 eV and 3.0 eV, respectively (Robert and Malato, 2002).

The shift of absorption to the longer wavelengths, towards visible part of solar spectra, has been a major quest in TiO_2 and visible light related research. High absorption of visible light wavelengths would enable the semiconductor as a photocatalyst to absorb more photons of the sunlight wavelengths which reach the Earth’s surface thus improving photocatalytic performance also under visible light irradiation. Even though there are some studies published which claim the same photoreactivity of both crystalline phases, most of them claim the anatase to be the principal photocatalytic TiO_2 phase (Bouras et al., 2007).

Dopant is an impurity element added to a crystal or semiconductor lattice in low concentrations with the aim to alter the optical/electrical properties of the semiconductor. Dopant substitutes atoms in the crystal lattice of the semiconductor. Dopant elements (transitional metal ions: Cr, W, Ru, or non-metal ions: S, C, N) are added in different ratios to the TiO_2 solution (Ellis et al.,

1993). On contrary to nanocrystallite size changing where decrease of band gap energy is achieved, doping creates new energy levels within the band gap of the semiconductor. And consequently the “red shift” towards longer wavelengths takes place and is more pronounced than in case of size changing (Bouras et al., 2007).

N- and p-type semiconductors are defined according to the functioning of the silicon semiconductor. But since silicon and titanium both form tetravalent ions in the semiconductor, the principle behaviour in the case of dopant addition is the same also for TiO_2 semiconductor. In the n-type semiconductor pentavalent impurities (i.e. P, Sb, As) are added which contribute free electrons that greatly increase conductivity of the intrinsic semiconductor. In the p-type semiconductor trivalent impurities (for example B, Al, Ga) are added which creates deficiencies of valence electrons, called "holes". In an n-type material there are electron energy levels near the top of the band gap which can be easily excited into the conduction band and used in reduction reactions. In p-type material, extra holes in the band gap allow excitation of valence band electrons, leaving mobile holes in the valence band for oxidation of OH^- ions (Fig. 4) (Ellis et al., 1993).

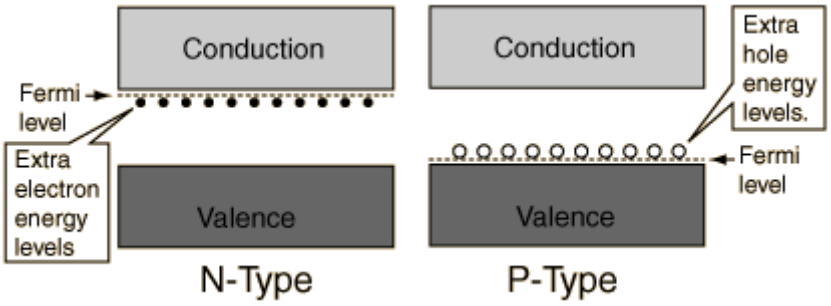

Figure 4: Extra electron energy levels within the band gap of a semiconductor (*http://hyperphysics.phy-astr.gsu.edu/hbase/solids/dope.html#c4*, 22.4.2008).

There are limits to the extent of doping. The dopant addition shifts the absorption onset, but it doesn't necessarily improve the catalytic performance. There are also detrimental effects of doping. There is an optimum level of dopant addition which usually lies at very low concentrations. This also means that low absorbance shift is achieved. If the level is surpassed, dopants become recombination sites and worsen the overall performance. Another drawback is the energy of the emitted electrons from the dopant trapping states (Kumbhar and Chumanov, 2005). Due to shifted Fermi level, they have lower energy compared to those in anatase conduction band and subsequently lower reductive capacity (Bouras et al., 2007).

Doping process benefits to absorption of water and hydroxyl group. Fe^{3+} doping introduces more oxygen vacancies in/on the crystal lattice and surface of TiO_2, which favour H_2O adsorption and formation of surface hydroxyl group and so promote the photocatalytic activity. The beneficial effect of Fe^{3+} can be also explained by efficient separation of photogenerated electrons and holes. Fe^{3+} can act as photogenerated hole trapper (Eq. 2) due to Fe^{3+} /Fe^{4+} energy level above the valence band edge of anatase TiO_2. The Fe^{4+} trapped holes then migrate to the surface where reaction with adsorbed hydroxyl ion produces hydroxyl radical (Eq. 3) (Zhu et al., 2006):

$$Fe^{3+} + h_{vb}^{+} \rightarrow Fe^{4+} \quad (2)$$

$$Fe^{4+} + OH^{-}_{(ads)} \rightarrow Fe^{3+} + OH^{\bullet}_{(ads)} \quad (3)$$

To reach charge compensation for electro-neutrality in doped TiO_2, O^{2-} in the surface lattice or adsorbed to the surface can trap photogenerated holes (Eq. 4) and produce hydroxyl radicals (Eq. 5).

$$O^{2-} + h_{vb}^{+} \rightarrow O^{-} \quad (4)$$

$$O^{-} + H_2O_{(ads)} \rightarrow OH^{\bullet}_{(ads)} + OH^{-}_{(ads)} \quad (5)$$

Fe^{3+} can also serve as photogenerated electron trapper (Eq. 6). Subsequently, Fe^{2+} can be oxidized to Fe^{3+} by transferring electrons to absorbed O_2 on the surface of TiO_2 (Eq. 7) and a neighbouring surface Ti^{4+} (Eq. 8) which then leads to interfacial electron transfer (Eq. 9) (Zhu et al., 2006):

$$Fe^{3+} + e_{cb}^{-} \rightarrow Fe^{2+} \quad (6)$$

$$Fe^{2+} + O_{2(ads)} \rightarrow Fe^{3+} + O_2^{-} \quad (7)$$

$$Fe^{2+} + Ti^{4+} \rightarrow Fe^{3+} + Ti^{3+} \quad (8)$$

$$Ti^{3+} + O_{2(ads)} \rightarrow Ti^{4+} + O_2^{-} \quad (9)$$

As already mentioned, Fe^{3+} ions can also act as recombination centres for the photogenerated electrons and holes. Recombination process works as a combination of reactions in equations 2 and 6 and equations 10 to 12 (Zhu et al., 2006). When dopant concentration is too high, the recombination rate will increase and compete with the redox processes since the distance between trapping sites decreases. And this can have a detrimental effect on photocatalytic performance.

$$Fe^{4+} + e_{cb}^{-} \rightarrow Fe^{3+} \quad (10)$$

$$Fe^{2+} + h_{vb}^{+} \rightarrow Fe^{3+} \quad (11)$$

$$Fe^{2+} + OH^{\bullet} \rightarrow Fe^{3+} + OH^{-} \quad (12)$$

3.3.5. Addition of noble metals to thin films' surface

In a metal sputtered TiO_2 semiconductor the light is absorbed by the semiconductor; the valence band electron is ejected into the conduction band. There it reacts with the metal ion on the surface by reducing it and so recombination is prevented or it reacts with oxygen atom to form oxide radical (Carneiro et al., 2007).

Metal/ TiO_2 (in our case Au/TiO_2) nanocomposites are used in broad range of applications due to their interesting chemical-physical properties. A key role in promoting interactions is played by phenomena occurring at the Au nanoparticle/TiO_2 matrix interface (weak Au/TiO_2 contact). Synergic competition between deposition/ablation phenomena which distinguishes the sputtering processes from glow discharges is a key step in order to obtain nanoparticles with tailored size and distribution. In these processes, plasma activation of both gas phase species and growth surface induces intermixing processes between the host matrix and the guest phase (Armelao et al., 2004).

As a general rule, the functional performances of Au/TiO_2 materials are strongly dependent on the Au particle size and distribution determined by the adopted synthetic procedure. The technique used to deposit gold (experimental part, Au/TiO_2 nanocomposites) on the surface of prepared TiO_2 films is based on the RF-sputtering of gold (guest) on porous TiO_2 xerogels (host) obtained by the sol-gel route. This combined synthetic pathway unites advantages of both techniques: sol-gel layers (porosity) and advantages of plasmochemical methods (conformal coverage, infiltration power) (Armelao et al., 2004).

The main advantages of the plasma liquid phase hybrid approach are the flexibility (various metals and dielectric materials) and the capability to produce uniformly distributed metal clusters (Sunghun et al., 2000). Another important advantage of the used synthetic pathway is its versatility and feasibility for the preparation of a wide range of host/guest metal/metal oxide systems, featuring properties hardly attainable by other synthetic routes (Armelao et al., 2006).

3.3.6. Photocatalytic degradation of textile dyes

3.3.6.1. Photocatalytic oxidation

When dye molecules are adsorbed on the surface of the semiconductor or in the solution, the following reactions take place; e^- can directly reduce the dye or react with electron acceptors on the surface of the semiconductor or dissolved in water. The photogenerated holes can oxidise organic molecules to form R^+ or react with OH^- or H_2O oxidising them to $OH^\cdot$ radicals. Relevant reactions at the semiconductor surface which result in dye degradation are the following (Konstantinou and Albanis, 2004):

$$\text{Dye} + OH^\cdot \rightarrow \text{degradation products} \quad (13)$$

$$\text{Dye} + h^+_{VB} \rightarrow \text{oxidation products} \quad (14)$$

$$\text{Dye} + e^-_{CB} \rightarrow \text{reduction products} \quad (15)$$

Most of the azo dye oxidation and final mineralization is attributed to the reaction with hydroxyl radicals. Role of reductive pathway in dye degradation has also been suggested but it is considered to have a minor role compared to oxidation in overall mineralization rate (Konstantinou and Albanis, 2004).

3.3.6.2. Photosensitized oxidation

Photosensitized oxidation or photo-assisted degradation by visible light irradiation ($\lambda > 420$ nm) takes place when the visible light excitation of the adsorbed dye molecule takes place to appropriate singlet or triplet state. Subsequently follows the electron injection from the excited dye molecule onto the conduction band of the semiconductor. The dye itself is converted to cationic dye radical and undergoes a series of reactions to yield the following products (Eq. 16-19), (Konstantinou and Albanis, 2004):

$$\text{dye} + hv\ (\text{Vis}) \rightarrow {}^1\text{dye}^* \text{ or } {}^3\text{dye}^* \quad (16)$$

$^{1}dye^{*}$ or $^{3}dye^{*} + TiO_2 \rightarrow dye^{\cdot +} + TiO_2 (e^{-}_{CB})$ (17)

$TiO_2 (e^{-}_{CB}) + O_2 \rightarrow O_2^{\cdot -} + TiO_2$ (18)

$dye^{\cdot +} \rightarrow$ degradation products (19)

Cationic dye radicals readily react either with hydroxyl anions to get oxidation products or interact with excited species to generate intermediates leading to final mineralization (Eq. 20-26), (Konstantinou and Albanis, 2004):

$dye^{\cdot +} + OH^{-} \rightarrow dye + HO^{\cdot}$ (20)

$dye + 2HO^{\cdot} \rightarrow H_2O +$ oxidation products (21)

$O_2^{\cdot -} + H^{+} \rightarrow HO_2^{\cdot}$ (22)

$HO_2^{\cdot} + H^{+} + TiO_2 (e^{-}_{CB}) \rightarrow H_2O_2 + TiO_2$ (23)

$H_2O_2 + TiO_2 (e^{-}_{CB}) \rightarrow HO^{\cdot} + HO^{-} + TiO_2$ (24)

$dye^{\cdot +} + O_2^{\cdot -} \rightarrow DO_2 \rightarrow$ degradation products (25)

$dye^{\cdot +} + HO_2^{\cdot}$ (or $HO^{\cdot}$) $\rightarrow$ degradation products (26)

In experiments, where both UV and Vis light is used to irradiate the samples, both, photodegradation and photosensitization mechanisms are supposed to occur. It hasn't been undoubtedly proven which of the mechanisms is superior in its performance, but photosensitization improves overall performance and makes photodegradation with solar light more feasible (Konstantinou and Albanis, 2004). Presumably the photocatalytic degradation reactions proceed in the following rates: oxidation by positive hole majorly contributes to intermediates' disappearance; reduction by the conduction band electron contributes to disappearance of the dye molecule (dye molecule can be reduced by conduction band electrons but the intermediates cannot be further degraded by reduction) and electron injection from the sensitized dye into the conduction band contributes to some extent to overall degradation (Tanaka et al., 2000; Epling and Lin, 2002).

3.3.6.3. Effect of dye concentration and its adsorption on the degradation

Adsorption of the dye onto the surface of the semiconductor is an important parameter determining the photocatalytic degradation rate (Tanaka et al., 2000). No competition between the water and dye molecules to occupy TiO_2 surface sites was found. Since the adsorption isotherms fit well the Langmuiran type this implies a monolayer adsorption model (Konstantinou and Albanis, 2004).

In general the rate of degradation depends on the probability of radical formation on the surface of the catalyst and the probability of reaction between the radical and the pollutant molecule. The observed degradation rate increases with an increasing dye concentration up to a certain level until further increase in the dye concentration decreases its degradation rate. Initial enhancement of the degradation rate is attributed to a higher probability of reaction between reactive oxygen species and the dye molecule (Konstantinou and Albanis, 2004).

The following decrease in degradation rate is presumed to be caused by the reduction in generation of the $OH^{\cdot}$ radicals since active sites on the surface of the catalyst are covered by dye ions. The other possible explanation is that the dye molecules colour the solution up to a degree which causes screening effect. Dye molecules absorb the UV irradiation and prevent it from reaching the surface of the catalyst. Consequently the catalytic reaction efficiency is reduced and concentrations of $OH^{\cdot}$ and $O_2^{\cdot -}$ decrease. Retardation in light penetration with increasing dye concentration requires higher catalyst surface for the same degradation rate to be achieved as in lower dye concentrations (Konstantinou and Albanis, 2004).

The effect of the pH value of the solution on the dye degradation in general is dependent on the type of dye and on the properties of the surface of the semiconductor. For azo dyes' degradation in solution different optimal pH values

have been established as the most favourable in degradation terms. For the majority of azo dyes it can be predicted that at pH < 6 strong adsorption of the dye will occur due to electrostatic attraction forces between the dye and the negatively charged TiO_2 surface. The opposite, electrostatic repulsion is predicted at pH > 6.8 due to dye/surface repulsion, as dyes are negatively charged in alkaline media. An increase in concentration of the TiO^- groups on the surface of the semiconductor is also expected to affect the dye adsorption (Konstantinou and Albanis, 2004).

For the reasons mentioned above, the photocatalytic activity of the anionic dyes mainly reaches maximum values in acidic conditions and decreases when pH has alkaline values. But for other types of azo dyes reported optimal conditions are at pH values 6-7 and degradation decreases in alkaline and acidic conditions. It can be concluded, that the pH effect on each of the dyes' degradation should be related to the changes occurring to a single dye molecule under certain experimental conditions. Namely, protonation and deprotonation of the dye can change its adsorption characteristics and redox activity (Konstantinou and Albanis, 2004).

The effect of pH values and piezoelectric characteristics of the photocatalytic paper surface are described in 3.3.7.

3.3.6.4. Intermediate degradation products and mineralization rate

The degree of mineralization achieved by photocatalytic decomposition is assessed through CO_2 and inorganic ions formation. But for the real wastewaters this two categories would give only a very global estimation of the performance and not the contaminant decay rate. Parameters which more accurately assess the degradation rate are COD, BOD and TOC. These are parameters which are generally used for monitoring mineralization of the dye (Konstantinou and Albanis, 2004).

In general the reactant disappearance and mineralization level proceed with similar rates in photodegradation of compounds with low recalcitrant levels, when compounds don't form important intermediates. On the other hand, with high recalcitrant levels and formation of important intermediates during the degradation pathway, mineralization is slower than parent compound degradation (Konstantinou and Albanis, 2004).

COD and TOC values decrease with irradiation time and amount of inorganic ions increases or increases initially and after reaching plateau remains constant. COD and TOC drop curves have exponential or sigmoid shape. The sigma shaped curve indicates formation of relatively tolerant by-products or intermediate products during the irradiation. The pattern indicates that during the first phase, when solution is still coloured, the decrease in COD is low since the parent compound is decomposed to lower molecular weight compounds and intermediates formed are not mineralized yet (Konstantinou and Albanis, 2004). As the initial dye concentration increased also the formation of tolerant intermediate products increased which contributed to an increase of COD values of the solution. An increase in initial dye concentration finally resulted in slower overall mineralization process (Soustas et al., 2010).

After decolouration the COD values decrease sharply, indicating that oxidation of the intermediate products takes place; it results in mineralization of most of the organic matter (Konstantinou and Albanis, 2004).

Intermediate products formed during irradiation were identified for most of the degraded dyes. The initial reaction usually takes place near the azo bond area and it leads to fading of the solution. Aromatic intermediates like aromatic amine and phenolic compounds are formed. Formation of aminobenzenesulfonate indicates reductive cleavage of azo group before aromatic ring opening. Aromatic amines are also a result of anaerobic azo dye reduction, on contrary to

phenolic compounds which occurred as a consequence of photocatalytic degradation of aromatic compounds (Konstantinou and Albanis, 2004).

Aliphatic intermediates occur in the form of organic acids, mainly formic and acetic acid. As formic acid has higher photocatalytic degradability compared to acetic acid, presumably more intermediate products are degraded through formic acid. Other reported acids were oxalic, glycolic and malonic acids (Tanaka et al., 2000). Formation of these acids is presumably a result of aromatic and naphthalene ring opening followed by several oxidation steps leading to lower molecular weight acids finally resulting in CO_2 formation. CO_2 is formed through “photo-Kolbe” reaction via decarboxylation of carboxylic acid (Konstantinou and Albanis, 2004).

Ions formed during mineralization are ammonium, nitrate and sulphate ions, since these are the most common heteroatoms in textile dyes. In the degradation reactions, nitrogen from the parent compound is mineralized into NH_4^+, NO_3^- and N_2. The proportion between different ions depends on the initial oxidation degree of nitrogen, substrate structure and irradiation time. Since the stoichiometry based amount of nitrogen ions in the final solution after mineralization is usually lower, presumably some of the N-containing species remain adsorbed onto the surface and significant amount of N_2 and/or NH_4 is transferred to gas phase (Konstantinou and Albanis, 2004; Garcia et al., 2009).

As in azo dyes the both nitrogen atoms forming azo group are already formally in zero oxidation state, this oxidation state together with double bond in the parent compound being degraded favours the evolution of the gaseous dinitrogen. Formation of nitrogen gas represents an ideal case of decontamination which results in a completely innocuous final product (Guillard et al., 2003a). In the case of sulphur atoms, they are mineralized into sulphate ions. In most cases the studies revealed almost stoichiometric relation between

the expected and formed amount of ions. They are formed as initial products, resulting from the initial attack on the sulfonyl group of the dye. The non-stoichiometric relation between the expected and formed ions is attributed to the strong adsorption on the surface of the catalyst (Konstantinou and Albanis, 2004).

It is generally acknowledged that nitrate anions have little effect on the rate of degradation, but sulphate, chloride and phosphate ions at higher concentrations can reduce the rate 20-70 % due to competitive adsorption on reaction sites on the surface of the catalyst (Konstantinou and Albanis, 2004).

3.3.6.5. Toxicity exhibited after irradiation

As referred to in the previous chapter, aromatic intermediates and phenolic compounds are commonly observed compounds formed during photocatalytic degradation. As the molecular fragments, generated during irradiation can be more toxic compared to the parent compound, toxicity measurements of the photo-treated solutions are necessary. It is important to emphasise that toxicity of the solution is not necessarily sum of compounds' toxicity but interactions have to be taken into account (Konstantinou and Albanis, 2004).

There are two methods in general which are usually applied in toxicity studies, *Escherichia Coli* bacterial respiration inhibition and *Vibrio fischeri* bioluminescence inhibition. The second one appears to be the best available method with high sensitivity and reliability for field monitoring and toxicity screening of industrial effluents (Konstantinou and Albanis, 2004).

The remaining toxicity together with persisting TOC content after degradation indicates that molecular fragments, produced during degradation and possible remaining mother compounds in the solution exhibit toxicity towards test organism (Konstantinou and Albanis, 2004).

3.3.7. Photocatalytic paper as a catalyst form

TiO_2 has been immobilised on several kind of supports or anchoring materials like silica, glass, alumina, fibre glass, clay and zeolite, even acoustic panels forming false ceilings. Photocatalytic paper is one of the forms of supported TiO_2 catalyst. The expression “photocatalytic paper” namely represents a range of materials based on paper and non-woven fabrics which perform a function based on light-activated catalysis. The first mention of photocatalytic paper was published in 1995 describing catalytic destruction of acetaldehyde in vapour phase (Matsubara et al., 1995).

Ahlstrom, France, started to manufacture photocatalytic paper in the 1990s and remains one of the two producers on the market. The other one is a Japanese company named Nippon paper, which also developed a so called “light catalyst newsprint” together with the Japanese largest newspaper publisher (Pelton et al., 2006).

3.3.7.1. Non-woven photocatalytic paper

Photocatalytic paper is made by rapid filtration of a very dilute (less than 1 wt. %) water suspension of cellulose fibres. The term non-woven can be referred to a range of materials made by different techniques (plastic, cellulose fibres). Different densities are available, depending on the foreseen use. Their large attribute is their strength; they are stronger than paper when wet and are mostly used in high performance applications like filtration and disposable fabrics used in medicine (Pelton et al., 2006).

The photocatalyst can be added to a non-woven base in the following ways (Pelton et al., 2006):

- by “size press treatment” also referred to as coating: dry paper is impregnated with the photocatalyst by passing it through a bath of TiO_2, binder and starch. TiO_2 is concentrated near the paper surface and is

coated with a binder. The majority of paper in use is fabricated with the size press method.

- by “wet-end addition”: TiO_2 is deposited onto individual fibres before the sheet is formed and TiO_2 occurs in the whole sheet but surfaces are likely to have lower TiO_2 content compared to the interior of the sheet since draining forces can wash away the surface filler particles.

Since polyolefin and other plastic fibres constituting the non-wovens are hydrophobic, low energy surfaces, a binder has to be introduced to fix the TiO_2 catalyst. It is also important to secure the cellulose base from photochemical degradation since up to 30 % reduction in strength of the paper was reported after UV irradiation (Pelton et al., 2006). The use of ceramic fibres was introduced to separate the TiO_2 from the cellulose fibres to minimise the loss of strength after irradiation (Iguchi et al., 2003).

Photocatalytic paper applications can be divided into mineralization of organic pollutant molecules and disinfection. Very low density filters and high density low permeability paper - cellulose substrates are used for this. It is used in applications targeted to treat water and air, in liquid or vapour phase. The first publication on the photocatalytic paper application for the degradation of water pollution was published in 2003 when they compared performance of a laboratory prepared photocatalytic paper to the same but unsupported catalyst to degrade water solution of bisphenol A (Fukahori et al., 2003).

Azo dyes were first published to be degraded by photocatalytic paper in water phase in 2005 (Aguedach et al., 2008). It has been found out that the rate determining step is the adsorption of the dye onto the semiconductor surface. Since the adsorption is driven by electrostatic forces, the influence of the pH value on the degradation of the colour molecules was established. The initial, dark adsorption onto the TiO_2 surface was much higher at pH 3 compared to

dark adsorption at 4.5 or higher. This is attributed to the value of the TiO_2 piezoelectric point and acid-base equilibrium. At low pH the TiO_2 surface is more positive and consequently dye adsorption is higher and degradation faster. But dye degradation took place also at higher pH values, proving that reactive oxygen species can diffuse into solution and degrade the dye molecules (Aguedach et al., 2008).

One of the first pilot-scale experiments of photocatalytic decomposition was pesticide and dye degradation in sunlight irradiated compound parabolic concentrator and “STEP” reactors. A comparison was done between the degradation efficiency with slurry in a CPC reactor and Ahlstrom non-woven paper in a “STEP” reactor. The “STEP” reactor with paper catalyst was proven to be less efficient compared to CPC slurry reactor. But it has been proven that even if the paper proved to be less efficient, total decolouration could be achieved. The pH of the solution during the treatment remained neutral through the experiment, possibly due to simultaneous release of sulphate and ammonia during the experiment (Guillard et al., 2003b).

The drop in TOC values was considerably slower compared to the drop in remaining colouration of the solution. Slow TOC drop, especially pronounced at the beginning of the irradiation, is attributed to the slow formation and degradation of hydroxylated compounds, which are considered to be the main primary intermediates formed during the photodegradation (Guillard et al., 2003b).

Photocatalytic paper with coated TiO_2 catalyst on a non-woven paper has different surface characteristics compared to a non coated one. When the silica binder is used as a binder to the non-woven support material, it influences the surface characteristics since it is negatively charged. The surfaces of both oxides TiO_2 and SiO_2 in water are amphoteric, their surface charge being

dependant on the pH of the solution. The pzc point of SiO_2 is ≈ 2 and is much lower compared to the lower pzc of TiO_2. Adsorption of the azo dye onto the surface of the semiconductor could be attributed to the electrostatic attraction between sulfonic moiety of the azo dye and positive charges of the oxide when pH is inferior to the pH_{pzc} of the oxide. On the other hand, at basic pH values, the electrostatic repulsion between $-SO_3^-$ and TiO_2 /SiO_2 prevents the adsorption (Aguedach et al., 2008).

When cations are added to the solution exposed to photocatalytic decomposition, positive ions diminish the electrostatic repulsion and the dye molecules can penetrate closer to the surface of the semiconductor and adsorption occurs. Addition of salts and consequent increase in ionic strength hinders the electrostatic repulsive effect by compressing the electric double layer. In this regard, the higher valence cations like Ca^{2+} are more successful in compressing the double layer (Guillard et al., 2003a). But unlike the general effect of cations in compressing the double layer, there were differences observed between the three monovalent ions. This is attributed to the fact, that each ion must also have a specific interaction between either the substrate or the oxide (Aguedach et al., 2008). It can be concluded, that cation addition hinders the electrostatic repulsion of the double layer and non-electrostatic interactions between the substrate and the dye can take place (Aguedach et al., 2008).

At pH values above the pH_{pzc} the main electrostatic interactions taking place are those between cations and the negatively charged oxide surface. If the surface is considered uniformly negatively charged, than the anions in the solution are not expected to influence the adsorption capacity. But if heterogeneity of the surface charge (pK_{a2} of TiO_2 is 8) is taken into account (presumably there is a distribution of the positive, negative and neutral sites) the presence of anions implies electrostatic interactions between them and positive surface sites. In this

case the anions can compete with dyes for the adsorptions sites in the semiconductor surface. At the addition of salts, the added anions could compete with the dye molecules, but the phenomenon was not considered to predominate over beneficial effect of cations, since the amount of negative and neutral sites outnumbers the amount of positive sites at neutral pH values (Aguedach et al., 2008).

3.3.8. Photocatalytic ozonation of textile dyes

Although photocatalysis has proven to be a successful approach in degrading a large variety of pollutants, in some cases complete mineralization and pollution abatement is attained slowly and consequently it is an energy consuming process. Ozone is also used as a powerful oxidant for degradation of organic matter in water. Its electrochemical oxidation potential is 2.07 V compared to hydroxyl radicals' 2.8 V (Augustina et al., 2005).

However industrial scale applications of ozonation process to treat organic contaminants in wastewaters are not widely used due to high operational costs. Costs arise from high production costs and low mass transfer rate of ozone. A combination of ozonation with other methods of water treatment has proven to be more efficient in organic compound mineralization since it increases considerably the amount of highly reactive oxygen based radicals being formed and in consequence it increases the rate of mineralization of organic compounds (Augustina et al., 2005).

The synergy effect of TiO_2 based photocatalysis combined with ozonation results from a series of reactions which are often conditioned by products of the preceding reaction. The synergistic effect of combining UV irradiation with ozonation in the presence of TiO_2 catalyst possibly originates from ozone adsorption onto the TiO_2 surface through the following interactions: physical

adsorption, weak hydrogen bonds formation with surface hydroxyl groups and molecular or dissociative adsorption into Lewis acid sites (Addamo et al., 2005).

Synergistic effect between the TiO_2/UV photocatalytic degradation and ozonation has been proven for a pH range 3-8.5 when pesticide samples were irradiated and simultaneously ozonated. At higher pH values the synergy was presumably lost due to fast ozone degradation and consequent low ozone concentration in the solution. The synergy was most pronounced at pH below 7 when ozone is mainly in molecular form and as such capable of extracting electrons form conduction band of the semiconductor (Černigoj et al., 2007).

When wastewater is ozonated there are two reactions taking place between the ozone molecule and the organic matter and different reaction pathways can simultaneously contribute to degradation. At low pH ozone only reacts with compounds with specific functional groups like electrophilic, nucleophilic and dipolar addition reaction (direct degradation pathway). But at high pH values the stability of ozone is lower, its decomposition faster and produced hydroxyl radicals accelerate degradation of organic molecules (Sevimli and Sarikaya, 2002).

When the ozone molecule is adsorbed to the surface of the semiconductor it is more easily reduced by a photogenerated electron since it is a stronger oxidant compared to oxygen. In reaction the ozonide radical anion is formed which in the following reactions 27-32 generates hydroxyl radical (Kopf et al., 2000; Hernandez-Alonso et al., 2002):

$$O_3 + TiO_2\,(e^-_{CB}) \rightarrow O_3^{\cdot -} + TiO_2 \qquad (27)$$

$$O_3^{\cdot -} + H^+ \rightarrow HO_3^{\cdot} \qquad (28)$$

$$HO_3^{\cdot} \rightarrow O_2 + OH^{\cdot} \qquad (29)$$

Another pathway of hydroxyl radical formation through ozone mediation is the reaction of superoxide anion with ozone, again resulting in ozonide radical anion which gives hydroxyl radical through Eqs. 28 and 29 (Kopf et al., 2000; Hernandez-Alonso et al., 2002):

$$O_2 + TiO_2\,(e^-_{CB}) \rightarrow O_2^{\bullet -} + TiO_2 \qquad (30)$$

$$O_2^{\bullet -} + O_3 \rightarrow O_3^{\bullet -} + O_2 \qquad (31)$$

Ozonide radical anion can also be formed when ozone reacts with H_2O_2 which is produced when molecular oxygen is reduced on the surface of the semiconductor (Černigoj et al., 2010):

$$O_3 + HO_2^- \rightarrow O_3^{\bullet -} + HO_2^{\bullet} \qquad (32)$$

According to the proposed reactions of hydroxyl radical formation through conduction band electrons scavenging by ozone, the ozone molecule adsorption to the surface of the semiconductor is an inevitable step. It has been proven, that the surface area of the catalyst plays a decisive role in determining the degree of synergy (Černigoj et al., 2010). It has also been proven, that synergy between ozonation and photocatalysis depends on the ozone dosage (Černigoj et al., 2007).

At ozone introduction into dye water solution, the reactions can take place also directly between the ozone molecule and the pollutant entity. It has been established that the structure of azo dye influences the kinetics of ozone degradation reaction since the velocity of reaction depends on the size of the functional group. The order of reactivity has been established for the following functional groups: benzene < naphthalene < phenantrene < pyrene < anthracene (de Souza et al., 2010). It has also been established that ozone mediated dye degradation is fastest at alkaline pH values since alkaline

environment promotes ozone decomposition in favour of hydroxyl radical formation (Sevimli and Sarikaya, 2002; Konsowa, 2003).

With increasing the ozone dose the decolouration of the sample was faster and COD drop was more pronounced. But the ozone utilization ratio decreased since consumed ozone per unit of colour and COD removal remained almost the same, regardless the ozone dose applied. According to the two-film theory, overall mass transfer mechanism of the ozone molecule from the gaseous phase into the bulk aqueous phase occurs in several steps. Increasing the applied ozone dose enhances the mass transfer and subsequently increases ozone concentration in the liquid phase where degradation reactions are faster (Sevimli and Sarikaya, 2002).

3.4. COMBINATION OF TREATMENT APPROACHES FOR POLLUTION ABATEMENT

The use of a large variety of dyes and auxiliary chemicals in the textile industry results in large volumes of wastewater containing the named substances. A question arises how to maintain a profitable level of production and on the other hand how to reduce the intake of fresh water or at least the release of large volumes of contaminated waters. Biological degradation of a chemical is determined as elimination of a pollutant by the metabolic activity of living organisms, usually microorganisms and in particular bacteria and fungi that live in natural water and soil (EUR 20418 EN/2). As already stated in 3.1.3. conventional treatment methods (biological or/and physicochemical) are generally not successful in reducing pollution loads to the level for the effluents to meet the limits for discharge into the environment due to their recalcitrant, complex and toxic nature (Hai et al., 2007).

None of the named methods, shown in Fig. 1, tested for the textile wastewater pollution abatement, have proved to be a panacea, a universally applicable

method for treating these extremely recalcitrant wastewaters. Since a single, widely applicable end-of-pipe solution has not been established so far, a combination of the proposed and tested techniques seems to be essential when technically and economically feasible method is the set goal (Hai et al., 2007).

In general cost-competitive biological methods are many times ineffective without a supplementary method. Physicochemical methods on the other hand have restrictions in operation scale and pollution profile of the effluent. A number of biological approaches have been tested (activated sludge, fluidised bed biofilm, several different fixed bed systems) as well as their combinations. A combination with municipal wastewater is proposed, whenever applicable. Their main disadvantage lies in the fact that dyes are very toxic and resistant to biodegradation, some highly soluble and exhibit poor adsorption to activated sludge (Hai et al., 2007).

Simultaneous or sequential utilisation of biological and physicochemical treatment approaches combines coagulation, absorption and numerous other approaches; combinations can be divided into biological/physicochemical combinations (i.e. fluidised bed biofilm/coagulation/electrochemical oxidation, Fenton/biofilm/Fenton, bio/electroflocculation/flotation/filtration), integrated partial oxidation/biodegradation (i.e. chemical oxidation as pre-treatment to enhance biodegradation, …), biodegradation/adsorption combinations (activated carbon added to activated sludge), biodegradation/membrane filtration (nanofiltration for water reuse). With AOPs there are generally two major combinations: sequential biological/AOP treatment and partial preoxidation followed by biological stage (Hai et al., 2007). There are also many physicochemical methods/AOP combinations combining coagulation, adsorption and membrane methods with AOPs (Hai et al., 2007).

Advanced oxidation methods offer an alternative or complementary but highly competitive method to decolourise and reduce recalcitrant (stable, non biodegradable) wastewater loads. Although chemical oxidation for complete mineralization is usually expensive, a combination with biological treatment is widely reported to reduce the operational costs. They offer an alternative for final pollution abatement of biologically resistant wastewater pollution (Oller et al., 2010).

The potentials offered by AOP and CW treatment can be used to integrate biological treatment and oxidative degradation of toxic or refractory substances. The oxidative treatment can be done either before entering or after leaving the biological stage. A suitable application of AOPs for wastewater treatment must consider the fact that they use expensive reagents or UV light sources and demanding setup for carrying out the treatment. So it is obvious that their application should not replace whenever possible the less expensive biological treatment but the combination of both systems is a self bidding opportunity (Malato et al., 2002).

One possibility is application of AOP as a pre-treatment to convert initially persistent organic compounds into more biodegradable intermediates which can be in turn treated in a biological oxidation process with considerably reduced costs. In this case the percentage of the pre-treatment mineralization should be minimal, since lower operational costs are achieved through biological mineralization (Oller et al., 2010).

Combination strategy can also have the opposite direction. Also pollution load of wastewater expressed as COD is to be considered in this regard. Only wastewater with relatively low COD (< 2.0 g/L) can be cost-efficiently treated by AOPs. At higher COD values the reagents consumption raises costs and the method becomes unattractive (Malato et al., 2002). So it is more feasible to first

eliminate high organic loads of biodegradable components from the wastewater in our case in the CW and then proceed with the degradation of recalcitrant contaminants and their final mineralization.

In an experiment where only textile dyes were tested for decolouration and degradation (glucose was added only as a carbon source) the suggested sequence was first AOP followed by biological treatment (Brosillon et al., 2008). But in the case when also high organic loads are taken into account and in absence of toxicity of wastewaters towards faecal microorganisms the other sequence seems to be a more reasonable choice – organic load reduction followed by AOP until final mineralization is achieved. Azo dyes are resistant to decolouration under aerobic conditions but are readily decolourised under anaerobic treatment. But aromatic amines formed during decolouration which are more toxic than the dye molecule itself, are easily mineralized under aerobic conditions or oxidised to CO_2 and H_2O (de Souza et al., 2010).

A combination of TiO_2 photocatalysis and wetland reactor was already suggested with the aim to treat pesticide loaded wastewaters (Arana et al., 2008). In the named case CW followed the photocatalysis stage but samples treated in the experiment were only pesticide solutions and not those of real (or prepared) wastewaters.

A review was done on an array of potential hybrid technologies for treatment of dye loaded waters in general and specially textile wastewaters where also available costs were included. It has been concluded, that the biological hybrid technologies appear to be the most promising due to the fact, that the effectiveness of combining biological and other treatment methods is designed in a way to assure synergy rather than just a sum of both methods' performance (Hai et al., 2007).

3.5. LEGISLATION ON TECHNICAL WATER EFFLUENT LIMITS

In the Directive 2006/11/EC of the European Parliament and of the Council in February 2006 (Directive 2006/11/EC) on pollution caused by certain dangerous substances discharged into the aquatic environment of the Community, it has been established that there is a need for general and simultaneous action by the member states to protect the aquatic environment of the Community from pollution, particularly that caused by certain persistent, toxic and bioaccumulable substances. In the named directive the term ‘pollution’ is defined as means of discharge by man, directly or indirectly, of substances or energy into the aquatic environment, the results of which are such as to cause hazards to human health, harm to living resources and to aquatic ecosystems, damage to amenities or interference with other legitimate uses of water (Directive 2006/11/EC).

Based on the named directive the Slovene government introduced a regulation on the emission of substances and heat at wastewaters release from installations for manufacturing, processing and finishing of textile fibres (Official Gazette RS 7/2007). The regulation among other defines also the parameters’ limit values for emissions of wastewater and special measures to be taken in regard with reducing emissions of substances. Among other parameters also limit values of effluents’ colouration, biological degradability (70 % of the biodegradability of water at treatment plant) and organic pollution are defined and given in Table 1. The limits are set for two possible treatments. In the case the water is directly released into the surface waters the limits are set higher and in case the water is released into the sewage treatment system the limits are set in the way not to obstruct the operation of the treatment plant.

Spectral absorption coefficient (SAC) value is determined (according to ISO 7887) at peak absorbance values (λ), characteristic for each of the dyes. SAC is calculated according to the following equation (33):

$$SAC(\lambda) = \frac{A}{l} * f \qquad (33)$$

In Eq. 33 A is absorbance at certain wavelength, l - optical pathway given in mm and f is a unit conversion factor.

Table 1: Limit values of single wastewater parameters from textile factories released into surface waters or into sewage system (Official Gazette RS 7/2007) and from industrial wastewaters in general (Official Gazette RS, 45/2007).

	TEXTILE FACTORIES DISCHARGE (Official Gazette RS 7/2007)		INDUSTRIAL DISCHARGE IN GENERAL (Official Gazette RS, 45/2007)	
PARAMETER	RELEASE INTO SURFACE WATERS	RELEASE INTO SEWAGE SYSTEM	RELEASE INTO SURFACE WATERS	RELEASE INTO SEWAGE SYSTEM
TOTAL ORGANIC CARBON (TOC)	60 [mg/L]	h	30 [mg/L]	_
CHEMICAL OXYGEN DEMAND (COD)	200 [mg/L]	h	120 [mg/L]	_
BIOLOGICAL OXYGEN DEMAND 5 (BOD_5)	30 [mg/L]	–	25 [mg/L]	_
SAK (436 nm)	7 [m^{-1}]	b	7 [m^{-1}]	b
SAK (525 nm)	5 [m^{-1}]	b	5 [m^{-1}]	b
SAK (620 nm)	3 [m^{-1}]	b	3 [m^{-1}]	b

b – the limit value is defined in the "environmental permission document" as a value at which treated discharge from coloured wastewaters treatment plant doesn't exceed surface waters colouration limits

h – the discharge of wastewater is permitted in the case the biodegradability of the discharge, expressed as COD or TOC accounts for at least 70 % of municipal wastewaters' biodegradability

4. THIN FILMS FOR PHOTOCATALYSIS

4.1. EXPERIMENTAL

4.1.1. Sol-gel procedure for TiO_2 thin films preparation

The first step was the silica sol deposition on soda–lime glass microscope slides to create a barrier silica layer in order to prevent the sodium ions from the glass to penetrate into the semiconductor. By single dipping prepared films were heat treated at 500 ºC for 30 min (L. Štangar et al., 2006).

SiO_2 sol: Tetraethoxysilane (15.96 mL) was dissolved in ethanol (32.64 mL). Separately 11.5 % solution of nitric(V) acid was prepared by dissolving concentrated (65 %) nitric(V) acid (1.32 mL) in water (10.5 mL). After ten minutes both solutions were mixed. The sol was used after ageing at room temperature for at least two hours. Since the sol rapidly gels it was prepared fresh on the day of use.

TiO_2 sol: Titanium(IV) isopropoxide ($Ti(OiPr)_4$) (17.92 mL) was added to ethyl acetoacetate (7.88 mL) during constant stirring. The solution was then dissolved in iso-propanol (C_3H_7OH) (64.8 mL) after 5 minutes. As last the surfactant Pluronic F-127 (9.4 g) was added. The resultant alkoxide solution was stirred overnight at room temperature for solvolysis and condensation reactions and for the surfactant to dissolve. Between sequential uses the sol was kept in the refrigerator. It was conditioned by heating to reach 50 ºC just prior to the next use.

4.1.2. Doping

In the case of preparation of Fe doped TiO_2 sol, various amounts of $Fe(NO_3)_3$ x $9H_2O$ were added in the sol at the step before adding surfactant. Quantities of $Fe(NO_3)_3$ x $9H_2O$ for different doping ratios are listed in Table 2.

Table 2: The amounts of $Fe(NO_3)_3$ x $9H_2O$ added corresponding to the % of doping (n(Fe)/n(Ti) x 100).

% of doping	$Fe(NO_3)_3$ x $9H_2O$ [g]
0.5	0.0606
1	0.1212
5	0.6058
10	1.2116
20	2.4232

4.1.3. Deposition

Films were deposited on microscope glass slides (75 mm x 25 mm x 1 mm), washed with ethanol and dried before use. The SiO_2 films were deposited using dip-coating technique with a withdrawal speed of 10 cm/min. Thickness of the film and consequential cracking (if too thick) depended also on the outside temperature. At high ambient temperatures (around 30 ºC), 10-20 % of initial ethanol volume was added to the sol to prevent cracking.

TiO_2 films were deposited on silica protected glass slides using dip-coating technique with a fixed withdrawal speed - 10 cm/min. Glass slides coated with gel films were left at room temperature in air to dry for 30 min and then they were calcined at 500 °C for 15 min. In the case of deposition of thicker films with more layers, after calcination the whole procedure was repeated. After the last layer deposition and air drying, the calcination was 60 min long.

Deposition of the TiO_2 films subsequently sputtered by gold was done at the University of Padova, Italy, by the group of Department of Chemical Sciences.

4.1.4. Sputtering of gold nanoparticles

Radio frequency (RF) sputtering of gold was performed on sol-gel TiO_2 xerogels at temperatures as low as 60 ºC, to avoid thermally induced modifications of the xerogel morphology and structure. After sputtering the samples were annealed for 1h at 200, 400 or 600 ºC in air.

Au depositions on TiO_2 xerogels were performed by a custom-built Radio Frequency Plasmochemical reactor (v = 13.56 MHz) using electronic grade Ar (purity 5.0) as plasma source. A 2'' diameter gold target (0.1 mm thick; BAL-TEC AG, 99.99 %) was fixed on the RF electrode. Samples were placed on a second ground electrode whose temperature was measured by a thermocouple inserted into the resistively heated sample holder. Deposition was carried out at 60 ºC substrate temperature, with an electrode-to-electrode distance of 50 mm, under optimized conditions.

Sputtering of gold nanoparticles onto the TiO_2 films was done at the University of Padova, Italy, by the group of Department of Chemical Sciences.

4.1.5. Thin films characterisation

4.1.5.1. UV-Vis Spectroscopy

UV-Vis spectra of the films used in photocatalytic experiments were recorded on a Hewlett-Packard 8453 UV-Vis spectrophotometer. Transmittance spectra were recorded in the spectral range from 190 nm to 1100 nm.

4.1.5.2. XRD

X-ray diffraction (XRD) measurements were done on powder samples on a Philips PW1710 automated X-ray diffractometer using graphite monochromatized Cu-Kα (λ = 0.1542 nm) radiation in the step-by-step mode.

The grain size (the effective size of coherently scattering domain) has been calculated from the XRD pattern by the Scherrer's equation (34):

$$D = \frac{0{,}9\lambda}{\beta \cos\theta} \qquad (34)$$

The diameter of the particles (D) in the equation 34 is calculated from λ - wavelength of the X-ray, β - the full width at half maximum of the pattern peak, corrected for the instrumental broadening and θ is the diffraction angle in degrees.

4.1.5.3. AFM

Surface topography of TiO_2 films was evaluated by atomic force microscopy (AFM) on a CP-II scanning probe microscope (Veeco) in non-contact mode at constant force in air. The tip was also a Veeco product (model RFESPA-M).

4.1.5.4. XPS

Surface and in-depth composition of films were analyzed by XPS on a Perkin Elmer Φ 5600ci spectrometer using standard Al and Mg radiations (1486.6 eV) working at 350 W. The working pressure was < $5x10^{-8}$ Pa. The spectrometer was calibrated by assuming the binding energy (BE) of the $Au4f_{7/2}$ line at 83.9 eV with respect to the Fermi level.

Standard deviation for the BE values was 0.15 eV. The reported BE were corrected for the charging effects, assigning, in the outer layers where contamination carbon is still present, to the C1s line of carbon the BE value of 284.6 eV (Moulder et al., 1992, Briggs et al., 1990). Survey scans (187.85 pass energy, 1 eV/step, 25 ms per step) were obtained in the 0-1300 eV range. Detailed scans (58.7 eV pass energy, 0.1 eV/step, 100 ms per step) were recorded for the O1s, C1s, Ti2p, Fe2p, TiKLL, Si2p and FeKLL regions.

Depth profiles were carried out by Ar^+ sputtering at 3 keV with an argon partial pressure of 5×10^{-6} Pa. A specimen area of 2×2 mm^2 was sputtered. Samples were introduced directly, by a fast entry lock system, into the XPS analytical chamber. The assignments of the peaks were carried out by using the values reported in (Moulder et al., 1992) and in the NIST XPS Database (http://srdata.nist.gov/XPS, Dec. 2007). XPS measurements were performed at the University of Padova by dr. Silvia Gross (Gross, 2008).

4.1.6. Photocatalytic activity

For the photodegradation experiments a continuous flow reactor (Fig. 5) (Černigoj et al., 2006) was used. Photocatalytic performance of the films deposited on microscope glass slides (25 mm × 70 mm) was tested.

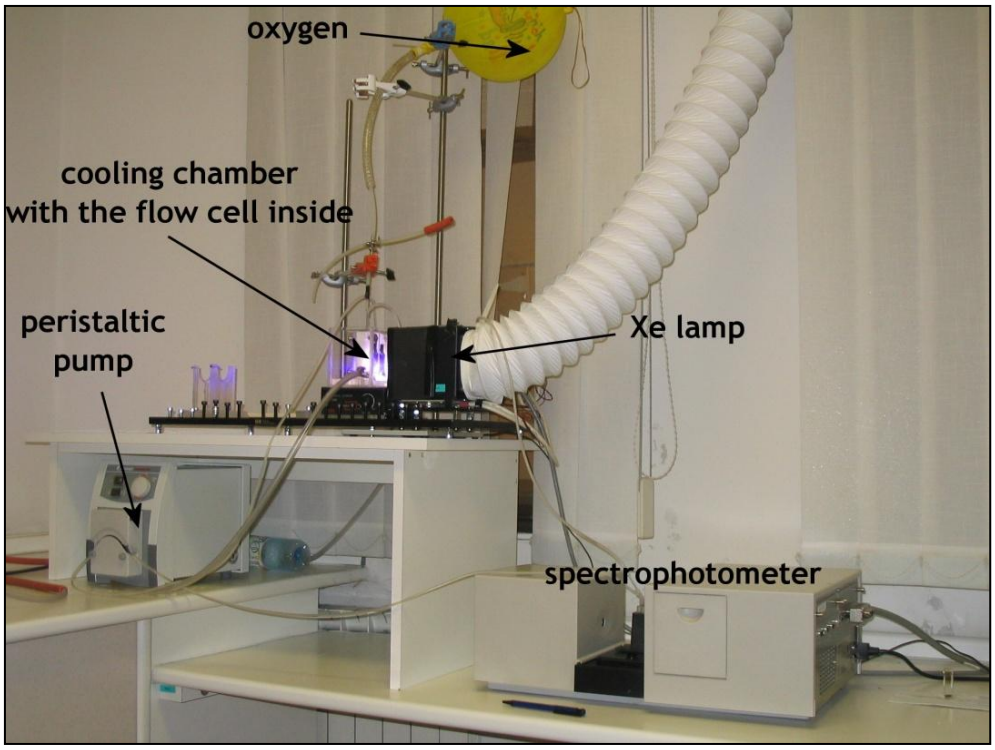

Figure 5: Continuous flow reactor for TiO_2 thin-film photodegradation experiments (Černigoj et al., 2006).

The flow cell was constructed from Teflon and boral glass; it allows purging of the sample with a chosen gas and uses tap water for cooling (Fig. 5). On-line absorbance measurements of the solution were done on Hewlett-Packard 8453 UV-Vis spectrophotometer.

A 10 mm thick 335 nm cut-off filter solution (NaBr (110 g), $Pb(NO_3)_2$ (0.69 g) in water (230g)) was used in front of the photocatalytic cell. An irradiation source was a 125 W Xe lamp (Cermax xenon parabolic lamp). The area of 23 mm x 23 mm on one side of TiO_2 thin film was irradiated along the normal direction. Aqueous solution (6 mL) of Plasmocorinth B - 3-(5-chloro-2-hydroxyphenylazo)-4,5-dihydroxy-2,7-naphthalene disulfonic acid, disodium salt (Fig. 6) - (40 mg/L) was used as a sample solution. The Plasmocorinth B dye solution was chosen as a model substance since it has been proved to be stable in the absence of TiO_2 photocatalyst under the irradiation conditions used for all photocatalysis experiments (Černigoj et al., 2006).

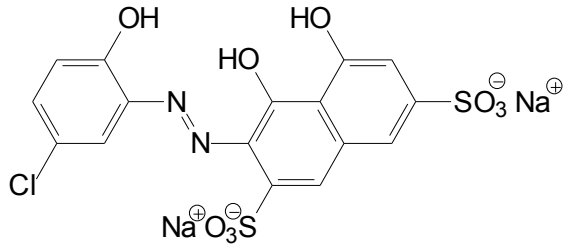

Figure 6: Chemical structure of Plasmocorinth B.

During irradiation the solution was constantly purged with oxygen. A peristaltic pump Heidolph PD 5001 with silicon hose was used to drive the solution at the rate of 80 rpm from the flow cell to the sample compartment of the UV-Vis spectrophotometer and back. Thus, on-line measurement of the absorbance of the solution was enabled.

4.2. RESULTS AND DISCUSSION

4.2.1. Optical properties of Fe doped and Au sputtered thin films

All TiO_2 films obtained by high-temperature sol-gel process and doped with different amounts of iron exhibited high optical quality. They were crack-free and transparent over the whole visible spectral range (Fig. 7). The brownish colouring of the films increased with increased amount of Fe doping.

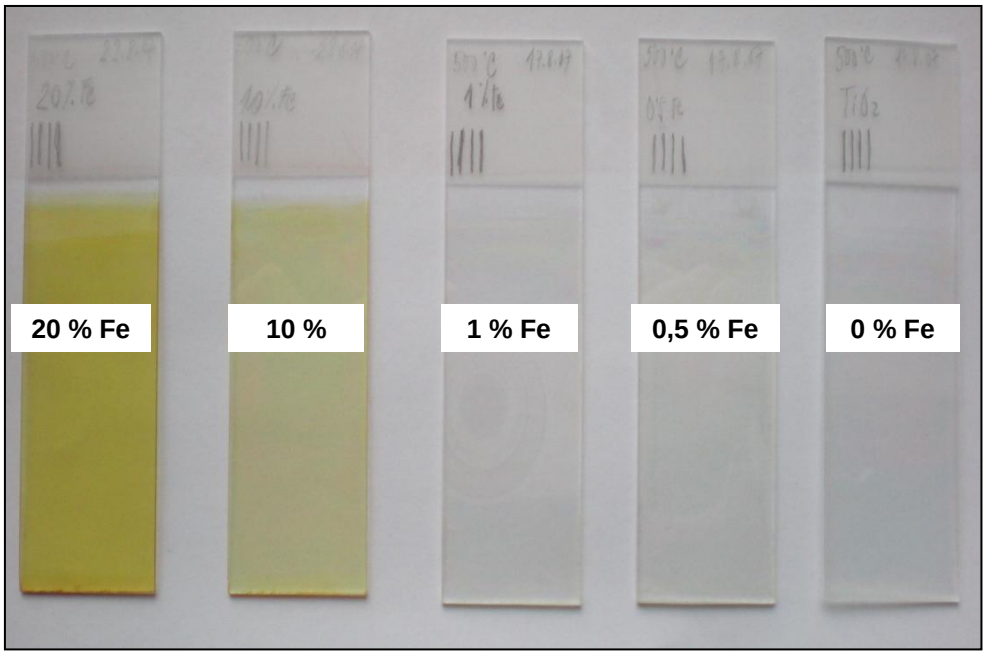

Figure 7: Photo of various % iron doped TiO_2 thin films, made by four dipping-heating cycles. From left to right follow 20, 10, 1 and 0.5 % iron doped films.

At lower dopant concentrations addition - 0.5 and 1 at. % Fe, the colouring of films is not pronounced (Fig. 7). Also a shift in absorption to the visible part of spectra - the “red shift” is not exhibited (Fig. 8).

When comparing curves in the spectra (Fig. 8) of doped films to undoped one, it is clearly seen that addition of the dopant produced a red shift of absorbance onset. Different amounts of iron added to the sol had a diverse affect on the absorbance onset. There is a clearly exhibited “red shift” towards longer wavelengths (visible part of spectra) in thin films with 5, 10, 20 at. % doping.

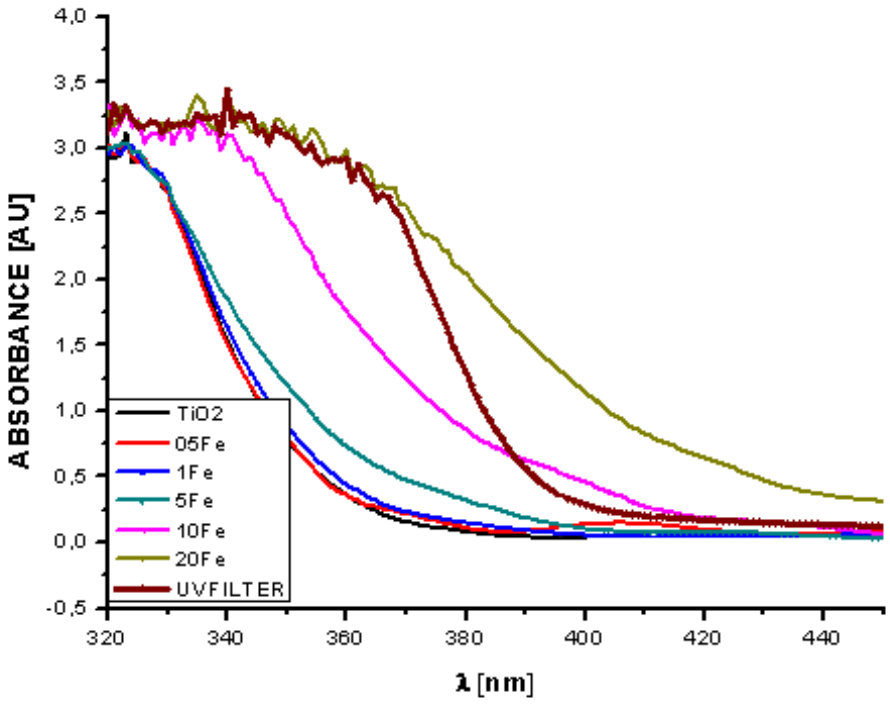

Figure 8: Absorbance spectra of various % iron doped TiO_2 thin films.

According to the films’ absorbance in visible region, the photocatalytic activity of films is expected to be higher or lower, depending on the light source used for irradiation of the films (see photocatalytic performance chapter 4.2.3). The brown curve represents the absorbance of the filter used to filter out most of the UV light. As such it was used to imitate natural sunlight reaching the Earth’s surface. This is the type of light which would irradiate the semiconductor if it was used in a pilot reactor outdoor.

Transmittance of the filter at the wavelengths of TiO_2 band gap is given in Table 3. Transmittance of the UV filter was calculated from the absorbance results, equation (35).

$$T = (1 - A) \times 100 \qquad (35)$$

Table 3: Transmittance of the UV filter at TiO_2 band gap wavelengths.

WAVELENGTH [nm]	TRANSMITTANCE [%]
380 (corresponding to Eg = 3.267 eV)	62
388 (corresponding to Eg = 3.2 eV)	81

Photo in the Fig. 9 shows unsputtered and gold sputtered thin films of various TiO_2 layers. There is a clearly exhibited difference among the coloured Au sputtered films and the non-coloured 2 and 1 layer pure TiO_2 thin films. There is also a difference in colouration among Au sputtered samples of different TiO_2 layers.

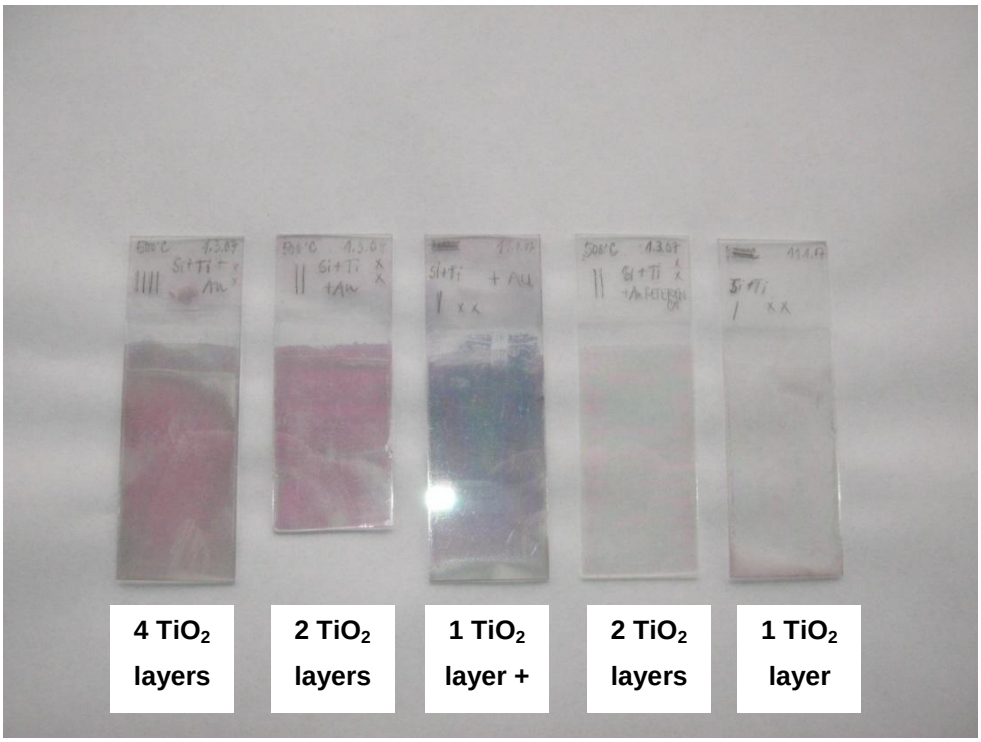

Figure 9: Photo of various TiO_2 layers, gold sputtered and unsputtered TiO_2 thin films. From right to left, 4, 2 and 1 layer TiO_2 films sputtered with Au are shown, followed by 2 and 1 layer pure TiO_2 thin films.

The difference in colouration among Au sputtered films of different TiO_2 layers is also exhibited in their absorbance spectra (Fig. 10). Additional TiO_2 layers slightly shift the absorbance towards longer wavelengths.

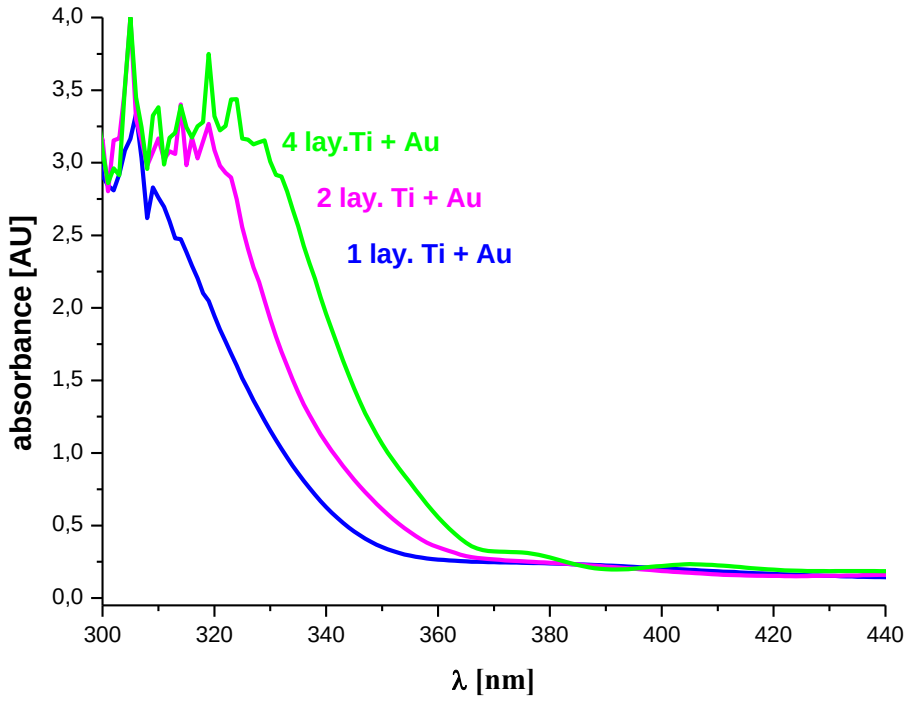

Figure 10: Absorbance spectra of gold sputtered thin films of various TiO_2 layers.

4.2.2. Structural and morphological features of doped thin films

4.2.2.1. XRD results

X-ray diffraction measurements show that all films, regardless the percentage of iron added as dopant, consist of a dominant anatase crystalline phase. Identification of the crystalline phases was performed on the ”film powder” samples. Powder samples were used instead of immobilized thin films to be able to obtain diffractograms with higher intensities of peaks and consequently better peak identification.

Powders were obtained by drying sols with different percent of doping on a large substrate (Petri dish), mechanically scratched and calcined in the oven at the

same temperature and length as the films were. This procedure provided sufficient quantity of the powder for the XRD analysis.

X-ray diffractograms of the undoped and different amounts of iron doped powders are presented in Fig. 11. In the undoped sample the anatase phase is present with a characteristic peak of highest intensity at 2θ = 25.4 °. Also all the doped samples exhibit this peak. The value of 2θ = 27.4 ° (Fig. 11 samples with 5 and 10 % iron added) is representative for rutile. Values for anatase and rutile peaks are in accordance with published values (Natl. Bur. Stand., 1969). The presence of dopant ions in the sample induces a change in nanocrystallinity of the films in favour of rutile in some cases.

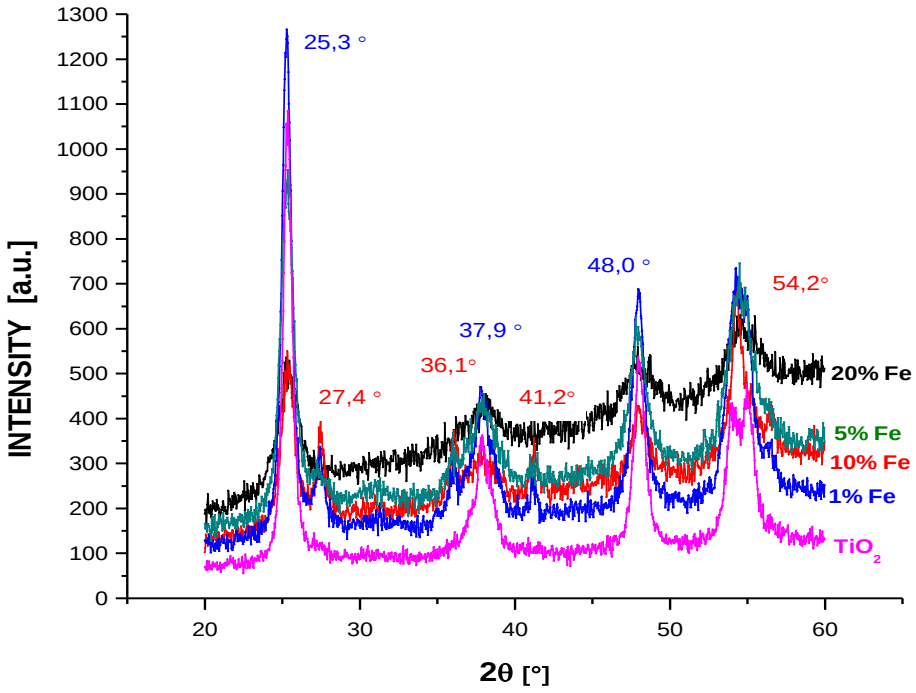

Figure 11: X-ray diffractograms of the undoped and different amounts iron doped powders.

With the increasing amount of dopant added, progressively increasing amount of amorphous phase is present in the samples. Even though high atomic % of iron

was added in the case of 10 % and 20 % doping, no other iron containing crystalline phase was observed - no presence of ferric oxides has been detected by the XRD. This is in accordance with the published data (Bouras et al., 2007).

Compared to pure TiO_2, the pattern peaks for Fe-doped TiO_2 slightly weaken and broaden. Channels along the c-axis in pure TiO_2 are of 0.77Å length. The radius of Ti^{4+} atom is 0.68 Å and of Fe^{3+} is 0.64 Å. From the given numbers it is possible to assume that Fe^{3+} diffuses along the c-axis in the TiO_2 lattice and substitutes Ti^{4+}. But since the Fe^{3+} radius is a little smaller than Ti^{4+} the different atomic sizes of Fe^{3+} and Ti^{4+} introduce some extent of deformation into the crystal lattice of TiO_2 (Zhu et al., 2006) .

As a result of crystal lattice deformation, the crystallite growth of Fe^{3+} - doped TiO_2 grains is restrained during thermal treatment, this results in a slight broadening of XRD peaks.

A crystallite size of the undoped and doped samples calculated from Scherrer's formula (Eq.34) is given in Table 4.

Table 4: The grain size D of different samples calculated according to Eq. 34.

SAMPLE	SIZE, D [nm]
TiO_2	16
1 % Fe	14
5 % Fe	11
10 % Fe	11
20 % Fe	7

Size of the grains differs significantly among the samples. As it was already mentioned growth of the Fe^{3+} - doped TiO_2 grains is restrained due to addition of Fe into the crystal lattice. Dopant addition and consequential lattice deformation

results in progressively smaller grain size. At the highest dopant addition, the grain size is less than half the size of pure TiO_2 grains.

In the patterns of Au/TiO_2 systems (Fig. 12) the anatase crystallization was almost unperturbed even though Au was added on the surface. This is indicated by anatase diffraction peaks at $2\theta = 25.3^{\circ}$ and 48.0°. Diffractograms are dominated by the gold peaks at $2\theta = 38.4^{\circ}$ and 44.5° which undergo an intensity increase and a progressive sharpening with the annealing temperature.

These trends correspond to nanocrystal sizes between 12 and 15 nm for Au and lower than 20 nm for anatase, and suggest a progressive structural/morphological evolution of the obtained systems upon thermal treatment.

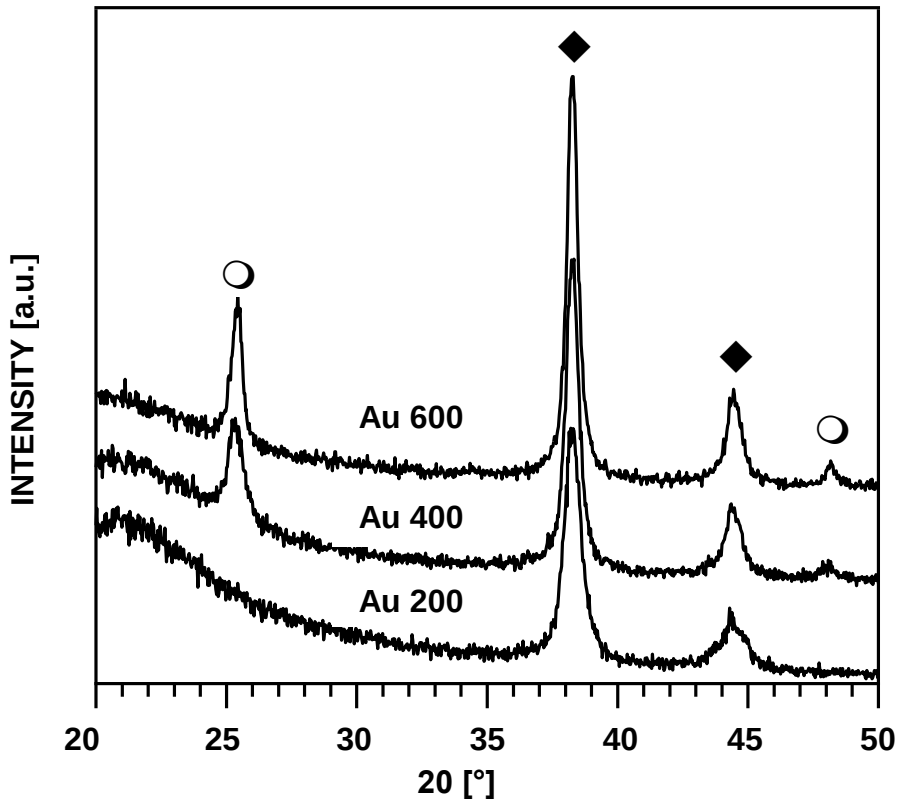

Figure 12: XRD patterns of Au/TiO_2 nanocomposites as a function of the annealing temperature. Peak positions for anatase TiO_2 (○) and Au (♦) are indicated.

4.2.2.2. AFM results – Fe doped TiO_2

In Fig. 13, atomic force microscopy images are presented. Photos differ in the amount of added dopant in the sol preparation.

AFM photos confirm the results of grain size calculation from XRD measurements (see 4.2.1). A progressive variation of grain size and shape takes place with increased amount of dopant addition. At higher dopant addition percentage the grain size is progressively smaller.

In the case of pure TiO_2 thin film, the grains' form is well expressed and of spherical shape. Very much the same can be said for grains of 1 % doped sample. The calculated size - the Scherrer's formula estimation gave similar size values (Table 4).

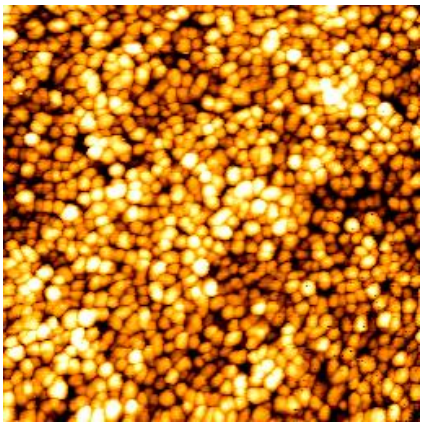

Pure TiO_2

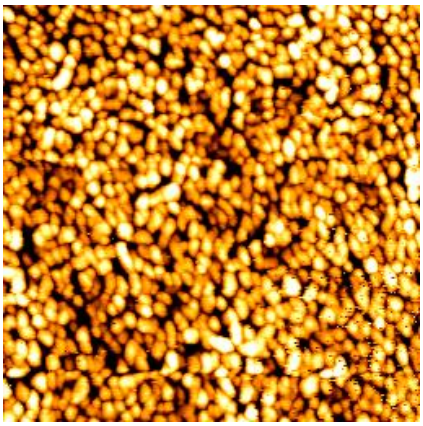

1 % Fe doping

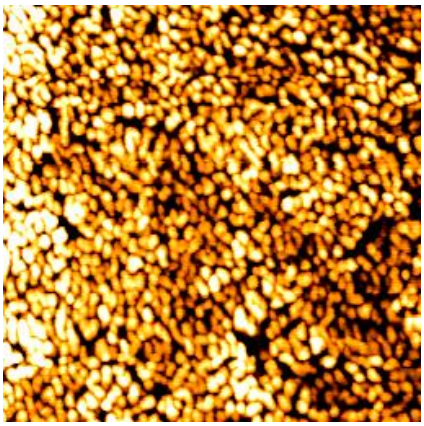

5 % Fe doping

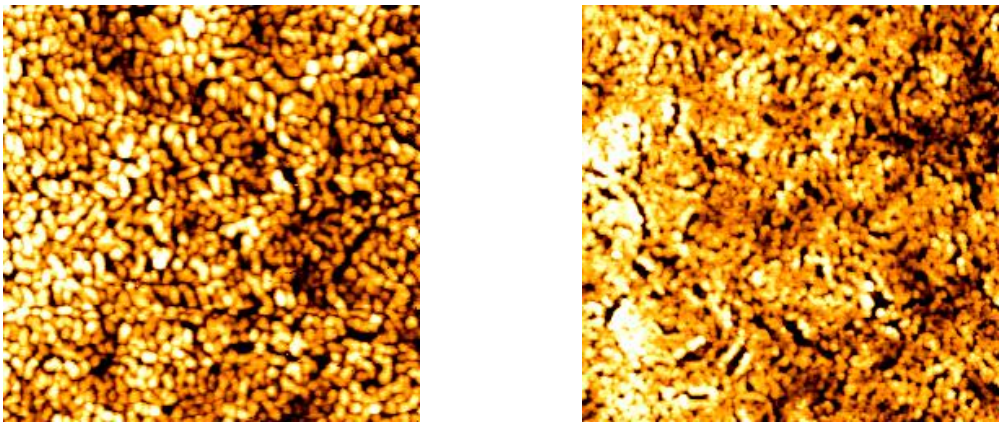

10 % Fe doping 20 % Fe doping

Figure 13: 500 nm x 500 nm atomic force microscopy images of thin films with various dopant additions.

In the case of higher dopant addition, the grains become smaller and less pronounced. Their shape is less expressed. In the case of 10 and especially 20 % doping, particle agglomeration is present. On the 20 % doping image, chains of agglomerated particles can be clearly observed.

4.2.2.3. FE-SEM results - Au/TiO_2 thin films

Photos done by Field Emission Scanning Electron Microscopy (FE-SEM) (Fig. 14) show homogeneous distribution of gold nanoaggregates on the TiO_2 surface. Even though the deposited Au amount was the same in all samples, their surface density and morphological features differ according to the calcination temperature. A progressive shape variation of gold particles from island-like to almost spherical takes place and an increase in the average interparticle distance is observed with increasing treatment temperature.

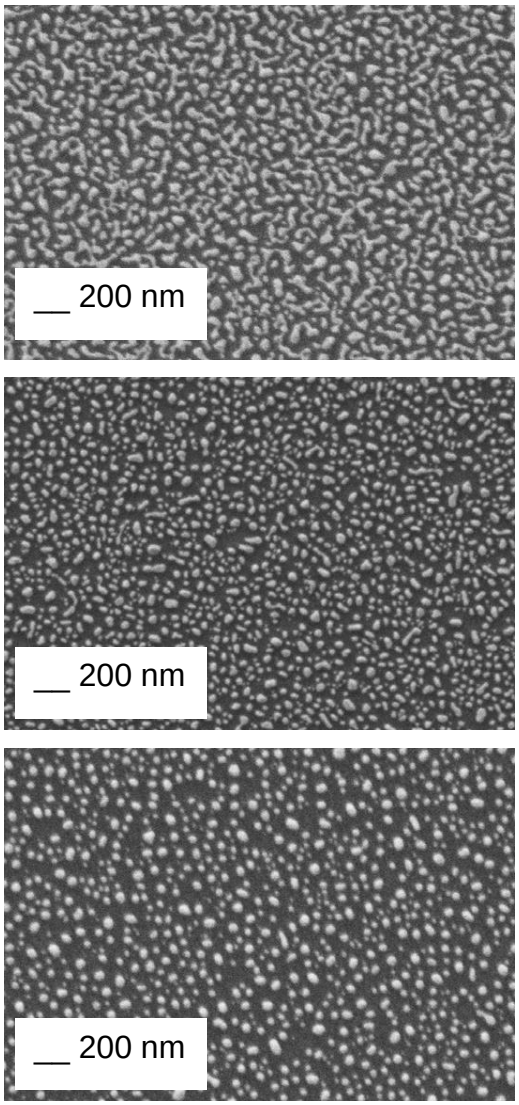

Figure 14: Plane-view FE-SEM micrographs of Au/TiO_2 samples annealed at different temperatures: 200 ºC, 400 ºC and 600 ºC.

A progressively decreasing TiO_2 coverage (44.0 %, 32.0 % and 28.0 % for samples in Fig. 14) indicates gold redistribution on the surface due to particle agglomeration during thermal treatment.

Morphological and size changes of gold nanoparticles are attributed to the influence of ex situ thermal treatment. As the annealing temperature was increased larger particles grew at the expense of smaller ones (Ostwald

ripening), and coalescence/agglomeration processes became progressively more marked with a concomitant evolution of the particle shape (Armelao et al., 2006).

4.2.2.4. XPS results

X-ray photoelectron spectroscopy (XPS) analysis provides information about composition, electronic structures, and chemical environment of each element on a surface and up to a few nanometers in depth. It is a widely used technique in the study of doped TiO_2 nanoparticles. For small nanoparticles, especially for particles with diameters <10 nm, the XPS provides a profile of the whole material (Qiu et al., 2007).

XPS is a powerful tool to study electronic structure and atomic environment of a chemical species (Hüfner et al., 1995). Oxidation state of different species is provided from the information on chemical shifts in the core levels. So the method also provides a powerful tool to investigate in-depth distribution of the species in thin films.

XPS was used to analyze atomic composition and chemical state of the species both on surface and in-depth of the thin films. Depth profiles were done by controlled removal (sputtering) of the samples' surface by Ar^+ ions bombardment followed by analysis at each depth.

In Figs.15 and 16 survey spectrum of the surface and Ti2p peak of 20 % Fe-doped TiO_2 sample before sputtering are given. Peaks of all the involved species - O1s, Fe2p, C1s, Ti2p, Si2s, TiLMM and OKLL are well pronounced.

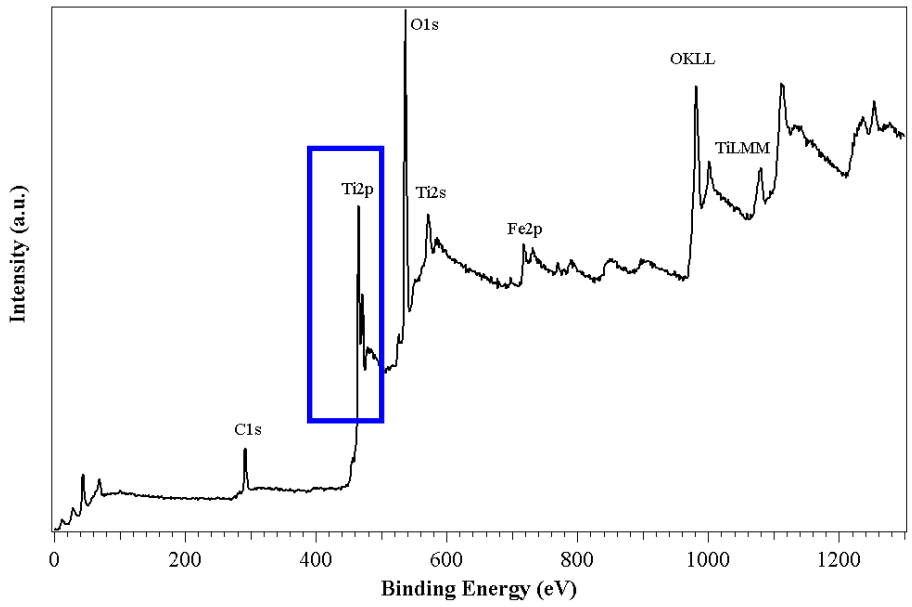

Figure 15: XPS survey spectrum of 20 % Fe-doped TiO_2 thin film before sputtering.

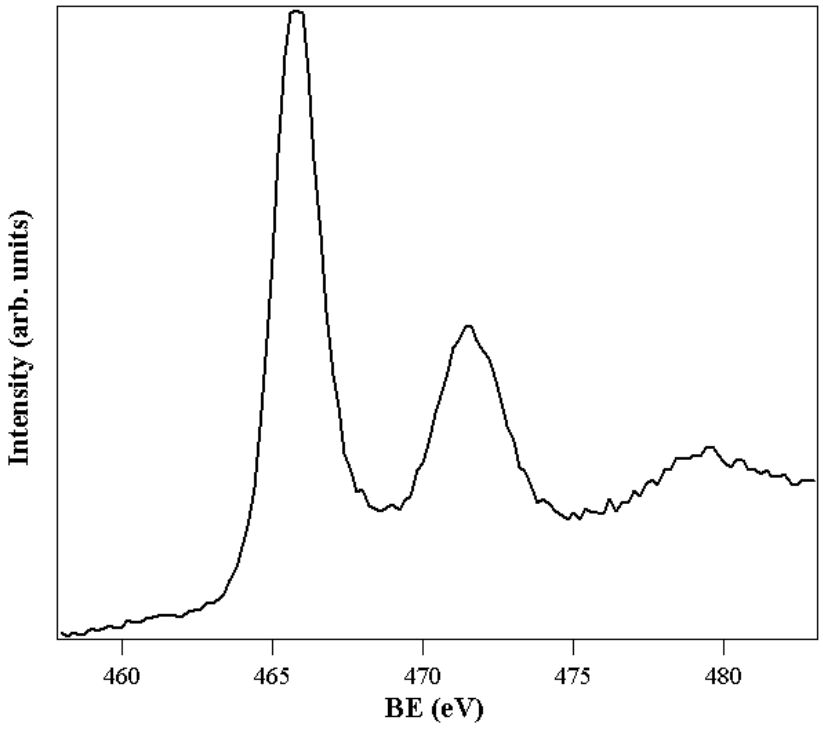

Figure 16: Ti2p peak from the XPS spectrum of 20 % Fe-doped TiO_2 sample before sputtering.

In Table 5 the atomic percentage of oxygen, titanium, iron and carbon is given as a function of sputtering time. In the last column the titanium to iron ratio is given. The data is given for two samples – the 20 % and 10 % doped TiO_2 samples.

Table 5: Atomic percentage of different chemical species as a function of sputtering time.

SAMPLE	TIME OF SPUTTERING [min]	% O	% Ti	% Fe	% C	Ti/Fe ratio
20 % Fe TiO_2_2	0	55.4	17.3	4.6	22.7	3.8
20 % Fe TiO_2_4	3	52.5	21.5	5	21.1	4.3
20 % Fe TiO_2_6	6	53.6	24.6	5.1	16.8	4.8
20 % Fe TiO_2_8	10	56.4	28.3	5.1	10.2	5.5
20 % Fe TiO_2_10	15	48.9	24.8	8.9	17.5	2.8
20 % Fe TiO_2_12	25	55.9	26.5	5.4	10.2	4.9
20 % Fe TiO_2_14	40	53.4	26.3	6.8	13.5	3.9
20 % Fe TiO_2_16	60	52.2	24.0	6.7	17.0	3.6
10 % Fe TiO_2_2	0	55.2	20.4	1.7	22.7	12.0
10 % Fe TiO_2_4	5	57.4	29.2	2.4	10.9	12.2
10 % Fe TiO_2_6	15	59.1	34.2	2.6	4.1	13.2
10 % Fe TiO_2_8	60					9.3

In Fig. 17 the Ti/Fe atomic ratio is plotted in relation to time of sputtering. From the values in Table 5 and curves in Fig. 16 it can be concluded that iron is rather homogeneously distributed in the TiO_2 matrix all along the investigated thickness.

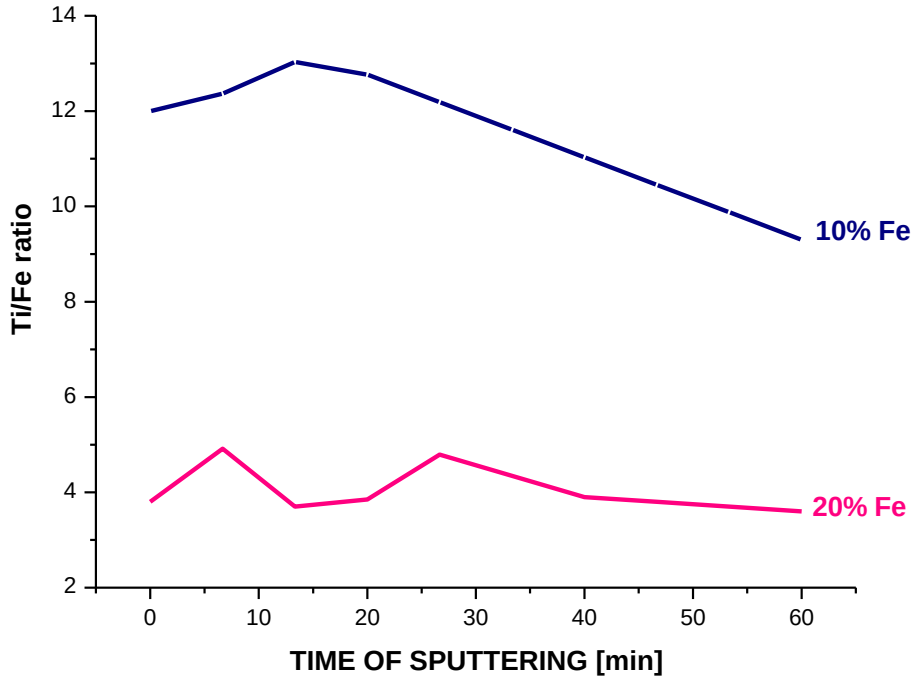

Figure 17: Ti/Fe atomic ratio in relation to time of sputtering.

The average experimental values obtained through XPS analysis are 4.2 for 20 % doped TiO_2 and 11.7 for 10 % doped TiO_2. These values are in good agreement with the nominal values in the solution for the sample preparation which would be 5 and 10, for 20 % and 10 % doping, respectively. This shows that the adopted experimental route allows good control of final composition of the thin film.

After 60 min of sputtering, iron, titanium and oxygen are still detected in the survey spectrum, whereas no silicon signal could be found. This indicates that the interface with deposited SiO_2 layer or the soda-lime substrate was not yet reached.

The amount of carbon on the surface of the layer is noticeable (22.7 at. %) due to presence of outside carbon contamination. The carbon amount decreases

considerably upon sputtering, but some amount still remains. This can be ascribed to presence of organic residuals in the film. It can be in fact argued that the temperature of annealing (500 °C) was not high enough to achieve a complete combustion of all the organic parts and some carbonaceous material still remained in the sample.

Binding energy gives the information on the chemical state of single species. In Table 6, the binding energies of Ti2p and Fe2p peaks are listed.

Table 6: Binding energies of Ti2p and Fe2p peaks as a function of sputtering time.

TIME OF SPUTTERING [min]	BE Ti2p [eV]	BE Fe2p [eV]
0	457.5	710.7
3	458.4	709.6
6	458.7	709.5
10	458.4	709.3
15	458.4	708.5
25	458.6	708.8
40	458.6	708.6
60	458.4	708.8

BE of the Ti2p peak ranges from 457.5 eV (on the surface of the film) to 458.7 eV (the bulk of the film in depth), these are values typical for Ti2p in TiO_2. Upon sputtering, a broadening of the Ti2p region was observed, which can be ascribed to a partial reduction of Ti(IV) to Ti(III) due to the preferential sputtering of oxygen induced by the Ar^+ ion sputtering during experimental procedure.

The same phenomenon was observed for Fe2p region. In the upper part of Fe2p [eV] column the measured data correspond to the surface of the sample. The presented BE values are values typical of Fe_2O_3 (Fe(III)). But during analysis when sputtering of the sample is carried out a progressive decrease of BE values is observed. Also appearance of a second component can be detected, which is ascribed to the presence of Fe(II).

Magnetic energy of the electron spin in presence of internal magnetic field caused by the orbital motion splits the 2p level into two states with angular

momentum j = 3/2 and j = 1/2. This is the so called spin-orbit effect. The Fe2p spectra are split by the 2p spin–orbit effect into the 2p3/2 and 2p1/2 regions.

On the surface, the BE value of 2p3/2 is 710.7 eV, a value close to those reported in literature for Fe(III) in Fe_2O_3 (Pereira et al., 2000) whereas after sputtering these values are in the range 708.5-709.3 eV, which are typical for Fe(II) species (XPS Database 20, 2007). It can be concluded that during sputtering, preferential sputtering of O takes place due to Ar^+ usage. This leads to reduction of Fe(III) into Fe(II) and consequentially progressive decrease of BE is observed.

XPS surface spectra of all three Au sputtered samples, annealed at 200, 400 and 600 °C displayed main peaks of C, O, Au, and Ti. Carbon was present throughout the whole film thickness at samples annealed at T < 400, indicating that applied annealing temperatures were not successful for a complete TiO_2 network /anatase formation. This hypothesis was confirmed by observing the evolution of O1s signal, which could be fitted by three different BE, ascribed to lattice oxygen in Ti(IV)oxides, adsorbed -OH groups and H_2O, respectively. In the sample annealed at 600 °C, presence of the latter two components decreased. At all applied annealing temperatures, the Ti2p3/2 BE was always close to 459.0 eV, which is in agreement with literature values for Ti(IV). Also the Au4f7/2 component was close to 84.0 eV value for all specimens, characteristic for metallic gold (Armelao et al., 2004).

4.2.3. Photodegradation results

In all photodegradation experiments aqueous solution of Plasmocorinth B - 3-(5-chloro-2-hydroxyphenylazo)-4,5-dihydroxy-2,7-naphthalene disulfonic acid, disodium salt azo dye was used. This azo dye is suitable for photoefficiency experiments because it is stable under the light used in the experiments, it doesn’t absorb to the surface of the photocatalyst (decolouration is proportional

to decomposition) and as it is degraded no coloured products are formed so UV-Vis spectroscopy can be used to follow degradation.

4.2.3.1. Fe - TiO_2 thin films

Figs. 18 and 19 show photodegradation data for aqueous solution of Plasmocorinth B in the presence of pure TiO_2 and different atomic % Fe doped TiO_2 thin films. Absorbance measured at the beginning of the experiment is set as a starting point (100 %). Because degradation is measured as % of the dye decomposition, the curves represent efficiency of photodegradation as a function of time. The performance of various thin films is compared through degradation %.

UV – Vis irradiation, λ> 335 nm

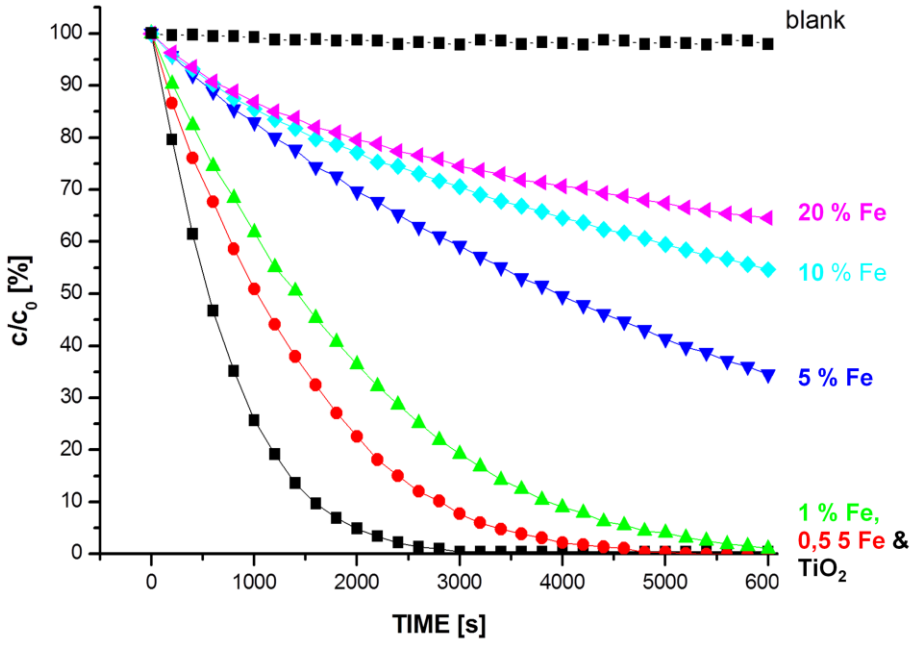

Figure 18: Percentage of photodegradation of Plasmocorinth B by different atomic % iron doped thin films, use of UV and Vis irradiation.

Vis irradiation, λ > 375 nm

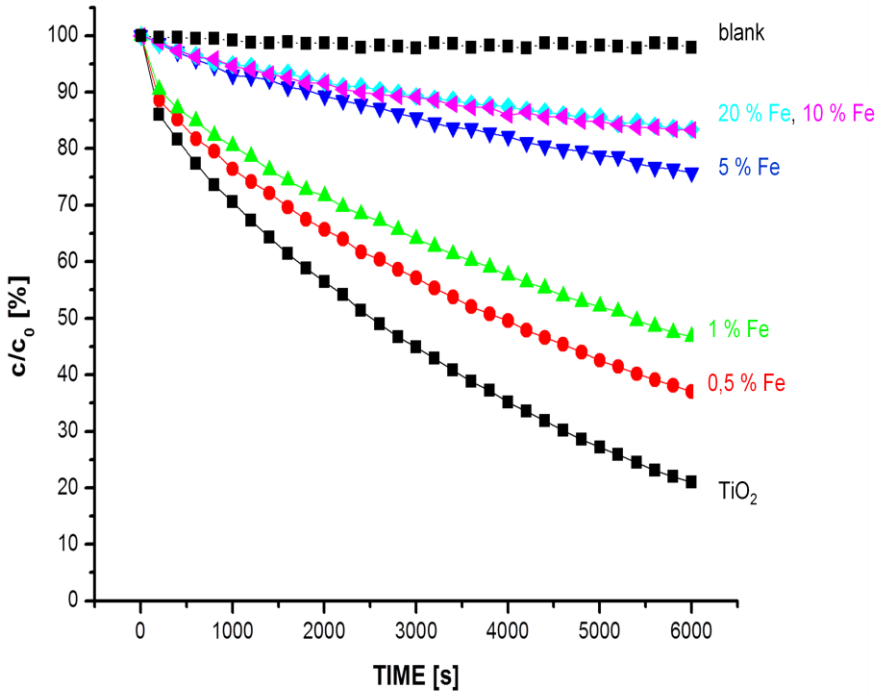

Figure 19: Percentage of photodegradation of Plasmocorinth B by different atomic % iron doped thin films, use of Vis irradiation.

Degradation curves of 6 different thin films and blank are shown. Blank is a result of dye solution decolouration, without the use of catalyst. All other degradation curves show dye decomposition in presence of pure TiO_2, 0.5 %, 1 %, 5 %, 10 % and 20 % iron doping. TiO_2 films are composed of four layers made by four sequential coating/heating cycles. As irradiation source, UV and Vis light was used of wavelengths longer than 335 nm. In Fig. 19 the degradation curves represent photocatalytic action of the same films but irradiated with only Vis light of wavelengths longer than 375 nm.

When degradation curves in Figs. 18 and 19 are compared, we see a pronounced difference in photocatalytic activity. The sequence of thin films from

the best performing to worst performing one is the same in both figures. The best performing thin film in both experiments was pure TiO_2 film. Then followed 0.5 %, 1 %, 5 %, 10 % and 20 % iron doped films.

In the case of UV and Vis irradiation the 10 % doped film exhibited better performance compared to 20 % doped one. But when films were irradiated with only Vis light, the performance of both of them was practically the same.

When Figs. 18 and 19 are compared a clear difference in films' catalytic performance is seen and influence of iron doping is exhibited. The reason why doping is done in general is to achieve higher absorbance of catalyst in the Vis part of solar spectra. As showed in chapter 4.2.1. a "red shift" in absorbance was achieved in the case of 10 and 20 % iron doped samples.

As a consequence also a better performance of iron doped films was expected compared to undoped ones when irradiated with Vis light – from this point of view, the sequence in curves in Figs. 18 and 19 was expected to be the opposite. But the results show that even though a beneficial effect of band gap shift was achieved, the doping had an overall detrimental effect on photocatalytic performance of all the doped films. The detrimental effect was exhibited at low dopant additions of 0.5 and 1 % as well as at higher additions of 5 %, 10 and 20 % of iron. It can be concluded that high or low iron addition had a detrimental effect for catalytic performance when irradiated with either UV-Vis or Vis light. There are some possible reasons why this happened.

On the AFM photos in Fig. 13 a progressive change in size and shape of nanoparticles at different percentage of iron addition is evident. With iron addition, the size of particles decreases, this was also proved with the calculation results shown in Table 4. Also a progressive agglomeration of particles takes place. At the 20 % iron addition, the exhibited agglomeration is

substantial. Agglomeration of particles decreases the accessible surface area of active particles and consequently detrimentally affects the photocatalytic activity. As a consequence of the dopants presence in the sample, crystallinity loss is observed, shown by the broadening of the XRD peaks. With the increasing amount of dopant added a significant presence of amorphous phase is present in the samples and at the highest dopant concentration the amorphous phase prevails. This is attributed to crystal lattice deformation due to introduction of smaller Fe atoms in the TiO_2 lattice. Crystallite growth of Fe^{3+} - doped TiO_2 grains is restrained during thermal treatment and this results in a broadening of XRD peaks.

In the case of 10 % doping co-presence of rutile phase is observed. Rutile is generally a worse performing catalyst compared to anatase (Bouras et al, 2007). Presence of rutile on expense of anatase can be therefore another reason for performance deterioration.

Another important fact in dopant addition is the formation of recombination sites by dopant introduction into the crystal lattice. The electron hole recombination rate of a semiconductor significantly influences its photocatalytic performance. The aim of doping is also to introduce atoms (Fe) which would act as electron scavengers to prevent recombination before oxidation and reduction reactions can take place. It seems that with the dopant addition in the case of iron introduction, the iron atoms act as recombination sites in the crystal lattice rather than e^- scavengers and so deteriorate the semiconductors performance since recombination of photogenerated electrons and holes takes place. In theory the recombination of e^-_{CB} and h^+_{VB} on dopant sites takes place when above optimum metal ions concentration is reached in the bulk of the semiconductor (Kumbhar and Chumanov, 2005). But in our case also very low dopant concentrations detrimentally affected the performance.

Another possible reason for lower activity of the doped TiO_2 lies in the energy of the shifted band gap of a doped semiconductor. With dopant addition lower energy states are created within the band gap as Fermi level is shifted. As lower-lying dopant E states (2.4 eV) have lower energy compared to undoped semiconductor, this in turn means that electrons occupying this level have a lower electron reductive capacity to reduce substances as they react with them on the surface of the semiconductor.

A possible reason for unexpectedly good performance of pure TiO_2 and also low iron addition TiO_2 thin films under Vis irradiation are the wavelengths of irradiation used for these experiments. The UV filter used progressively filtered out shorter wavelengths (see Fig. 8). But the filter's transmission of light was in the region of TiO_2 band gap still more than 50 % - at 380 nm it was 62 % and at 388 nm it was 81 %.

The filter used was chosen in order to imitate natural sunlight which reaches the surface of the Earth. The percent of filters transmission in the TiO_2 band gap region is an explanation why the pure TiO_2 and low dopant thin films exhibit the best photocatalytic performance even though most of the near Vis UV light is filtered out. In conclusion, iron doping may enhance visible light activity of TiO_2, but not solar light activity.

4.2.3.2. TiO_2 – Au 1-layer thin films

Photocatalytic activity of TiO_2 and Au/TiO_2 samples was analyzed as a function of the annealing temperature. In the case of pure TiO_2 samples the photocatalytic activity increases with higher annealing temperature used. Higher annealing temperature improves the systems' crystallinity (see 4.2.2.1) which in turn reduces the number of defects in the system, which act as recombination sites of photogenerated holes and electrons.

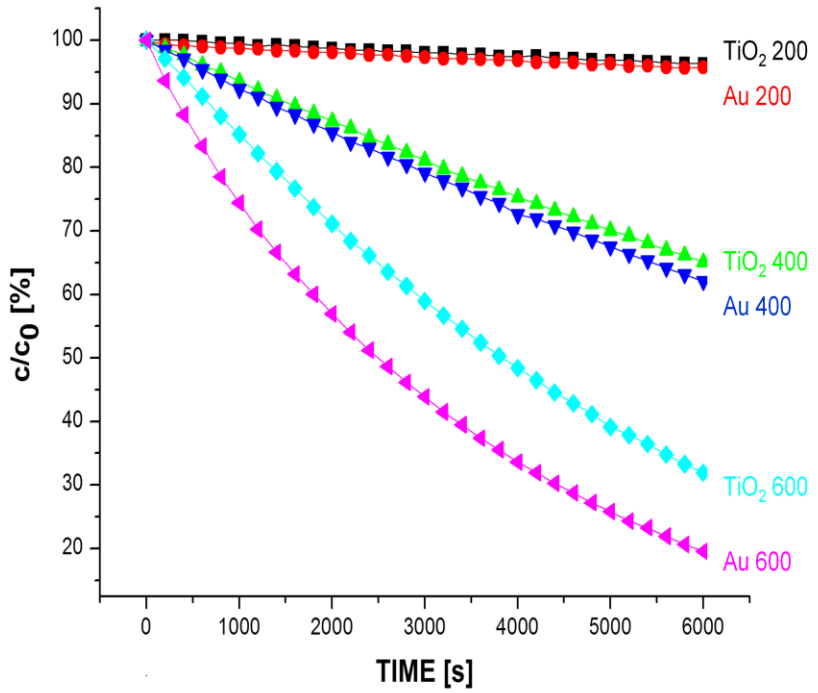

Figure 20: Percentage of photodegradation of Plasmocorinth B by pure TiO_2 and Au/TiO_2 thin films annealed at 200, 400 and 600 ºC.

In samples with gold nanoparticles on the TiO_2 surface, the gold presence enhanced the dye degradation (Fig. 20). Same as in the case of pure TiO_2 films, the Au/TiO_2 performance was increased at higher annealing temperature. The results suggest a direct influence of the morphological features on the photocatalytic performances of the films which are significantly affected by the size and shape of the gold particles.

The annealing temperature influences surface coverage, size and shape of Au nanoparticles which, in turn, play a key role in influencing the interfacial charge transfer during irradiation. SEM results (see 4.2.2.3.) show that an increase in annealing temperature from 200 to 600 ºC results in decreased TiO_2 coverage. Less coverage means more TiO_2 surface directly exposed to the irradiation and available for pollutant adsorption and light absorbance.

The improvement resulting from gold introduction can be explained by the fact that the obtained photocatalyst represent a composite surface acting both as a photon-capturing system and as gold promoted substrate. In Au/TiO_2 composites photocatalytic activity is enhanced by the interfacial charge transfer promoted by the gold particles. The photoejected electrons in the conduction band are attracted by the metal particles which act as their scavengers and thus prevent electron–hole recombination (Armelao et al., 2007).

It has been reported that the Au/TiO_2 contact has a Schottky barrier character. As a consequence, electrons excited by illumination at the gold particles are likely to move to the metal surface driven by the radiation electric field. Thus light-induced charge separation becomes easier, improving photocatalytic efficiency with respect to pure TiO_2. This mechanism beneficially affects photocatalytic activity up to an optimal Au/TiO_2 loading. The excess loading of metal particles may cover active sites on the TiO_2 surface and so reduce photodegradation efficiency (Sakthivel et al., 2006).

4.2.3.3. Multiple layers TiO_2 – Au thin films

Photocatalytic activity of TiO_2 and Au/TiO_2 samples was analyzed as a function of the number of TiO_2 layers and gold addition. TiO_2 was deposited as described in chapter 4.1.3. Samples were afterwards sent to Padova University, where gold was sputtered on the surface and consequently they were annealed at 500 ºC.

From the results in Figs. 21 and 22 can be concluded that in all cases the number of deposited TiO_2 layers had a pronounced effect on the photocatalytic performance of the films. In pure TiO_2 thin films and in gold sputtered ones the increased number of layers increased the photocatalytic activity of the thin films but there are some differences among the same number of layers and their performance under UV compared to UV-Vis irradiation.

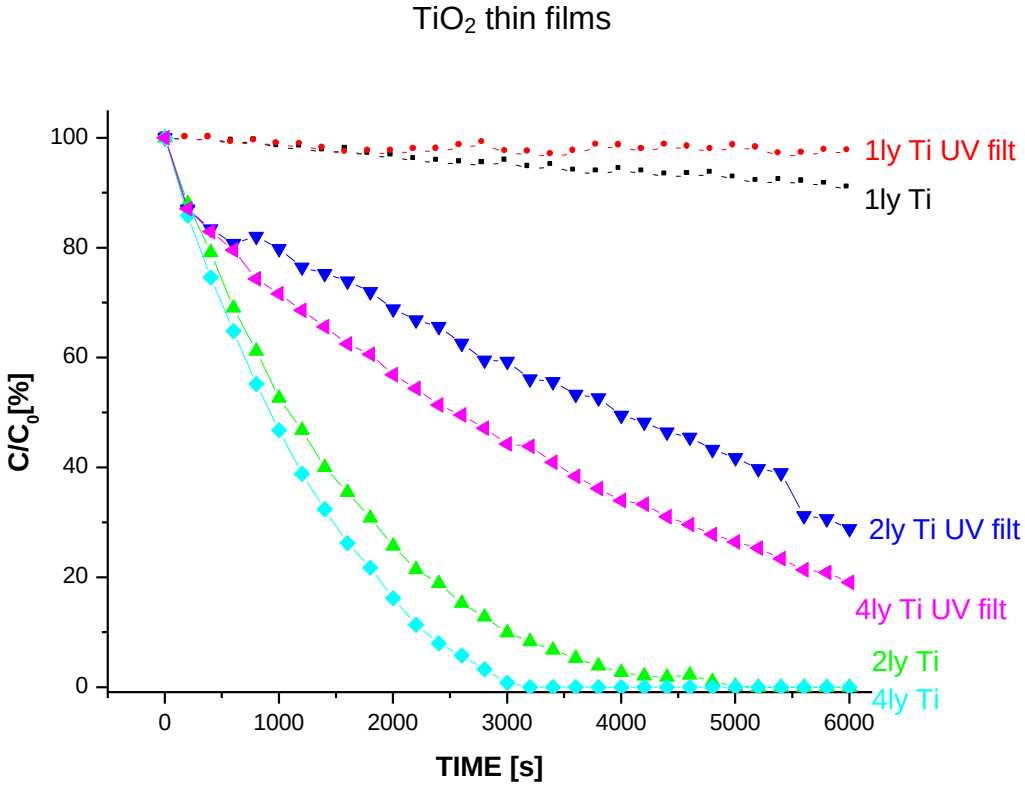

Figure 21: Percentage of photodegradation of Plasmocorinth B by different layers of TiO_2 thin films, with the use of UV and Vis irradiation (filter used to cut off the UV wavelengths).

gold sputtered TiO_2 thin films

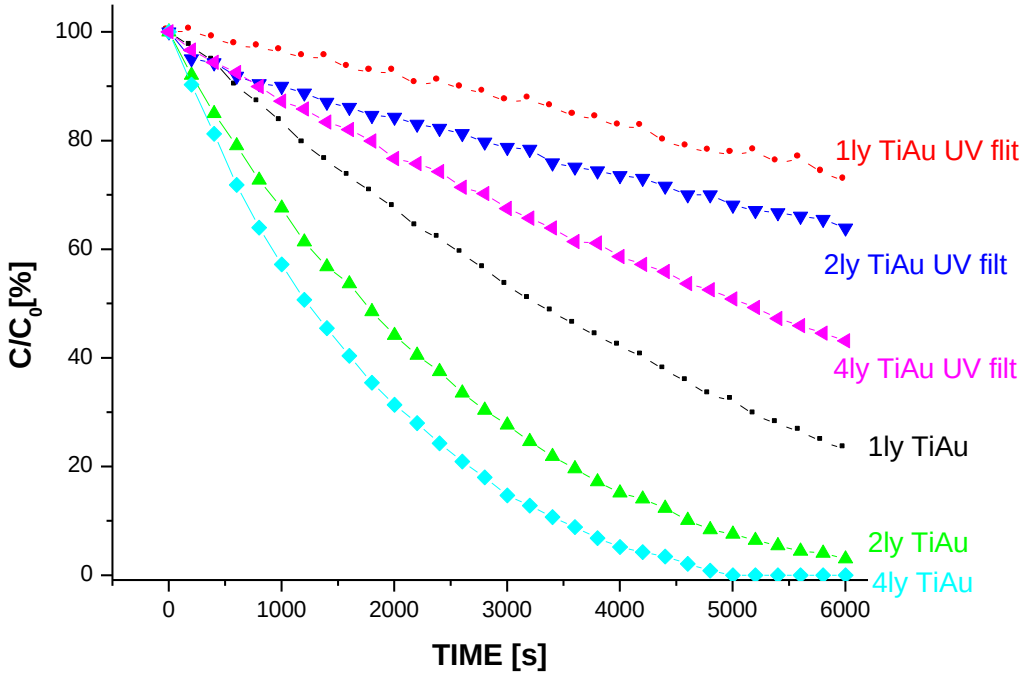

Figure 22: Percentage of photodegradation of Plasmocorinth B by different layers of TiO_2 gold sputtered thin films, with the use of UV – Vis or Vis irradiation.

There is a distinct difference in the 1 layer film's performance compared to 2 and 4 layer films, with regard to whether samples were gold sputtered or not. In the case of pure TiO_2 films (Fig. 21), the 1 layer films exhibited far the worst performance under UV–Vis and Vis light compared to 2 and the 4 layer films. The performance of a gold sputtered 1 layer TiO_2 films under Vis light was also rather poor, but under UV–Vis their performance was improved to a great extent compared to the unsputtered ones (Fig. 22).

In the case of 1 layer TiO_2 film, the pure TiO_2 version exhibits poor photocatalytic performance (under UV-Vis and UV light) because within a single layer of deposited semiconductor only a limited amount of photogenerated electrons and holes are produced. When the 1 layer TiO_2 film is sputtered with

gold, the charge transfer is facilitated and the obtained performance better. Gold particles on the surface act as photoejected electron scavengers thus reducing the recombination in the bulk of the semiconductor (Armelao et al., 2007). So in the case of 1 TiO_2 layer the gold addition acts beneficially on the films performance, as observed also in 4.2.3.2.

In the case of 2 and 4 layer films the situation is the opposite. Under UV-Vis and Vis light the sputtered films performance is deteriorated compared to unsputtered samples. The deterioration is indicated by a longer irradiation time needed to decolourise the dye solution. A clearly exhibited difference in performance of 2 and 4 layer gold sputtered films compared to pure TiO_2 ones can be attributed to hindering of the charge separation and transfer within the bulk of the semiconductor by the gold particles. It can also be attributed to the fact that gold, at the amount used, shields the semiconductor surface. The shielding effect which results in preventing the generation of conduction band electrons and valence band holes surpasses the beneficial effect of charge separation noticed in the case of 1 layer film.

As follows from the Fig. 21 the 2 and 4 layer films without any addition exhibit the best performance. Enough electrons and holes are generated in the bulk of the semiconductor to produce reactive oxidative species (ROS) to perform photobleaching of the used water sample.

4.3. CONCLUSIONS

The results of photodegradation experiments show that even though the band gap shift was achieved, the doping with iron had an overall detrimental effect on photocatalytic performance of all the doped films. The detrimental effect for catalytic performance was exhibited at all applied dopant concentrations, when irradiated with either UV-Vis or Vis light imitating solar irradiation on the Earth surface.

This is explained by several aspects of doping. Doping causes agglomeration of particles which in turn decreases the overall surface area. Also crystallinity loss is exhibited, shown by the broadening of the XRD peaks. With increasing amount of dopant addition amorphous phase becomes evident in the samples. This arises from crystal lattice deformation due to introduction of smaller Fe atoms into the TiO_2 lattice. In the case of 10 % doping also co-presence of rutile phase deteriorates the catalyst performing.

Moreover, doping forms recombination sites, namely iron atoms act as recombination sites in the crystal lattice rather than e^- scavengers and so deteriorate the semiconductors' performance. In our case also very low dopant concentrations detrimentally affected the performance. Furthermore, lower-lying dopant E states (2.4 eV) with lower energy compared to undoped semiconductor are introduced to the sample where electrons have lower electron reductive capacity to reduce substances.

When photocatalytic activity of TiO_2 and Au/TiO_2 samples was analyzed it has been established that under UV-Vis and Vis light in the pure TiO_2 samples the number of layers plays the most important role in determining photocatalytic performance which can be explained by the charge transfer within the bulk of the semiconductor.

The 1 layer TiO_2 film exhibited poor photocatalytic performance due to a limited amount of photogenerated electrons and holes produced, but when single layer TiO_2 film was sputtered by gold (it acts as electron scavenger), the charge transfer was facilitated as the gold particles acted as photoejected electron scavengers thus reducing the recombination in the bulk of the semiconductor which resulted in an increased performance.

However, in the case of 2 and 4 TiO_2 layers, the gold addition had a detrimental effect on the photocatalytical performance which is attributed to the hindering of the charge separation and transfer within the bulk of the semiconductor by the gold particles and to the shielding effect of the gold particles. The shielding effect (prevents generation of conduction band electrons and valence band holes) surpasses the beneficial effect of charge separation noticed in the case of 1 layer film. Among all tested films, the 2 and 4 layer films without any addition exhibit the best performance.

It can be concluded that in the case of multi layer pure TiO_2 thin films the best photocatalytic performance was obtained without various percent of dopant additions and without addition of noble metal on their surface. In the case of multilayer films both types of modifications turned out to have a deteriorating effect on the films performance. Only in the one layer film the gold addition substantially increased the photocatalytic performance of the film.

5. CONSTRUCTED WETLAND MODEL

5.1. EXPERIMENTAL

5.1.1. Model's geometry

A laboratory scale constructed wetland model was setup (Figs. 23, 24). Water was stored in a $1m^3$ reservoir.

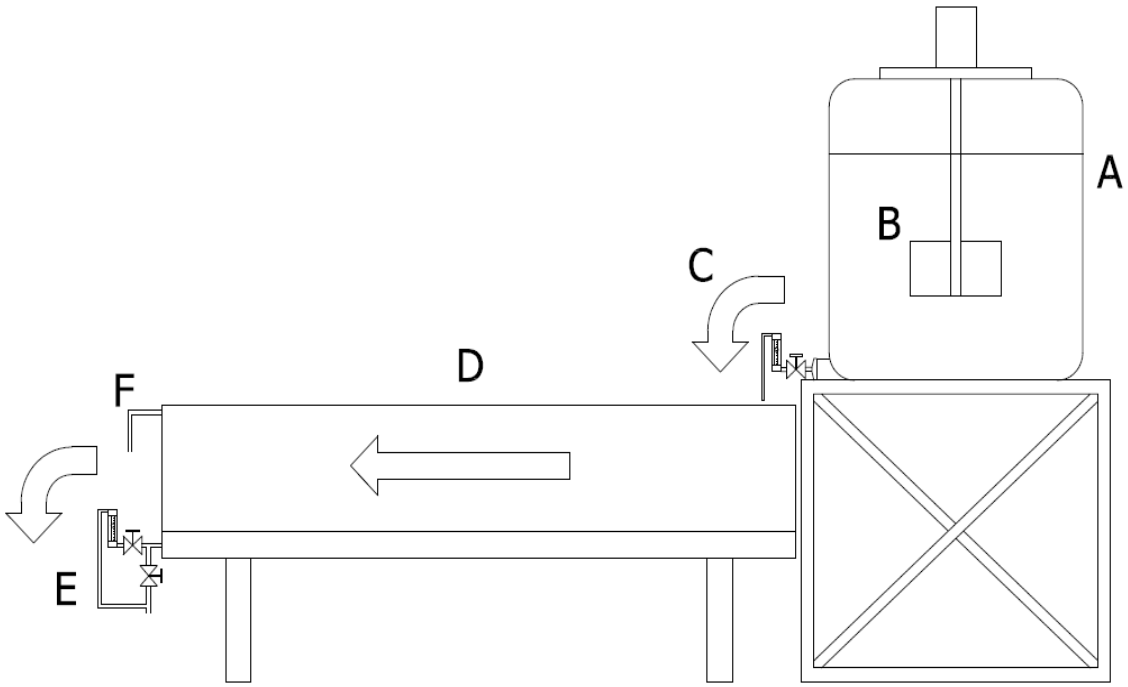

Figure 23: Scheme of the constructed wetland's setup with the reservoir and media compartment: A – reservoir, B – centrifuge reductive stirrer, C – inflow ball-bearing valve, D – CW model, E- outflow ball-bearing valve, F – bypass hose.

CW model had the following dimensions:

- 2.5 m in length (L),
- 0.5 m in height,
- 0.5 m in depth and
- 0.5 m in width (W).

The chosen width to length aspect ratio (L : W = 3) of the media filled part of the model is in accordance with the guidelines published by EPA (EPA Manual, 2000).

Figure 24: Photo of the CW model with reservoir, reductive stirrer and measuring valve.

The model had a wooden support construction. It had a high density polyethylene (HDPE) foil lining (Sinteza lining d.o.o., Slovenija), to assure impermeability. The reservoir was placed on a plinth, to enable gravitational flow towards model's inlet. Prepared wastewater in the reservoir was stirred by centrifuge reductive stirrer (Fig. 23, B) (RM– 600 PP series, Lastratech d.o.o.), in 10 s intervals. Two ball-bearing valves (Fig. 23, C and E) were installed at the inflow and outflow of the model. Ball-bearing valves were connected to flow-meters Hosco (USA), measuring range: 10-660 mL/min.

Model's porous volume was measured and it amounted for 250 L. Compartments are separated by wooden framed inox perforated plates, (φ = 5 mm), (Fig. 25, I), to stabilise media within the compartment. Silt media compartment was additionally lined with felt fabric (Fig. 25, F).

The model was longitudinally divided into four compartments:

- a media free influent compartment of 25 cm in length, from which water percolated evenly through whole media's cross section,
- media filled compartment of 150 cm in length,
- media filled compartment of 25 cm in length,
- a media free effluent compartment of 50 cm in length.

The water homogeneously percolated through the model, as observed in the last (media free) compartments' cross section at each model's filling. Sampling was done by means of two vertical tubes, (φ = 10 cm), installed at the distance of 45 cm and 141 cm (Figs. 25, 26) from the inflow into the sand media compartment.

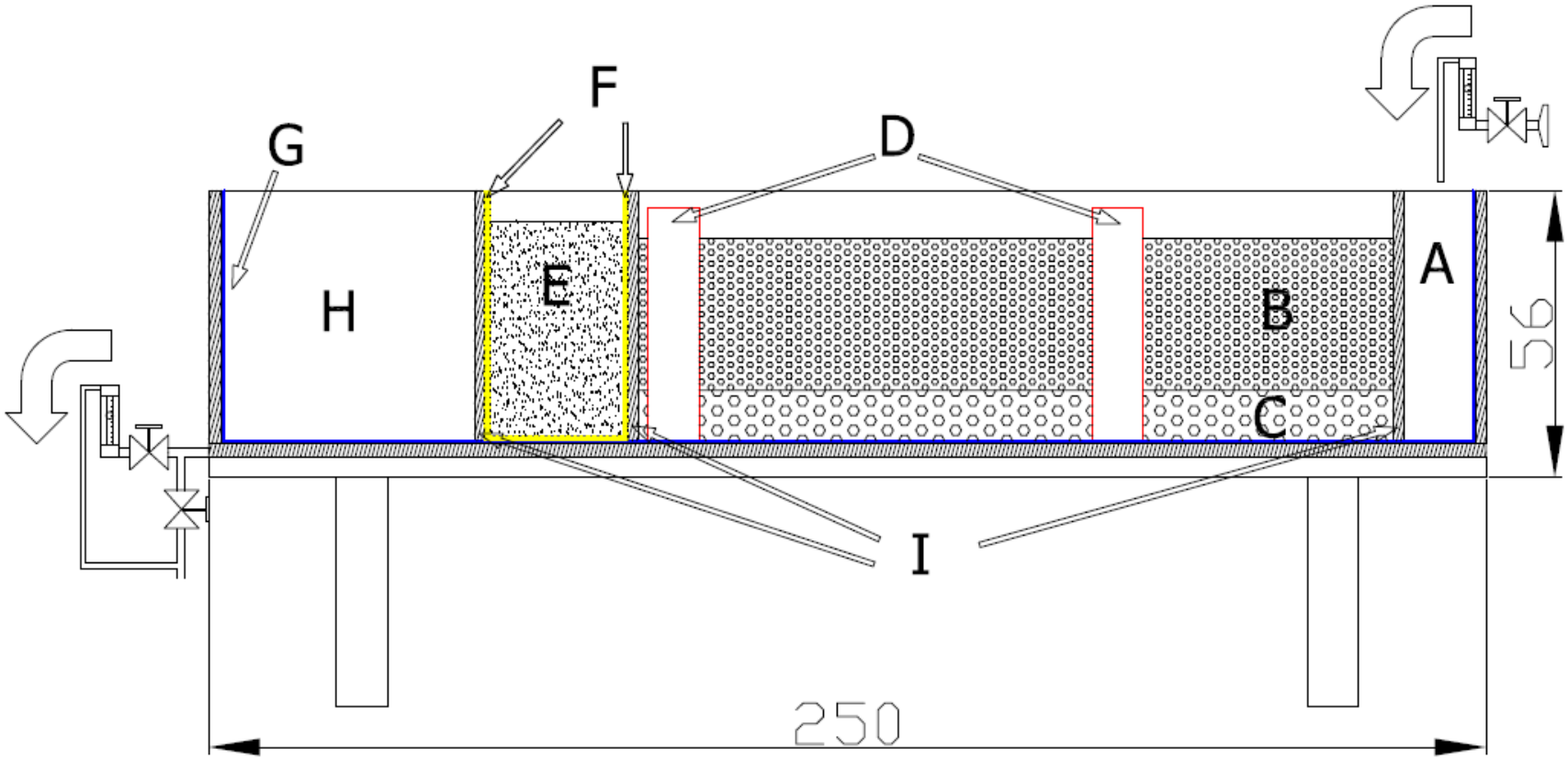

Figure 25: Scheme of the constructed wetland's media compartment: A - inflow compartment, B - media (sand, 2-4 mm), C - media (sand, 8-11 mm), D - vertical sampling tubes, E - media (silt, 0-1mm), F - felt lining, G - HDPE folium, H - outflow compartment, I - perforated membrane (courtesy of Marko Kete).

5.1.2. Media composition

Media in the first compartment was crushed and washed limestone sand of the following fractions:

- bottom 10 cm: sand of 8-11 mm particle size (Fig. 25, C);
- upper 40 cm: sand of 2-4 mm particle size (Fig. 25, B).

Crushed sand was obtained from Cestno podjetje Nova Gorica d.d., repository in Vrtojba, as washed sand. Sand was additionally washed under running water, to wash off the 0-2 mm fraction. Media in the second media filled compartment was flint stone silt, 0-1 mm in particle size (Fig. 25, E).

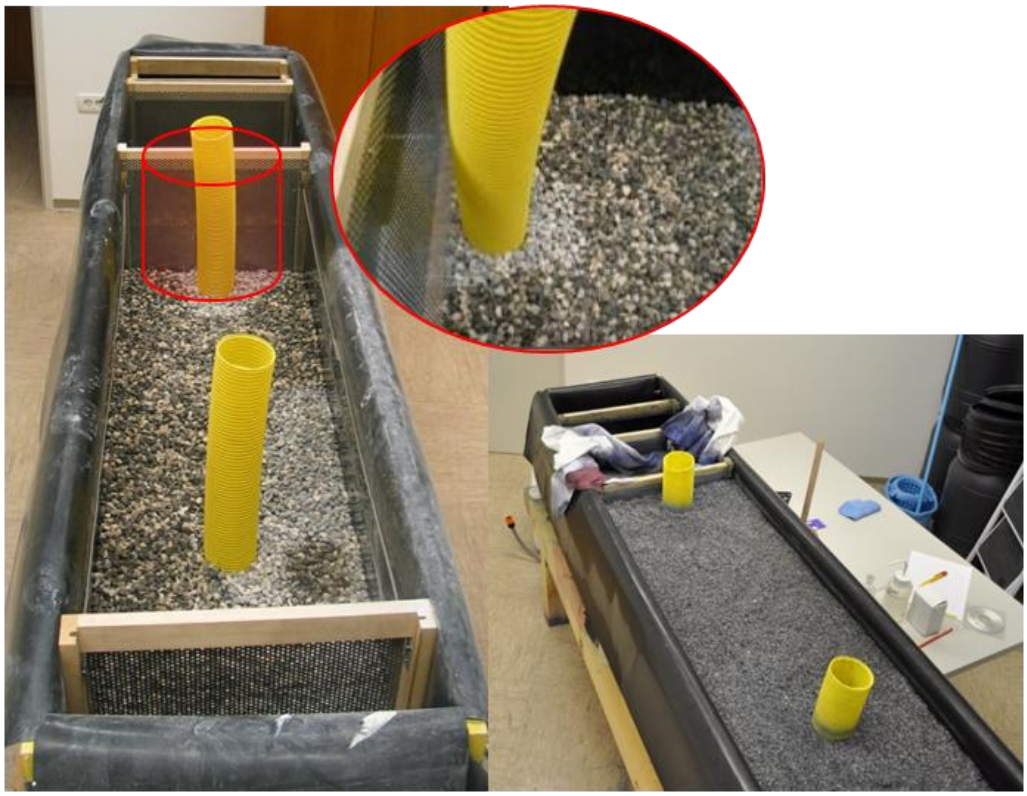

Figure 26: Photo of the media filled compartment, close look of the vertical sampling hose.

5.1.3. Colour absorbance to media

Adsorption of two dyes on the media used in the CW model was tested. Reactive Blue 19 and Reactive Black 5 in 33 and 100 mg/L concentration were added to prepared wastewater (as described in 5.1.5.).

20 g of 2-4 mm washed sand was weighted and dried in the oven (WTB Binder, Germany). 100 mL of prepared wastewater was mixed with media in 250 mL Erlenmeyer flasks. Samples were incubated at room temperature for 24 h on a shaker at 160 rpm. Adsorption at pH = 8.5 and 7 was tested. After the 24 h incubation time the samples were centrifuged for 10 min at 2500 rpm since the liquid part showed turbidity due to friction of sand particles during incubation. Absorbance was measured prior to and after incubation, degree of adsorption was calculated from Eq. (36):

$$\text{Degree of adsorption [\%]} = \frac{A_0 - A_a}{A_0} * 100 \quad (36)$$

5.1.4. Control of hydraulic retention time and flow in the CW model

Due to very low hydraulic retention time (HRT) of the media used in the model, the experimental HRT was controlled by ball-bearing valves at the inflow and outflow of the model. The flow, needed to achieve the chosen HRT was calculated from the model's porous volume (250 L). At 24 h HRT the flow was 175 mL/min. The inlet hydraulic load was 28.8 cm/day.

5.1.5. Preparation of textile wastewater used in the experiments

Wastewater used in the experiments was prepared according to parameters measured at the outflow of a local textile plant (Tekstina Ajdovščina). In this particular textile plant water from technological process and companies' domestic wastewater are mixed before discharge into the sewage system (Bulc

Griessler, 2005). The average values of wastewater parameters are given in Table 7.

Table 7: Average values of parameters measured during monitoring in year 2004 (E! 2983 "TEXTILE WET" report).

PARAMETER	AVERAGE VALUE
pH	8.2
COD [mg/L]	414
BOD_5 [mg/L]	148
TOC [mg/L]	94

Technological wastewater from the exhaust dying process has alkaline pH values (average pH = 12.5) in order to obtain maximal fixation of dyes onto the cellulose fibres. However, since in "Tekstina Ajdovščina" the technological wastewater from the dyeing step is later mixed with water from rinsing steps and companies' domestic wastewater, the average pH of water effluent drops considerably (Table 7).

Meat peptone, as nutrient which mimics the composition of municipal wastewater (Roš and Vrtovšek, 2004; Marques et al., 2008), and textile auxiliaries were added to simulate the actual wastewater composition from "Tekstina Ajdovščina". Information on dye concentration in the wastewater was obtained from Mr. Martin Krečič, textile technology department at "Tekstina Ajdovščina" (Krečič, 2009). Concentrations of textile auxiliaries (sequestering and wetting agent) were calculated from the dye dilution factor (dilution factor = 150). The concentration of alkalifying agent to be added was established experimentally with the aim to meet the wastewater pH value according to Table 7. Prepared wastewater composition is given in Table 8.

Table 8: Prepared wastewater composition and concentrations of added agents.

AGENT	CONCENTRATION	COMMERCIAL NAME
dye Reactive Blue 19	33 or 100 mg/L	Bezaktiv Blau V-RN SPE2
dye Reactive Red 22	100 mg/L	Bezaktiv Rot V-BN
dye Reactive Black 5	100 mg/L	Bezaktiv Schwartz V-B 150
sequestering agent	3.3 µL/L	KOLLASOL CDA®
wetting agent	13.2 µL/L	COLORCONTIN SAN®
levelling agent	30 µL/L	EGASOL SF®
meat peptone	0.25 mg/L	Meat Peptone, Fluka, 70174
stream water	~ 25 L/m^3	

All chemicals except meat peptone were purchased from Bezema Company (Switzerland), and used without further purification. Tap water was used to prepare the wastewater. Fresh wastewater was prepared prior to the start of each experiment.

The quantity of meat peptone added was established experimentally to meet the BOD_5 concentration of the company's effluent. Different amounts (0.03-0.5 mg/L) of meat peptone were mixed with nutrients (according to ISO 5815) and bacterial BOD_5 seed, R.T. Corporation (USA), to determine the quantity of peptone which gave the same BOD_5 results after 5 days of incubation as the effluent from the textile company. After the amount was established, the dyes and auxiliaries were added and the peptone addition was tested again to confirm the correct quantity.

5.1.5.1. Dyes used in the experiment

Wastewaters of three different colours were prepared with three dyes of different structure in order to establish colour reduction and treatment efficiency for structurally different dyes (Fig. 27).

- Reactive Blue 19 (Bezaktiv Blau V-RN SPE2) (RBL19), anthraquinone dye, a monofunctional dye with one vinylsulphonic group, molecular mass = 626 g/mol.

- Reactive Red 22 (Bezaktiv Rot V-BN) (RRD22), monoazo dye, a monofunctional dye with one vinylsulphonic group, molecular mass = 590 g/mol.
- Reactive Black 5 (Bezaktiv Schwartz V-B 150) (RBK5), a diazo, difunctional group with two vinylsulphonic groups and molecular mass = 991 g/mol.

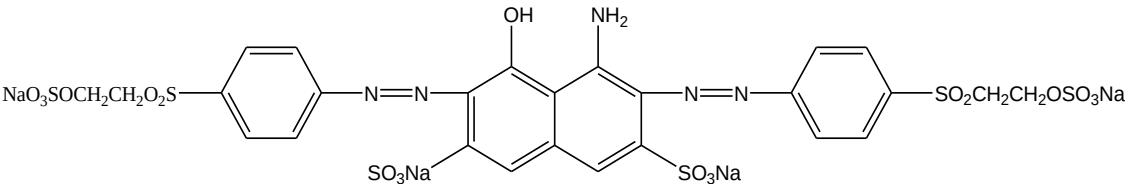

Reactive Black 5

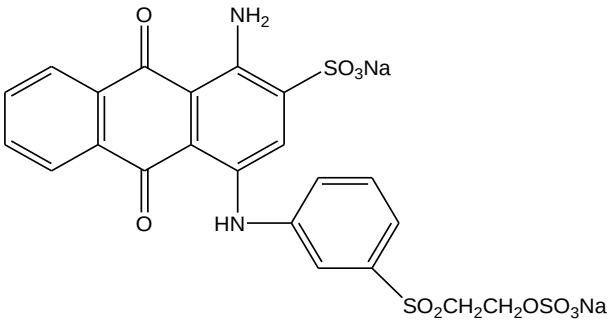

Reactive Blue 19

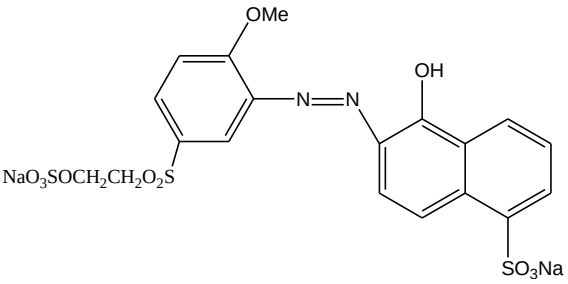

Reactive Red 22

Figure 27: Chemical structure of dyes used in the experiment.

5.1.6. Population of media with microorganisms

Prior to start of experiments the model was populated with faecal microorganisms from a local municipal wastewater treatment plant (WWTP). 400 L of wastewater were pumped from first (mechanical) treatment stage basin at the WWTP and transported to the laboratory where the water was pumped into the reservoir. The wastewater percolated through the CW model media. A week later the same procedure was repeated.

As the prepared wastewater for decolouration and degradation experiments didn't contain any microorganisms, approximately 25 L of water from a stream near the university building was added. This water was a large source of uncertainty concerning the prepared wastewater composition since seasonal and precipitation variation influenced flow and temperature and consequently concentration of microorganisms the stream's water. Seasonal and precipitation variation was considered to minimise the uncertainty. Streams' catchment area is a valley with family houses, connected to septic tanks which are usually not waterproof. With the uncertainty in mind, the stream water was still chosen as the best source of similar microorganism composition to be added to prepared wastewater as the consortium brought to the media from the WWTP (Jamieson, et al., 2004).

With the stream water added to each reservoir of prepared wastewater the intention was to provide similar microorganisms' consortium for each experiment and to avoid a decrease in microorganisms' number due to washing out of the system by sequential experiments.

5.1.7. CW model operation

Prior to onset of experiments, the model was operated with the prepared wastewater containing textile dyes for four weeks, HRT was 24 h.

5.1.7.1. 33 mg/L Reactive Blue 19 degradation experiments

During each experiment the model worked under continuous operation regime. The RBL19, 33 mg/L experiment was performed in the following steps, given in Table 9.

Table 9: Steps of the 33 mg/L Reactive Blue 19 degradation experiments.

DAY, APPROXIMATE SAMPLING TIME	STEP OF THE EXPERIMENT
day 0 - 9 h	fresh wastewater prepared in the reservoir and fed to the CW model
	when the model was full, the valves at the inflow and outflow were closed → the same volume of water was left in the model for 24 h
day 1 - 9 h	day 1 sampling - after 24 h from the start of experiment
	inflow and outflow valves were opened and set at a flow of 175 mL/min
day 2 - 9 h	day 2 sampling - after 48 h from the start of experiment
day 3 - 9 h	day 3 sampling - after 72 h from the start of experiment
day 4 - 9 h	day 4 sampling - after 96 h from the start of experiment

At day 4 sampling the water level was already decreased to half of the media height and later on day 4 the CW media dried. Residual volume of the reservoir was emptied (through the model) and the CW was left dry for 2.5 days until the next experiment.

5.1.7.2. 100 mg/L Reactive Blue 19, Reactive Red 22 and Reactive Black 5 degradation experiments

During each experiment the model worked under continuous operation regime. The 100 mg/L dye concentration experiments were performed in the following steps, given in Table 10.

Table 10: Steps of the 100 mg/L Reactive Blue 19, Reactive Red 22 and Reactive Black 5 degradation experiments.

DAY, APPROXIMATE SAMPLING TIME	STEP OF THE EXPERIMENT
day 0 - 9 h	fresh wastewater prepared in the reservoir and fed to the CW model
	when the model was full, the valves at the inflow and outflow were closed → the same volume of water was left in the model for 24 h
day 1 - 9 h	inflow and outflow valves were opened and set at a flow of 175 mL/min
day 1 - 14 h	day 1 sampling - after 29 h from the start of experiment
day 2 - 14 h	day 2 sampling - after 53 h from the start of experiment
day 3 - 14 h	day 3 sampling - after 77 h from the start of experiment

On contrary to chapter 5.1.7.1. in chapter 5.1.7.2. experiments the valves in the CW model were opened 5 h prior to sampling of the day 1 sample (and 24 h after the reservoir was filled with freshly prepared wastewater). Namely, as following from the Table 9, the water sampled at the outflow at the time of valve opening was water from outflow compartment and not the water, which was actually in the media between day 0 and day 1. With the span of 5 h between valve opening and sampling (Table 10) some of the water from the media percolated to the outflow compartment. Due to the changed sampling regime, the sampling on day 4 wasn't possible; after sampling on day 3 the reservoir was empted and the CW was dried up for 3.5 days and then filled again with a freshly prepared wastewater.

5.1.8. Model performance

Assessment of the model's performance was evaluated by the following physical – chemical parameters: pH, temperature (T), dissolved oxygen concentration (DO) and electric conductivity measurement (EC). These parameters were measured in situ at 4 measuring points – inflow, outflow and two vertical tubes in the media.

Sampling was carried out at the inflow compartment and at the outflow from the model. Samples were directly analysed for the following parameters:

colouration, chemical oxygen demand (COD) and biological oxygen demand (BOD_5). Samples for *Vibrio fischeri* toxicity test were frozen and analysed later. Total organic carbon (TOC) and total nitrogen (TN) measurements were done only for the first set of experiments (5.1.7.1.) due to persistent problems with the TOC analytic instrument in later in 2010.

5.1.8.1. Methods

- ABSORBANCE of the samples was measured across the UV and Vis spectra (190–1100 nm) in quartz cell with 10mm optical length, on Hewlet Packard 8453 UV-Vis spectrophotometer. Calibration curves were done for each of the used dyes, to establish relation between the absorbance and dye concentration.

- pH, T, DO and EC: parameters were measured using the WTW MultiLine P4 portable universal pocket-size meter with pH electrode (measurement uncertainty = 0.01), SenTix 41 temperature probe (measurement uncertainty = 0.1), Cell Ox 325 dissolved oxygen probe (measurement uncertainty = 0.5 %) and TetraCon 325 standard conductivity cell (measurement uncertainty = 0.5 %).

- COD measurements were done with determined photometrically on Nanocolor 500 D photometer (Macherey-Nagel, Germany) using standard COD (ISO 15705) digestion solutions in 100-1500 mg/L range (measurement uncertainty = ±3 %). 2 mL of the sample was introduced into the digestion solution, shaken and thermostated at 148 °C for 210 min, left to cool and COD was photometrically measured.

- BOD_5 was determined after incubation in WTW OxiTop measuring bottles. 250 mL of samples were incubated according to standardised

procedure (ISO 5815) (measurement uncertainty = ±1 %). Samples were stirred by a magnetic stirrer and incubated at 20 °C for 5 days.

- TOC and TN measurements were done by differential method measuring total carbon, inorganic carbon and total nitrogen, on the Analytic Jena, series 3200 analyzer. Due to problems with catalyst clogging in the instruments' furnace column, the method was adapted for measurements of the raw and pre-treated prepared wastewater samples. Samples were diluted in sample: water ratio = 1:3 and manually acidified (0.1 M HCl, 30 µL) to values below pH 6 prior to beginning of measurement, due to very fast catalyst ageing. The volume of the sample was 300 µL; furnace temperature 750 °C.

- Toxicity of the samples was measured on LUMIStox (dr. Lange, Germany) toxicity test for the inhibition of bioluminescence of *Vibrio fischeri*. After sampling the samples were frozen to – 23 °C, then defrosted and analysed at the end of each experiment (after 4^{th} day) according to the procedure (ISO 11348). The pH of the samples was corrected and salt was added to reach the salinity demanded by the test organism. Incubation time of the solutions was 30 min at 15 °C. Results of the samples were compared to an aqueous control with colour correction.

5.2. RESULTS

5.2.1. Model's geometry

Due to the position of valve and flow meter at the reservoir's outlet which needed to be below water level, the reservoir had a 70 L residual volume. This amount of water, left in the reservoir after each experiment, was washed out before fresh wastewater was prepared.

The model had an additional hose mounted at the top of the wooden frame, to prevent the possible flooding events (Fig. 25, F). Silt media compartment (Fig. 25, F) was additionally lined with felt fabric, since the inox membrane didn't prevent it from washing out.

5.2.2. Dye absorbance to the media

Results of dye absorption experiments of to the media are given in Table 11.

Table 11: Average absorption values measured prior to and after 24 h incubation time.

DYE, CONCENTRATION	ABSORBANCE BEFORE INCUBATION		ABSORBANCE AFTER INCUBATION	
	pH = 7.0	pH = 8.5	pH = 7.0	pH = 8.5
Reactive Blue, 33 mg/L	0.332	0.326	0.397	0.385
Reactive Blue, 100 mg/L	0.899	0.935	0.961	0.972
Reactive Black, 100 mg/L	3.213	3.198	3.331	3.204

5.2.3. Hydraulic retention time

As the model was filled with sand media, expectedly HRT was very short (6 min). To increase the retention time of sand media, silt media was added. Silt addition assured even percolation of the water through the whole cross section and prolonged the actual hydraulic retention time of the media to 35 min.

The 24 h HRT was chosen with the aim to obtain feasible conditions in the CW media which would promote dye decolouration and degradation. Since, according to the literature, dyes are decolourised under anaerobic conditions (Yoo et al., 2000; Beydilli et al., 2000; Isik and Sponza, 2008), the chosen HRT enabled the establishment of anaerobic locations in the media, where reductive decolouration reactions took place. To establish a HRT in the chosen range, valves had to be installed at the inflow and outflow of the model.

5.2.4. Prepared textile wastewater composition

The concentration of dyes in the prepared wastewater in the first set of experiments (with RBL19) was chosen as 1/3 of the actual dye concentration (100 mg/L) (Krečič, 2009) in the textile effluent, with the aim to test systems performance.

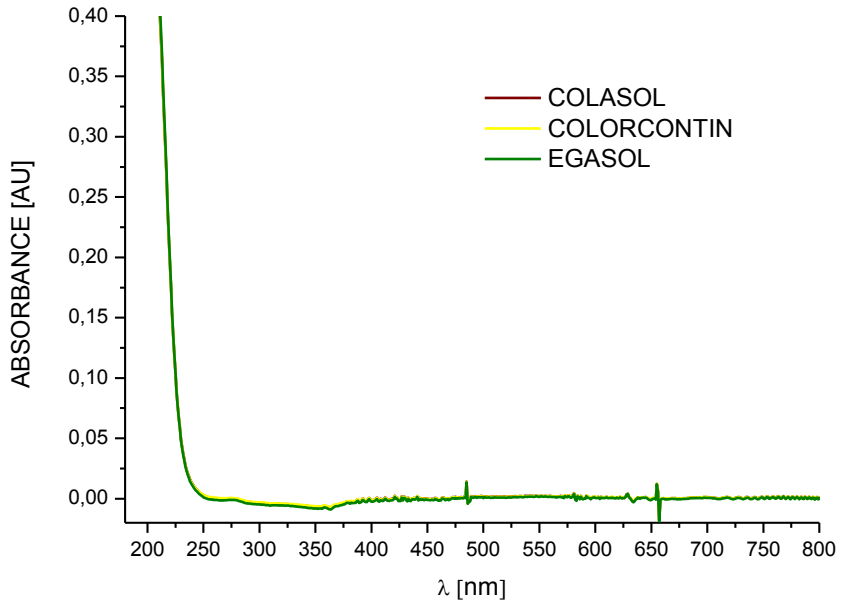

Figure 28: Absorbance spectra of all textile auxiliaries used in the experiment, Colasol, Colorcontin and Egasol in the concentrations used in the prepared wastewater.

As can be seen from the spectra in Fig. 28, the absorbance spectra of the auxiliaries used in the experiment exhibit no absorbance in the visible range which could interfere with the dyes' absorbance spectra.

5.2.5. Degradation experiments, RBL19, 33 mg/L

Program SAS/STAT (SAS Software, Version 8.01) was used for statistical analysis of experimental data. Basic statistical parameters were calculated by MEANS procedure and UNIVARIATE procedure was used to test normality of data distribution. Pearsons correlation coefficients were calculated with CORR procedure.

5.2.5.1. pH, O_2, EC and T measurements, RBL19, 33 mg/L

Model was operated at room conditions. Day 0 water temperature was tap water temperature, which depended on the outside temperature (seasonal variation). From day 0 to day 4 the inflow compartment water temperature increased for 8 °C since water, stored in the reservoir under room conditions, warmed. Also water temperature in the outflow compartment increased with days of experiment, but the difference was less than 2 °C.

pH of prepared wastewater measured in the reservoir was 8.2 on average, as following from the "Tekstina Ajdovščina" wastewater composition obtained during monitoring in the year 2004 (Table 7). In the inflow compartment the pH was on average 8.0 on day 0. On days 1 and 2 it decreased to 7.4 on average and increased again to 7.8 through the days 3 and 4. The pH values in the outflow compartment ranged between 7.2 and 7.4 on days 1 to 4. On general they are lower compared to inflow values but on day 2 and 3 the values differ for only up to 0.2 (all Table 12).

Table 12: measured pH, O_2, EC and T values at the inflow compartment and outflow of the model.

DAY		INFLOW		OUTFLOW	
AVERAGE, RANGE			T [ºC]		T [ºC]
	pH	8.0 (7.9 - 8.2)		7.5 (7.3 - 7.9)	
0	O_2 [mg/L]	6.4 (2.06 - 9.58)	10.4 (9.7 - 11.2)	1.8 (1.07 - 2.75)	15.7 (13.9 - 18.9)
	EC [µS]	334 (313 - 358)		437 (391 - 524)	
	pH	7.4 (7.2 - 7.6)		7.3 (7.2 - 7.5)	
1	O_2 [mg/L]	0.7 (0.07 - 2.69)	13.2 (12 - 14.4)	0.08 (0.06 - 0.1)	15.4 (13.7 - 17.3)
	EC [µS]	356 (334 - 390)		442 (412 - 497)	
	pH	7.4 (7.3 - 7. 6)		7.4 (7.2 - 7.6)	
2	O_2 [mg/L]	0.1 (0.08 - 0.12)	16.8 (15.3 - 17.6)	0.09 (0.07 - 0.11)	15.8 (13.8 - 16.9)
	EC [µS]	385 (361 - 404)		488 (468 - 519)	
	pH	7.5 (7.3 - 7.6)		7.2 (7.2 - 7.3)	
3	O_2 [mg/L]	1.2 (0.08 - 3.4)	17.9 (16.6 - 18.9)	0.09 (0.08 - 0.1)	16.6 (15.1 - 17.5)
	EC [µS]	446 (426 - 473)		490 (478 - 494)	
	pH	7.8 (7.5 - 8.4)		7.2 (7.1 - 7.3)	
4	O_2 [mg/L]	2.8 (0.14 - 4.3)	18.4 (15.8 - 20.6)	0.1 (0.07 - 0.13)	17.1 (15.2 - 19.1)
	EC [µS]	454 (432 - 468)		479 (464 - 498)	

Electric conductivity (EC) values (Table 12) at the inflow compartment increased from day 0 to day 4 for more than 100 µS, for 35 % of the initial value on average. Values at the outflow compartment on days 1, 2 and 3 exhibited an

increase in the EC value compared to the inflow values for more than 100 µS. The difference between the inflow and the outflow on day 4 falls and accounts for 33 µS.

The dissolved oxygen (DO) concentration (Table 12) changed rapidly from day 0, when the fresh wastewater was prepared, to the following days of experiment. In freshly prepared wastewater the oxygen concentration was high and accounted for 6.4 mg O_2/L. After one day in the reservoir the concentration in the inflow compartment decreased to 0.7 mg O_2/L and on day 2 it accounted for only 0.1 mg O_2/L. On days 3 and 4 it increased again to 1.2 and 2.8 mg O_2/L respectively. Water in the reservoir was mixed in 10 s intervals by centrifuge reductive stirrer as described in 5.1.1.

An increase on days 3 and 4 took place due to the fact, that the water level in the reservoir dropped and the reductive stirrer mixed the water more vigorously through the whole depth of the water volume, namely, the stirrers' propellers were placed close to the bottom of the reservoir. Vigorous mixing introduced more oxygen into the remaining wastewater and measured concentration at the inflow compartment increased.

DO concentrations at the outflow compartment decreased considerably compared to the model's inflow compartment on days 1 and 2, when the difference accounted for several orders of magnitude - concentrations in the inflow were 0.7-6.4 mg O_2/L and at outflow 0.08 and 0.1 mg O_2/L. The difference lowered on the third day when concentration dropped to 0.1 mg O_2/L in the inflow compartment and it lowered to 0.09 mg O_2/L in the outflow compartment.

5.2.5.2. COD results, RBL19, 33 mg/L

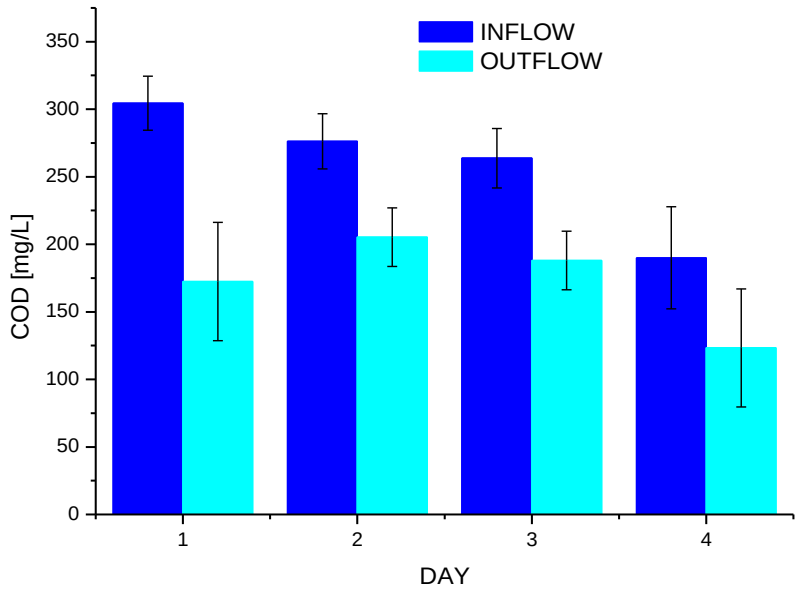

Figure 29: COD values at inflow compartment and outflow from CW model, RBL19, 33 mg/L.

COD values of prepared wastewater (Fig. 29) at the inflow compartment on day 1 were 305 (±25) mg/L on average and decreased to 190 (±33) mg/L on average on day 4. The outflow COD values were lower on the day 1, 173 (±44) mg/L, increased on day 2 to 205 (±22) mg/L and decreased to the end of experiment - day 4 - to on average 123 (±44) mg/L. The removal efficiency ranged from 26 to 43 %. COD value was found to (negatively) correlate with EC values ($r = -0.89979$, $p < 0.0001$).

The COD data in mass flow is given in Table 13.

Table 13: Mass flow in g/day for COD.

COD	INFLOW [g/day]	OUTFLOW [g/day]
day 1	77	44
day 2	70	52
day 3	67	47
day 4	48	31

5.2.5.3. BOD_5 and TOC results, RBL19, 33 mg/L

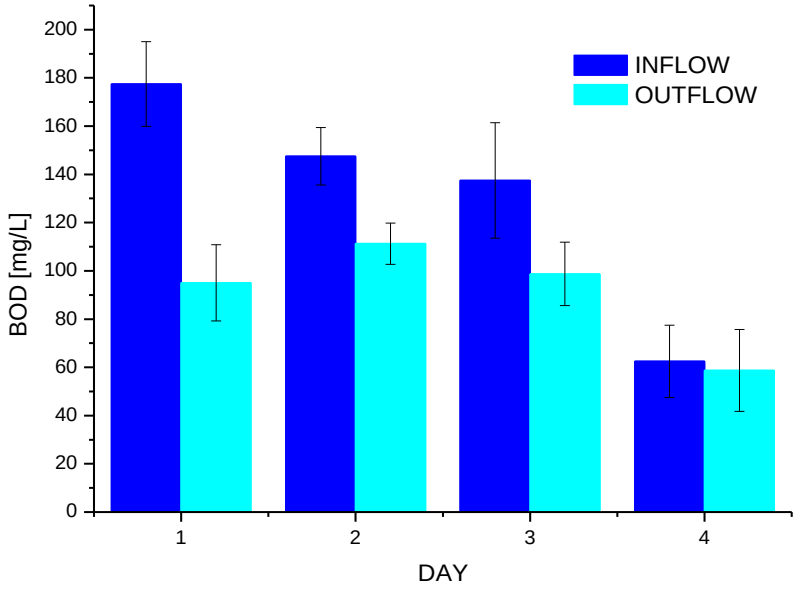

Figure 30: BOD_5 values at inflow compartment and outflow from CW model, RBL19, 33 mg/L.

BOD_5 and TOC values (Fig. 30 and 31) exhibit the same trend as COD values at the inflow compartment and outflow from the model. The average BOD_5 value on day 0, as wastewater was prepared, was 178 (±18) mg/L. BOD_5 values at the inflow decreased with days from the start of the experiment. A more pronounced decrease was exhibited between day 3 and 4 when average BOD_5 value

decreased from 138 (±24) to 63 (±15) mg/L and average TOC value from 89 (±4) to 56 (±1) mg/L. BOD value was found to (negatively) correlate with EC values ($r = -0.79789$, $p < 0.0002$).

As the level of water in the reservoir decreased below half of the volume, reductive stirrers' water mixing was more vigorous due to lower water volume. When the level in the reservoir decreased below ¼ of the reservoirs' volume, more air bubbles were present in the remaining water volume (visible observation). Consequently DO in the water started to increase on the day 3 and increased substantially by day 4, from 0.1 mg/L or lower to on average 2.8 mg/L (Table 12).

BOD_5 and TOC outflow values exhibited the same trend as COD outflow values; lower on the day 1, increased on the day 2 and a decrease towards the end of the experiment due to removal reduction.

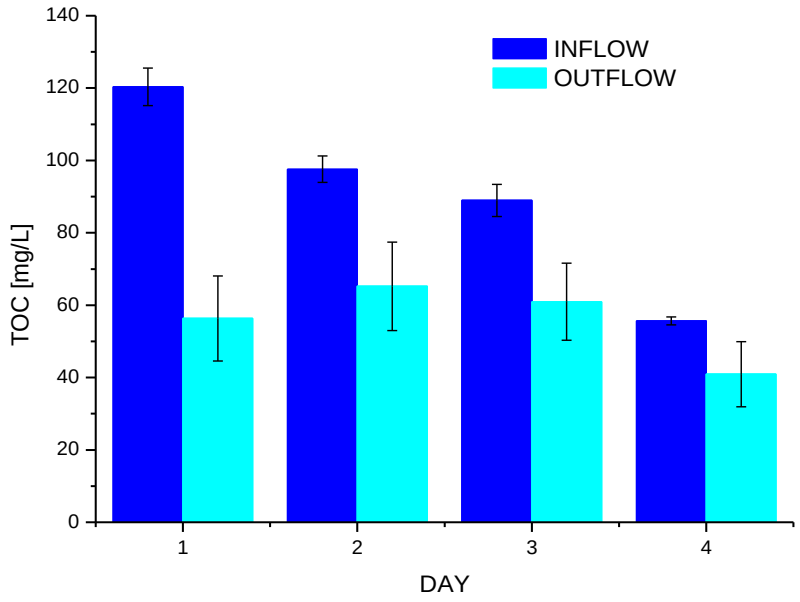

Figure 31: TOC values at inflow compartment and outflow from CW model, RBL19, 33 mg/L.

In Table 14 the BOD_5/COD ratio at inflow compartment and outflow from CW model is given.

Table 14: BOD_5/COD ratio at inflow compartment and outflow from CW model, RBL19, 33 mg/L.

DAY	INFLOW BOD_5/COD RATIO	OUTFLOW BOD_5/COD RATIO
1	0.58	0.55
2	0.53	0.54
3	0.52	0.53
4	0.33	0.48

5.2.5.4. Toxicity results, RBL19, 33 mg/L

The samples' toxicity values are shown in the Fig. 32. Prepared wastewaters' toxicity in the inflow compartment was 61 % (SD±10) on days 1 and 2 and it dropped to 42 % (SD±5) on the last day of the experiment. But at the outflow it was near to 100 % on the day 1 and 100 % on all following days.

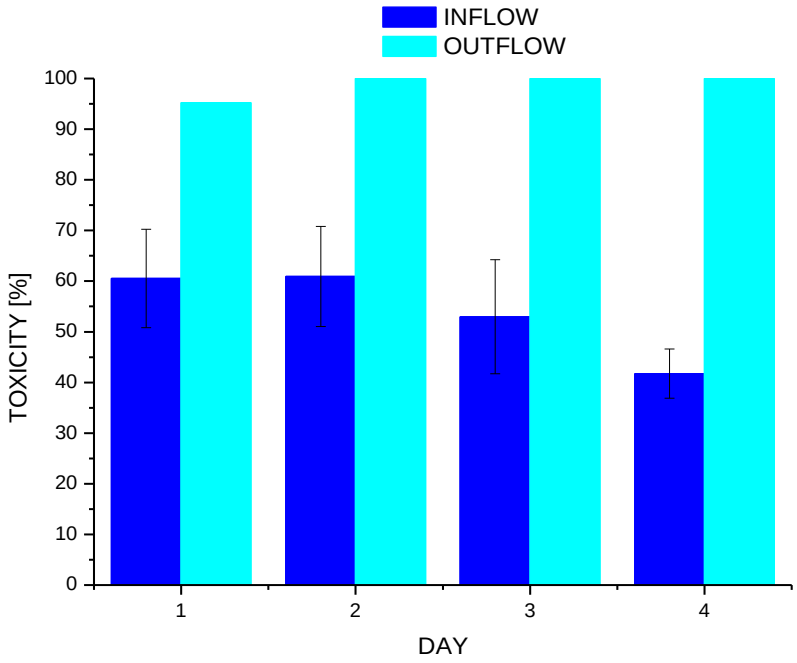

Figure 32: Toxicity values at inflow compartment and outflow from CW model, RBL19, 33 mg/L.

5.2.5.5. Decolouration results, RBL19, 33 mg/L

In the Fig. 33 decolouration data of the 33 mg/L RBL19 are shown. On day 1, when sampling was done at the same time as the valves were opened (as following from the 5.1.7.1.), decolouration percentage was very low (4 % on average). On following days it increased, to 36 % on day 2 and then for 10 % each day and reached 56 % on day 4. RBL19 decolouration was found to negatively correlate with oxygen concentration (r = -0.60589, p = 0.0129) and positively correlate with EC (r = 0.73105, p = 0.0013).

On day 1 the average decolouration was 4 % but the SD was high, 14 % namely. In two experiments, no. I and no. II some dye remained in the system from the previous experiment and increased the absorbance of the CW model effluent. But as can be seen from the Fig. 34 on average the absorbance in the first 24 hours didn't change.

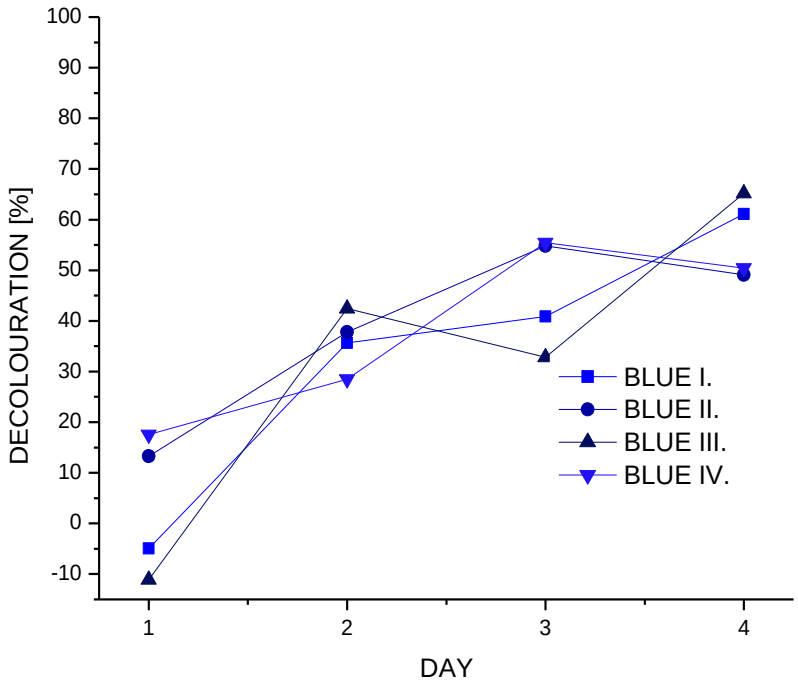

Figure 33: Decolouration % in separate experiments on different days of experiment, Reactive Blue 19, 33 mg/L.

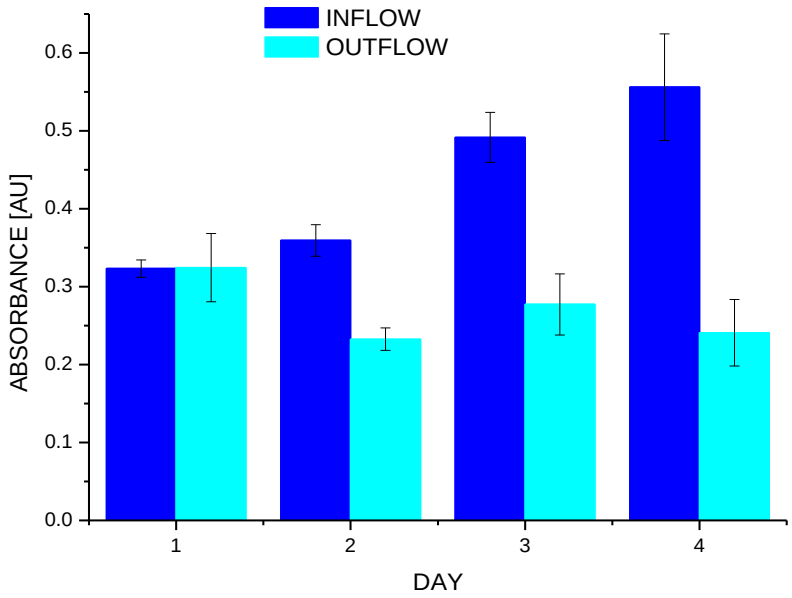

Figure 34: Average absorbance on different days of experiment, Reactive Blue 19, 33 mg/L.

5.2.6. Degradation experiments, RBL19, RRD22 and RBK5, 100 mg/L

5.2.6.1. pH, O_2, EC and T measurements, RBL19, RRD22 and RBK5, 100 mg/L

The sampling was done at the inflow compartment of the CW model, at the tube no. I., tube no. II. and at the outflow from the model (Fig. 25). The results are given in Table no. 15.

CW model was operated under same conditions as those described in 5.2.5.1. Initial water temperature was tap water temperature, which depended on seasonal variation in outside temperature. Compared to experiments with RBL19, 33 mg/L, experiments with a 100 mg/L concentration of all three dyes

were performed in the spring and summer months. Consequently, T of water in the model increased for 1-3 °C due to high outside temperatures.

pH on day 0 was adjusted to the values after the Table 7, as described in chapter 5.1.5. Again, as water reached the inflow compartment, the pH dropped to 8.17 on average. On days 1, 2 and 3 the pH was 7.5 on average. pH values in the outflow compartment ranged between 7.4 and 7.6. Measured outflow values are lower compared to inflow for 0.1-0.2 (Table 15).

Table 15: Measured pH, O2, EC and T values at the inflow and outflow of the model.

DAY		INFLOW		TUBE I.		TUBE II.		OUTFLOW	
AVERAGE, RANGE			T [ºC]		T [ºC]		T [ºC]		T [ºC]
	pH	8.2 (7.7 - 8.7)		8.0 (7.6 - 8.6)		7.9 (7.5 - 8.4)		7.6 (7.3 - 7.9)	
0	O_2 [mg/L]	6.5 (5.5 - 7.7)	13.6 (11.9 - 15.1)	3.5 (2.2 - 5.9)	14.8 (14 - 15.5)	1.2 (0.2 - 3.7)	15.3 (14.7 - 15.7)	0.9 (0.3 - 1.8)	17.2 (15.2 - 18.7)
	EC [µS]	373 (344 - 445)		388 (364 - 454)		403 (369 - 458)		549 (425 -911)	
	pH	7.7 (7.5 - 8.2)		7.5 (7.3 - 7.9)		7.4 (7.2 - 7.9)		7.5 (7.3 - 7.8)	
1	O_2 [mg/L]	0.6 (0.1 - 3.2)	17.1 (15.1 - 18.8)	0.1 (0.1 - 0.2)	16.9 (14.9 - 18.6)	0.1 (0.1 - 0.1)	16.8 (14.8 - 18.5)	0.2 (0.1 - 0.6)	16.8 (14.2 - 19)
	EC [µS]	393 (374 - 430)		461 (420 - 496)		506 (451 - 533)		531 (472 - 600)	
	pH	7.5 (7.3 - 7.8)		7.3 (7.2 - 7.5)		7.3 (7.2 - 7.4)		7.4 (7.3 - 7.5)	
2	O_2 [mg/L]	0.1 (0.1 - 0.3)	18.4 (15.9 - 20.2)	0.1 (0.1 - 0.1)	18.2 (16.6 - 19.4)	0.1 (0.1 - 0.1)	17.8 (16.6 - 18.9)	0.1 (0.1 - 0.1)	17.8 (15.8 - 19.4)
	EC [µS]	440 (406 - 533)		492 (425 - 554)		542 (472 - 596)		544 (480 - 611)	
	pH	7.6 (7.3 - 8.1)		6.2 (7.2 - 7.7)		6.1 (7.2 - 7.6)		7.4 (7.2 - 7.4)	
3	O_2 [mg/L]	1.4 (0.1 - 4.1)	19.3 (17.9 - 20.6)	0.1 (0.1 - 0.1)	19.2 (17.8 - 20.5)	0.1 (0.1 - 0.1)	19.1 (17.8 - 20.3)	0.1 (0.1 - 0.1)	18.9 (17.8 - 20.4)
	EC [µS]	471 (447 - 512)		423 (480 - 531)		458 (488 - 588)		530 (496 - 560)	

Again as in RBL19, 33 mg/L also in RBL19, RBK5 and RRD22, 100 mg/L experiments, DO changed rapidly since day 0 (6.5 mg O_2/L), when wastewater was prepared. On day 1 it dropped to 0.6 mg O_2/L and day 2 to 0.1 mg O_2/L, same value as in 33 mg/L RBL19 experiments. On the day 3 it increased again to 1.4 mg O_2/L. As previously described (5.2.5.1.), DO in the inflow compartment increased as vigorous mixing in reservoir introduced more oxygen into remaining wastewater.

On day 0 as prepared wastewater was introduced into the media, DO measured in both tubes exhibited gradual decrease from inflow compartment to the outflow one. Oxygen was consumed while fresh wastewater percolated through the media as the concentration at the outflow was 7 times lower compared to the inflow. On days 1, 2 and 3 decreased DO was measured in the inflow compartment and kept at constant value of 0.1 mg O_2/L.

EC values increased in the reservoir and during percolation through media which resulted in increased values at the outflow and inflow compartment. Values at the outflow on days 1 and 2 exhibited an increase compared to inflow values for more than 150 µS. On day 3 the difference between inflow and outflow lowered to 90 µS. The same has been noted in 5.2.5.1.

5.2.6.2. COD results, RBL19, RRD22 and RBK5, 100 mg/L

In the Fig. 35 and Table 16 the average COD values are shown. In Fig. 35 values are given in mg of COD per mL and in Table 16 mass flow is given in g of COD per day. Increase in prepared wastewaters' dye concentration resulted in 50 mg/L higher COD for RBL19 (Figs. 29 and 35). Initial COD values of prepared wastewater containing three different colours differed among blue, red and black and ranged between 331 and 374 mg/L.

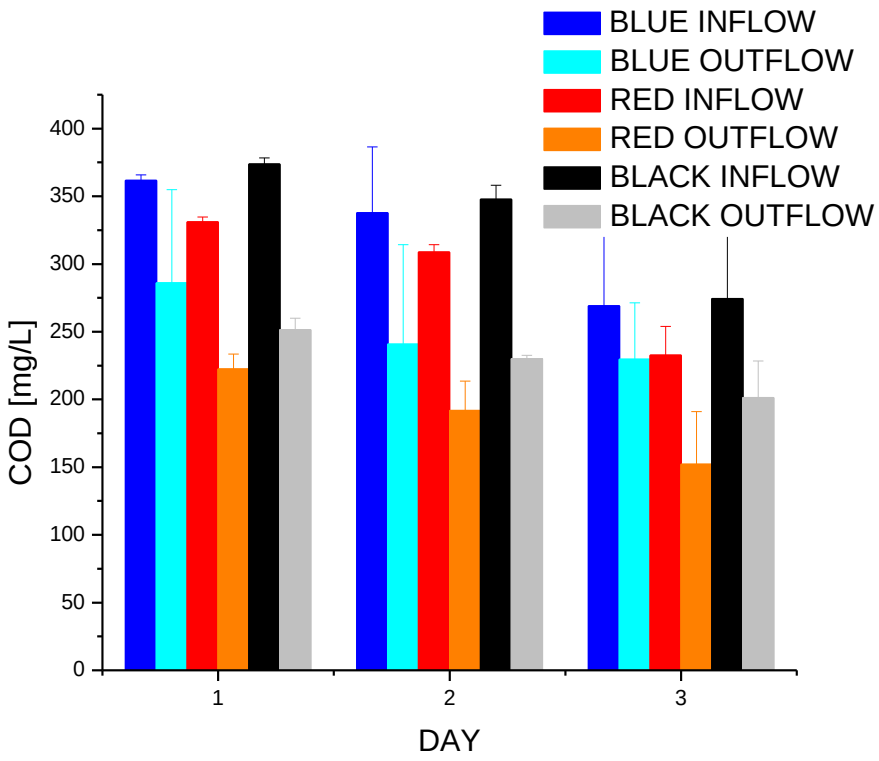

Figure 35: Average COD values at inflow compartment and outflow from CW model, RBL19, RRD22 and RBK5, 100 mg/L.

COD removal reduction was the same for RBK5 and RRD22, 33 % and lower for RBL19, 22 % on day 1. On days 2 and 3 again RBL19 exhibited the lowest removal rate, 29 and 15 % respectively. For RBK5 the removal reduction was 34 and 27 % and for RRD22 38 and 35 %. Average removal rate was the highest for RRD22, 35 %, RBK5 followed (31 %) and lowest was RBL19 (21 %). COD

removal reduction on day 4 decreased all three colours. By day 4 COD decreased already prior to inflow compartment and lower efficiency is attributed to the lower inflow value. The removal reduction efficiency was always assessed as the difference in the inflow and outflow values, regardless the initial concentration. Due to changed sampling regime (chapter 5.1.7.2) DO in the inflow didn't increase as much as in 5.2.5.1. on day 3. The concentration of DO didn't increase to a level which would in turn help to decrease the COD value due to the high oxygen availability. COD values were again found to correlate with EC value (r = -0.55525, p = 0.0026).

Table 16: Mass flow in COD [g/day].

	BLUE		RED		BLACK		AVERAGE	
COD	INFLOW [g/day]	OUT-FLOW [g/day]	INFLOW [g/day]	OUT-FLOW [g/day]	INFLOW [g/day]	OUT-FLOW [g/day]	INFLOW [g/day]	OUT-FLOW [g/day]
day 1	91	72	83	56	94	63	90	64
day 2	85	61	78	48	88	58	84	56
day 3	68	58	59	38	69	51	65	49

5.2.6.3. BOD_5 results, RBL19, RRD22 and RBK5, 100 mg/L

In the Fig. 36 average BOD_5 results for all three dyes are shown. BOD_5 values at the inflow on day 0 are considerably lower compared to COD, for 50 % on average. BOD_5 removal reduction for RBL19 was 34 % on day 1, lowered to 16 % on day 2 and increased to 20 % on day 3. For RBK5 reduction was 23 % on day 1, followed by 31 and 13 % day 3. And for RRD22 the removal reduction was 44 % on day 1 and increased on days 2 and 3 to 46 and 57 %. Overall reduction removal was the same (23 %) for RBL19 and RBK5, notwithstanding the BOD_5 reduction differed by days. For RRD22 it was considerably higher - 49 %. Before entering the model BOD_5 decreased for 20 % for RBL19, 32 % for RBK5 and 43 % for RRD22 between day 0 and day 3. BOD values were again found to correlate with EC values (r = -0.66891, p = 0.0136).

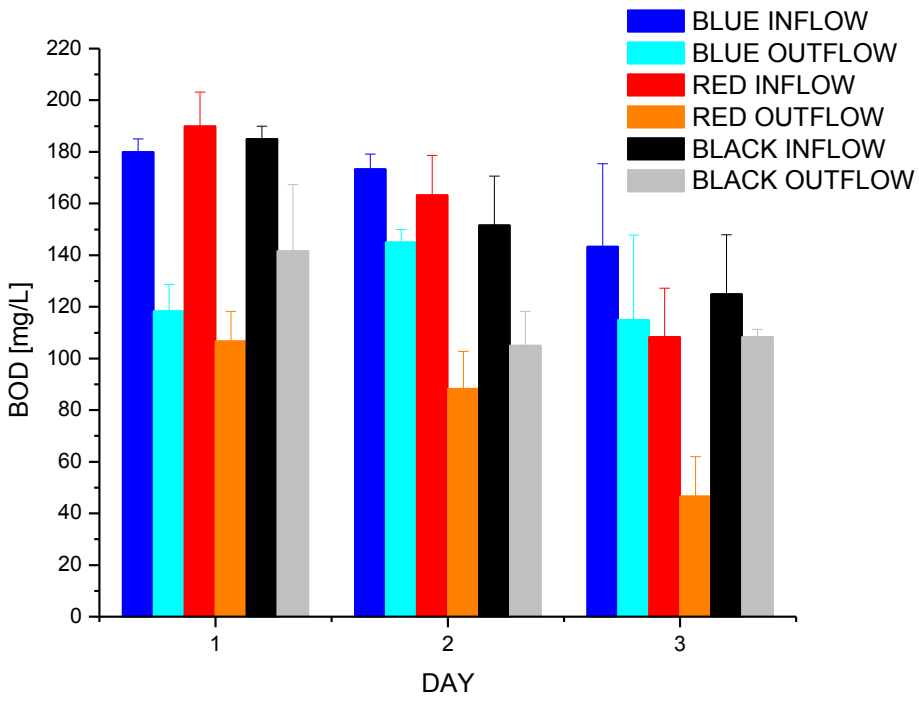

Figure 36: Average BOD_5 values at inflow compartment and outflow from CW model, RBL19, RRD22 and RBK5, 100 mg/L.

In the Table 17 BOD_5/COD ratio at inflow compartment and outflow from CW model for all three dyes is given.

Table 17: BOD_5/COD ratio at inflow compartment and outflow from CW model, RBL19, RRD22 and RBK5, 100 mg/L.

DAY	BLUE		RED		BLACK	
	INFLOW	OUTFLOW	INFLOW	OUTFLOW	INFLOW	OUTFLOW
1	0.50	0.41	0.57	0.48	0.50	0.56
2	0.51	0.60	0.53	0.46	0.44	0.46
3	0.53	0.50	0.47	0.31	0.46	0.54

5.2.6.4. Toxicity results, RBL19, RRD22 and RBK5, 100 mg/L

Samples' average toxicity values are shown in Fig. 37. On contrary to lower RBL19 concentration (33 mg/L), at 100 mg/L on day 3 toxicity at the inflow compartment slightly increased. Increase can be explained by the fact that also

absorbance increased on day 3, due to flocculation of RBL19 dye in the reservoir. For RRD22 some extent of concentration (but not flocculation) was also observed and confirmed in Fig. 37, inflow toxicity increased to 100 % on day 3. RBK5 exhibited very high toxicity through the whole experiment.

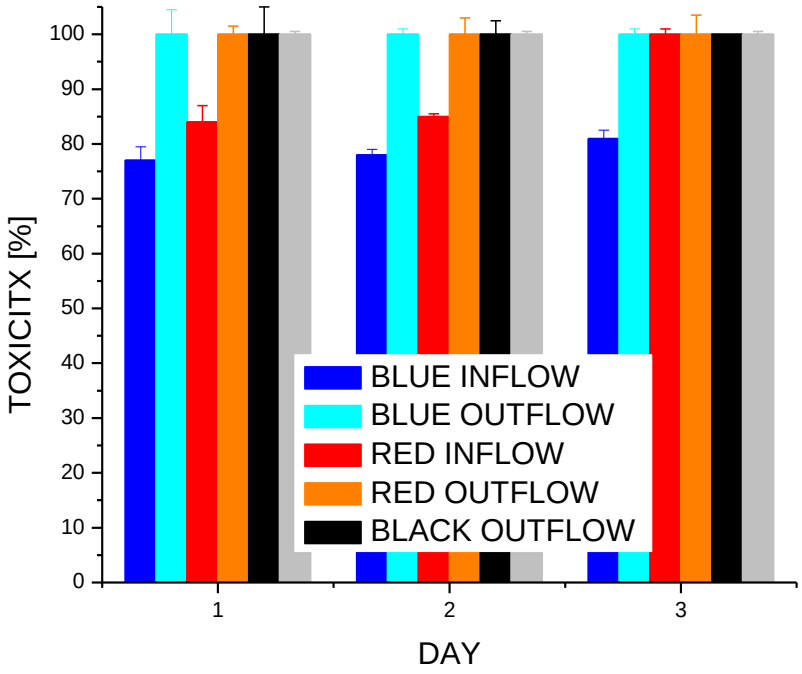

Figure 37: Average toxicity values at inflow compartment and outflow from CW model, RBL19, RRD22 and RBK5, 100 mg/L

5.2.6.5. Absorbance results, RBL19, RRD22 and RBK5, 100 mg/L

In Fig. 38 decolouration data for 100 mg/L concentration of all three dyes is given. RBL19 and RRD22 absorbance slightly increased at the inflow from day 1 to day 3. For RBL19 the increase is attributed to a minor flocculation observed to take place inside the reservoir. For RRD22 flocculation event was visually hardly perceivable. RBK5 concentration didn't increase but decreased substantially until day 3. The drop accounted for 10 % of initial dye absorbance.

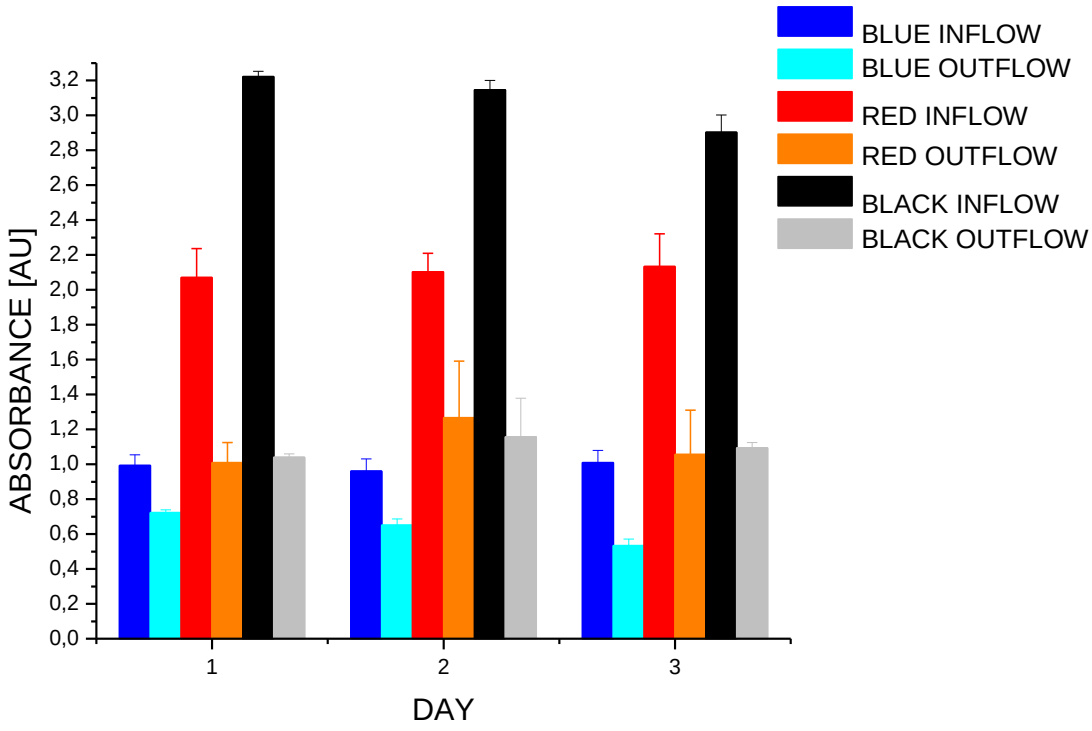

Figure 38: Average absorbance values at inflow compartment and outflow from CW model, RBL19, RRD22 and RBK5, 100 mg/L.

RBL19 decolouration was 37 % on average (range 27-48 %) and was increasing from day 1 to day 3, which confirmed results from 5.2.5.5. As in 5.2.5.5. efficiency was increasing regardless the fact that the dye concentrated in the reservoir. RRD22 decolouration was 46 % on average (range 39-50 %) and was also increasing. On contrary RBK5 didn't exhibit increasing decolouration trend; its decolouration was 61 % on average (range 67-58 %).

Decolouration was found to negatively correlate with oxygen concentration. The correlation coefficients were for RBL19 ($r = -0.71507$, $p = 0.0304$), for RBK5 ($r = -0.5308$, $p = 0.1351$) and for RRD22 ($r = -0.59964$, $p = 0.36066$). Decolouration was also found to positively correlate with EC ($r = 0.6432$, $p = 0.0304$) for all three dyes.

Under reservoir conditions (aeration, 10 s stirring intervals) RBK5 dye partly decolourised (for 10 %) already in the reservoir. Absorbance peak was shifted (broadened) from initial max. at 595 nm to a max. at 563 nm. The 563 nm peak exhibited slightly higher absorbance on days 2 and 3. The same broadening of the peak absorbance and occurrence of a second maximum is observed during photocatalytic degradation of RBK5 (Fig. 41).

5.3. DISCUSSION

5.3.1. pH, O_2, EC and T measurements RBL19, 33 mg/L, RBL19, RRD22 and RBK5, 100 mg/L

Drop in average pH (Tables 12 and 15) towards neutral values is attributed to the CWs' buffering capacity. Reportedly biological reduction of azo bond and formation of aromatic amine metabolites results in pH increase due to their alkalinity (Pearce et al., 2003). Thus pH decrease in the CW model is attributed to microbial metabolism of wastewaters' organic matter; in the wetland system acids are produced by acetogenic microorganisms, which is in accordance with the literature (Bulc and Ojstršek, 2008; Mbuligwe, 2005).

Increase in EC values was measured at the inflow and outflow compartment. Measured EC values give evidence of microbial enhanced EC increase, as a consequence of organic matter decomposition (Atekwana et al., 2004). Nevertheless the organic matter decomposition started already in the reservoir, there was a clearly exhibited contribution of the model since EC values were consistently higher (25 % on average) after 24 h HRT. The correlation between decolouration and EC also confirms degradation of dye molecules.

Also decrease in DO at the inflow compartment is attributed to biological degradation which is confirmed by gradual BOD_5 removal reduction showed in the Figs. 30 and 36. As the prepared wastewater contained stream water as a

source of microorganisms and peptone as carbon source, the conditions were in favour of organic matter decomposition.

5.3.2. COD values RBL19, 33 mg/L, RBL19, RRD22 and RBK5, 100 mg/L

Increase in COD values at the outflow between day 1 and 2 in RBL 19, 33 mg/L concentration are explained by the fact that CW model was under continuous feed operation. Prior to start of each experiment, the media was left to dry and aerate. High DO concentration at the inflow on day 0 (6.4 mg O_2/L), as water was fed into CW model and aerated media attributed to higher COD removal compared to the following days, when DO dropped considerably already in the inflow compartment. With the changed sampling regime (introduction of 5 h interval between valve opening and sampling) at 100 mg/L concentration, COD increase is not present. Removal reduction range was 26-35 % for RBL19 (33 mg/L), 33-38 % for RRD22, 27-33 % for RBK5 and 15-29 % for RBL19 (100 mg/L).

COD removal reduction is lower than reported for similar systems treating textile wastewater (Bulc and Ojstršek, 2008; Mbuligwe, 2005; Bromley-Challenor et al., 2000). Partly this can be attributed to the fact, that the inflow concentration used in our experiments is lower compared to literature, where higher COD removal is reported (inflow values above 1000 mg/L). It has been reported that CW performance is more efficient at higher loads where the removal rates are consequently higher (Kadlec and Reddy, 2001). The same has been found out in case of an anaerobic reactor, where textile dyes were degraded under methanogenic conditions; the removal rate for RBL19 doubled as the initial dye concentration increased from 50 mg/L to 100 and 200 mg/L (Lee and Pavlostathis, 2004). It should also be noted, that the COD of the textile wastewaters was found to be highly recalcitrant due to their specific composition (Oller et al., 2010).

In a study with an anaerobic - aerobic reactor of 2.5 L in volume, HRT proved to be a determining criterion influencing COD removal efficiency. At HRT of 100 days, the COD removal was 80 %. At decreased HRT (6 h), colour removal remained almost the same, but COD removal dropped to 29 %. At the same HRT as in our experiment, the removal efficiency was 60 % (Isik and Sponza, 2008).

In another experiment in an anaerobic upflow packed bed reactor, 24 % COD removal was achieved at HRT of 5 days for a simulated wastewater (Talarposhti et al., 2001), but a different efficiency is reported for the anaerobic decolouration at the HRT of 10 days. COD removal was in the range of 78-94 % which is undoubtedly higher compared to all other literature data (Manu and Chaudhari, 2002). In the same study an interesting issue was raised, namely COD and colour removal were correlated; it has been shown that with nutrients (starch) addition, which led to reducing equivalents' production in sufficient quantity due to starch degradation, only dye reduction took place. This might be the case also in our experiment, where addition of meat peptone provided abundant nutrient source for dye reduction (decolouration) and as in (Manu and Chaudhari, 2002) low COD removal reduction is exhibited.

The other possible explanation for lower removal rates lies in the fact, that the CW was not planted. In planted CW, aerobic and anaerobic conditions are present. Compared to planted CW, the unplanted ones exhibit lower number of aerobic microlocations. As the first step of the dye molecule degradation is reduction, it takes place in anaerobic environment and it results in aromatic amines' formation. Since they are further degraded only aerobically by hydroxylation and ring-opening, the aerobic stage is essential for further degradation (Mbuligwe, 2005; Pearce et al., 2003). In another experiment, where anaerobic and aerobic reactors were sequentially used to treat textile effluent, the anaerobic part had 35 – 55 % COD removal reduction efficiency.

Overall treatment removal reached 80 - 90 %. But, interestingly, the bypass ofthe anaerobic reactor as a first treatment stage did not alter the overall COD removal efficiency (Frijters et al., 2006). This proves the fact that aerobic conditions play a crucial role, determining the success of the treatment process in COD removal and pollution mineralization. Comparable range of COD removal reduction as in anaerobic stage in (Frijters et al., 2006) was found in the CW model used in this experiment.

Moreover, in the literature a clear difference has been shown between planted and unplanted CW performance in terms of COD removal reduction. The planted beds, containing aerobic microlocations in the roots and rhizomes of the macrophytes exhibited up to 21 % higher removal rates compared to unplanted ones (Mbuligwe, 2005). Based on the written it can be concluded, that also in the case of our experiment, presence of more aerobic microlocations within the CW model would mean higher COD removal since degradation products from the colour molecules' reduction would be further degraded.

5.3.3. BOD_5 and TOC values, RBL19, 33 mg/L, RBL19, RRD22 and RBK5, 100 mg/L

Higher BOD_5 removal reduction exhibited for RBL19, 33 mg/L, on day 4 (Fig. 30) was attributed to DO increase in remaining wastewater in the reservoir due to more vigorous mixing. As more oxygen became available, further aerobic decomposition of organic compounds was rendered more feasible. Trend in inflow TOC values confirmed the BOD_5 results with a higher drop in TOC value between day 3 and 4.

When BOD_5 and COD results for RBL19, 33 mg/L are compared, the only major difference observed is on day 4. Interestingly, inflow TOC values on day 4 didn't decrease to the same extent compared to BOD_5 values. Consequently TOC at inflow and outflow still differed for 33 % but BOD_5 was almost the same (7 %

difference). Presumably this could arise from the degradation of organic material which attributed to lowering of BOD_5 values. But since it was degraded only to (more recalcitrant) lower molecular weight compounds, they still contributed to the overall TOC value.

Before entering the CW model BOD_5 decreased for 20 % for RBL19, 32 % for RBK5 and 43 % for RRD22. This hints to the fact, that RRD22 is more easily degraded under conditions present in the reservoir. Also within the CW model RRD22 exhibited the highest BOD_5 (and COD) reduction removal, compared to other two dyes. This indicates that dyes' chemical structure didn't prove to be a determining factor for COD and BOD_5 removal since RRD22 and RBK5 are both azo dyes (one mono and one diazo dye) and RBL19 is an anthraquinone dye. In the case of dyes applied in this experiment it has been shown that dyes' structure didn't play a role in its removal efficiency.

In experiments with dyes in 100 mg/L concentration there was no significant drop in BOD_5 value at the inflow exhibited on the last day (Fig. 36) as was the case for RBL19, 33 mg/L. As already mentioned the sampling regime was changed and DO concentration in the inflow compartment didn't show a pronounced increase like it was in lower RBL19 concentration which could contribute to a substantial BOD_5 decrease at the inflow on day 3.

High BOD_5/COD ratio values obtained at the inflow compartment show high samples' degradability, which is attributed to the meat peptone degradability (Table 17). Persisting high values obtained at outflow of the model hint to the fact, that there was still organic matter present in the sample, which could be degraded if higher oxygen concentrations were available. As already established, the RRD22 dye exhibited the highest BOD_5 reduction removal, which is also shown by the pronounced decrease in BOD_5/COD ratio for this particular dye.

5.3.4. Toxicity values, RBL19, 33 mg/L, RBL19, RRD22 and RBK5, 100 mg/L

Inhibition of photo-bacteria' natural luminescence is regarded as toxicity indication. When samples cause less than 20 % inhibition, they are considered not toxic, on contrary bioluminescence inhibition higher than 20 % indicates toxicity (Girotti et al., 2008). Toxicity (cytotoxicity, genotoxicity and bioaccumulation) of textile dyes has been confirmed and published (Gottlieb et al., 2003; Jadhav et al., 2010).

High complexity is characteristic for textile wastewater samples which include degraded textile dyes, mixture of textile auxiliaries, salts, surfactants, dye and other degradation products. But most of the samples' toxicity after (in our case partly) anaerobic treatment is attributed to the formation of aromatic amines during reductive cleavage of azo bonds (Gottlieb et al., 2003). In our experiment increase in UV absorbance, exhibited in the samples' UV-Vis spectra, confirmed aromatic amine formation (Figs. 40, 41 and 42 – pre-treated samples).

Dye molecules in prepared wastewater solution were only partially hydrolyzed (full hydrolysis would be at 100 °C, for 10 min, at high pH values), since hydrolysis of the unreacted dye molecules (no bonding with the cellulose fibres) at room temperature is slow. It has been found that partially hydrolyzed dye solution exhibits higher toxicity towards bioluminescent bacteria compared to the fully hydrolyzed one (Libra et al., 2004). The 30 to 80 times more inhibitory effect was exhibited by a partially hydrolyzed dye due to the presence of the vinyl form of the reactive group (compared to the hydroxyl group) (Libra et al., 2004). In our experiment it can be presumed, that hydrolysis occurred slowly since the start of each experiment, which explains the 30 % drop in toxicity of the solution between days 1 and 2 and day 4 at dye concentration of 33 mg/L.

Toxicity in the outflow compartment was nearly 100 % on day 1 and 100 % on all following days. It has been confirmed by other studies, that toxicity level after anaerobic treatment increased considerably and decreased after a following aerobic stage. The bioluminescence inhibition in effluent was doubled after anaerobic treatment and dropped to one third after aerobic treatment (Libra et al., 2004). Another study showed that a combination of anaerobic and aerobic treatment was successful in decolouration and toxicity removal but only in combination of anaerobic phase followed by the aerobic one. If anaerobic phase was bypassed, aerobic phase effluent exhibited significant increase in toxicity. This implies to the fact, that both of the processes are important in the overall decrease of toxicity of textile effluent. And, importantly, the wastewater effluent was found not to cause inhibition of the anaerobic phase and in turn its products did not inhibit the aerobic treatment process itself (Frijters et al., 2006).

Decreasing toxicity at the CW inflow compartment in 33 mg/L RBL19 was attributed to dye hydrolysis occurring from onset of each experiment. This presumption was not confirmed at higher tested concentration. It can be speculated that at higher concentration of RBL19, 100 mg/L, effect of hydrolysis wasn’t so pronounced and no drop in toxicity was observed.

Toxicity at the outflow for all 100 mg/L dye samples was 100 % on all days. As already stated the toxicity level of samples after anaerobic treatment was found to increase considerably due to the presence of aromatic amines, anaerobic degradation intermediates and decreases after a following aerobic stage (Libra et al., 2004; Frijters et al., 2006).

For our experiment, the increased luminescence inhibition can be attributed to two facts. Wastewater was only partly decolourised, so not all the initial toxicity was diminished by the wastewater treatment. Toxicity caused by degradation products was added to remaining initial toxicity and already high initial values

thus reached 100 %. Consequently, as increase in toxicity is attributed to anaerobic treatment phase, it can be again confirmed, that at least partly anaerobic conditions (microlocations) were present in the CW model.

Based on the fact, that aerobic phase is essential for a high degree of COD removal which has not been achieved at treatment conditions in the CW model but, at the same time a certain degree of BOD_5 and TOC removal has been exhibited by the system, it can be concluded that both, aerobic and anaerobic conditions were present in the CW model. Moreover, since COD removal reduction can be compared to the one quoted for anaerobic treatment conditions (Frijters et al., 2006) and toxicity results indicate presence of anaerobic effluent, it can be concluded, that anaerobic conditions were prevailing in the bulk of media in CW model.

5.3.5. Decolouration degree, RBL19, 33 mg/L, RBL19, RRD22 and RBK5, 100 mg/L

As following from results in Table 11 there was no absorption of both tested dyes onto the substrate used as media in the CW model. This was confirmed by absorbance spectra since there were no peaks of the previous dye present in the spectra of the next dye applied in the CW model (Figs. 40, 41 and 42 – pre-treated samples).

Since inflow and outflow valves were opened in 33 mg/L, RBL19 experiments, on day 1 only after the samples were taken, water sampled on day 1 at outflow was actually the same water, which percolated through media on day 0 (when model was filled with wastewater) and was actually in the media for only cca. 35 min. This explains the absence of decolouration on day 1 since 35 min HRT in the media couldn’t assure conditions feasible for decolouration. In the next set of experiments, this was changed to a different sampling regime, which assured that samples taken on day 1 to be partly those with HRT in the media.

As indicated by 33 mg/L RBL19 results in Fig. 33 a certain degree of flocculation was observed in the reservoir from day 0 to day 4. Increase in absorbance is attributed to concentration in the reservoir. Consequently, comparison of inflow and outflow absorbance values shows an interesting result. Even though the dye concentration at the inflow increased, the outflow values were almost the same, ranging between 0.23 and 0.28 AU on days 2 to 4. This proves the fact that efficiency of CW model increased as the inflow concentration increased, achieving higher decolouration efficiency each consecutive day. 100 mg/L RBL19 experiments, flocculation was observed visually but results don't show high degree of dye concentration.

In RBK5 degradation broadening of peak absorbance and occurrence of a second maximum was observed in the inflow samples. The same broadening occurred during RBK5 photocatalytic degradation (Fig. 41). This hints to the fact, that partial degradation of dye molecules and decolouration started already under the conditions present in the reservoir, before the inflow into the CW model.

Decreasing decolouration efficiency from day 1 to day 3 for RBK5 is explained by the fact that the inflow absorbance value decreased; consequently also difference between inflow and outflow lowered, in turn lowering the overall decolouration efficiency. Nevertheless, overall decolouration efficiency was still the highest for RBK5. In spite of the fact that decolouration started already before entering the CW model, RBK5 dye with two azo chromophore groups and the highest initial absorbance exhibited the highest decolouration rate. This confirms the fact, that CW exhibits higher performance at higher pollution loads since a considerably higher performance (Kadlec and Reddy, 2001) (25 % more than RRD22 and 40 % more than RBL19) was established for dye with considerably higher initial absorbance rate. Lower decolouration efficiency was

expected for the RBL19 dye, since only partial decolouration of anthraquinone dyes is characteristic for other than azo group dyes (Harrelkas et al., 2008).

Decolouration achieved in CW model for 33 mg/L RBL19 was lower compared to published values. Literature data states 69 and 74 % removal reduction for Acid orange 7 dye in a vertical flow reactor (Davies et al., 2005) and up to 90 % removal reduction in pilot CW for real textile effluent samples (Bulc and Ojstršek, 2008). Average decolouration efficiencies were also for 100 mg/L concentration of all three dyes lower compared to published data (Bulc and Ojstršek, 2008; Mbuligwe, 2005).

Interestingly, in experiment where planted and unplanted CW units' performance was compared, results showed very high differences in decolouration efficiency. The unplanted (control) unit exhibited 14.62 % decolouration and planted units exhibited - 72.16 % and 77.13 % decolouration (cattail and cocoyam, respectively). Planted units outperformed the unplanted one for 60 % in average and exhibited a more stable performance (Mbuligwe, 2005). Comparable results were achieved in a study, where agricultural residues like wheat straw, wood chips and corn cob shreds were used to absorb dye mixtures from a solution. After absorption, the residues were found to be suitable media for solid-state fermentation for white rot fungi and as such proved to be a suitable method for textile effluent remediation (Nigam et al., 2000).

Further on, it has been reported, that a 15 day mixed culture incubation at anoxic - anaerobic conditions resulted in up to 92 % decolouration. Initial rate of decolouration was increased for several folds (up to 12.6 times) at long term acclimation (5 months to 2 years) of methanogenic culture (Beydilli et al., 2000). In this and another study (Yoo et al., 2001) the cultures' performance was significantly higher after the oxidation-reduction potential (ORP) dropped to less than -50 mV. As the culture was kept at anoxic conditions the ORP further

dropped to -250 mV which resulted in higher decolouration performance. Alternating reduced and oxidised conditions were found to fundamentally influence microbial consortia, favouring the aerobic facultatives adjusted to varying nutrient and redox conditions (Faulwetter et al., 2009).

In general oxidised and reduced zones are present in CW models, but overall the reduced environment prevails (Headley et al., 2005). Redox potential increases with length due to progressive pollution degradation and mechanical filtration. And it decreases with depth since higher potential close to surface zone (5–20 cm) is a result of passive oxygen diffusion and plant oxygen release (Faulwetter et al., 2009). However since there is vertical mixing of water present in the matrix, the depth variation is not always present (Headley et al., 2005). In general it has been proven, that longer HRT generate more aerobic conditions and provide higher pollution removal rates (Huang et al., 2005).

In a study with anaerobic - aerobic reactor of 2.5 L in volume, HRT proved to be a determining criterion influencing colour removal efficiency. At 100 days HRT, colour removal was 91 % and COD 80 %. As HRT decreased to 6 h, colour removal remained almost the same, but COD removal dropped to 29 %. Decolouration as a consequence of complete azo bond reduction was very high even at very short HRT. Decolouration is attributed to electrons which are produced by carbon sources used in microorganisms' metabolic pathways under anaerobic conditions. Catabolism of glucose, starch and other carbonaceous substances is used to reduce enzyme cofactors which are oxidised through reductive decolouration reaction (azo bond cleavage) (Isik and Sponza, 2008).

In our experiment there are several aspects to be considered in regard with the decolouration efficiency. Acclimation was shorter that the one described in the literature (Beydilli et al., 2000), the media was exposed to prepared wastewater mixture for four weeks prior to start of experiments. But most importantly, the

length of incubation and the changing conditions were those which strongly influenced the decolouration rate. Each experiment in the CW model was operated under continuous feed operation but between two sequential experiments the media was completely dried (and so aerated). This implies that aerobic conditions were repeatedly established before the start of each new experiment. When DO concentration in the inflow compartment dropped decolouration was observed and its rate increased on each following day. This was also confirmed by a negative correlation between decolouration and O_2 value.

But it must be emphasised, that conditions in the model were not only anaerobic. At the start of each experiment aerobic conditions prevailed due to previous media drying; later measured DO concentrations indicated hypoxic conditions but certainly some aerobic microlocations remained, which is confirmed by COD and BOD_5 decrease exhibited on all days except the last one (when decolouration was actually the highest).

This hints to the fact that CW model should have been operated under more anaerobic conditions and at prolonged HRT to obtain better decolouration.

There is one more presumption in regard with the operation efficiency. The metabolic production of reduced enzyme cofactors which are oxidised through azo bond cleavage when electrons are passed to the dye molecule was not facilitated to the same extent, since in this case meat peptone was used as a carbon source and not glucose or starch. Since proteins represent a more hardly accessible energy source (not primary carbon source like glucose) compared to sugars and the protein metabolism produces less energy to the unit of mass, the production of reduced equivalents is presumed to be slower and in turn more time would be needed for higher decolouration to take place (Horton et al., 2006).

5.4. CONCLUSIONS

COD removal reduction in the CW model was lower than reported for similar systems treating textile wastewater. Partly this can be attributed to the fact, that the inflow concentration used in our experiments was lower compared to literature, where higher COD removal was reported. Since it has been established that aerobic conditions play a crucial role in COD removal and overall pollution mineralization; it can be concluded, that presence of more aerobic microlocations within the CW model would mean higher COD removal since degradation products from the dyes' reduction would be further degraded.

Since the highest BOD_5 and COD removal reduction was established for RRD22 dye, it can be concluded that dyes' chemical structure didn't prove to be a determining factor for COD and BOD_5 removal since RRD22 and RBK5 didn't exhibit similar removal rates. With RBL19 it has been confirmed that anthraquinone dyes are more recalcitrant towards degradation compared to azo dyes.

Toxic aromatic amines' formation through reductive azo bonds' cleavage was confirmed by an increase in UV absorbance, exhibited in the samples' UV-Vis spectra. Increased bioluminescence inhibition can be attributed to the fact that wastewater was only partly decolourised, so not all the initial toxicity was diminished by the treatment. Namely, degradation products' toxicity was added to remaining initial toxicity and already high initial values thus reached 100 %. As increase in toxicity is attributed to anaerobic treatment phase, it can be established, that at least partly anaerobic conditions (microlocations) were present in the CW model.

Average decolouration efficiencies for 100 mg/L concentration of all three dyes were lower compared to published data. Length of incubation and changing conditions were those which strongly influenced the decolouration rate. Since

alternating reduced and oxidised conditions favour aerobic facultatives, adjusted to varying nutrient and redox conditions, the periodic aeration of media while it was dry didn't have a favourable effect on decolouration efficiency. For an ultimate decolouration to be achieved also longer HRT would have to be applied since the measured DO concentrations indicated hypoxic rather than anaerobic conditions, which favour decolouration.

It can be concluded, that both, aerobic and anaerobic conditions (microlocations) were present in the model. At the start of each experiment aerobic conditions prevailed due to previous media drying; later measured DO concentrations indicated hypoxic conditions but some aerobic microlocations remained, which was confirmed by COD and BOD_5 decrease. For higher decolouration and COD removal rate to be achieved the CW model should have been operated under more anaerobic conditions and at prolonged HRT.

6. PHOTOCATALYSIS IN LAB SCALE PHOTOREACTOR

6.1. EXPERIMENTAL

6.1.1. Photoreactor setup

Samples of raw and CW pre-treated wastewater were subject to photocatalysis in a Carberry type photoreactor (Černigoj et al., 2007). Photocatalytic cell consisted of a DURAN glass tube (240 mm, inner diameter 40 mm), which was closed on the lower side with a glass frit with a valve at the lower end to allow the sample to be gas purged – oxygen and ozone (Fig. 39, a). Effective volume of the glass tube was 250 mL. Initial volume of the irradiated sample was 280 mL. Samples were irradiated by a UVA source - 6 low pressure mercury fluorescent lamps (CLEO 20 W, 438 x 26 mm, Philips; broad max at 355 nm). The photocatalytic cell was put in the centre surrounded by lamps.

Spinning basket which fitted into the photocatalytic cell was made of Teflon and inox parts to enable fastening of the photocatalytic paper. Photocatalytic paper (Ahlstrom, France) was adjusted to a steel support and radially fastened with 24 thin bars to form a 12 angle star (Fig. 39, b. and c.). Area of the photocatalytic paper used was 0.069 m^2. Mass of the catalyst per unit area (paper+TiO_2) was 75 g/m^2, the total mass being 5.18 g. Ahlstrom photocatalytic paper with Millennium PC-500 powder was used as the catalyst. Prior to fastening the paper onto the support, flowing water was used to rinse off the redundant catalyst.

a. b. c.

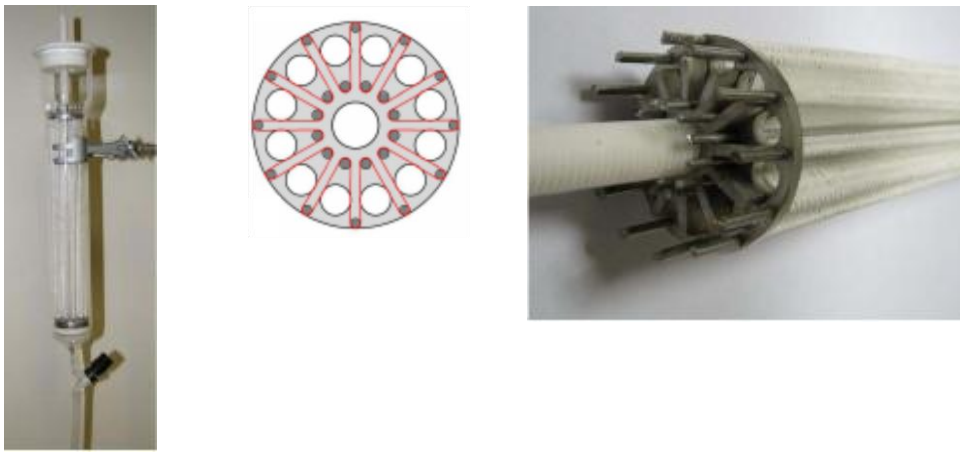

Figure 39: a. Photocatalytic cell. b. Geometrical shape of the steel paper holder (top view). c. Photocatalytic paper immobilised to the support (Kete, 2008).

6.1.2. Photocatalytic oxidation

In photocatalytic oxidation (PCOx) experiments, raw and pre-treated samples of prepared textile wastewater were irradiated in a Carberry type photoreactor in the presence of photocatalytic paper to assess the time needed for decolouration to be reached. Degradation of pollutant molecules and toxicity of the samples was followed. Prepared textile wastewater was obtained as explained in chapter 5.1.5. Pre-treated samples were taken from the CW on the second day of treatment and then irradiated. The second day of treatment was chosen due to the fact, that hypoxic conditions in the CW model were already established (after the model was filled with prepared wastewater) and relatively high decolouration was achieved. Samples from the same day were also chosen to follow the aim of repeatibility among different irradiated samples.

Dye solutions were exposed to UVA irradiation under constant oxygen purging according to the time needed to achieve decolouration. Oxygen was bubbled through the lower end frit into the reactor tube. Gas flow was kept constant through the whole set of experiments to keep the solution saturated.

Time at which the decolouration was achieved differed among dyes and accounted for 90 to 210 min. 5 mL aliquots of irradiated sample were taken at time = 0 and in time intervals (5-20 min), which were found to best suit the decolouration speed. Absorbance in UV-Vis, COD and toxicity were measured. pH of the solutions was measured as well. Analytical procedures are explained under 5.1.8.1. In the Table 18 values of measured parameters are given for the raw and pre-treated samples before photocatalytic degradation experiments.

Table 18: Characteristics of raw and pre-treated textile wastewater, subjected to photocatalysis.

parameter	raw sample			CW pre - treated sample		
	BLUE	RED	BLACK	BLUE	RED	BLACK
PEAK ABSORBANCE [AU]	0.88	1.99	3.1	0.55	0.99	1.1
COD [mg/L]	372	351	360	280	215	245
BOD [mg/L]	183	185	187	148	93	100
pH	8.1 - 8.2	8.1 - 8.2	8.1 - 8.2	~ 7.3	~ 7.3	~ 7.3
TOXICITY [%]	84	100	100	73	100	100

6.1.3. Photocatalytic ozonation

Photocatalytic ozonation (PCOz) experiments were done on the same type of prepared wastewater – raw and pre-treated one as in 6.1.2. Experiments were performed in the same way, only the irradiation was shorter, since the decolouration was achieved in shorter time (in 20 to 30 min) compared to oxygen purging.

During the experiment, samples was taken in constant intervals and analyzed. After aliquots were taken from the irradiated solution, argon was introduced into the samples to prevent further oxidation of the sample. The absorbance was measured; COD test and Lumistox toxicity test was done to evaluate the possible decrease in toxicity.

Ozone was generated by Pacific Ozone Technology instrument; model LAB 21, fed with pure oxygen (99.5 %). The gaseous concentration of ozone was calculated from iodometric titration with a standard tiosulphate solution. The flow rate of ozone was calculated to be 0.13 g/h.

6.2. RESULTS AND DISCUSSION

6.2.1. Changes in absorbance spectra after pre-treatment and during photocatalytic oxidation

In the Figs. 40, 41 and 42 time dependent UV-Vis absorbance spectra of Reactive Blue 19 (RBL19), Reactive Black 5 (RBK5) and Reactive Red 22 (RRD22) containing wastewater are presented. Absorbance peaks for all three colours in UV and Vis region decreased with time of irradiation and no new absorbance peaks occurred. Measurements at their reference wavelengths indicated decolouration of the solution, leading to a complete absence of colouration.

The same starting concentration of all three commercial dyes, i.e. 100 mg/L, exhibited significantly different absorbance at respective characteristic absorbance peaks in the visible spectra. RBL19 dye exhibited the lowest absorbance at 100 mg/L, 0.8 AU on average, RBK5 the highest absorbance – 3.1 AU on average and RRD22 on average 1.9 AU. This is explained by different structure of the dyes under study.

From the spectra in Figs. 40, 41 and 42 it can be observed that pre-treatment in the CW model had a uniform effect on all three dyes – it decreased absorbance in the Vis part of spectra and increases the absorbance in the UV part. This is in agreement with the fact that in anaerobic conditions the azo bonds are reduced and chromophore cleaved. Aromatic amines which absorb in the UV part of

spectra are formed. The obtained results are in accordance with the previous findings (Harrelkas et al., 2008; van der Zee et al., 2005).

The major difference between both sets of RBL19 spectra (Fig. 40) is that spectrum of the pre-treated sample shows simultaneous decrease in UV and Vis absorbing components (peak at 592 nm), but the raw sample shows only minor drop in UV absorbance. Part of dye molecules was during pre-treatment degraded into degradation products which still absorb in the UV region. These degradation products proved to be more susceptible to photocatalytic degradation compared to parent compound.

Remaining UVC absorbance after photocatalysis (left graph) is attributed to well-known high resistance of the anthraquinone dyes to changes in this spectral range. Aromatic organic intermediates in the solution such as quinones and phenols cause UV-C absorbance which is in accordance with previously published data (Marques et al., 2010). According to the literature in mild experimental conditions different degradation products like quinones, phenols and mono and diacids (maleic, acetic, oxalic) are formed (Saquib et al., 2002; Marques et al., 2010).

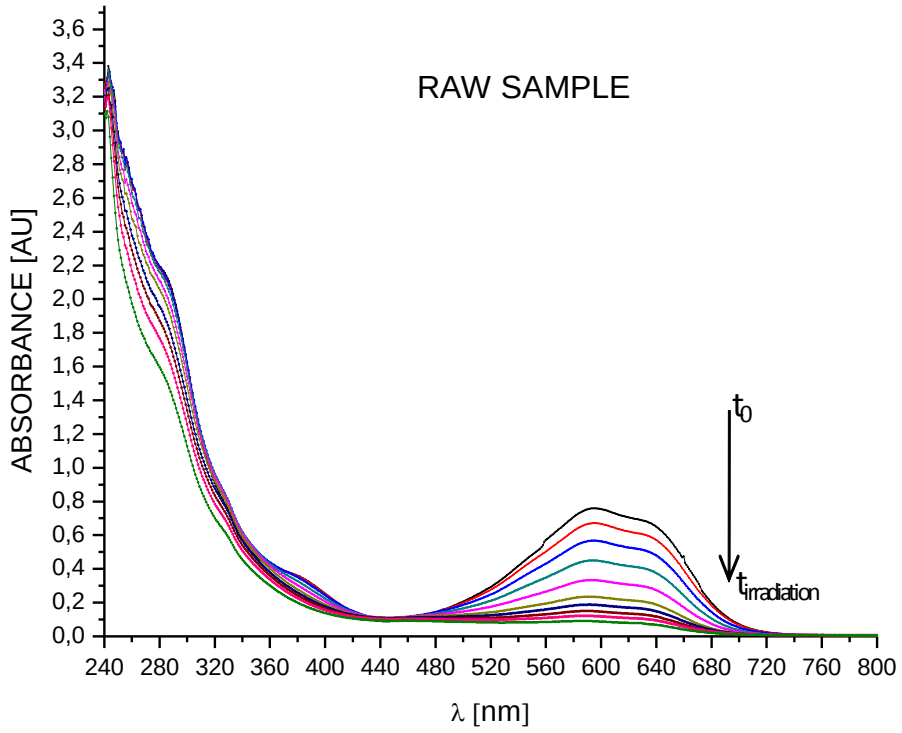
RAW SAMPLE
ABSORBANCE [AU]
λ [nm]
t0
tirradiation
3,6
3,4
3,2
3,0
2,8
2,6
2,4
2,2
2,0
1,8
1,6
1,4
1,2
1,0
0,8
0,6
0,4
0,2
0,0
240 280 320 360 400 440 480 520 560 600 640 680 720 760 800

a.

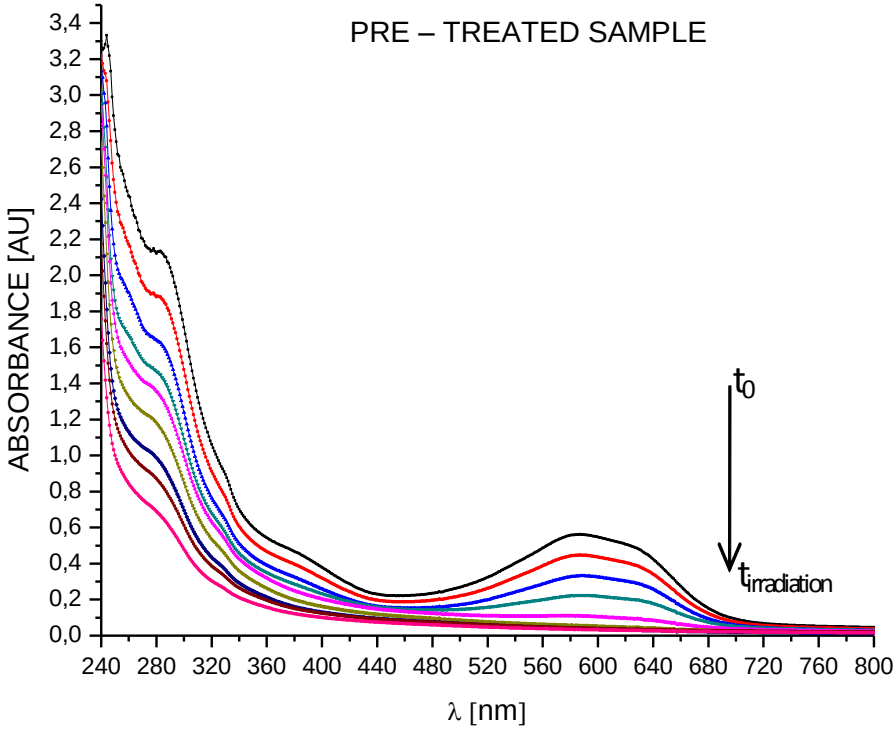

b.

Figure 40: UV-Vis spectral changes as function of time of irradiation of raw (a) and pre-treated (b) RBL19 textile effluent taken in 5-15 min intervals, the irradiation time was 90 min.

In Fig. 41 UV-Vis spectra during photocatalytic treatment of raw and pre-treated samples of RBK5 are shown. Raw RBK5 sample exhibits a characteristic absorbance peak at 598 nm; in the pre-treated sample the peak is shifted to 567 nm. In both spectra there is a pronounced absorbance in the UV region. On contrary to RBL19, the degradation of RBK5 in the raw and pre-treated samples is manifested simultaneously in the UV and Vis part of spectra.

In raw RBK5 sample a new peak is formed after 80' of irradiation at 255 nm; it increases for the next 20 min of irradiation, and with further irradiation it decreases. The pre-treated sample has two pronounced peaks in the UV, at 335

and 255 nm, the latter one being extremely pronounced - probably main anaerobic degradation product. The same UV peak can also be found in literature (Gottlieb et al., 2003b). In another photocatalytic study with the same dye but with slurry TiO_2 semiconductor, temporal changes in spectra also show a newly occurring peak in the 250-260 nm region, after 90 min of irradiation (Kritikos et al., 2007). The GC-MS analysis revealed that compounds with aromatic rings (benzaldehyde) and short chain aliphatic oxygenated hydrocarbons (like butanoic and propanoic acid) are organic compounds formed during RBK5 photocatalytic degradation (Kritikos et al., 2007). Since the absorbance at 255 nm is in our case present in both sets of spectra it can be assumed that the same degradation products are formed during anaerobic degradation and after 80 min of raw sample irradiation.

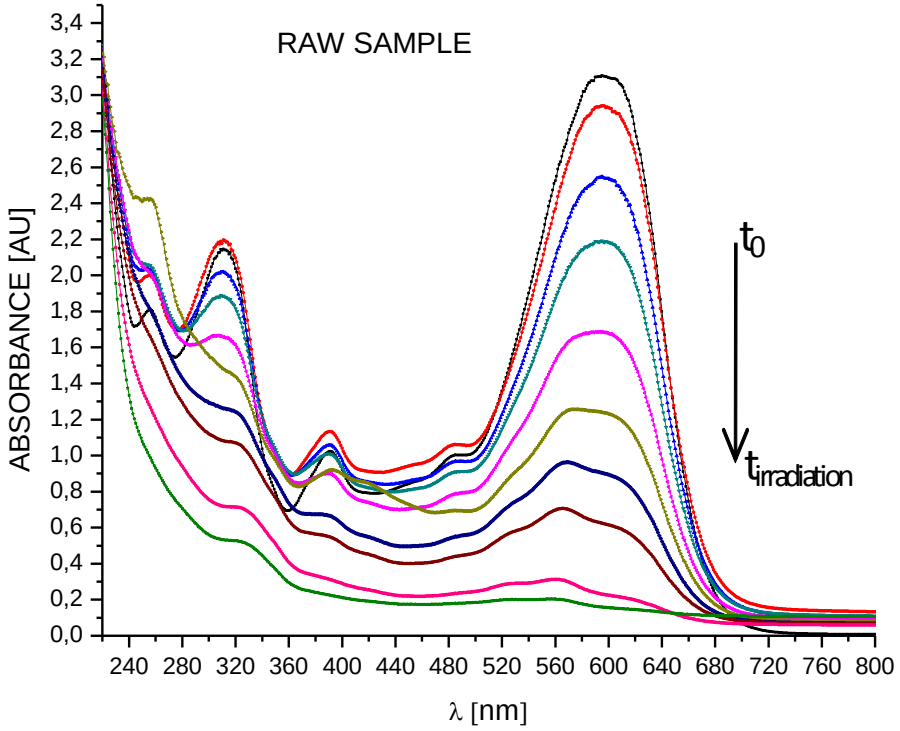

a.

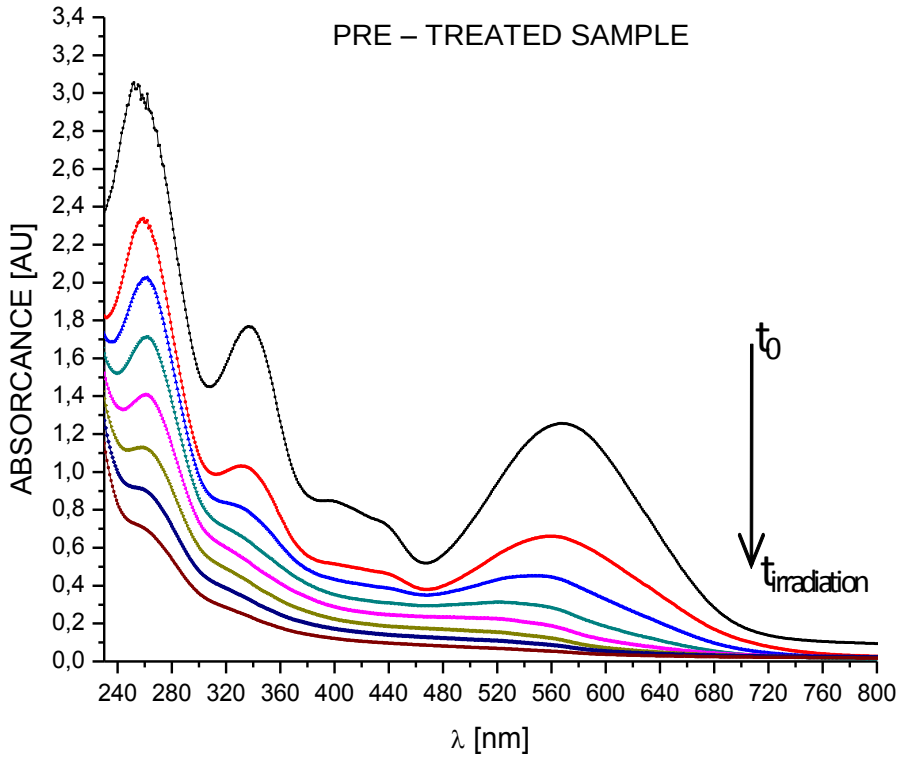

b.

Figure 41: Temporal changes in absorbance spectra of raw (a.) and pre-treated (b.) RBK5 textile effluent taken at 5-15 min intervals, the irradiation time was 210 min.

In Fig. 42 UV-Vis spectra during photocatalytic treatment of raw and pre-treated samples of RRD22 are shown. Both wastewater samples exhibit characteristic absorbance peak at 520 nm. Again in the pre-treated sample the dye degradation is exhibited as a decrease in absorbance in the Vis range and increase in absorbance in the UV range indicating aromatic product formation. Like in RBK5 case (both azo dyes) photocatalytic degradation of the raw and pre-treated samples of RRD22 took place simultaneously in the UV and Vis part of spectra. In both sets of spectra there is a pronounced absorbance in the UV region at wavelengths between 250 and 300 nm. Unfortunately (to our knowledge) no scientific literature data on red dye of the same chemical

structure is available, so no degradation products are suggested except those generally characteristic for textile dye degradation, where formic and acetic acid are main degradation products while the others include oxalic, glycolic and malonic acids (Tanaka et al., 2000).

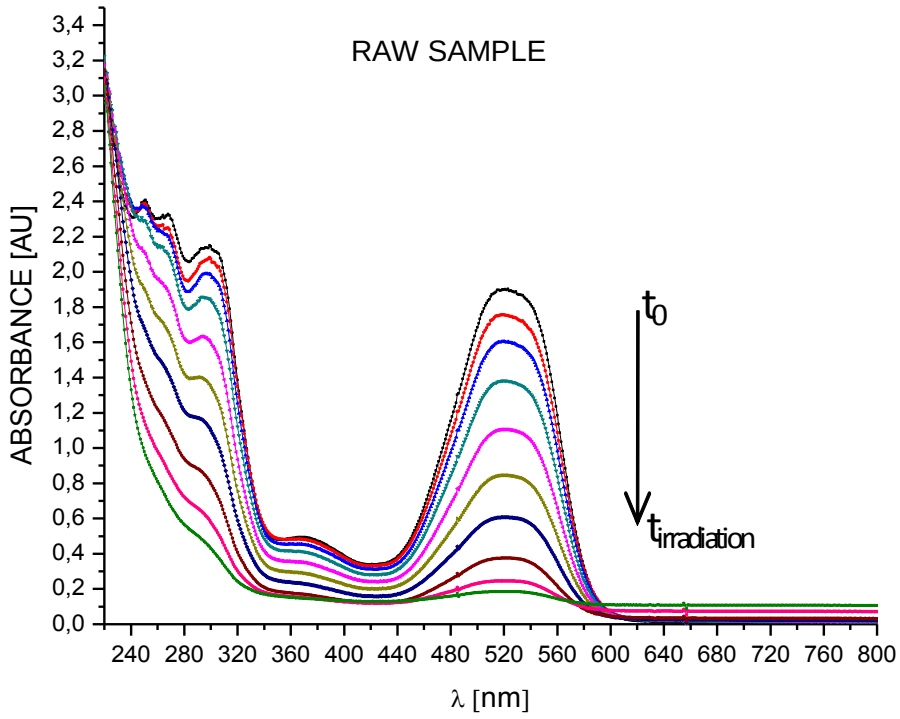

a.

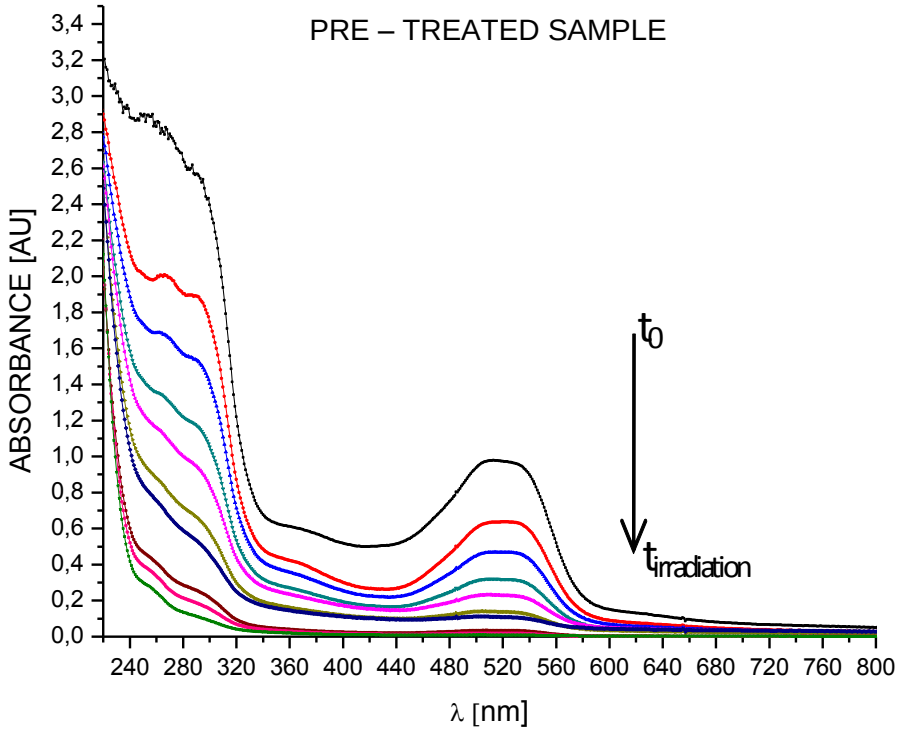

b.

Figure 42: Temporal changes in absorbance spectra of raw (a.) and pre-treated (b.) Reactive red 22 textile effluent taken at 5-15 min intervals, the irradiation time was 210 min.

Absorbance of dyes on the photocatalytic paper after 2-3 min immersion in solution was observed. By the end of irradiation as solution decolourised, also the photocatalytic paper was decolourised. Reversible adsorption of the dye would result in an unchanged spectrum after irradiation. Since spectra of all three dyes exhibit completely altered shape, this confirms that the oxidative transformation rather than dye adsorption took place.

6.2.2. Comparison of photocatalytic oxidation of pre-treated and raw samples

In following Figs. 43, 44 and 45, normalised absorbance (main Vis absorbance peaks) and COD values of samples taken at the same irradiation intervals are plotted as a function of time of irradiation (average values of 2-6 irradiation experiments). Difference in initial absorbance values between the raw and pre-treated samples is exhibited. Irradiation time was chosen according to the time needed for each dye to be completely decolourized.

Decrease in absorbance during CW model pre-treatment was, compared to the other two dyes, the lowest for RBL19. It has been reported elsewhere that anthraquinonic dyes are more recalcitrant under anaerobic conditions compared to azo dyes (Firminio et al., 2010). Degradation percent of three different dyes in our experiment confirms this as the average decolouration percent was 35 for RBL19 and much higher for both azo dyes - up to 60 % for RBK5 and over 50 % for RRD22.

When photocatalytic reactions take place on the surface of the catalyst, the pH value of solution is an important factor since it dictates the surface charge properties of the catalyst. Starting pH of raw and pre-treated wastewater (Table 8) was higher than the point of zero charge of TiO_2 and SiO_2 (used as binder in photocatalytic paper) oxide surfaces (6.2 and 2.5 respectively), which creates electrostatic repulsive effect (ERL) which in turn hinders adsorption of dye onto the photocatalyst surface. During reaction the pH values didn't alter significantly. Even though they would be expected to drop due to formation of degradation products like butanoic and propanoic acid as reported elsewhere (Stylidy et al., 2003; Tanaka et al., 2000), the values oscillated up to 0.2 pH units from the initial value (different for raw and pre-treated samples). However, it has to be taken into consideration that prepared wastewater, beside dyes also contained

textile auxiliaries and organic material (BOD) which also influenced (to a considerable extent) pH values of the solution.

As prepared wastewater contained also easily degradable organic material it contributed to the concentration of different ions. Electric conductivity of pre-treated samples was higher compared to raw samples, indicating presence of higher concentration of ions. Increased ion concentration proved to lower the ERL and promote further decolouration and degradation. Cations on one hand separately neutralize the negative charge and thus promote low energy interactions between dye molecule and catalyst surface. Anions on the other hand can compete with the dye for surface adsorption sites, but the effect of anions is presumed to be less pronounced since negative and neutral sites on surface of the semiconductor outnumber the positive ones (Aguedach et al., 2008). Nevertheless, acidic conditions proved to be more feasible for dye degradation in many studies, so in acidified conditions degradation rate would be expected to increase due to no ERL and more efficient electron-transfer process between the positive charged catalyst and negatively charged dye molecule (Pekakis et al., 2006). As in this study the aim was to mimic real conditions in industrial wastewater and its composition, the degradation in acidic media has not been tested.

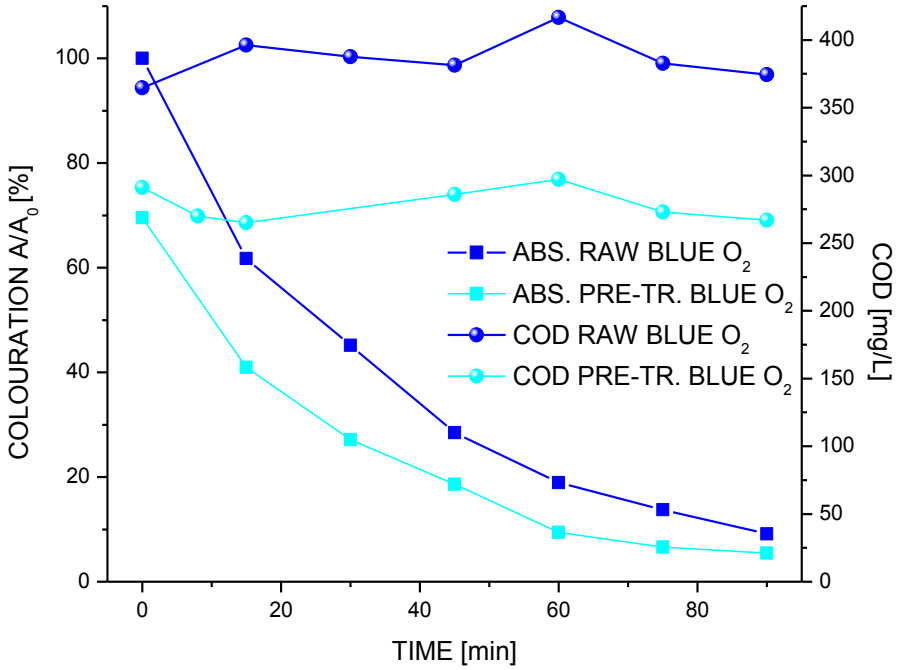

Figure 43: Colouration expressed as A/A_0 and COD values of RBL19 containing samples at different times of PCOx irradiation. Square symbols in all graphs represent absorbance values of raw and pre-treated samples, sphere symbols represent COD values of the same samples taken at the same times.

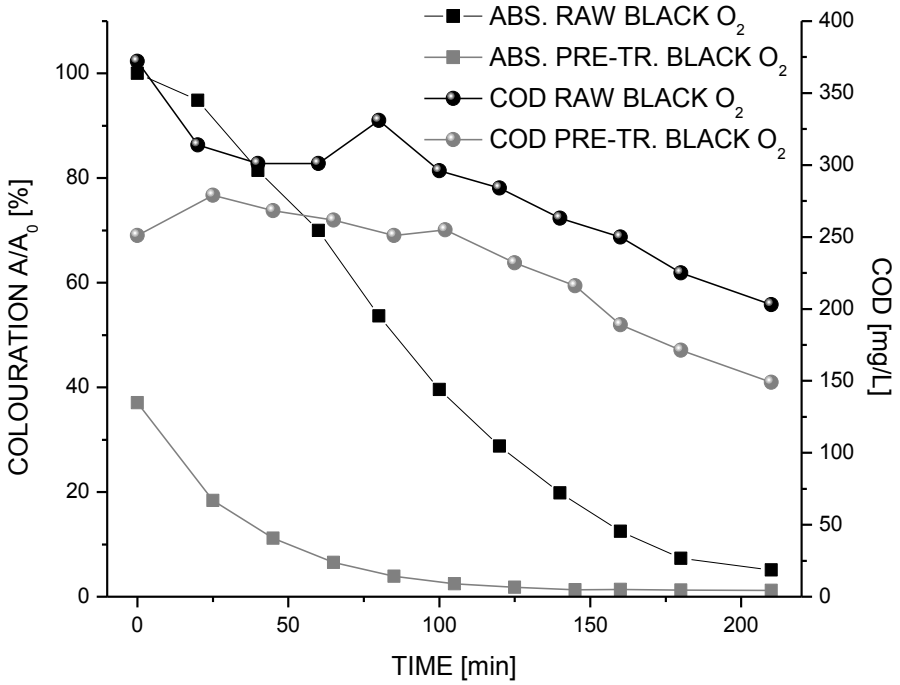

Figure 44: Colouration expressed as A/A_0 and COD values of Reactive Black 5 containing samples at different times of PCOx irradiation.

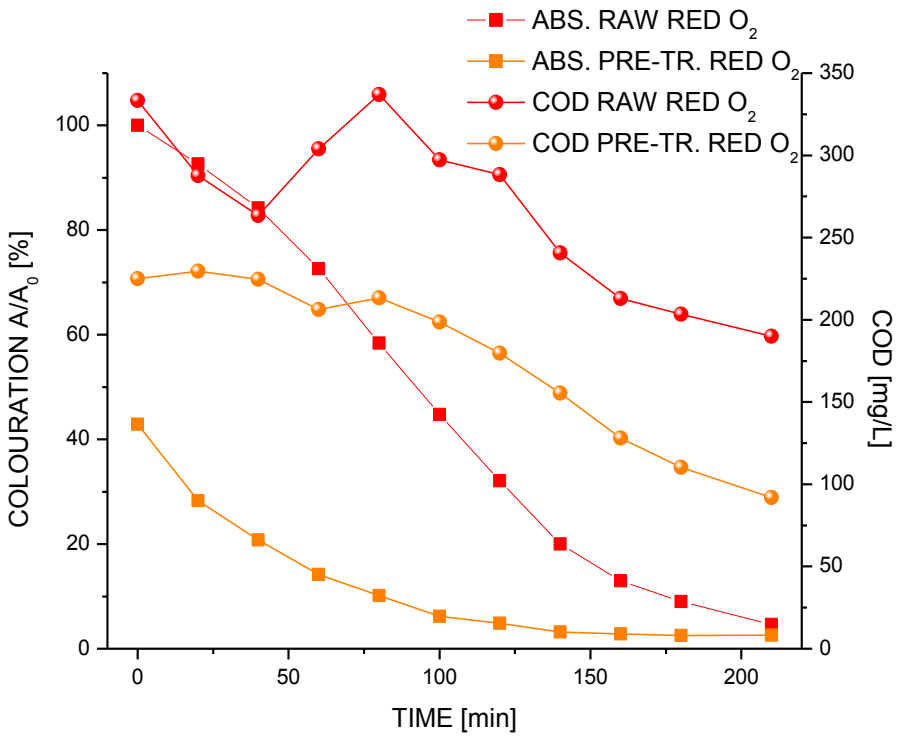

Figure 45: Colouration expressed as A/A_0 and COD values of Reactive Red 22 containing samples at different times of PCOx irradiation.

Adsorption of dye onto surface of the semiconductor is an important parameter determining the photocatalytic degradation rate due to the catalyst surface area (Tanaka et al., 2000; Aguedach et al., 2008). In case of Degussa P25 TiO_2/UV aqueous suspension and a lower dye concentration compared to the one used in our experiment, the decolouration was reached in 15 to 90 min, depending on the catalyst load (Kritikos et al., 2007). A complete mineralization was reached after 200 min of irradiation of an 85 mg/L reactive black dye (Tang et al., 2004). Literature data on dye degradation or mineralization is very scarce in case of photocatalytic paper use. Irradiation in a similar immobilised TiO_2 reactor with H_2O_2 addition reached complete removal of colouration in 30 to 60 min, depending on the concentration of H_2O_2 added (Wang et al., 2002). A direct comparison is difficult since the reactor setup and the type of TiO_2 were different.

For RBL19 (Fig. 43) the shortest time of irradiation, i.e. 90 min, was needed to reach complete degradation, compared to RBK5 and RRD22. This is attributed to the fact that by using the same dye concentration RBL19 dye exhibited much lower absorbance indicating lower colour intensity. It is interesting that even though the pre-treated sample had lower initial absorbance, complete decolouration was achieved at the same irradiation time. Our experiment proved the recalcitrance of this anthraquinone dye since it showed that 35 % difference in initial colouration of the pre-treated sample didn't shorten the irradiation time needed to reach complete decolouration.

Longer irradiation time (210 min) was needed to reach complete decolouration of RRD22 and RBK5. As it can be concluded from Figs. 44 and 45, decolouration course of red and black pre-treated and raw samples exhibits a clear difference in favour of the pre-treated samples regarding irradiation time needed to reach complete decolouration (about 40 % shorter time of irradiation).

Dye molecules colour the solution up to a degree which causes screening effect as they absorb the UV irradiation and prevent it from reaching the surface of the catalyst and thus reduce reaction efficiency and concentrations of reactive radicals. In Table 18 the initial absorbance values which imply to the intensity of colouration are given. Among both azo dyes and the anthraquinone one the difference in initial absorbance was substantial and was also exhibited in almost 60 % shorter time for the decolouration of RBL19 to be achieved. Retardation in light penetration with increasing dye concentration requires higher catalyst surface for the same degradation rate to be achieved (Konstantinou and Albanis, 2004; Tang et al., 2004).

Raw samples' decolouration curves comparison shows that RBL19 exhibits first order exponential decay but RRD22 and RBK5 curves are more of a sigmoid shape in the first part of the irradiation experiment. Only after the first 60 min of

irradiation, when initial absorbance dropped for 30 %, decolouration curves acquired exponential decay shape. Exhibited characteristic of the curves is attributed to the screening effect of red and black dyes in first part of irradiation due to initially high intensity values. When initial colouration intensity drops for a certain percent, screening effect is no longer present and further decolouration proceeds exponentially. These findings are in accordance with the published results (Stylidy et al., 2003). Additionally the screening effect is confirmed by the fact that none of the decolouration curves of the pre-treated samples has sigmoid shape.

Toxicity of the raw and pre-treated samples towards *Vibrio fischeri* test organism prior to irradiation was very high (only for the blue coloured wastewater was lower than 100 %) (Table 18). This is attributed to the fact that textile auxiliaries and dyes exhibit toxicity; they or their degradation products are carcinogenic or mutagenic (Wang et al., 2002).

During PCOx of textile wastewater samples, only RRD22 pre-treated sample exhibited pronounced decrease in toxicity. In all cases the toxicity during irradiation first increased and then, after reaching maximal values, started to decrease. As also the COD values showed sigmoid shape during irradiation, toxicity of the samples can be attributed to toxic intermediates formed during first stages of reaction. This confirms the published results by (Lizama et al., 2002). Considering COD values, prolonged irradiation would be expected to result in further toxicity abatement since COD values started to decrease in the second half of irradiation period.

6.2.3. COD values and sample mineralization during photocatalytic oxidation

From Figs. 43, 44 and 45 it can be concluded that decolouration was achieved much faster compared to mineralization. Since irradiation time was chosen

according to the time needed for disappearance of visible colouration, the COD decrease is not very significant.

All raw wastewater samples exhibit a sigmoid shape of the COD curve. In RBL19 samples an increase occurs after 60 min and no correlation with decolouration of the solution can be established. Due to short irradiation time, no drop in COD values was achieved during irradiation. If irradiation of RRD22 and RBK5 samples was stopped at the same time, approximately the same results would be obtained as all COD curves in the first 90 min exhibit the same tendencies.

For RRD22 and RBK5 samples irradiation time was longer; formation of recalcitrant intermediate species takes place after 80 min of irradiation. Sigmoid shape of COD curve indicates formation of more tolerant intermediate products, which temporarily increase the COD of the solution (Soustas et al., 2010). Increase in COD occurs approximately 20 min after the decolouration changes from sigmoid to exponential. Average drop in COD values for raw samples is similar for red and black dye, reaching 143 and 169 mg/L respectively which accounts for 43 and 45 % drop. This numbers are in agreement with the published data for textile wastewaters for similar irradiation lengths (Alinsafi et al., 2007). Irradiation of a textile dye solution in a similar immobilised TiO_2 reactor as the one used in our experiment, but with H_2O_2 addition reached 50 mg/L after 240 min of irradiation. In our experiment drop in COD values was higher compared to the irradiation with H_2O_2 addition (Wang et al., 2002). After decolouration of the solution is achieved, the COD is reported to decrease sharply (Konstantinou and Albanis, 2004).

The CW pre-treatment contributed to a drop in average COD values of all the wastewater samples ranging from 73 mg/L for RBL19 up to 108 mg/L and 121 mg/L for RRD22 and RBK5, respectively. It can be concluded that for all dyes, the pre-treatment exhibits advantage in COD drop which for real scale textile

wastewater treatment plants means shorter time of irradiation in order to meet the effluent limits. Sigmoid shape of the curve of pre-treated samples is far less pronounced; there is a slight increase in COD value after the same irradiation time as in raw samples. In the second half of irradiation the COD value starts to decrease. Pre-treated samples of red and black dye exhibited an average difference of 133 and 102 mg/L before and after irradiation.

It has to be taken into account that in case of prepared wastewater solution the COD drop does not depend solely on dye degradation mechanism but it is rather influenced by many additional photocatalytic decomposition processes taking place in the irradiated solution.

6.2.4. Comparison of photocatalytic ozonation of pre-treated and raw samples

When ozone molecule is adsorbed onto the surface of the semiconductor an ozonide radical anion is formed finally resulting in hydroxyl radical formation. Another pathway of its formation through ozone mediation is reaction of superoxide anion with ozone, again leading to hydroxyl radical formation (Kopf et al., 2000).

Furthermore, a synergy effect of TiO_2 based photocatalysis combined with ozonation has been reported (Addamo et al., 2005; Černigoj et al., 2010). It results from a series of reactions which are often conditioned by products of the preceding reaction. Synergistic effect possibly originates in ozone adsorption on the TiO_2 surface through the following interactions: physical adsorption, weak hydrogen bonds to surface hydroxyl groups and molecular or dissociative adsorption.

As in the case of PCOx also during PCOz absorbance spectra of raw wastewater samples and CW pre-treated samples (not shown) indicated a

decrease in absorbance peaks for all dyes in UV and Vis region; no new absorbance peaks occurred. After PCOz irradiation, spectra show complete degradation of VIS wavelengths absorbing molecules, while some absorbance in the UV persists and is more pronounced in the untreated sample.

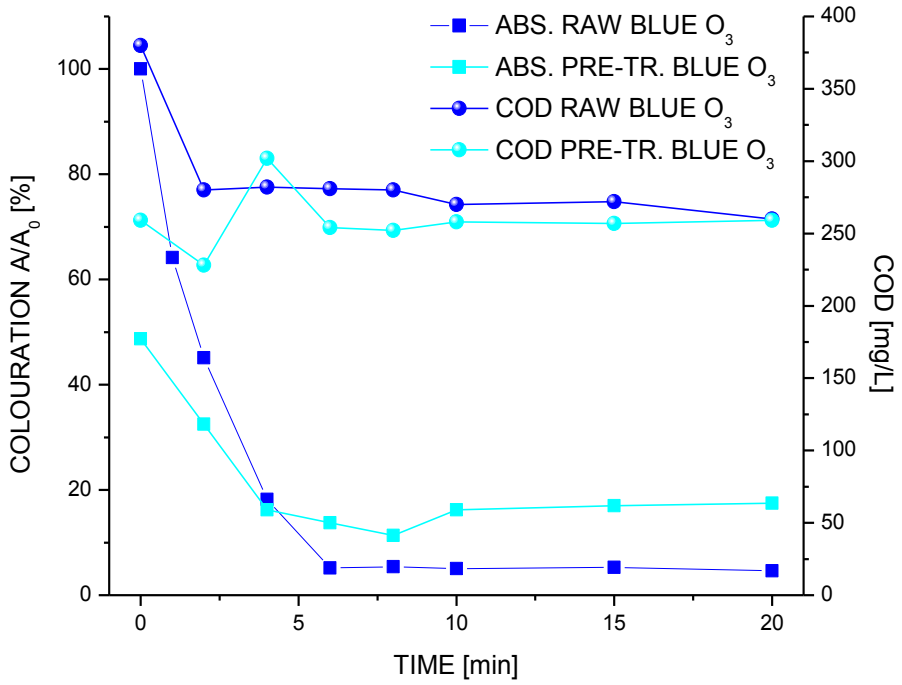

Figure 46: Colouration expressed as A/A_0 and COD values of the samples taken at the same time intervals of irradiation, RBL19.

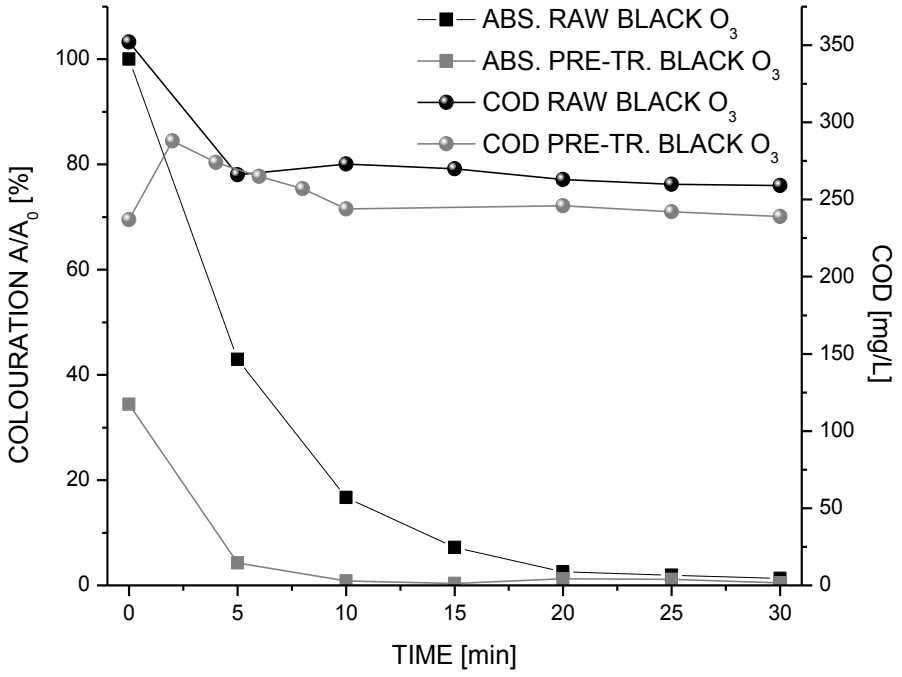

Figure 47: Colouration expressed as A/A_0 and COD values of the samples taken at same time intervals of irradiation, RBK5.

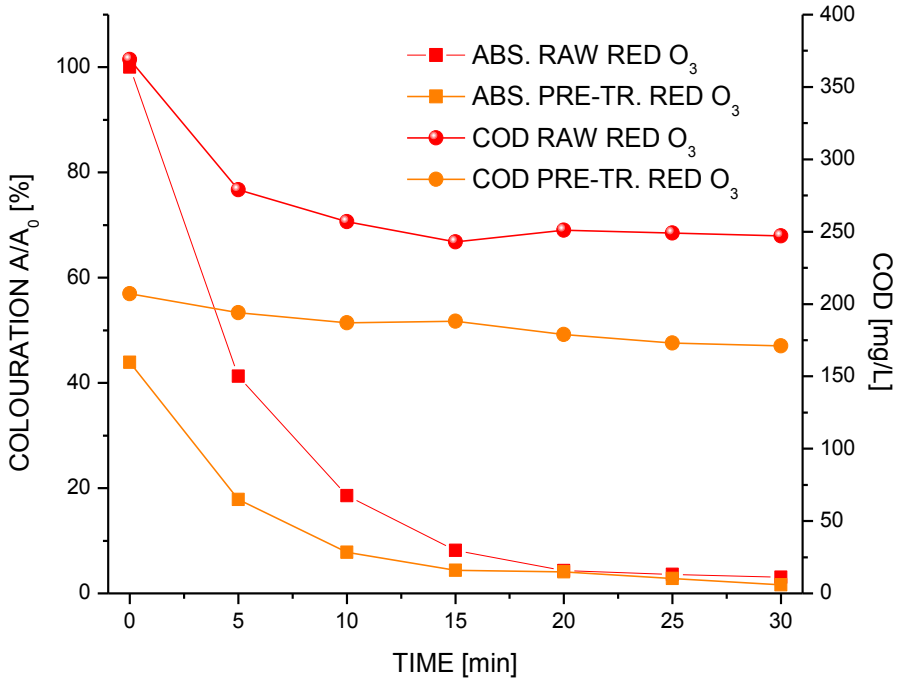

Figure 48: Colouration expressed as A/A_0 and COD values of the samples taken at same time intervals of irradiation, RRD22.

From Figs. 46, 47 and 48 it can be concluded that all raw and pre-treated samples reached complete decolouration in much shorter time with PCOz compared to PCOx. Complete decolouration was achieved in 20 min for raw RRD22 and RBK5 samples, and even faster for RBL19 samples, only 10 min were needed. This is attributed to the action of ozone which increases rate of decolouration (Augustina et al., 2005). Difference in irradiation time for colouration abatement of pre-treated samples compared to raw ones in PCOz was much lower compared to PCOx. For RBL19 samples the same time of irradiation was needed to reduce visible colouration; for RRD22 the difference was only 5 min. Only the RBK5 pre-treated sample needed considerably shorter irradiation time (50 % reduction, i.e. 20 min for raw samples to 10 min for pre-treated ones).

Since ozone molecule adsorption to the semiconductor surface is an inevitable step for hydroxyl radical formation (through conduction band electrons scavenging by ozone molecules) type of catalyst, its load and surface area play an important, rate determining role (Černigoj et al., 2007; 2009). This statement was also proven by (Wu et al., 2008) where addition of different amounts of TiO_2 didn't considerably improve decolouration of Reactive Red dye. To our knowledge, so far there are no publications yet on the PCOz dye decolouration with Ahlstrom photocatalytic paper. The data on PCOz irradiation with P25 Degussa TiO_2 catalyst for monochloroacetic acid and pyridine degradation (Kopf et al., 2000) has proven to be 4 times and 5 times more efficient respectively, compared to PCOx.

It has been established that ozone mediated dye degradation is the fastest at alkaline pH values since alkaline environment promotes ozone decomposition in favour of hydroxyl radical formation (Mehmet and Hasan, 2002; Konsowa, 2003). Since pH values were around 7.3 for pre-treated samples and above 8 for raw ones, the values are in favour of radical formation. In case of even more alkaline wastewaters, pH would further increase decolouration and degradation rate, since the difference between pH 2 and 12 was found to be 32 % (Konsowa, 2003).

6.2.5. COD values and sample mineralization during photocatalytic ozonation

In Figs. 46, 47 and 48 the COD values of samples obtained during 20 to 30 min irradiation time are also shown (right scale). For RBL19 pre-treated sample no drop is exhibited while the raw sample exhibits 32 % drop in COD. For RBK5 the drop in COD values is evident for raw samples (26 %, 93 mg/L) but was again absent in pre-treated samples. Only in case of RRD22 wastewater the PCOz proved to be successful in COD abatement - 33 % and 17 % for the raw and pre-treated samples, respectively. All COD curves show more or less

pronounced sigmoid shape, indicating formation of degradation reaction products, which can act as ozone scavengers, thus decreasing rate of mineralization and consequent COD removal. Again it has to be kept in mind that all samples were actually prepared wastewater and not dye solution samples, containing also textile auxiliaries and organic material.

Since irradiation time used in this experiment was chosen to reach decolouration of the solution, consequential low or even no drop in COD values of solution was expected. In the case of textile effluent, PCOz treatment with P25 Degussa catalyst resulted in almost complete decolouration after 60 min of irradiation and more than 60 % drop in TOC values (Gomes et al., 2000). This implies to the fact that reaction intermediates compete with pollutant molecules in O_3 scavenging and only their further degradation to mineralization decreases overall TOC values. In case of prepared textile wastewaters prolonged irradiation time would be needed to reach not only decolouration goal but also higher degree of COD removal.

As in the case of PCOx also during PCOz the samples' toxicity during and after irradiation was high. Again only RRD22 wastewater exhibited a drop in toxicity values to 82 % in the raw samples and below 20 % (the limit value of toxicity after standardised *Vibrio fischeri* toxicity test) in the pre-treated samples. Also RBL19 samples' toxicity dropped just below 100 %, to 98 and 90 % for raw and pre-treated samples, respectively.

In our subsequent studies of photocatalytic degradation of raw and pre-treated prepared textile wastewater samples prolonged irradiation time was applied with the aim to reach both decolouration and mineralization of the samples in order to meet the limits set by the legislation on technical water effluent limits (Chapter 7).

6.2.6. Comparison of photocatalytic oxidation and photocatalytic ozonation

General comparison of irradiation times needed for decolouration to be achieved (Table 19) shows large differences between PCOx and PCOz. Irradiation time for RBL19 samples is for both, raw and pre-treated samples with PCOz shorter for 93 %. But pre-treatment played no role at all in shortening irradiation length of RBL19 samples.

Table 19: Irradiation times given in minutes needed to obtain the decolouration of different samples and the difference between both methods and between raw and pre-treated samples within each method (PCOx and PCOz).

SAMPLE/ DYE	TREATMENT / SAMPLE	**PCOx** (O_2 PURGING) [min]	**PCOz** (O_3 PURGING) [min]	DIFFERENCE BTW. **PCOx** AND **PCOz** [%]	DIFFERENCE BTW. RAW AND PRE-T. **PCOx** [%]	DIFFERENCE BTW. RAW AND PRE-T. **PCOz** [%]
BLUE, RBL19	RAW	90	6	93	0	0
	PRE - TREATED	90	6	93		
RED, RRD22	RAW	210	20	90	43	25
	PRE - TREATED	120	15	88		
BLACK, RBK5	RAW	210	20	90	69	50
	PRE - TREATED	65	10	85		

In case of RRD22 and RBK5, pre-treatment shortened the irradiation time for 25 to 69 %; the highest effect was exhibited in PCOx treatment of diazo dye RBK5 – 69 %. Irradiation time of RRD22 and RBK5 in PCOz compared to PCOx was shortened to a slightly lower extent compared to RBL but it was still much shorter, between 85 and 90 %.

For both azo dyes which exhibited higher initial absorbance compared to anthraquinone dye, RRD22 and RBK5 the COD drop was substantial, between 41 and 60 %; the highest in case of pre-treated PCOx RRD22 (Table 20). But it was again much lower at PCOz, in case of pre-treated RBK5 even absent due to

the already low initial COD. This confirms that length of irradiation played a crucial role in COD decrease. For RBL19 with the lowest initial peak absorbance and consequently the shortest irradiation time, the COD drop was low or negligible, at longer irradiation times applied for RRD22 and RBK5 the COD drop was more pronounced.

Regarding irradiation time scale, the PCOz proved to be much more efficient in terms of a much shorter time needed to decolourize the sample solution compared to PCOx. But as the irradiation time was much shorter also COD drop of the raw samples was lower except for the raw RBL19.

Table 20: % of the drop in COD values of samples during irradiation treatment.

SAMPLE / DYE	DROP IN COD [%] DURING IRRADIATION	**PCOx** IRRADIATION [%]	**PCOz** IRRADIATION [%]
BLUE, RBL19	RAW	0	32
	PRE - TREATED	8	0
RED, RRD22	RAW	43	33
	PRE - TREATED	60	17
BLACK, RBK5	RAW	45	26
	PRE - TREATED	41	0

For RBL19 with shorter irradiation times employed, the COD drop was substantial only during PCOz of raw sample. In other cases it was minor or even no drop at all was observed.

6.3. CONCLUSIONS

Textile wastewaters containing three different dyes were first treated in the CW model, followed by photocatalysis. Results of pre-treated and raw samples were compared. Unexpectedly in the case of blue dye irradiation time needed to decolourize the sample solution was not shortened by the CW model pre-treatment. For other dyes, red and black, pre-treatment considerably shortened irradiation time and proved to be a successful approach to increase efficiency in wastewater treatment.

Regarding irradiation time scale, PCOz proved to be much more efficient in terms of a much shorter time needed to decolourize the sample solution compared to PCOx. On the other hand, since the irradiation time was much shorter also COD drop of raw samples was lower except for the raw RBL19.

It can be concluded that pre-treatment has proven to be successful in shortening the irradiation time for final decolouration in the case of both azo dyes, RRD22 and RBK5 in both photocatalytic degradation and ozonation experiments. This was not the case for RBL19 since irradiation time is exactly the same regardless of the samples' origin. Overall irradiation time was found to be dependent on initial colouration intensity since blue dye with the lowest initial absorbance decolourised much quicker compared to the other two dyes which exhibited screening effect due to initially high colouration of the solution. During CW pre-treatment of simulated textile wastewater considerable level of decolouration and partial drop in COD levels was achieved.

7. PHOTOCATALYSIS IN PILOT SCALE PHOTOREACTOR

7.1. EXPERIMENTAL

7.1.1. Photoreactor and catalyst setup

The compound parabolic concentrator (CPC) reactor, produced by Ao Sol, Energias Renovaveis (Portugal), was used to irradiate higher sample volumes (Fig. 49).

Figure 49: CPC photoreactor setup.

CPC reactor of 196 cm x 198 cm (length and width) was elevated under angle of 42 ° (Fig. 50). Length of tubes in the photoreactor is 150 cm; their outer and inner diameter is 50 mm and 46 mm, respectively. In the distance of 30 cm and under the same angle a rectangular frame was set up to support the lamps

(EVERSUN 100W/79, 1760 x 38 mm, Osram). Since lamps were mounted under the same angle as the whole reactor setup, they were parallel to tubes with the sample solution and irradiated them perpendicularly. Above the supporting frame aluminium plates were placed to direct most of the light sheaf into the reactor, to hinder UVA irradiation from leaving the reactor (Kete, 2008).

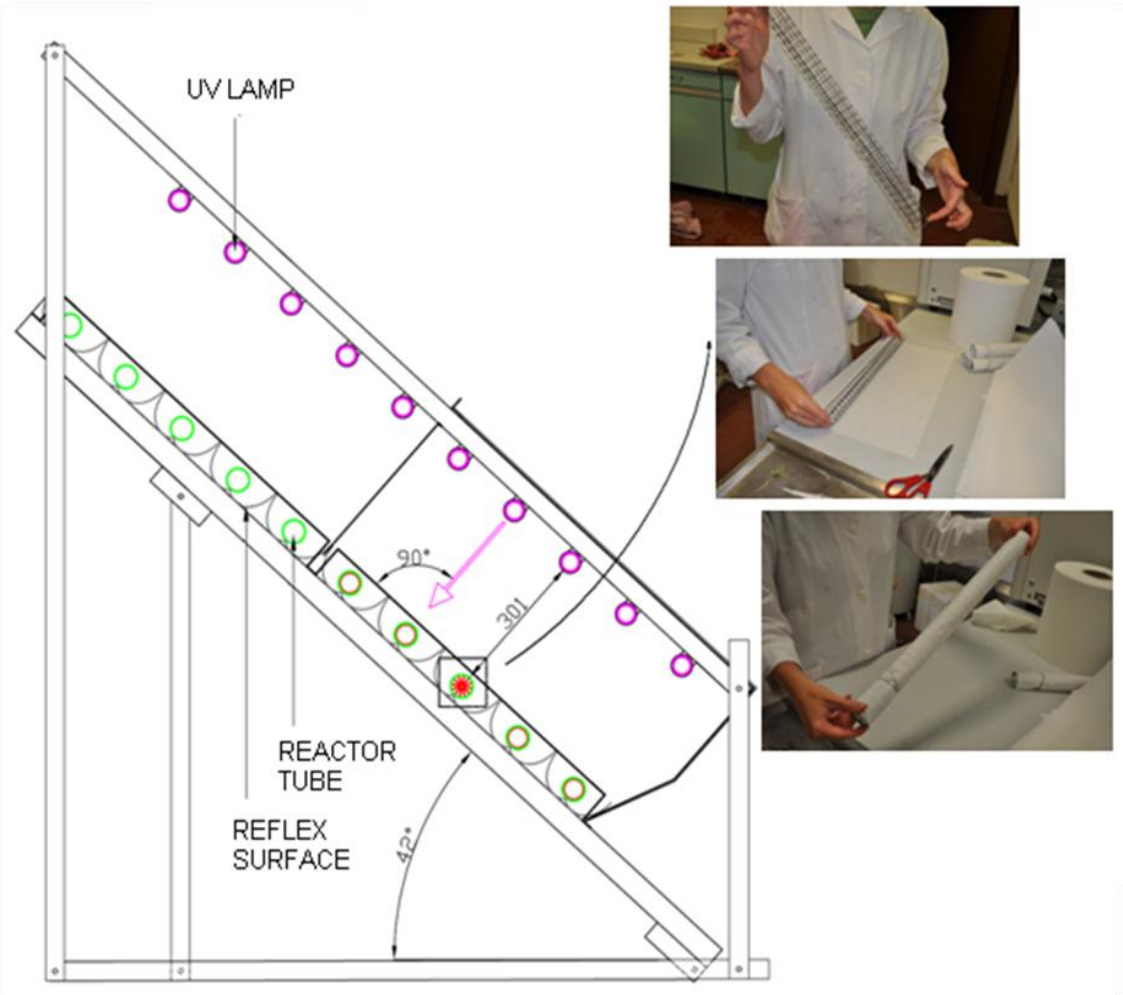

Figure 50: CPC photoreactor setup: angle of reactor tubes and lamps elevation (Kete, 2008), fastening of the photocatalytic paper onto wire support.

From 10 glass tubes of CPC reactor, the lower 5 were used in irradiation experiment. Reactor tubes were connected among themselves and through a Teflon hose to a centrifugal bearing-less pump (RXL-50 INOX, 0.25 kW, Lastra

Tech, Slovenija) (Fig. 51 a) which enabled flows between 0 and 50 L/min. The pump enabled circulating, mixing and aeration of solution.

a. pump **b. automatic sampler**

Figure 51: Centrifugal bearing-less pump (a) and tailor-made automatic sampler with a peristaltic pump (b).

Volume of the whole reactor setup was 20 L. However, each reactor's recharge volume was only 17.5 L since there was approximately 2.5 L of a residual volume, which stayed in reactor tubes due to their horizontal position and didn't flow out of when the lower tube was opened for reactor to be drained.

Photocatalytic paper (Ahlstrom, France) was used as a catalyst source. It was adjusted and fastened with elastic bands to the steel support. The supports were made out of a galvanized wire. Three supports of 49 cm in length were banded to form a circle. The whole length of the support in each tube was 147 cm and the irradiated surface was 0.623 m^2 in one tube resulting in 3.115 m^2 in all five tubes.

A tailor-made sampler (Fig. 51 b) was connected to a peristaltic pump which enabled automatic sampling of 6 samples in chosen periods. Heidolph PD 5001 peristaltic pump (Heidolph Instruments GmbH & Co. KG, Germany) with silicon

hose was used to pump the samples from the stock solution (at the circular pump of the CPC reactor) into the sampling bottles.

7.1.2. Photocatalytic oxidation

Raw and CW model pre-treated wastewater samples were irradiated in the presence of photocatalytic paper to establish time needed for the decolouration to be reached. 2 - 4 repetitions were made for each sample. UV-Vis absorbance and COD measurements were used to assess degradation of pollutant molecules and samples' toxicity was monitored. Simulated textile wastewater was prepared as explained in chapter 5.1.5. Pre-treated samples were taken from CW model on day 2 or 3 of individual CW experiments and subjected to photocatalytic oxidation.

Approximately 17.5 L of dye solutions was exposed to UVA irradiation. Because of reactor's residual volume, a sample solution was, prior to beginning of each experiment, diluted by 2.5 L of water. The flow rate (at the maximum speed allowed by the pump used in the experiment) was 7.2 L/min.

The duration of experiments was 24 h in order to reach complete decolouration and substantial mineralization through reduction in COD values. 20 mL aliquots of the irradiated sample were taken at time 0 and in time intervals (2 - 6 h) manually and/or by automatic sampler. Absorbance, COD and toxicity were measured. Temperature changes were followed and pH was measured at the beginning and at the end of experiment. All analytical procedures are explained in 5.1.8.1.

Additionally, spectral absorption coefficient (SAC) value was calculated (according to ISO 7887) at peak absorbance values (λ), characteristic for each of the dyes, Eq. (33).

7.2. RESULTS AND DISCUSSION

7.2.1. Changes in absorbance spectra after pre-treatment and during photocatalytic degradation

In Figs. 52, 53 and 54 time dependent UV-Vis absorbance spectra of RBL19, RBK5 and RRD22 containing wastewater is given. The same as in Carberry reactor, absorbance peaks for all three dyes in UV and Vis region decreased with time of irradiation and no new absorption peaks occurred. Measurements at respective reference wavelengths indicated complete degradation of dye molecules leading to a complete absence of colouration of the solution in all samples except for the raw RRD22, where slight pink colour of the solution was present at the end of irradiation.

Again the CW model pre-treatment had a uniform effect on all three dyes – it decreased Vis spectra and increased UV spectra absorbance. This is in agreement with the fact that under anaerobic conditions azo bonds are reduced and chromophore cleaved. Aromatic amines which absorb in the UV part of spectra are probably formed. Obtained results are in accordance with the literature data (Harrelkas et al., 2008; van der Zee and Villaverde, 2005).

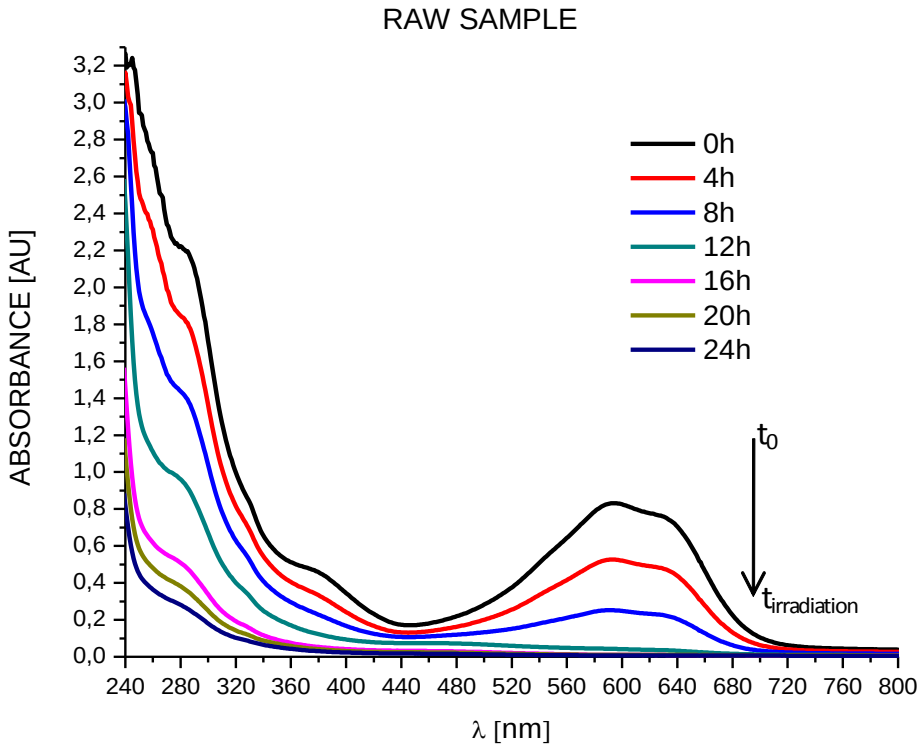
RAW SAMPLE
ABSORBANCE [AU]
λ [nm]
0h
4h
8h
12h
16h
20h
24h
t0
tirradiation

a.

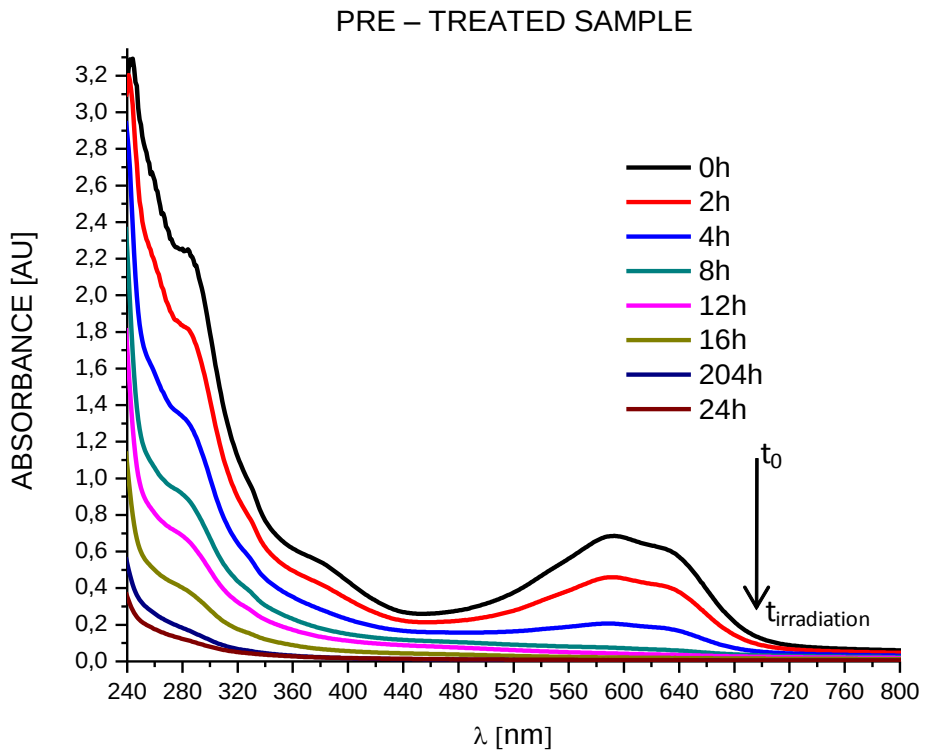

b.

Figure 52: Temporal changes in absorbance spectra of raw (a.) and pre-treated (b.) RBL19 samples taken in 2-4h intervals, the irradiation time was 24h.

In case of RBL19 dye the main difference between degradation in the Carberry reactor and prolonged degradation in the CPC reactor is in UV spectra absorbance of the raw sample. At prolonged irradiation time (compared to experiments in 6.2.1) used in the CPC reactor also disappearance and mineralization of substances absorbing in the UV part of spectra is exhibited (Fig. 52). This was not the case in Carberry photoreactor degradation, where UV absorbance after irradiation still remained high (Fig. 40). In CPC reactor complete decolouration was achieved within 12 h as well as (not complete) degradation of UV absorbing compounds.

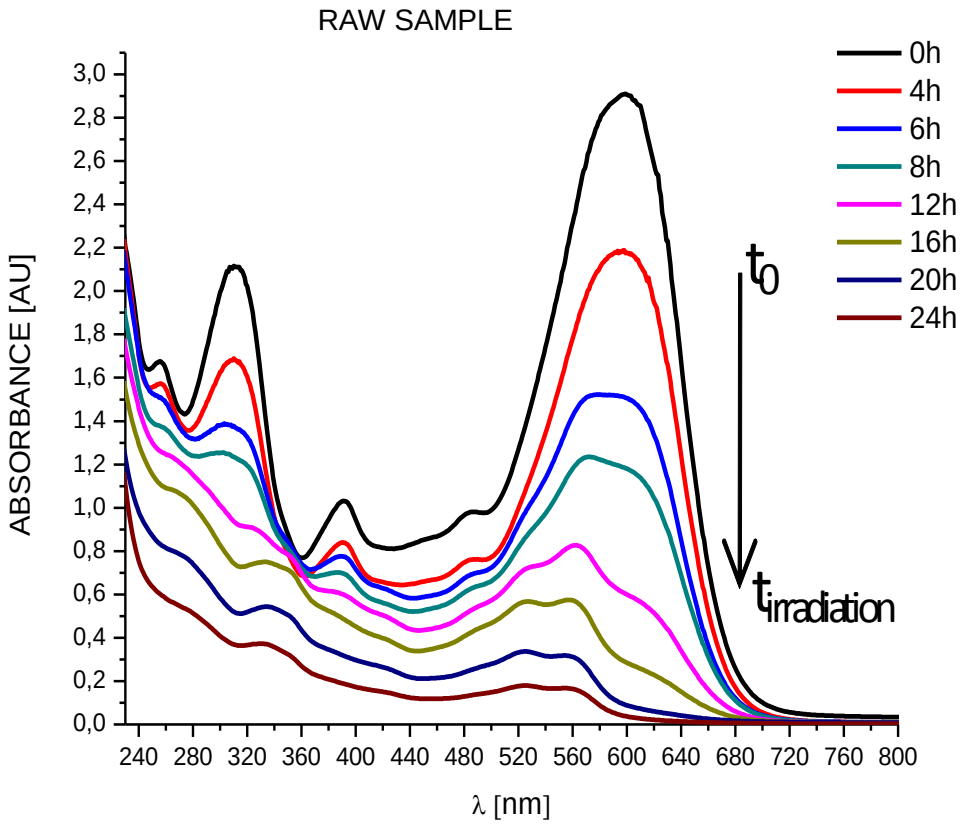
RAW SAMPLE
ABSORBANCE [AU]
λ [nm]
0h
4h
6h
8h
12h
16h
20h
24h
t0
tirradiation

a.

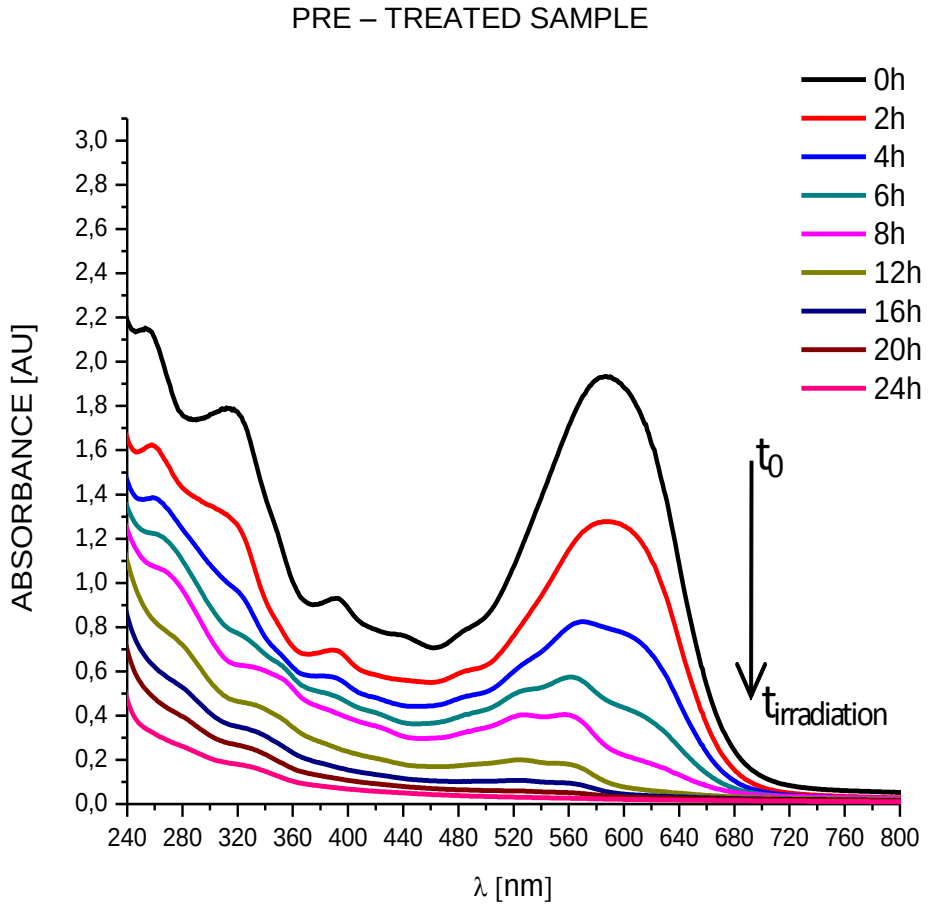

b.

Figure 53: Temporal changes in absorbance spectra of raw (a.) and pre-treated (b.) RBK5 samples taken in 2-4h intervals, the irradiation time was 24h.

In Fig. 53 raw and pre-treated samples of RBK5 are shown. The raw sample of RBK5 containing wastewater exhibits a characteristic absorbance peak at 598 nm and in the pre-treated sample the peak is shifted to 567 nm. In both spectra there is a pronounced absorbance in the UV region which is evenly decreasing with the irradiation time.

On contrary to the Carberry photoreactor reactions, a formation of a new peak at 255 nm is not observed in the case of CPC reactor. The pre-treated sample has two pronounced peaks in the UV, at 330 and 255 nm, the latter one being

extremely pronounced and is attributed to the main anaerobic degradation product.

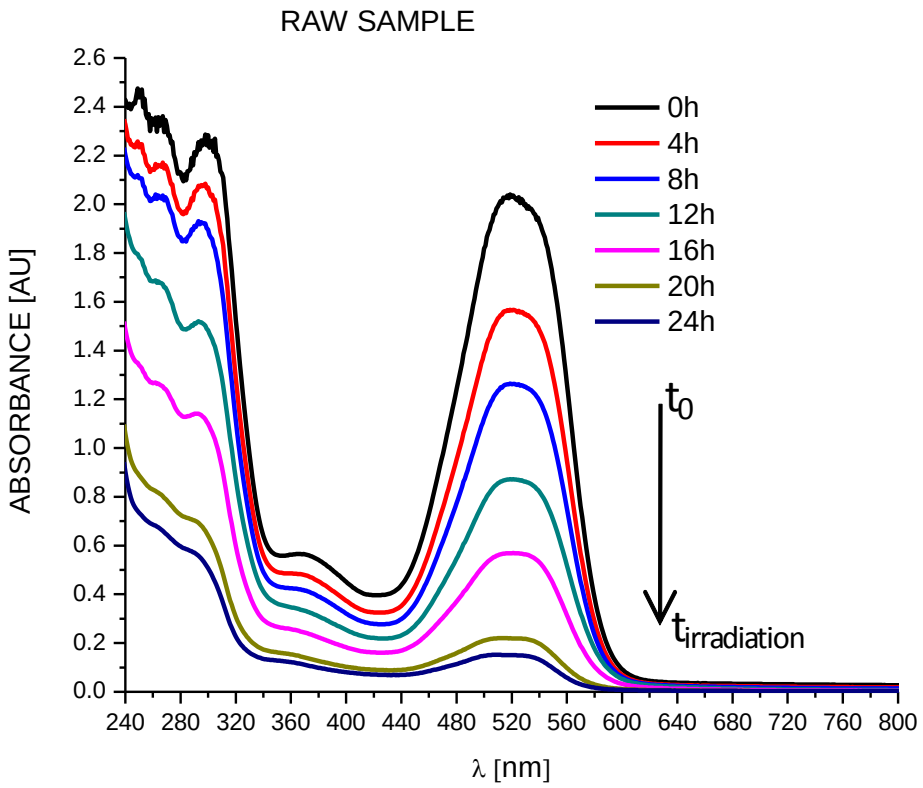

a.

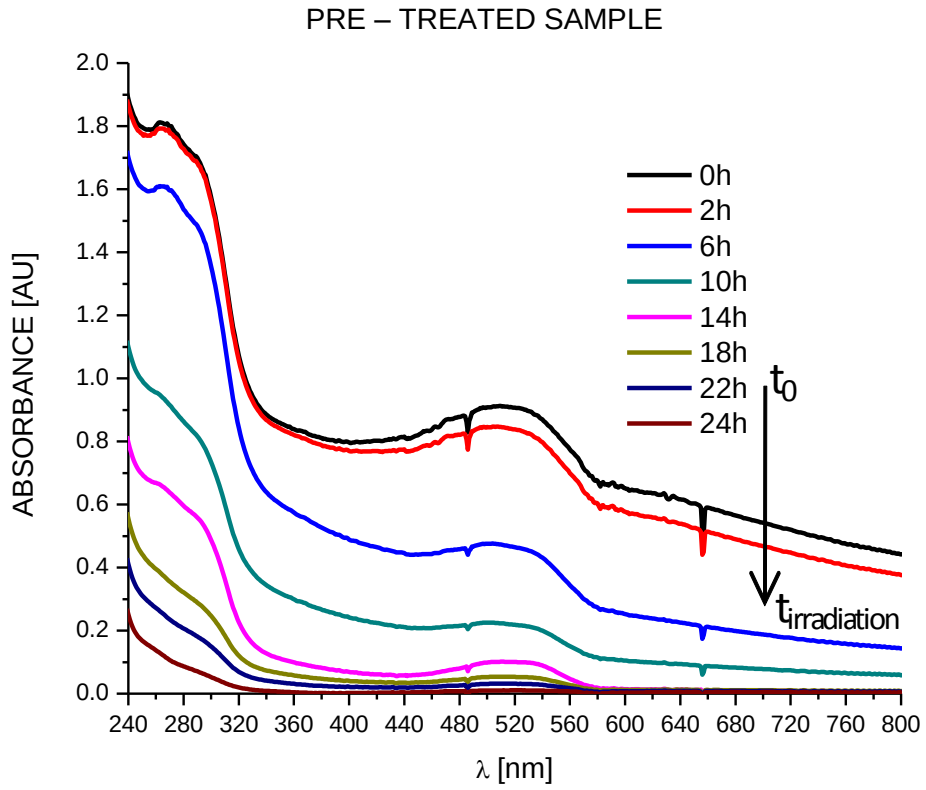

b.

Figure 54: Temporal changes in absorbance spectra of raw (a.) and pre-treated (b.) RRD22 samples taken in 2-4h intervals, the irradiation time was 24h.

In Fig. 54 raw and pre-treated samples of RRD22 are shown. Both wastewater samples exhibit characteristic absorbance peak at 520 nm. Again in the pre-treated sample the degradation of dye is exhibited as a decrease in absorbance in the Vis range and increase in absorbance in the UV range indicating aromatic product formation (Pinheiro et al., 2004; Harrelkas et al., 2008). In both spectra there is a pronounced absorbance in the UV region at wavelengths between 250 and 300 nm.

Absorbance of dyes on the photocatalytic paper was observed after 2-3 min immersion into wastewater solution. As in the Carberry photoreactor also in CPC reactor spectra of all the three dyes exhibit completely altered shape after

irradiation, this confirms the oxidative transformation rather than that dye adsorption took place. By the end of irradiation as the solution decolourised, also the photocatalytic paper was decolourised in all cases except in the case of raw red dye wastewater solution.

7.2.2. Comparison of photocatalytic oxidation of pre-treated and raw samples

In Fig. 55 the drop in colouration and COD values during photocatalytic treatment of Reactive Blue 19 is shown. In the 24 h photocatalytic treatment water was continuously circulating around the system while exposed to UV light source. RBL19 dye's visible colouration diminished after 12 h in both cases, for raw and CW pre-treated samples. But legislative SAC limit value at 620 nm is achieved already after 6h for the raw and after 3h for the pre-treated samples. RBL19 exhibited the lowest initial absorbance (0.83 AU) compared to the other two dyes used in experiment, RBK5 and RRD22 (2.9 and 2.03 AU). The CPC reactor results confirm the results obtained in the Carberry type photoreactor were also the same length of irradiation was needed to decolourise raw and pre-treated samples.

On the contrary to results obtained in the Carberry photoreactor (Fig. 43), the COD values obtained in the CPC reactor decreased during the course of irradiation. Curves of both samples, the raw and pre-treated one exhibit the same shape. Since a certain drop (27 %) in COD values for pre-treated samples was obtained already in the CW model, the legislative limit for discharge into surface waters is met after shorter irradiation time compared to raw samples. The raw samples met the legislative limit of 200 mg/L (Official Gazette RS 7/2007) after 7 h and pre-treated samples met the limit after 2 h of photocatalytic degradation. The lower limit values, 120 mg/L namely, which are set for the discharge of industrial waters in general (Official Gazette RS 45/2007), are met after 17.5 h for raw and after 8 h for pre-treated sample.

In all experiments, cuvette tests used to determine COD values ranged from 100–1500 mg/L, consequently COD values below the tests' lower limit (also below legislative limit) were not detected.

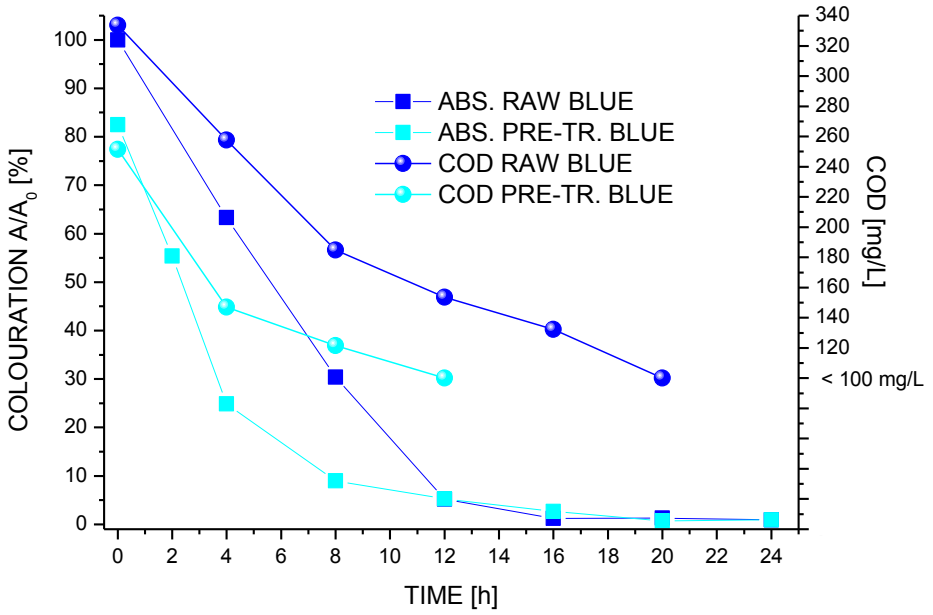

Figure 55: Colouration expressed as A/A_0 and COD values of samples taken at the same time intervals of irradiation, RBL19.

In Fig. 56 the drop in colouration and COD values during photocatalytic treatment of Reactive Black 5 is shown. Much longer irradiation time was needed for RBK5 decolouration compared to RBL19, which exhibited the highest initial absorbance. Raw sample was decolourised after 20 h (legislative SAC – spectral absorption coefficient - limit value at 620 nm was achieved after 16h) and the pre-treated one after 16 h of photocatalytic degradation (legislative SAC limit value at 620 nm was achieved after 7 h). These results confirm results obtained in the Carberry photoreactor (Fig. 44) where faster decolouration was obtained with pre-retreated samples. Since the CW pre-treated samples, irradiated in the CPC, were not decolourised to the same extent as those which were irradiated in the Carberry reactor (decolouration after pre-treatment was

over 60 % compared to 44 % in CPC) also the difference in time needed to achieve complete decolouration is lower and accounts for 20 %.

As in case of RBL19, also RBK5 COD values exhibited a decreasing trend. Curves of both, raw and pre-treated samples, exhibit the same shape. Since a 20 % drop in COD values of pre-treated samples was obtained already in CW model, the legislative limit for discharge into surface waters is met after shorter irradiation time compared to raw samples. Raw samples met the legislative limit of 200 mg/L (Official Gazette RS 7/2007) after 6.3 h and pre-treated samples met the limit already after less than an hour of photocatalytic degradation. The lower limit values, 120 mg/L namely, which are set for the discharge of industrial waters in general (Official Gazette RS 45/2007), are met after 14.3 h for raw and after 6 h for the pre-treated sample.

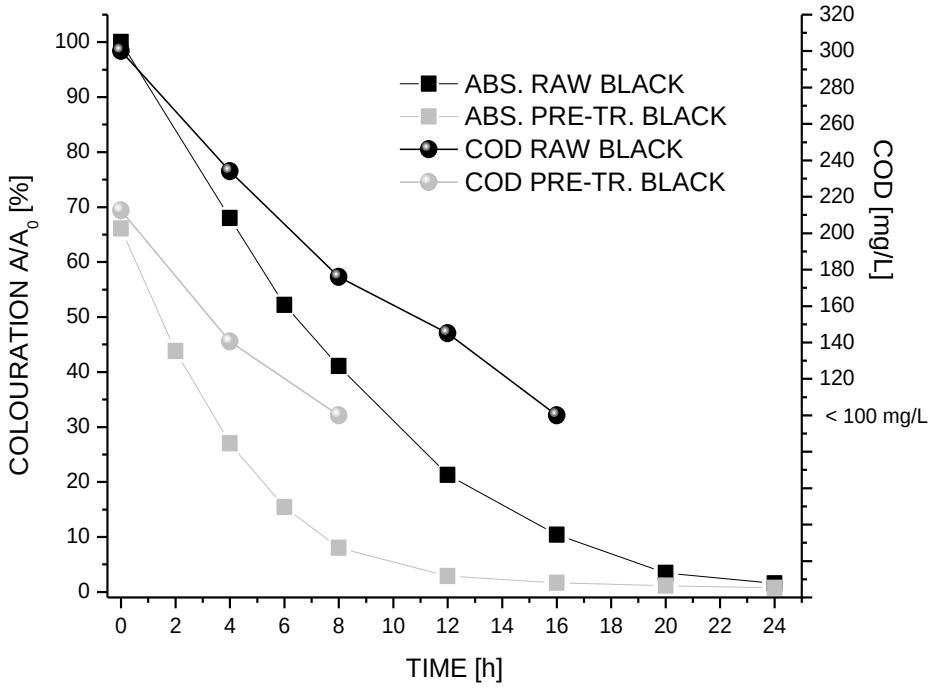

Figure 56: Colouration expressed as A/A_0 and COD values of the samples taken at the same time intervals of irradiation, RBK5.

In Fig. 57 drop in colouration and COD values during photocatalytic treatment of RRD22 is shown. For RRD22 visible colouration ceased after 12 h for the pre-treated sample. However for the raw sample some colouration remained present even after 24 h irradiation time. RRD22 exhibited middle initial absorbance (2.03 AU) compared to the other two dyes used in experiment, RBK5 and RBL19 (2.9 and 0.83 AU). CPC reactor results confirmed results obtained in the Carberry photoreactor (Fig. 45) where pre-treated samples reached complete decolouration in half the time needed for raw samples. In CPC reactor the difference was higher, since raw samples didn't reach complete decolouration in 24 h irradiation. The remaining 7 % colouration (also visible) represents the SAC of 15 m^{-1} which is 3 times more than the legislative limit for 525 nm (5 m^{-1}). Decolouration of pre-treated samples was much faster and limit values as well as decolouration were achieved after 12 h of irradiation.

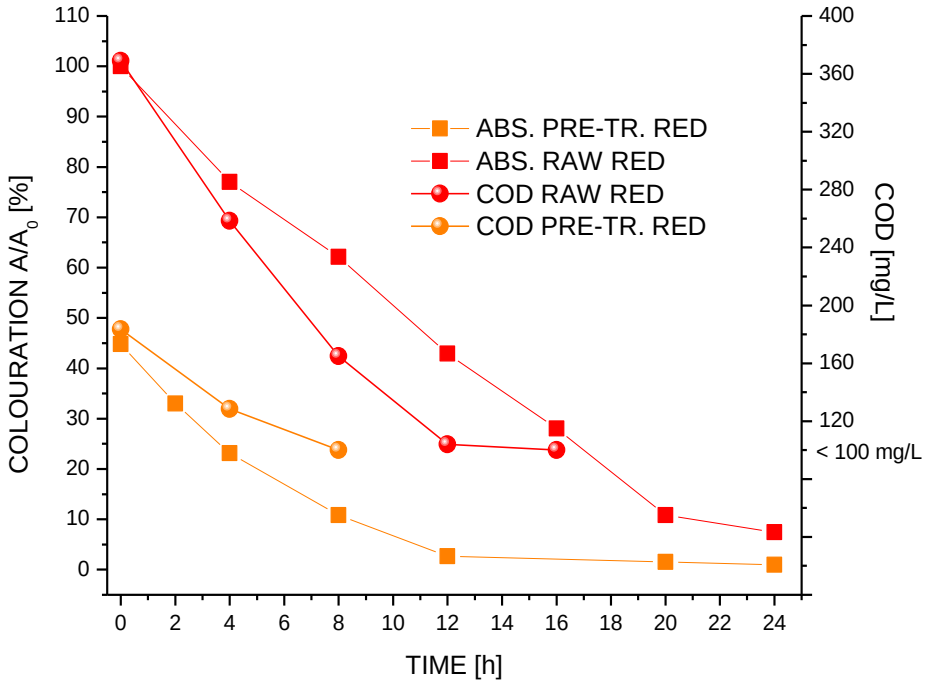

Figure 57: Colouration expressed as A/A_0 and COD values of the samples taken at the same time intervals of irradiation, RRD22.

RRD22 COD values exhibit a decreasing trend. COD values of raw RRD22 samples decreased faster compared to the other two dyes. This is attributed to the fact that the starting values were higher in RRD22 sample compared to RBK5 and RBL19. The limit values (200 mg/L) for discharge into surface waters were for pre-treated sample achieved already during treatment in the CW model. On the other hand, a 6.8 h irradiation was needed to achieve legislative limits for the raw sample. The stricter limit values for industrial waters in general (120 mg/L) were achieved in 11 h for the raw and 5.5 h for the pre-treated sample.

Decolouration curves of RRD22 and RBK5 wastewater in experiments performed in Carberry photoreactor exhibited sigmoid shape which after certain time altered to exponential. This shape of curves was attributed to the screening effect of red and black dyes in the first part of irradiation due to initially high absorbance values (Stylidy et al., 2003). This effect has not been observed during degradation in the CPC reactor. The difference is attributed to different geometry and consequently different positions of photocatalytic paper in different reactors. In Carberry reactor the paper was fastened to a support placed centrally in the reaction tube. As consequence, there was a larger volume of sample solution present between the catalyst and reaction tube wall, which caused shielding effect. Due to the support geometry in the CPC reactor, also placed centrally, but closer to the reaction tube, the volume of sample between catalyst and reaction tube wall was much lower and no shielding effect was exhibited in decolouration curves.

In another study (Guillard et al, 2003b), Congo Red and Indigo Carmine textile dyes were photocatalytically degraded in a STEP reactor with non-woven paper used as a catalyst. Instead of irradiation time the quantity of accumulated energy (in kJ/L) is given, so the irradiation length cannot be compared. Also the concentrations of dyes used are not comparable but considerably lower. It can be noted anyway that the shape of the kinetic curves is very similar as in the

case of our experiment. A difference between the two dyes has been established, the red dye proved to be more recalcitrant compared to indigo dye and it decolourised only after prolonged irradiation.

Also in case of our experiment, raw RRD22 samples proved to be more recalcitrant toward photodegradation and didn't reach complete decolouration; prolonged irradiation time (>24 h) would be needed to reach it. Red dye also exhibited a slightly different shape of kinetic curve compared to blue and black one. Results of the irradiation experiments are summarised in Table 21 (times needed to reach absence of visible colouration and to meet the legislative limit regarding decolouration before discharge for the raw and pre-treated textile wastewater samples).

Table 21: Irradiation times in hours needed to reach absence in visible colouration and to meet the legislative SAC limits.

DYE	TREATMENT / SAMPLE	ABSENCE OF VISIBLE COLOURATION	LEGISLATIVE SAC LIMIT MET AT
BLUE	RAW	12 h	6 h (620 nm)
	PRE-TREATED	12 h	3 h (620 nm)
BLACK	RAW	20 h	16 h (620 nm)
	PRE-TREATED	16 h	7 h (620 nm)
RED	RAW	> 24 h	/
	PRE-TREATED	12 h	12 h (525 nm)

When a comparison was done between degradation efficiency with slurry in a CPC reactor and Ahlstrom non-woven paper in STEP reactor, the STEP reactor with paper catalyst has proven to be less efficient compared to CPC slurry reactor. Nevertheless, even if photocatalytic paper proved to be less efficient, total decolouration could be achieved with at longer irradiation times applied (Guillard et al., 2003b). Decrease in TOC values was considerably slower compared to decrease in remaining colouration of the solution in both STEP and CPC reactors. Slow TOC drop, especially pronounced at the beginning of

irradiation, is attributed to the slow formation and degradation of hydroxylated compounds, which are considered to be main primary intermediates formed during photodegradation reactions (Guillard et al., 2003b).

The same has been established for Carberry photoreactor experiments (6.2.3.) and was also confirmed in the CPC reactor for black and blue dye and pre-treated red sample (Table 22). Only in case of raw red sample was the COD decrease actually faster compared to decolouration in the CPC reactor, on contrary to the results from the Carberry reactor. Also in case of Congo Red degradation, the red dye proved to be more recalcitrant toward degradation compared to Indigo Carmine even though the concentration of the red dye used in the experiment was 50 % lower compared to Indigo Carmine one (Guillard et al., 2003b). It has been explained that the lower rate constant of Congo red photocatalytic degradation is attributed to the steric hindrance of a large aromatic molecule which leads to a smaller number of the dye molecules adsorbed on the surface (Guillard et al., 2003a).

Table 22: CPC irradiation times in hours needed to meet the legislative COD limits.

DYE	TREATMENT / SAMPLE	COD under 200 mg/L	COD under 120 mg/L
BLUE	RAW	7 h	17.5 h
	PRE-TREATED	2 h	8 h
RED	RAW	6.8 h	11 h
	PRE-TREATED	0 h	5.5 h
BLACK	RAW	6.3 h	14.3 h
	PRE-TREATED	<1 h	6 h

7.2.3. Temperatureand pH values during samples' irradiation

The samples temperature in our experiment was constantly increasing from the start to the end of the experiment. The average temperature at the beginning of experiment was 27.1 °C and increased to 32.1 °C. The increase of irradiated solutions' temperature was thus expected to occur during the experiment.

It has been emphasised that adsorption of the dye onto the semiconductor's surface is an important parameter determining photocatalytic degradation rate. Temperature of the solution was found to influence dye's adsorption on the semiconductor; an increase in temperature of the solution from 20 to 40 °C increased the quantity of adsorbed dye from 16 mg/m^2 to 21 mg/m^2 (Barka et al., 2008). In temperature range between 25 and 35 °C the adsorbed quantity remained the same. According to the calculated enthalpy based on obtained data, the adsorption reaction is endothermic. A positive effect of higher temperature of the solution was also established for the degradation rate. Even though generally the rate of photocatalysis is not very temperature dependent, a faster degradation and complete decolouration were achieved when the temperature of the solution was gradually increased from 20 to 40 °C. This is attributed beside higher adsorption also to the lower recombination rate at higher temperature due to faster reactions on the surface of the semiconductor (Barka et al., 2008; Daneshvar et al., 2004). It can be concluded that the increasing temperature most probably didn't substantially increase the quantity of the adsorbed dye but overall it did contribute to the resulting decolouration and mineralization rate through accelerating the reactions on the catalyst surface.

The solution's pH value also influences the extent of adsorption of dye onto the surface through both, surface state of TiO_2 molecule and ionisation state of ionisable organic molecule of the dye and other molecules in solution (Barka et al., 2008). In pre-treated samples, pH values oscillated around starting values

(7.3) as it was also found for the degradation in the Carberry photoreactor where pH didn't change considerably during the course of photodegradation. The same has been found out in a STEP and CPC photoreactor degradation study of the two dyes, where the pH of the solution remained neutral through the experiment, possibly due to simultaneous release of sulphate and ammonia during the experiment (Guillard et al., 2003b).

For raw samples on the other hand, the pH dropped from 8.2 on average to 7.8 on average. Based on this it can be presumed that the pH of the sample dropped as a consequence of photocatalytic degradation of dyes, auxiliaries and organic compounds from meat peptone.

According to literature (Aguedach et al., 2008; Barka et al., 2008), repulsion between dye molecules and catalyst surface is presumed to take place at basic pH values. It is a consequence of electrostatic repulsion between $-SO_3^-$ and TiO_2/SiO_2 and prevents adsorption onto the semiconductor. As already discussed in 6.2.5. in our experiment not only distilled water solution of dye was used but a prepared wastewater which was a mixture of dyes, textile auxiliaries and meat peptone nutrient. In the pre-treated samples also all the products of degradation processes in the CW model were present which increased the concentration of different ions proven by higher electric conductivity in the pre-treated samples, indicating presence of higher concentration of ions. All this contributed to the visible adsorption of the dye onto the surface of the catalyst.

Increase in ion concentration proved to lower the ERL and to promote further decolouration and degradation. Cations on one hand separately neutralize the negative charge and thus promote low energy interactions between the dye molecule and the catalyst surface. The negative effect of anions which can compete with the dye for surface adsorption sites is presumed to be less pronounced since negative and neutral sites on the surface of the

semiconductor outnumber the positive ones (Aguedach et al., 2008). This explains the observed good absorption of the dyes in the wastewater solution onto the surface of the catalyst and their efficient degradation.

7.2.4. Toxicity

In Fig. 58 the toxicity percentage before, during and after photocatalytic degradation of raw and pre-treated samples of all the three dyes are shown. In the case of decolouration and mineralization in the Carberry photoreactor the toxicity of the samples didn't drop at all due to the short irradiation times. The same has been established for the mineralization behaviour.

For RBK5, the toxicity was very high through all the course of the experiments in CPC reactor. The diluted samples exhibited a minor decreasing trend in toxicity values but the decrease was not high enough to be evident also after volume correction. It can be concluded that even prolonged 24 h of photocatalytic oxidation didn't decrease the toxicity of the black dye sample.

For the other two dyes, photocatalytic oxidation decreased the toxicity after several hours of irradiation. For RRD22 toxicity started to drop in the last 4 h of irradiation; after 24 h it was 64 %. Pre-treated RRD22 sample exhibited a toxicity decrease after 20 h; after 24 h the toxicity was 52 %.

Only in the case of pre-treated RBL19 sample the toxicity during irradiation decreased below the value indicating absence of toxicity (green line indication in Fig. 58) (Girotti et al., 2008). The sample became non toxic to *Vibrio fischeri* test organisms after 20 h of irradiation; its toxicity after 24 h of irradiation was 8 %. Raw RBL19 sample approached the non-toxic limit after 24h of irradiation, its toxicity was 26 %.

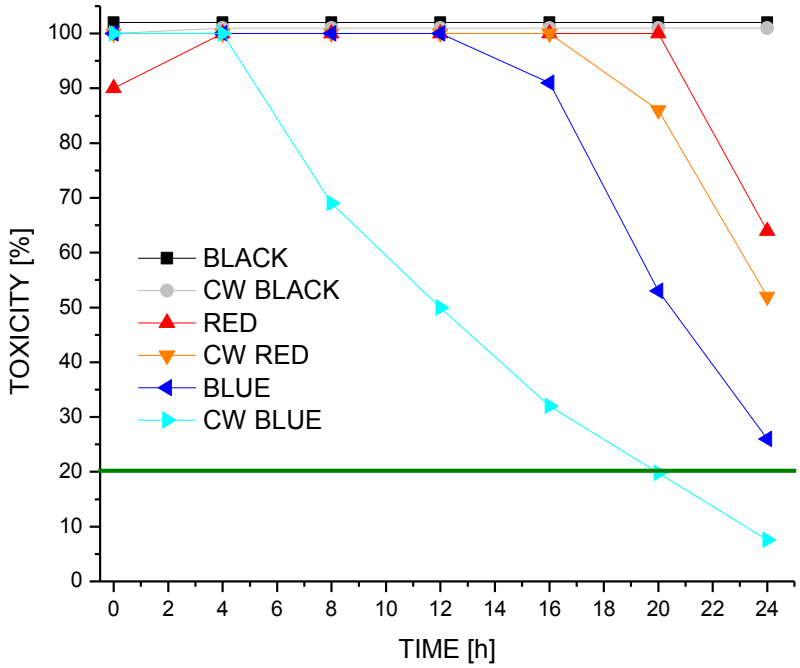

Figure 58: *Vibrio fischeri* toxicity expressed in % for raw and pre-treated samples of RBK5, RRD22 and RBL19.

7.3. COST ESTIMATION

Two treatment methods or approaches, both feasible and promising techniques for textile wastewater pollution abatement were combined with the aim to propose an environmentally and economically feasible combination of wastewater treatment methods. The following cost estimation was done with the intention to serve as an approximate comparison between the costs of both treatment approaches used in the experiment and different factors, which have to be taken into account. Figures are partly based on estimations and not all relevant factors could be taken into account.

Cost analysis of photocatalytic treatment should be based on investment, operational and maintenance costs and necessary collector area to provide the desired retention time (Goswami et al., 1997).

Prices used in calculation are based on current (spring 2011) available prices from material and services suppliers. All investment costs were calculated per 1m³ of wastewater. Investment costs for the chosen treated wastewater volume (1m³) were divided into 10 year operation period, which is supposed to be the minimum lifetime for a reactor (Augsten, 2004). The CW media was supposed to be changed 2 times within the spam of 10 year operation. The price of land where CW would be constructed is not included due to large differences in land prices even within Slovenija. Also the exact size and number of lagoons in not foreseen since the amount of wastewater to be treated is not known. All numbers given are calculated for treatment of 1m³ of wastewater (also the number of reactors). Maintenance costs and material consumption are calculated per hour of operation. With the intention to obtain approximate comparison between the costs of both treatment approaches, all costs were then summed based on 1 hour of treatment of 1m³ of textile wastewater (with similar inflow parameters compared to those used in our experiment for both systems, CW and CPC reactors).

In cost calculations it was assumed that the CW will work continuously with the foreseen HRT. Cost estimation was done based on the experiment presented in Chapter 5 but the number of operational hours could decrease on account of a different feeding regime. After the CW a storage lagoon is foreseen to collect the wastewater before photochemical treatment. For photochemical treatment two sets of costs estimations are given. In the first set (I.) wastewater is irradiated under artificial light source (same lights as used in the experiment) and photoreactors are operated during working hours, which means 8 hours a day, 5 days a week. Photoreactor setup availability due to necessary maintenance was estimated to be 90 %. The time used in calculation was the time obtained in our experiment.

In the second set (II.) the wastewater is irradiated under natural conditions; 10 hours a day, 5 days a week and photoreactor availability due to weather conditions and necessary maintenance will be 70 %. The irradiation time used in calculation was 1.5 times longer than the irradiation time obtained in our experiment; this presumption is based on lower intensity of natural light compared to artificial irradiation source.

In Table 23 estimation ofinstallation costs per 1 m³ per hour according to operational hours in sets I. and II. is presented. In Tables 24-27 an estimation of electricity costs per hour per 1 m³ of wastewater and estimation of nondurables' costs per hour per 1 m³ of wastewater is presented for both sets of experiments.

Table 23: Installation costs per 1 m³ per hour according to operational hours in sets I. and II.

PRODUCT	PRODUCER	PRICE /ARTICLE [EUR]	REQ. NO.	SUM [EUR]	**SET I. COSTS/ h [EUR/h]**	**SET II.COSTS/ h [EUR/h]**
PUMP	Lastratech (Slovenia), 0.55 kW	350	25	8750	0.4674	0.3425
CPC REACTOR	Ao Sol (Portugal)	1000	25	25000	1.3355	0.9785
INSTALLATION COSTS		75	25	1875	0.1002	0.0734
CONST. WETLAND	Limnos d.o.o. (Slovenia)	1500	2	3000	0.0351	0.0351
STORAGE LAGOON	/	1000	1	1000	0.0117	0.0117
PUMP from CW to CPC system - ELECTRICITY	Lastratech (Slovenia), 0.55 kW	350	1	350	0.0187	0.0137

Two CWs are foreseen in the no. of articles, price of 1 is the first installation, and in the price of the second two times media change is included in the foreseen 10 years of operation. The CW construction costs for 1 m³ of wastewater were calculated from construction costs for one PE (1 PE = 150 L of wastewater per day, needed CW area is 2.5 m^2). Based on the given data the CW lagoon area needed to treat 1m³ of textile wastewater which doesn't exceed the BOD of one

PE (as the one used in our experiment) would be 16.675 m^2. According to the capacity of the CPC reactor obtained from Ao Sol (Portugal), 25 such reactors are needed to simultaneously irradiate 1m^3 of wastewater.

Table 24: Estimation of electricity costs for set I. experiments per hour per 1 m^3 of wastewater.

PRODUCT/ SERVICE	PRODUCER	QUANT.	POWER CONSUMPT. [W]	ELECTR. PRICE [EUR/Wh]	**COST/h [EUR]**
LAMPS - ELECTRICITY	Osram Eversun 100W	250	100	0.000105	2.625
PUMPS - ELECTRICITY	Lastratech (Slovenia), 0.55 kW	25	250	0.000105	0.656
PUMP from CW to CPC system - ELECTRICITY	Lastratech (Slovenia), 0.55 kW	1	250	0.000105	0.026

Each reactor is irradiated by 10 lamps and a pump is foreseen between each CPC module.

Table 25: Estimation of nondurables' costs for set I. experiments per hour per 1 m^3 of wastewater.

PRODUCT	PRODUCER	QUANT.	PRICE /ART. [EUR]	SINGLE PURCHASE PRICE	NO. OF h OF OPERATION	**COST /h [EUR]**
LAMPS	Osram Eversun 100W (800h)	250	29.5	7375	800	9.219
CATALYST	Ahlstrom (France) (720)	155.75	13.2	2055.9	720	2.855
CW MAINTENANCE	/	1	400	400	8760	0.046

The calculated catalyst area in all 25 reactors was 155.75 m^2.

Table 26: Estimation of electricity costs for set II. experiments per hour per 1 m³ of wastewater.

PRODUCT/ SERVICE	PRODUCER	QUANT.	POWER CONSUMPT. [W]	ELECT. PRICE [Wh]	**COST/h [EUR]**
PUMPS - ELECTRICITY	Lastratech (Slovenia), 0.55 kW	25	250	0.000105	0.656
PUMP from CW to CPC system - ELECTRICITY	Lastratech (Slovenia), 0.55 kW	1	250	0.000105	0.026

Table 27: Estimation of nondurables' costs for set II. experiments per hour per 1 m³ of wastewater.

PRODUCT	PRODU-CER	QUANT.	PRICE /ARTICLE [EUR]	SINGLE PURCHA-SE PRICE	NO. OF h OF OPERATION	**COST/h [EUR]**
CATALYST	Ahlstrom (France) (720)	155.75 [m^2]	13.2	2055.9	720	2.855
CW MAINTENANCE	/	1	400	400	8760	0.046

CPC reactors maintenance costs were not calculated due to lack of information and experience, according to (Goswami et al., 1997) they account for 2 % of the total fixed costs. Logistic costs were also not estimated; they depend heavily on general approach to treatment set-up like scale and location of the plant. Logistics and maintenance costs, but most importantly human resource costs depend to a large extent on the treatment plant size. For small plants human resource costs constitute more than 50 % of the total treatment costs and they diminish significantly with upsizing. Due to the fact, that all the cost estimations are given per hour per 1 m³ of wastewater, the human resource costs would introduce a high source of uncertainty and are thus not included in the estimation. But it has been estimated that for a middle range treatment plant, 1 full time employee would be an appropriate estimation given, outsourcing is assumed at bigger maintenance events.

In Tables 28 and 29 estimation of costs according to the irradiation times needed to meet legislative limits on discharge colouration and COD limits for both sets is given.

Table 28: Estimation of total treatment costs according to the irradiation times needed to meet legislative limits on discharge colouration and COD limits for set I. estimations – artificial irradiation.

SET I.		DECOLOURATION COSTS		COD DECREASE COSTS	
DYE	SAMPLE	TIME [h]	PCOx [EUR/h]	COD DECREASE [h]	PCOx [EUR/h]
BLUE	RAW	6	103.55	17.5	302.02
	PRE-TREATED	3	52.19	8	139.16
BLACK	RAW	16	276.13	14.3	246.79
	PRE-TREATED	7	121.77	6	104.37
RED	RAW	27	465.97	11	189.84
	PRE-TREATED	12	208.75	5.5	95.68
AVG. COSTS	RAW		281.88		246.21
	PRE-TREATED		127.57		113.08

According to data in Table 28 costs of treatment per 1m^3 per hour clearly differ wether the CW pre-treatment was applied or not. For all three prepared wastewaters containing textile dyes costs of treatment differ substantially based on the difference whether they were pre-treated or not. Nevertheless the pre-treatment costs are calculated, still the overall costs are on average 55 % lower compared to raw wastewater irradiation for the legislative SAC limits to be met. Costs needed to meet the COD limits are on average for 54 % lower with included pre-treatment.

Table 29: Estimation of costs according to the irradiation times needed to meet legislative limits on discharge colouration and COD limits for set II. – natural irradiation at prolonged irradiation times.

SET II.		DECOLOURATION COSTS		COD DECREASE COSTS	
DYE	SAMPLE	TIME [h]	PCOx [EUR/h]	COD DECREASE [h]	PCOx [EUR/h]
BLUE	RAW	9	44.15	26.25	128.78
	PRE-TREATED	4.5	22.67	12	60.46
BLACK	RAW	24	117.74	21.45	105.23
	PRE-TREATED	10.5	52.90	9	45.35
RED	RAW	40.5	198.69	16.50	80.95
	PRE-TREATED	18	90.69	8.25	41.57
AVG. COSTS	RAW		120.20		104.99
	PRE-TREATED		55.42		49.92

Total costs of treatment for one cubic metre of wastewater per hour including reactor investment, electricity, catalyst and CW maintenance for natural irradiation source are given in Table 29. Again a clear difference in cost is exhibited between raw and pre-treated samples and it accounts for 55 % on average.

When results from Tables 28 and 29 are compared, as expected the costs are much lower when natural sunlight is applied as irradiation source, nevertheless 50 % longer irradiation times were foreseen. This hints to the fact, that not only the catalyst but above all the artificial irradiation source is a large cost since lamps applied in our experiment have 800 h of life time and later have to be replaced.

7.4. CONCLUSIONS

Pre-treatment in the CW model proved again to have a uniform effect on all the three dyes – it decreased absorbance in the Vis part of spectra and increased the absorbance in the UV part.

As in the Carberry photoreactor also in CPC reactor spectra of all the three dyes exhibit completely altered shape after irradiation, confirming the oxidative transformation of the samples. The CPC reactor results agree with the results obtained in the Carberry type photoreactor - for RBL19 again the same length of irradiation was needed to decolourise raw and pre-treated samples. For RBK5 irradiation again faster decolouration was obtained for pre-retreated samples but the difference was lower due to lower degree of decolouration achieved in the CW.

Only in case of raw RRD22 sample, the CPC reactor irradiation didn't result in complete sample decolouration. The remaining 7 % colouration (SAC = 15 m^{-1}) is 3 times higher than the legislative limit for 525 nm (5 m^{-1}). As for the other two dyes decolouration of the pre-treated samples was much faster, limit values as well as decolouration were achieved after max. 12 h of irradiation.

As already established elsewhere, the drop in COD values was considerably slower compared to drop in remaining colouration. On average the raw samples met the legislative limit of 200 mg/L (Official Gazette RS 7/2007) after 6.7 h and pre-treated samples met the limit already after one hour of photocatalytic oxidation. The lower limit values, 120 mg/L namely, which are set for the discharge of industrial waters in general (Official Gazette RS 45/2007), were on average met after 14.3 h and after 6.5 h for raw and pre-treated samples, respectively. Nevertheless the COD decrease was slower compared to decolouration, the limit COD values were for RRD22 and RBK5 reached before the colouration limit values were reached.

Toxicity percentage before, during and after photocatalytic degradation of raw and pre-treated samples of all the three dyes was followed. Very high toxicity was obtained in the case of black dye (RBK5) through all the course of the experiment; even prolonged 24 h photocatalytic oxidation didn't decrease the toxicity of the samples.In the case of red dye (RRD22) the toxicity dropped as a consequence of irradiation to 64 % and 52 % for raw and pre-treated samples, respectively.

Only in the case of pre-treated blue dye sample the toxicity decreased below the value indicating absence of toxicity; the sample was non-toxic after 20 h of irradiation. Raw blue dye sample approached the non-toxicity limit; after 24 h of irradiation its toxicity was 26 %.

Total costs of treatment for one cubic metre of wastewater per hour including reactor investment, electricity, catalyst and CW maintenance for artificial and natural irradiation source were estimated. Based on the costs assessment it can be concluded that the pre-treatment introduction into the treatment approach and natural irradiation source are suggested as an efficient and cost effective combination of treatment approaches compared to artificial irradiation source.

8. CONCLUSIONS

TiO_2 thin films were doped with iron and the band gap shift was achieved towards Vis light absorption, but photodegradation experiments showed that doping had an overall detrimental effect on photocatalytic performance. This was attributed to particles' agglomeration and crystallinity loss exhibited in the doped samples and the fact, that doping forms recombination sites which deteriorate the semiconductor performance. When photocatalytic activity of TiO_2 and Au/TiO_2 samples was analyzed, it has been established, that under UV-Vis and Vis light in the pure TiO_2 samples the number of layers plays the most important role in determining photocatalytic performance. In multi layer pure TiO_2 thin films the best photocatalytic performance was obtained without various percent of dopant additions and without addition of noble metal on their surface. In the case of multilayer films both types of modifications turned out to have a deteriorating effect on the films performance. Only in the one layer film the gold addition substantially increased the photocatalytic performance of the film.

Pre-treatment in the CW model proved to have a uniform effect on all the three dyes – it decreased absorbance in the Vis part of spectra and increased the absorbance in the UV part. The decoluration rate of all thre dyes was 50 % on average and the legislative limits for water colouration were not met (SAC values at 525 and 620 nm). COD removal reduction and decolouration efficiency of the CW model were lower than reported for similar systems treating textile wastewater. Average COD values at the outflow compartment on day 2 of the experiment (when samples were taken for irradiation in Carberry and CPC reactors) were 221 mg/L (120 mg/L being the legislative discharge limit, Table 1). Avgerage BOD_5 values at the outflow compartment on day 2 were 177 mg/L (30 mg/L being the legislative discharge limit, Table 1). Partly this can be attributed to the fact, that the inflow concentration used in our experiments was lower compared to literature and consequently removal rates were lower. Length

of incubation and changing conditions were those which strongly influenced the decolouration rate. Since alternating reduced and oxidised conditions favour aerobic facultatives and decolouration occurs in anaerobic conditions, periodic aeration of media didn't have a favourable effect on decolouration efficiency. Toxic aromatic amines' formation through reductive azo bonds' cleavage is suggested, due to an increase in UV absorbance, exhibited in the samples' UV-Vis spectra, as porposed by (Pinheiro et al., 2004). As increase in toxicity is attributed to anaerobic treatment phase, it can be established, that at least partly anaerobic conditions (microlocations) were present in the CW model. For higher decolouration and COD removal rate to be achieved the CW model should be operated under more anaerobic conditions and at prolonged HRT.

Results of Carberry photoreactor photocatalytic oxidation and ozonation of pre-treated and raw samples of textile wastewaters with three different dyes were compared. Unexpectedly for blue dye the irradiation time needed to decolourize the sample solution was not shortened by the pre-treatment in the CW model. For red and black dye, the pre-treatment considerably shortened irradiation time and proved to be a successful approach to increase efficiency in wastewater treatment. Photocatalytic ozonation exceedingly shortened time needed to decolourize the sample solution but the COD decrease of the raw samples was much lower except for the raw RBL19. Overall irradiation time was found to be dependent on the initial colouration intensity since blue dye with the lowest initial absorbance decolourised much quicker compared to the other two dyes which exhibited screening effect due to initially high colouration of the solution.

The CPC reactor irradiation results confirmed the results obtained in the Carberry type photoreactor - for RBL19 again the same length of irradiation (12h) was needed to decolourise raw and pre-treated samples. SAC limits (SAC at 620 nm ≤ 3 /m) were met after 3 h for pre-treated samples and 6 h for raw ones. For azo dyes RBK5 and RRD22 faster decolouration was obtained for pre-

retreated samples (16 h compared to 20 h for RBK5 and 12 compared to more than 24 h for RRD22) but the difference was lower due to lower degree of decolouration achieved in the CW. SAC limits were met after 16 h and 7 h for RBK5 (SAC at 620 nm ≤ 3 /m) and after more than 24 h and 12 h for RRD22 (SAC at 525 nm ≤ 5 /m) raw and pre-treated samples, respectively. Only in case of raw RRD22 sample, the CPC reactor irradiation didn't result in complete sample decolouration. Very high toxicity was obtained for RBK5 containing samples throughout the course of experiment; even prolonged 24 h of photocatalytic oxidation didn't decrease it. For RRD22 the toxicity dropped as a consequence of irradiation to 64 % and 52 % for raw and pre-treated samples, respectively. RBK5 and RRD22 samples' toxicity did't decrease below the non-toxicity limit, only blue dyes' raw sample toxicity approached the 20 % non-toxicity limit and the pre-treated sample was found to be non-toxic after 20 h of irradiation. The toxicity discharge limit value for *Vibrio fischeri* test organism is not given in legislation. The drop in COD values was considerably slower compared to drop in remaining colouration. Nevertheless the COD decrease was slower, the limit COD values (120 mg/L) were for RRD22 (11 h and 5.5 h for raw and pre-treated samples) and RBK5 (14.3 h and 6 h for raw and pre-treated samples, respectively) reached before the colouration limit values were reached. For RBL19 legislative limits were met after 17.5 h and 8 h for raw and pre-treated samples, respectively.

Two treatment methods or approaches, both feasible and promising techniques for textile wastewater pollution abatement were combined with the aim to propose an environmentally and economically feasible combination of wastewater treatment methods. In cost estimation analysis the pre-treatment decreased the overall treatment costs for 55 % on average. Estimated treatment costs per hour of treatment, per cubic meter of wastewater, added up to 282 EUR for raw samples and 127 EUR for pre-treated samples irradiated under artificial irradiation source. Moreover, natural irradiation source is suggested as

the most cost efficient treatment approach since artificial irradiation costs were calculated to increase treatment costs for more than 100 %.

A proposed treatment combination with biological approach improvement/ optimisation (vertical flow CW introduction) would further decrease the irradiation times of photocatalytic degradation and in turn further reduce the overall operational costs of the wastewater treatment. An improved biological stage with natural irradiation source is thus proposed as the best treatment approach based on the results obtained in our experiment.

9. LITERATURE

Addamo M., Augugliaro V., García-López E., Loddo V., Marcì G., Palmisano L. 2005. Oxidation of oxalate ion in aqueous suspensions of TiO_2 by photocatalysis and ozonation. Catalysis Today 107-108: 612-618.

Aguedach A., Brosillon S., Morvan J., Lhadi E. K. 2008. Influence of ionic strength in the adsorption and during photocatalysis of reactive black 5 azo dye on TiO_2 coated on non woven paper with SiO_2 as a binder. Journal of Hazardous Materials, 150: 250-256.

Aguedach A., Brosillon S., Morvan J., Lhadi E.K. 2005. Photocatalytic degradation of azo-dye reactive black 5 and reactive yellow 145 over a newly deposited titanium dioxide. Applied Catalysis B, 57: 55-62.

Akpan U.G., Hameed B.H. 2009. Parameters affecting the photocatalytic degradation of dyes using TiO_2 basedphotocatalysis: A review. Journal of Hazardous Materials, 170: 520-529.

Akratos C. S., Tsihrintzis V. A. 2007. Effect of temperature, HRT, vegetation and porous media on removal efficiency of pilot-scale horizontal subsurface flow constructed wetlands. Ecological Engineering, 29: 173-191.

Alinsafi A., da Motta M., le Bonte S., Pons M.N., Benhammou A. 2006. Effect of variability on the treatment of textile dyeing wastewater by activated sludge. Dyes and Pigments, 69: 31-39.

Arana J., Garriga I Cabo C., Fernandez Rodriguez C., Herrera Melian J.A., Ortega Mendez J.A., Dona Rodriguez J.M., Perez Pena J. 2008. Combining

TiO_2 photocatalysis and wetland reactors for the efficient treatment of pesticides. Chemosphere, 71: 788-794.

Armelao L. Barecca D., Bottaro G., Gasparotto A., Maccato C., Maragno C., Tondello E., Lavrenčič Štangar U., Bergant M., Mahne D. 2007. Photocatalytic and antibacterial activity of TiO_2 and Au/ TiO_2 nanosystems. Nanotechnology, 18: 375709-375716.

Armelao L., Barecca D., Bottaro G. 2004. Au/TiO_2 nanosystems: a combined RF-sputtering/sol-gel approach. Chemical Materials, 16: 3331-3338.

Armelao L., Barecca D., Bottaro G., Gasparotto A., Gross S., Maragno C., Tondello E. 2006. Recent trends on nanocomposites based on Cu, Ag and Au clusters: A closer look. Coordination Chemistry Reviews. 250: 1294-1314.

Atekwana E. A., Atekwana E.A., Dale Werkema D., Allen J.P., Smart L.A., Duris J.W., Cassidy D.P., Sauck W.A., Rossbach S. 2004. Evidence of microbial enhanced electrical conductivity in hydrocarbon-contaminated sediments, Geophysical Research Letters, 31: L 23501.

Augsten E. 2004. Effects of the Parameters Temperature, Iron Concentration and Irradiation on the Reaction Rate of the Photo-Fenton Process using Alachlor as a Model Compound. M.Sc. Thesis, Fachhochschule Bingen. http://www.psa.es/webeng/projects/cadox/documents/EvaAugstenMasterThesis.pdf

Augustina T.E., Ang, H.M., Vareek V.K. 2005. A review of synergic effect of photocatalysis and ozonation on wastewater treatment. Journal of Photochemistry and Photobiology C: Photochemistry. Rev. 6: 264-273.

Barka N., Assabbane A., Nounah A., Aît Ichou Y. 2008. Photocatalytic degradation of indigo carmine in aqueous solution by TiO_2 – coated non-woven fibres. Journal of Hazardous Materials, 152: 1054-1059.

Baughman G. L., Perkins W. S. 2001. Treatment of textile effluents in constructed wetlands. AATCC Review, 1: 31-33.

Beydilli M. I., Pavlostathis S. G., Tincher W.C. 2000. Biological Decolorization of the Azo Dye Reactive Red 2 Under Various Oxidation - Reduction Conditions. Water Environment Research, 72: 698-705.

Bouras P., Stathatos E., Lianos P. 2007. Pure versus metal-ion-doped nanocrystalline titania for photocatalysis. Applied Catalysis B: Environmental, 73: 51-59.

Briggs D., Seah M.P. 1990. Practical Surface Analysis (2nd edn. ed.), Vol. 1. John Wiley and Sons, New York.

Brinker C.J., Sherer G. W. 1990. Sol-Gel Science. Academic Press Limited, London.

Bromley-Challenor K. C. A., Knapp J.S., Zhang Z., Gray N.C.C., Hetheridge M.J., Evans M.R. 2000. Decolorization of an azo dye by unacclimated activated sludge under anaerobic conditions. Water Research 34: 4410-4418.

Brosillon S., Djelal H., Merienne N., Amrane A. 2008. Innovative integrated process for the treatment of azo dyes: coupling of photocatalysis and biological treatment. Desalination, 222: 331-339.

Bulc Griessler T. 2005. The use of constructed wetland to treat textile dyes, E! 2983 “TEXTILE WET”, končno poročilo o rezultatih raziskovalnega projekta v okviru Eureke za leto 2005.

Bulc Griessler T., Ojstršek A. 2008. The use of constructed wetland for dye-rich textile wastewater treatment, Journal of Hazardous Materials, 155: 76-82.

Calheiros C.S.C., Rangel A.O.S.S., Castro P.M.L. 2007. Constructed wetland system vegetated with different plants applied to the treatment of tannery wastewater. Water Research, 41: 1790-1798.

Carneiro J.O., Teixeira V., Portinha A., Magalhaes A., Coutinho P., Tavares C.J., Newton R. 2007. Iron-doped photocatalytic TiO_2 sputtered coatings on a plastic for self cleaning applications. Material Science and Engineering, 138: 144-150.

Carp O., HuismanC.L., Reller A. 2004. Photoinduced reactivity of titanium dioxide. Progress in Solid State Chemistry, 32: 33-177.

Černigoj U., Lavrenčič Štangar U., Jirkovský J. 2010. Effect of dissolved ozone or ferric ions on photodegradation of thiacloprid in presence of different TiO_2 catalysts. Journal of Hazardous Materials, 177: 399-406.

Černigoj U., Lavrenčič Štangar U., Trebše P. 2007. Degradation of neonicotinoid insecticides by different advanced oxidation processes and studying the effect of ozone on TiO_2 photocatalysis. Applied Catalysis B, 75: 229-238.

Černigoj U., Lavrenčič Štangar U., Trebše P., Opara Krašovec U., Gross S. 2006. Photocatalytically active TiO_2 thin films produced by surfactant- assisted sol-gel processing. Thin Solid Films, 495: 327-332.

Černigoj U., Lavrenčič Štangar U., Trebše P., Sarakha M. 2009. Determination of catalytic properties of TiO_2 coatings using aqueous solution of coumarin: Standardization efforts. Journal of Photochemistry and Photobiology A, 201: 142-150.

Daneshvar N., Rabbani M., Modirshahla N., Behnajady M.A. 2004. Kinetic modeling of photocatalytic degradation of Acid Red 27 in UV/TiO_2 process.Journal of Photochemistry and Photobiology A: Chemistry Volume 168: 39-45.

Davies L.C., Carias C.C., Novais J.M., Martins-Dias S. 2005. Phytoremediation of textile effluents containing azo dye by using *Phragmites australis* in a vertical flow intemitten feeding constructed wetland. Ecological Engineering. 25: 594-605.

de Araujo B.S., Charlwood B.V., Pletsch M. 2002. Tolerance and metabolism of phenol and chloroderivatives by hairy root cultures of *Daucus carota L*. Environmental Pollution, 117: 329-335.

de Souza S.M., Bonilla K.A., de Souza A.A. 2010. Removal of COD and colour from hydrolyzed textile azo dye by combined ozonation and biological treatment. Journal of Hazardous Materials, 179: 35-42.

Directive 2006/11/EC of the European Parliament and of the Council (http://eur-lex.europa.eu/LexUriServ/LexUriServ.do?uri=OJ:L:2006:064:0052:0059:EN:PDF)

Dos Santos A. B., Cervantes F.J., van Lier J.B. 2007. Review paper on current technologies for decolorization of textile wastewaters: Perspectives for anaerobic biotechnology. Bioresource Technology, 98: 2369-2385.

Drew D., Hötzl H. 1999. Karst Hydrogeology and Human Activities, Impacts, Consequences and Implications. A.A. Balkema, Rotterdan, Brookfield.

Dvorak D.H., Hedin R.S., Edenborn H.M., McIntire P.E. 1992. Treatment of Metal-contaminated water using bacterial sulphate reduction: results from pilot scale reactors. Biotechnology and Bioengineering, 40: 609-616.

Ellis A.B., Geselbracht M.J., Johnson B.J., Lisensky G.C., Robinson W.R. 1993. Teaching General Chemistry: A Materials Science Companion. American Chemical Society, Washington DC.

EPA Manual. 2000. Constructed Wetlands Treatment of Municipal Wastewaters, EPA/625/R-99/010, September 2000, http://www.epa.gov/ORD/NRMRL.

Epling G. A., Lin C. 2002. Photoassisted bleaching of dyes utilizing TiO_2 and visible light. Chemosphere, 45: 561-570.

EUR 20418 EN/2. European Commission Joint Centre (2003). Technical Guidance Document on Risk Assessment in Support of Commission Directive 93/67/EEC, on Risk Assessment for new Notified Substances and Commission Regulation (EC) No. 1488/94, on Risk Assessment for Existing Substances and Directive 98/8/EC of the European Parliament and of the Council Concerning the Placing of Biocidal Products on the Market. Part II.

Farooqi I.H., Basheer F., Chaudhari R.J. 2008. Constructed wetland system (CWS) for wastewater treatment. Proceedings of Taal 2007: the 12th World Lake Conference: 1004-1009.

Faulwetter J.L., Gagnon V., Sundberg C., Chazarenc F., Burr M.D., Brisson J., Camper A.K., Stein O.R. 2009. Microbial processes influencing performance of treatment wetlands: A review. Ecological Engineering, 35: 987-1004.

Firminio P. I. M., da Silva M.E.R., Cervantes F.J., dos Santos A.B. 2010. Colour removal of dyes from synthetic and real textile wastewaters in one- and two-stage anaerobic systems. Bioresource Technology, 101: 7773-7779.

Forgacs E., Cserhati T., Oros G. 2004. Removal of synthetic dyes from wastewaters: a review. Environment International, 30: 953-971.

Frijters C.T.M.J., Vos R.H., Scheffer G., Mulder R. 2006. Decolorizing and detoxifying textile wastewater, containing both soluble and insoluble dyes, in a full scale combine anaerobic/aerobic system. Water Research, 40: 1249-1257.

Fujishima A., Honda K. 1972. Electrochemical photolysis of water at the semiconductor electrode. Nature, 238: 37–38.

Fukahori S., Ichiura Y., Kitaoka T., Tanaka H. 2003. Capturing of bisphenol A photodecomposition intermediates by composite TiO_2–zeolite sheets. Applied Catalysis B: Environmental, 46: 453-462.

Garcia J. C., Simionato J.I., da Silva A.E.C., Nozaki J., de Souza N.E. 2009. Solar photocatalytic degradation of real textile effluents by associated titanium dioxide and hydrogen peroxide. Solar Energy 83: 316-322.

Garcia J., Vivar J., Aromir M., Mujeriego R. 2003. Role of hydraulic retention time and granular medium in microbial removal in tertiary treatment reed beds. Water Research, 37: 2645-2653.

Gelover S., Mondragon P., Jimenez A. 2004. Titanium dioxide sol-gel deposited over glass and its application as a photocatalyst for water decontamination. Journal of Photochemistry and Photobiology A: Chemistry, 165: 241-246.

Girotti S., Ferri E.N., Fumo M.G., Maiolini E. 2008. Monitoring of environmental pollutants by bioluminescent bacteria. Analytica Chimica Acta, 608: 2-29.

Gomes de Moraes S., Sanches Freire R., Durán N. 2000. Degradation and toxicity reduction of textile effluent by combined photocatalytic and ozonation processes. Chemosphere, 40: 369-373.

Gonçalves I.M.S., Gomes A., Bras R., Ferra M.I.A., Amorim M.T.P., Porter R.S. 2000. Biological treatment of effluent containing textile dyes. Coloration Technology, 116: 393-397.

Goswami D.Y., Sharma S.K., Mathur G.D., Jotshi C.K. 1997. Techno-Economic Analysis of Solar Detoxification Systems. Journal of Solar Energy Engineering, 119: 108-113.

Gottlieb A., Shaw C., Smith A., Wheatley A., Forsythe S. 2003. The toxicity of reactive azo dyes after hydrolysis and decolourisation. Journal of Biotechnology, 101: 49-56.

Gross S. 2008. Report on XPS measurements, surface and in depth analysis. ISTM- CNR, January 2008.

Guillard C. Lachleb H., Houas A., Ksibi M., Elaloui E., Herrmann J.M. 2003a. Influence of chemical structure of dyes, of pH and of inorganic salts on their photocatalytic degradation by TiO_2 comparison of the efficiency of powder and

supported TiO_2. Journal of Photochemistry and Photobiology A: Chemistry: 158: 27-36.

Guillard C., Disdier J., Monnet C., Dussaud J., Malato S., Blanco J., Maldonado M.I., Herrmann J.M. 2003b. Solar efficiency of a new deposited titania photocatalyst: chlorophenol, pesticide and dye removal efficiency. Applied Catalysis B: Environmental, 46: 319-332.

Hai F. I., Yamamoto K., Fukushi K. 2007. Hybrid treatment systems for dye wastewater. Critical Reviews in Environmental Science and Technology, 37: 315-377.

Harrelkas F., Paulo A., Alves M.M., El Khadir L., Zahraa O., Pons M.N., van der Zee F.P. 2008. Photocatalytic and combined anaerobic-photocatalytic treatment of textile dyes. Chemosphere, 72: 1816-1822.

Hashimoto K., Irie H., Fujishima A. 2005. TiO_2 Photocatalysis: A Historical Overview and Future Prospects. Japanese Journal of Applied Physics, 12: 8269-8285.

Headley T.R., Herity E., Davidson L. 2005. Treatment at different depths and vertical mixing withina 1-m deep horizontal subsurface flow wetland. Ecological Engineering, 25: 567-582.

Hernandez-Alonso M.D., Coronado J.M., Javier Maira A., Soria J., Loddo V., Augugliaro V. 2002. Ozone enhanced activity of aqueous titanium dioxide suspensions for photocatalytic oxidation of free cyanide ions, Applied Catalysis B: Environmental, 39: 257–267.

Herrmann J.M., Duchamp C., Karkmaz M., Hoai B.T., Lachheb H., Puzenat E., Guillard C. 2007. Environmental green Chemistry as defined by photocatalysis. Journal of Hazardous Materials, 146: 624-629.

Horton R., Moran L.A., Scrimgeour G., Perry M., Rawn D. 2006. Principles of biochemistry, 4th edition. Prentice Hall, New Jersey.

Huang Y., Ortiz L., Aguirre P., Garcia J., Mujeriego R., Bayona J.M. 2005. Effect of design parameters in horizontal flow constructed wetland on the behaviour of volatile fatty acids and volatile alkylsulphides. Chemosphere, 59: 769-777.

Huett D.O., Morris S.G., Smith G., Hunt N. 2005. Nitrogen and phosphorus removal from plant nursery runoff in vegetated and unvegetated subsurface flow wetlands. Water Research, 39: 3259-3272.

Hüfner S. 1995. Photoelectron Spectroscopy. Springer, Berlin.

Iguchi Y., Ichiura H., Kitaoka T., Tanaka H. 2003. Preparation and characteristics of high performance paper containing titanium dioxide photocatalyst supported on inorganic fibre matrix. Chemosphere, 53: 1193-1199.

Isik M., Sponza D.T. 2008. Anaerobic/aerobic treatment of a simulated textile wastewater. Separation and Purification Technology, 60: 64-72.

ISO 11348-3 2007. Water quality - Determination of inhibitory effect of water samples on the light emission of *Vibrio fischeri* (Luminiscent bacteria test) - Part 3: Method using freeze-dried bacteria.

ISO 15705 2002. Water quality - Determination of the chemical oxygen demand index (ST-COD) - Small-scale sealed-tube method.

ISO 5815-2 2003. Water quality - Determination of biochemical oxygen demand after n days (BODn) - Part 2: Method for undiluted samples.

ISO 7887.1994. Water quality - Examination and determination of colour.

Jadhav J. P., Kalyani D.C., Telke A.A., Phugare S.S., Govindwar S.P. 2010. Evaluation of the efficacy of a bacterial consortium for the removal of colour, reduction of heavy metals and toxicity from textile dye effluent. Bioresource Technology, 101: 165-173.

Jamieson R., Gordon R., Joy D., Lee H. 2004. Assessing microbial pollution of rural surface waters. A review of current watershed scale modeling approaches. Agricultural Water Management, 70: 1–17.

Kadlec R. H., Wallace S. 2008. Treatment Wetlands, Second Edition. CRC Press/Taylor & Francis Group: Boca Raton, Florida.

Kadlec R.H., Reddy K.R. 2001. Temperature effects in treatment wetlands. Water Environment Research, 73: 543-557.

Kete M. 2008. Razvoj pilotnega sistema za čiščenje vode na principu TiO_2 fotokatalize. B.Sc. Thesis, University of Nova Gorica.
http://www.png.si/~vanesa/diplome/OKOLJE/slv/31Kete.pdf.

Ko S., Fleming P.D., Joyce M., Ari-Gur P. 2009. High performance of nano-titania photocatalytic paper composite. Part II: Preparation and characterisation

of natural zeolite-based nano-titania composite sheets and study of their photocatalytic activity. Materials Science and Engineering B, 164: 135-139.

Konsowa A.H. 2003. Decolorization of wastewater containing direct dye by ozonation in a batch bubble column reactor. Desalination, 158: 233-240.

Konstantinou I.K., Albanis T.A. 2004. TiO_2 assisted photocatalytic degradation of azo dyes in aqueous solution: kinetic and mechanistic investigations, A review. Applied Catalysis B: Environmental 49: 1-14.

Kopf P., Gilbert E., Eberle S.H., 2000. TiO_2 photocatalytic oxidation of monochloroacetic acid and pyridine: influence of ozone. Journal of Photochemistry and Photobiology A, 136: 163-168.

Krečič M. 2009. Textile technology department at Tekstina Ajdovščina, Slovenija. Oral communication, 17.2.2009.

Kritikos D.E., Xekoukoulotakis N.P., Psillakis E., Mantzavinos D. 2007. Photocatalytic degradation of reactive black 5 in aqueous solutions: effect of operating conditions and coupling with ultrasound. Water Research, 41: 2236–2246.

Kumbhar A., Chumanov G. 2005. Synthesis of iron(III)-doped titania nanoparticles and its application for photodegradation of sulforhodamine-B pollutant. Journal of Nanoparticle Research, 7: 489-498.

Lee Y. H., Pavlostathis S. G., 2004. Decolorization and toxicity of reactive anthraquinone textile dyes under methanogenic conditions. Water Research, 38: 1838-1852.

Li L., Li Y., Biswas D.K., Nian Y., Jiang G. 2008. Potential of constructed wetlands in treating the eutrophic water: Evidence from Taihu Lake of Chaina. Bioresource Technology, 99: 1656-1663.

Libra J. A., Borchert M., Vigelahn L., Storm T. 2004. Two stage biological treatment of a diazo reactive textile dye and the fate of the dye metabolites. Chemosphere, 56: 167-180.

Lizama C., Freer J., Baeza J., Mansilla H.D. 2002. Optimized photodegradation of Reactive Blue 19 on TiO_2 and ZnO suspensions. Catalysis Today, 76: 235-246.

Macek T., Mackova M., Kaš J. 2000. Exploitation of plants for the removal of organics in environmental remediation. Biotechnology Advances, 18: 23-34.

Malato S., Blanco J., Vidal A., Alarcon D., Maldonado M.I., Caceres J., Gernjak W. 2002. Photocatalysis with solar energy at a pilot-plant scale: on overview. Applied Catalysis B: Environmental, 37: 1-15.

Manu B., Chaudhari S. 2002. Aerobic decolourisation of simulated textile wastewater containing azo dye. Bioresource Technology, 82: 225-231.

Marques J.J., Souza R.R., Souza C.S., Rocha I.C.C. 2008. Attached biomass growth and substrate utilisation rate in a moving bed biofilm reactor. Brazillian Journal of Chemical Engineering, 25: 665-670.

Marques S.M., Tavares C.J., Oliveira L.F., Oliveira-Campos A.M.F. 2010. Photocatalytic degradation of C.I. Reactive Blue 19 with nitrogen-doped TiO_2 catalysts thin films under UV/visible light. Journal of Molecular Structures, 983: 147-152.

Mathur N., Bhatnagar P., Nagar P., Bijarnia M.K. 2005. Mutagenicity assessment of effluents from textile/dye industries of Sanganer, Jaipur (India): a case study. Ecotoxicology and Environmental Safety, 61: 105-113.

Matsubara H., Takada M., Koyama S., Hashimoto K., Fujishima A. 1995. "Photoactive TiO_2 Containing Paper: Preparation and its photocatalytic Activity under Weak UV Light Illumination. Chemistry Letters, 1995: 767-768.

Mays P.A., Edwards G.S. 2001. Comparison of heavy metal accumulation in a natural wetland and constructed wetlands receiving acid mine drainage. Ecological Engineering, 16: 487-500.

Mbuligwe S. E. 2005. Comparative treatment of dye-rich wastewater in engineered wetland system (EWS's) vegetated with different plants. Water Research, 39: 271-280.

Mehmet F. S., Hasan Z. S. 2002. Ozone treatment of textile effluents and dyes: effect of applied ozone dose, pH and dye concentration. Chemical Technology and Biotechnology, 77: 842-850.

Moulder J.F., Stickle W.F., Sobol P.E., Bomben K.D. 1992. Handbook of X-ray Photoelectron Spectroscopy. Perkin-Elmer Co., Eden Prairie, Minnesota.

NATIONAL BUREAU OF STANDARDS Monographs. Natl. Bur. Stand. (U.S.) Monogr. 25, 7, 82, 1969.

Nigam P., Armour G., Banat I.M., Singh D., Marchant R. 2000. Physical removal of textile dyes from effluents and solid state fermentation of dye-adsorbed agricultural residues. Bioresource Technology, 72: 219-226.

Nigam P., Banat I.M., Singh D., Marchant R. 1996. Microbial process for the decolorization of textile effluent containing azo, diazo and reactive dyes, Process Biochemistry, 31: 435-422.

Official Gazette RS 7/2007, Uredba o emisiji snovi in toplote pri odvajanju odpadne vode iz naprav za proizvodnjo, predelavo in obdelavo tekstilnih vlaken. http://okolje.arso.gov.si/onesnazevanje_voda/predpisi/53_20070131_094346_Tekstil.pdf

Official Gazette RS, 45/2007, Uredba o spremembah in dopolnitvah Uredbe o emisiji snovi in topolote pri dovajanju odpadnih vod v vode in javno kanalizacijo. Preglednica 1: Mejne vrednosti parametrov industrijske odpadne vode. http://www.uradni-list.si/files/RS_-2007-045-02463-OB~P001-0000.PDF

Ojstršek A., 2007. Application of different biomass supports on a dye-bath wastewater treatment. Ph.D. Thesis, University of Maribor.

Oller I., Malato S., Sanchez-Perez J.A. 2010. Combination of advanced oxidation processes and biological treatments for wastewater decontamination – A review. Science of Total Environment, Article in Press, available online 16th October 2010.

Ottova V., Balcarová J., Vymazal J. 1997. Microbial characteristics of constructed wetlands. Water Science and Technology, 35: 117-123.

Pandey A., Singh P., Iyengar L. 2007. Bacterial decolorization and degradation of azo dyes. International Biodeterioration & Biodegradation, 59: 73-84.

Pearce C. I., Lloyd J.R., Guthrie J.T. 2003. The removal of colour from textile wastewater using whole bacterial cells: a review. Dyes and Pigments, 58: 179-196.

Pekakis P.A., Xekoukoulotakis N. P., Pekakis D. M. 2006. Treatment of textile dyehouse wastewater by TiO_2 photocatalysis. Water Research, 40: 1276-1286.

Pelton R., Geng X., Brook M. 2006. Photocatalytic paper from colloidal TiO_2– fact or fantasy. Advances in Colloidal and Interface Science, 127: 43-53.

Pinheiro H.M., Touraud E., Thomas O. 2004. Aromatic amines from azo dye reduction: status review with emphasis on direct UV spectrophotometric detection in textile industry. Dyes and Pigments, 61: 121-139.

Qiu, X., Zhao, Y., Burda, C. 2007. Synthesis and Characterization of Nitrogen-doped Group-IVB Visible-light Photoactive Metal Oxide Nanoparticles. Advanced Materials, 19: 3995-3999.

Rampaul A., Parkin I.P., O'Neill S.A., DeSouza J., Mills A., Elliot N. 2003. Titania and tungsten doped titania thin films on glass; active photocatalysis. Polyhedron, 22: 35-44.

Robert D., Malato S. 2002. Solar photocatalysis: a clean process for water detoxification. The Science of the Total Environment, 291: 85-97.

Roš M., Vrtovšek J. 2004. The study of nutrient balance in sequencing batch reactor wastewater treatment. Acta Chimica Slovenica, 51: 779-785.

Sakthivel S., Shankar M.V., Palanichamy M., Arabindoo B., Bahnemann D.W., Murugesan V. 2004. Enhancement of photocatalytic activity by metal deposition: characterisation and photonic efficiency of Pt, Au and Pd deposited on TiO_2 catalyst. Water Research, 38: 3001-3008.

Saquib M., Muneer M. 2002. Semiconductor mediated photocatalysed degradation of an anthraquinone dye, Remazol Brilliant Blue R under sunlight and artificial light source. Dyes and Pigments, 53: 237-249.

Schubert U., Hüsing N. 2005. Synthesis of Inorganic Materials, 2nd, Revised and Updated Edition. Wiley–Vch Verlag GmbH & Co.

Sevimli M.F., Sarikaya H.Z. 2002. Ozone treatment of textile effluents and dyes: effect of applied ozone dose, pH and dye concentration. Journal of Chemical Technology and Biotechnology, 77: 842-850.

Soustas K., Karayannis V., Poulios I., Riga A., Ntampegliotis K., Spiliotis X., Papapolymerou G. 2010. Decolorisation and degradation of reactive azo dyes via heterogenus photocatalytic process. Desalination, 250: 345-350.

Štangar L.U., Černigoj U., Trebše P., Maver K., Gross S. 2006. Photocatalytic TiO_2 Coatings: Effect of Substrate and Template. Monatshefte fur Chemie, 137: 647-655.

Stylidy M., Kondarides D.I., Verykios X.E. 2003. Pathways of solar light induced photocatalytic degradation of azo dyes in aqueous TiO_2 suspensions. Applied Catalysis B: Environmental, 40: 271-286.

Sunghun C., Lee S., Oh S., Park S.J., Kim W.M., Cheong B., Chung M., Song K.B., Lee T.S., Kim S.G. 2000. Optical properties of Au nanocluster embedded dielectric films. Thin Solid Films, 377-378: 97-102.

Tabrizi, G. B., Mehrvar, M. 2004. Integration of Advanced Oxidation Technologies and Biological Processes: Recent Developments, Trends and Advances. Journal of Environmental Science and Health, 39: 3029-3081.

Talarposhti A.M., Donnelly T., Anderson G.K. 2001. Colour removal from simulated dye wastewater using two-phase anaerobic packed bed reactor. Water Research, 35: 425-432.

Tanaka K., Padermpole K., Hisanaga T. 2000. Photocatalytic degradation of commercial azo dyes. Water Research, 34: 327-333.

Tang C., Chen V. 2004. The photocatalytic degradation of reactive black 5 using TiO_2/UV in an annular photoreactor. Water Research, 38: 2775-2781.

Thullen J.S., Sartoris J.J., Nelson S.M. 2005. Managing vegetation in surface-flow wastewater-treatment wetlands for optimal treatment performance. Ecological Engineering, 25: 583-593.

van der Zee F. P., Villaverde S. 2005. Combined anaerobic - aerobic treatment of azodyes - A short review of bioreactor studies. Water Research, 39: 1425-1440.

Vrhovšek D., Kroflič B. 2007. Ekološka in ekonomska upravičenost rastlinskih čistilnih naprav na območjih razpršene poselitve. Geografski vestnik, 3/4: 13-16.

Vymazal J. 2005. Constructed wetlands for wastewater treatment. Editorial. Ecological Engineering, 25: 475-477.

Vymazal J., Brix H., Cooper P. F., Green M. B., Haberl R. 1998. Constructed wetlands for wastewater treatment in Europe. Backhuys Publishers, Leiden.

Wang C., Yediler A., Lienert D., Wang Z., Kettrup A. 2002. Toxicity evaluation of reactive dyestuffs, auxiliaries and selected effluents in textile finishing industry to luminescent bacteria *Vibrio fischeri*. Chemosphere, 46: 339-344.

Wiessner A., Kappelmeyer U., Kuschk P., Kastner M. 2005. Sulphate reduction and the removal of carbon and ammonia in a laboratory-scale constructed wetland. Water Research, 39: 4643-4650.

Yoo E.S., Libra J., Adrian L. 2001. Mechanism of decolorization of azo dyes in anaerobic mixed culture. Journal of Environmental Engineering, 127: 844-849.

Zhu J., Chen F., Zhang J., Chen H., Anpo M. 2006. Fe^{3+} - TiO_2 photocatalysts prepared by combining sol–gel method with hydrothermal treatment and their characterization. Journal of Photochemistry and Photobiology A: Chemistry, 180: 196–204.

Zupančič, M. 2001. Vloga substrata pri odstranjevanju kovinskih ionov v modelu rastlinske čistilne naprave. M. Sc. Thesis, Univerza v Ljubljani, Biotechnical Faculty, Biology department.